Static magnetic fields and nerve function.

Philip Leslie Cupitt

STATIC MAGNETIC FIELDS AND NERVE FUNCTION

Philip Leslie Cupitt

PhD Thesis

University of Durham
School of Engineering

2001

ABSTRACT

Hypothetical mechanisms by which magnetic fields may influence nerve function were investigated. The motivation for this interdisciplinary research was to devise a non-invasive method by which an anaesthetic effect may be produced, without the use of drugs or injections. If achievable, such a method would eliminate the risks to patient welfare posed by traditional anaesthetic drugs and could minimise the cost of surgery.

Two hypothetical methods of non-invasive anaesthesia were evaluated, each intended to prevent the propagation of action potentials along nerve fibres. The first method attempted to hyperpolarise a nerve with the use of a rotating magnetic field. The second method hypothesised that the rate of diffusion of sodium ions during the depolarisation of a nerve fibre could be reduced by a magnetic field aligned with the axis of the nerve. These methods were analysed by computer simulation of the electrical properties of a nerve fibre, *in vivo* experimentation and by experiments with ion exchange membranes, using applied magnetic fields in the range of 0.1-0.4 tesla. Both hypothetical techniques of non-invasive anaesthesia were concluded to be unfeasible.

A further benefit of this research is to clarify some of the potential risks to human health that may be caused by exposure to static magnetic fields.

ACKNOWLEDGEMENTS

I wish to thank my supervisor, Professor Alan Purvis, for his support and encouragement during my research. I express my gratitude to Keith Ions for his enthusiasm and invaluable assistance.

I would like to thank the technical staff of the School of Engineering for their assistance, without which this research would have been impossible; Dr. Stan White of Sheffield University and Dr. Rod King of Leeds University for their guidance on experiments with membranes; Dr. Geoff Endean for suggesting the method of non-invasive anaesthesia described in Chapter Four; Andrew Yates of the University of Durham Department of Physics for producing the scanning electron microscope images of Chapter Five; Nick Holliday, Richard McWilliam and Craig Robinson for their friendship and for providing a sounding board for ideas; and to the countless members of academic staff within the University of Durham who have shared their knowledge and experience during informal discussions.

Finally, I thank my parents, Leslie and Josephine, for their continued support throughout my education.

This research was funded by a research studentship from the Engineering and Physical Sciences Research Council.

CONTENTS

Abstract 2

Acknowledgements 3

Contents 4

Figures 7

Tables 12

Declaration 13

Nomenclature 14

1. Introduction 19

1.1. Physiology of Neurons 21

1.1.1. Basic Anatomy of Neurons 22

1.1.2. Resting Potential of Neurons 27

1.1.3. Electrical Properties of Neurons 31

1.2. Anaesthesia 41

1.3. The Effects of Magnetic Fields on Biological Systems 44

1.3.1. Effects of Static Magnetic Fields on Nerve Function 45

1.3.1.1. Theoretical Effects 46

1.3.1.2. Laboratory Studies 49

1.3.1.3. Clinical Studies 59

1.3.2. Effects of Time-Varying Magnetic Fields on Nerve Function 63

1.3.2.1. Use of Magnetic Stimulation for Pain Relief 66

1.4. References 68

2. Computer Simulation of Nerve Fibres 75

2.1. Axon Modelling 75

2.2. Development of a Simulated Nerve Fibre 86

2.3. Discussion 90

2.4. References 93

3. Non-invasive Anaesthesia by a Rotating Magnetic Field 96

3.1. Blocking of Action Potentials with an Extracellular Electric Field 96

3.2. Use of a Rotating Magnetic Field to Hyperpolarise Nerve Fibres 98
3.3. Computer Simulation of Action Potential Blocking by Hyperpolarisation 104
3.3.1. Method of Computer Simulation 110
3.3.2. Results of Computer Simulation 113
3.4. Experiments with Rotating Magnets 116
3.4.1. Apparatus 116
3.4.2. Experimental Method 117
3.4.3. Results 120
3.5. Discussion 121
3.6. References 135
4. Non-invasive Anaesthesia by a Static Axial Magnetic Field 137
4.1. Effect of a Magnetic Field on the Motion of a Charged Particle 137
4.2. Use of a Static Axial Magnetic Field to Block the Conduction of Action Potentials 139
4.3. Computer Simulation of the Effect of an Axial Magnetic Field on a Nerve Fibre 145
4.3.1. Method of Computer Simulation 147
4.3.2. Results of Computer Simulation 149
4.3.3. Discussion 154
4.4. References 159
5. Experimental Apparatus to Simulate the Effect of a Static Axial Magnetic Field on a Nerve Fibre 160
5.1. Artificial Membranes 160
5.2. Measurement of Membrane Potential 168
5.3. Magnetic Field 172
5.4. References 174
6. Effect of a Magnetic Field on Steady State Sodium Ion Flux 175
6.1. Experimental Method 175
6.2. Results 179
6.3. Discussion 184
6.4. References 189

7. Effect of a Magnetic Field on the Electrolysis of Sodium Chloride Solution 190
7.1. Experimental Method 190
7.2. Results 196
7.3. Discussion 209
7.4. References 220
8. Effect of a Magnetic Field on Transient Sodium Ion Flux 222
8.1. Experimental Method 224
8.1.1. Calculation of the Rate of Formation of Membrane Potential 229
8.1.2. Statistical Methods 231
8.2. Results 233
8.3. Discussion 254
8.4. References 275
9. Conclusions 280
9.1. Further Work 284
9.2. References 287
Appendix 1. Technical Drawings 290
Appendix 2. Supplementary Results 293

FIGURES

Figure 1.1	Structure of a typical neuron	23
Figure 1.2	Schematic diagram of a myelinated axon	24
Figure 1.3	Fluid-mosaic model of membrane structure	25
Figure 1.4	A typical action potential	32
Figure 1.5	Components of transmembrane current	32
Figure 1.6	Positive feedback cycle for sodium ion permeability	34
Figure 1.7	Strength-duration curve	37
Figure 2.1	Equivalent circuit of an axon	76
Figure 3.1	Schematic diagram of rotating magnet apparatus	99
Figure 3.2	Resulting charge distribution	101
Figure 3.3	Effect of grounding the extracellular fluid	102
Figure 3.4	Variation of intracellular and extracellular potential with distance from axis of rotating magnets	105
Figure 3.5	Possible distribution of membrane potential due to rotating magnetic field	108
Figure 3.6	Applied extracellular hyperpolarising voltage	109
Figure 3.7	Membrane potential due to applied extracellular voltage	109
Figure 3.8	Variation of threshold applied hyperpolarising voltage with nerve fibre diameter	115
Figure 3.9	Measurement of an EMF between the axis and circumference of a rotating magnet	119
Figure 3.10	Measurement of an EMF in a conductor placed between rotating magnetic poles	119
Figure 3.11	Calculation of ion motion due to a rotating magnetic field	126
Figure 3.12	Cancellation of induced EMFs in a closed loop within a rotating magnetic field	129
Figure 3.13	Generalised rotating magnet system	130
Figure 4.1	Effect of a magnetic field on the motion of a charged particle	138

Figure 4.2	Nerve fibre within a solenoid	139
Figure 4.3	Influx of sodium ions into a nerve fibre	140
Figure 4.4	Sodium ion colliding repeatedly with the ion channel in an applied magnetic field	141
Figure 4.5	Estimate of Larmor radius required to cause a collision	144
Figure 4.6	Dependence of threshold reduction in extracellular sodium ion concentration upon length of region of depleted ion concentration	152
Figure 4.7	Dependence of threshold extracellular ion concentration upon length of affected region	153
Figure 4.8	Ionic membrane currents during propagated and blocked action potentials	158
Figure 4.9	Intracellular currents during propagated and blocked action potentials	158
Figure 5.1	Scanning electron microscope image of cation exchange membrane (20000x magnification)	166
Figure 5.2	Scanning electron microscope image of cation exchange membrane (4300x magnification)	167
Figure 5.3	Cross section of apparatus	168
Figure 6.1	Apparatus for steady state experiment (plan view)	176
Figure 6.2	Apparatus for control experiment	178
Figure 6.3	Effect of magnetic field on membrane potential (constant current)	181
Figure 6.4	Effect of magnetic field on membrane potential in the absence of an applied current	182
Figure 6.5	Effect of potential difference in electrolyte (constant current)	183
Figure 6.6	Equivalent circuit of membrane	185
Figure 7.1	Apparatus for experiment *(a)*	192
Figure 7.2	Apparatus for experiment *(b)*	192
Figure 7.3	Apparatus for experiments *(c)* and *(d)*	195
Figure 7.4	Apparatus for experiments *(e)* and *(f)*	195

Figure 7.5	Effect of magnetic field on applied voltage (constant current)	199
Figure 7.6	Effect of magnetic field on applied voltage in absence of a membrane (constant current)	200
Figure 7.7	Effect of magnetic field on membrane potential (constant voltage)	201
Figure 7.8	Effect of magnetic field on applied current (constant voltage)	202
Figure 7.9	Effect of magnetic field on potential difference in electrolyte (constant voltage)	203
Figure 7.10	Effect of magnetic field on applied current in absence of a membrane (constant voltage)	204
Figure 7.11	Effect of prolonged magnetic exposure on applied current	207
Figure 7.12	Effect of prolonged magnetic exposure on applied current (reversed current direction)	208
Figure 7.13	Equivalent circuit of cation exchange membrane in sodium chloride solution	209
Figure 7.14	Total resistance of sodium chloride solution and platinum electrodes as a function of applied voltage	213
Figure 7.15	Equivalent circuit for electrolysis of sodium chloride solution	214
Figure 8.1	Experimental apparatus for transient experiments (plan view)	224
Figure 8.2	Calculation of rate of formation of membrane potential in the presence of noise	230
Figure 8.3	Membrane potentials measured in the absence of an applied magnetic field during first series of experiments	237
Figure 8.4	Mean membrane potentials measured during first series of experiments	238

Figure 8.5	Significance levels of differences between mean membrane potentials measured during first series of experiments	239
Figure 8.6	Membrane potentials measured in the absence of an applied magnetic field during second series of experiments	246
Figure 8.7	Variation of equilibrium membrane potential over a series of experimental runs	247
Figure 8.8	Mean rates of formation of membrane potential measured during second series of experiments	248
Figure 8.9	Significance of differences of mean rate of formation of membrane potential for second series of experiments	249
Figure 8.10	Mean membrane potentials measured during second series of experiments	250
Figure 8.11	Significance levels of differences between mean membrane potentials measured in the absence of a magnetic field and in the presence of an applied field in direction 1 during second series of experiments	251
Figure 8.12	Significance levels of differences between mean membrane potentials measured in the absence of a magnetic field and in the presence of an applied field in direction 2 during second series of experiments	252
Figure 8.13	Significance levels of differences between mean membrane potentials measured in the presence of an applied magnetic field in directions 1 and 2 during second series of experiments	253
Figure 8.14	Expected results from second set of transient experiments	257
Figure 8.15	Structure of a potassium channel	263

Figure 8.16	Cluster-network model of ion exchange membrane pore structure	265
Figure A1	Rotating magnet apparatus	290
Figure A2	Ussing chamber (bath 1)	291
Figure A3	Ussing chamber (bath 2)	292
Figure A4	Membrane potentials measured in the presence of an applied magnetic field during first series of experiments	293
Figure A5	Membrane potentials measured in the presence of a magnetic field applied in direction 1 during second series of experiments	294
Figure A6	Membrane potentials measured in the presence of magnetic field applied in direction 2 during second series of experiments	295

TABLES

Table 1.1	Intracellular and extracellular ion concentrations	27
Table 1.2	Summary of laboratory studies of the effects of static magnetic fields on nerve function	58
Table 2.1	Simulation parameters	88
Table 3.1	Threshold applied hyperpolarising voltages and membrane potentials	113
Table 4.1	Threshold extracellular sodium ion concentrations required to prevent propagation of action potentials	149
Table 4.2	Relationship between threshold extracellular sodium ion concentration and length of affected region	151
Table 7.1	Summary of experimental results	198
Table 8.1	Mean rates of formation of membrane potential and significance level of difference between means for first series of experiments	234
Table 8.2	Mean rates of formation of membrane potential for second series of experiments	242
Table 8.3	Significance levels of differences between mean rates of formation of membrane potential for second series of experiments	243

DECLARATION

I confirm that no part of the material offered has previously been submitted by me for a degree in this or any other university. If material has been generated through joint work, my independent contribution has been clearly indicated. In all other cases material from the work of others has been acknowledged and quotations and paraphrases suitably indicated.

NOMENCLATURE

Chapter 1

$[C]_i$	Intracellular ion concentration	mol dm^{-3}
$[C]_o$	Extracellular ion concentration	mol dm^{-3}
E	Induced EMF	V
F	Faraday constant (=96500)	C mol^{-1}
i_K	Potassium current density	A m^{-2}
i_L	Leakage current density	A m^{-2}
i_{Na}	Sodium current density	A m^{-2}
$[K]_i$	Intracellular potassium ion concentration	mol dm^{-3}
$[K]_o$	Extracellular potassium ion concentration	mol dm^{-3}
$[Na]_i$	Intracellular sodium ion concentration	mol dm^{-3}
$[Na]_o$	Extracellular sodium ion concentration	mol dm^{-3}
P_K	Potassium permeability constant	m s^{-1}
P_{Na}	Sodium permeability constant	m s^{-1}
R	Gas constant (=8.314)	J K^{-1} mol^{-1}
T	Absolute temperature	K
t	Time	s
V_{eq}	Equilibrium potential for ion species	V
V_r	Membrane resting potential	V
z	Ion valence	–
ϕ	Magnetic flux	Wb

Chapter 2

C_m	Membrane capacitance	F
c_m	Membrane capacitance per unit area	F m^{-2}
d	Diameter of axon	m
E	Membrane potential	V
F	Faraday constant (=96500)	C mol^{-1}
G_a	Internodal conductance	S
G_L	Leak conductance	S

g_L	Leak conductance per unit area	S m^{-2}
G_m	Membrane conductance	S
h	Sodium inactivation parameter	–
h_0	Initial (resting) value of sodium inactivation parameter	–
I	Applied stimulus current	A
$i_{i,n}$	Ionic transmembrane current density at node n	A m^{-2}
i_K	Potassium current density	A m^{-2}
i_L	Leakage current density	A m^{-2}
i_{Na}	Sodium current density	A m^{-2}
$[K]_i$	Intracellular potassium ion concentration	mol dm^{-3}
$[K]_o$	Extracellular potassium ion concentration	mol dm^{-3}
L	Length of internode	m
l	Length of node of Ranvier	m
m	Sodium activation parameter	–
m_0	Initial (resting) value of sodium activation parameter	–
n	Potassium activation parameter	–
n_0	Initial (resting) value of potassium activation parameter	–
$[Na]_i$	Intracellular sodium ion concentration	mol dm^{-3}
$[Na]_o$	Extracellular sodium ion concentration	mol dm^{-3}
P_K	Potassium permeability constant	m s^{-1}
P'_K	Maximum value of potassium permeability constant	m s^{-1}
P_{Na}	Sodium permeability constant	m s^{-1}
P'_{Na}	Maximum value of sodium permeability constant	m s^{-1}
R	Gas constant (=8.314)	J K^{-1} mol^{-1}
r	Distance from current source	m
T	Absolute temperature	K
$V_{e,n}$	Extracellular potential at node n	V
$V_{i,n}$	Intracellular potential at node n	V
V_L	Leakage potential	V

V_n	Reduced potential at node *n*	V
V_r	Membrane resting potential	V
α_m, α_n, α_h	Rate constants	s^{-1}
β_m, β_n, β_h	Rate constants	s^{-1}
ρ_e	Resistivity of extracellular medium	Ω cm
ρ_i	Resistivity of intracellular medium	Ω cm

Chapter 3

B	Magnetic flux density (vector)	T
B	Magnetic flux density (scalar)	T
c	Ionic concentration	$mol\ dm^{-3}$
E	Electric field (vector)	$V\ m^{-1}$
E	Electric field (scalar)	$V\ m^{-1}$
F	Lorentz force	N
F_E	Electrostatic force	N
i, ***j***, ***k***	Unit vectors along *x*, *y* and *z* axes	–
l	Path of integration	m
Q, Q_1, Q_2	Charge	C
r	Distance from axis of rotation	m
V	Voltage	V
V_r	Membrane resting potential	V
v	Velocity of charge relative to magnet	$m\ s^{-1}$
$\boldsymbol{v}_M$	Velocity of magnet relative to charge	$m\ s^{-1}$
v	Linear velocity of magnet	$m\ s^{-1}$
x	Distance of separation of charges	m
x_0	Interionic separation in cubic lattice	m
$\bar{y}$	Displacement from origin along *y* axis	m
$\bar{z}$	Displacement from origin along *z* axis	m
ε_r	Relative permittivity	–
ε_0	Permittivity of free space (=8.854 x 10^{-12})	$F\ m^{-1}$
ω	Angular velocity	$rad\ s^{-1}$

Chapter 4

$\boldsymbol{B}$	Magnetic flux density (vector)	T
B	Magnetic flux density (scalar)	T
$\boldsymbol{F}$	Lorentz force	N
F	Centripetal force	N
i_K	Potassium current density	A m^{-2}
i_L	Leakage current density	A m^{-2}
i_{Na}	Sodium current density	A m^{-2}
m	Mass	kg
Q	Charge	C
r	Larmor radius	m
$\boldsymbol{v}$	Velocity (vector)	m s^{-1}
v	Velocity (scalar)	m s^{-1}

Chapter 6

I	Applied current	A
R	Internal resistance of membrane	Ω
V_{mem}	Membrane potential	V
V_r	Resting potential of membrane	V

Chapter 7

B	Magnetic field	T
d	Thickness of conductor	m
F	Faraday constant (=96500)	C mol^{-1}
I	Current	A
$R_{electrode}$	Resistance of electrode/electrolyte interface	Ω
$R_{electrolyte1}$	Resistance of electrolyte in region of membrane	Ω
$R_{electrolyte2}$	Resistance of electrolyte in bulk solution	Ω
R_H	Hall coefficient	m^3 C^{-1}
$R_{membrane}$	Resistance of membrane	Ω
V_H	Hall voltage	V
V_{mem}	Membrane potential	V

Γ_+	Dimensionless coefficient for cation	–
Γ_-	Dimensionless coefficient for anion	–
η_0	Electrolyte concentration	mol m^{-3}
μ_+	Mobility of cation	$m^2 s^{-1} V^{-1}$
μ_-	Mobility of anion	$m^2 s^{-1} V^{-1}$
V_r	Resting potential of membrane	V

Chapter 8

$E_{kinetic}$	Kinetic energy	J
$E_{thermal}$	Thermal energy	J
F	Force	N
k	Boltzmann's constant (=1.38 x 10^{-23})	J K^{-1}
m	Mass	kg
N_x	Size of sample x	–
p	Significance level	–
Q_1, Q_2	Charge	C
r	Distance of separation of charges	m
T	Absolute temperature	K
t	t statistic	–
v	Velocity	m s^{-1}
$\bar{x}$	Mean value of sample x	Units of x
ε_r	Relative permittivity	–
ε_0	Permittivity of free space (=8.854 x 10^{-12})	F m^{-1}
ν	Number of degrees of freedom	–

1. INTRODUCTION

Electrical phenomena occur within all animals and are vital in sustaining life. For example, muscle action is completely dependent upon electrical effects and in the absence of these electrical phenomena the circulation of blood, occurring due to the electrically mediated contraction of the muscle fibres of the heart, would be impossible. One particularly interesting aspect of the electrical activity within animals is the transmission of electrical signals through the nervous system as a means of communication, decision making and memory. The nervous system serves an important role in integrating the functions of disparate organs of the body and life would cease without its vital controlling influence. Despite the precision and efficiency of these electrical activities, evolution has provided animals with an amazing level of 'fault tolerance' allowing normal bodily function to occur despite the wide variety of electrical and magnetic fields which are encountered in everyday life.

The aim of this research is to investigate the electrical characteristics of the nervous system, with a view to understanding the possible physiological effects of magnetic fields. The catalyst for this research was a surgeon's desire to develop a method by which to achieve anaesthesia without the need for drugs. Traditional anaesthetic agents present a significant risk to the welfare of patients, therefore there is a clinical need to develop an alternative to these drugs. 'Non-invasive anaesthesia' is a term used to describe techniques that produce an anaesthetic effect without the use of drugs or injections.

Two hypothetical methods of non-invasive anaesthesia were evaluated as part of this research, both involving the use of an applied magnetic field to disrupt the normal function of the nervous system. Devising a method to achieve non-invasive anaesthesia is an ambitious goal. However, this research also has far wider implications. The possible risks to human health associated with exposure to magnetic fields and electromagnetic radiation is a topic which has recently attracted much public concern. Therefore, the greater understanding of the physiological effects of magnetic fields which has resulted from the study of hypothetical non-invasive anaesthesia techniques can also be viewed as a contribution to mankind's knowledge of the health implications of exposure to magnetic fields.

The inherently interdisciplinary nature of this research has necessitated co-operation between many disparate academic disciplines: engineering, medicine, biology, physics and chemistry. Furthermore, the commercial potential of non-invasive anaesthesia has resulted in collaboration between academia and partners in the healthcare industry. However, this research has been approached from the perspective of an electronic engineer, with emphasis given to the quantitative appraisal of the effects of the magnetic field. It is envisaged that this thesis will provide a valuable contribution to a research field of much topical interest.

1.1. Physiology of Neurons

Despite the interdisciplinary topic of research, this thesis is considered as research within the field of electronic engineering. It is therefore necessary to familiarise the reader with the anatomical structure of the nervous system and the physiological processes that determine nerve function. This is not an exhaustive treatment of neurobiology, but is merely intended to provide a concise introduction to the biological concepts which are frequently referred to throughout this research. It is also hoped that this introduction will help to describe the context of the small area of neuroscience considered in this research within the much larger biological framework. For a more thorough treatment of the biological foundations of this work, the reader is referred to references [1, 2, 3].

1.1.1. Basic Anatomy of Neurons

Neurons, commonly known as nerve cells, are the means of information processing and an important medium of communication within all animals. Neurons can be classified as either components of the central nervous system (CNS) or of the peripheral nervous system. The CNS consists of all neurons within the brain and spinal cord, whereas the peripheral nervous system includes all neurons external to the central nervous system [1]. Neurons can be further described as afferent, efferent or interneurons. Afferent neurons transmit information from receptor cells, for example the receptors for temperature and pressure in the skin, into the CNS. Efferent neurons carry signals out of the CNS to effector cells such as muscles or glands. Interneurons, the most abundant type of nerve cell, exist within the central nervous system to connect afferent and efferent neurons.

A typical neuron consists of two main sections, the cell body and the axon, as shown in Figure 1.1. A large number of outgrowths from the cell body known as dendrites serve as locations where inputs from other neurons are received and processed. It should be noted that afferent neurons do not possess dendrites.

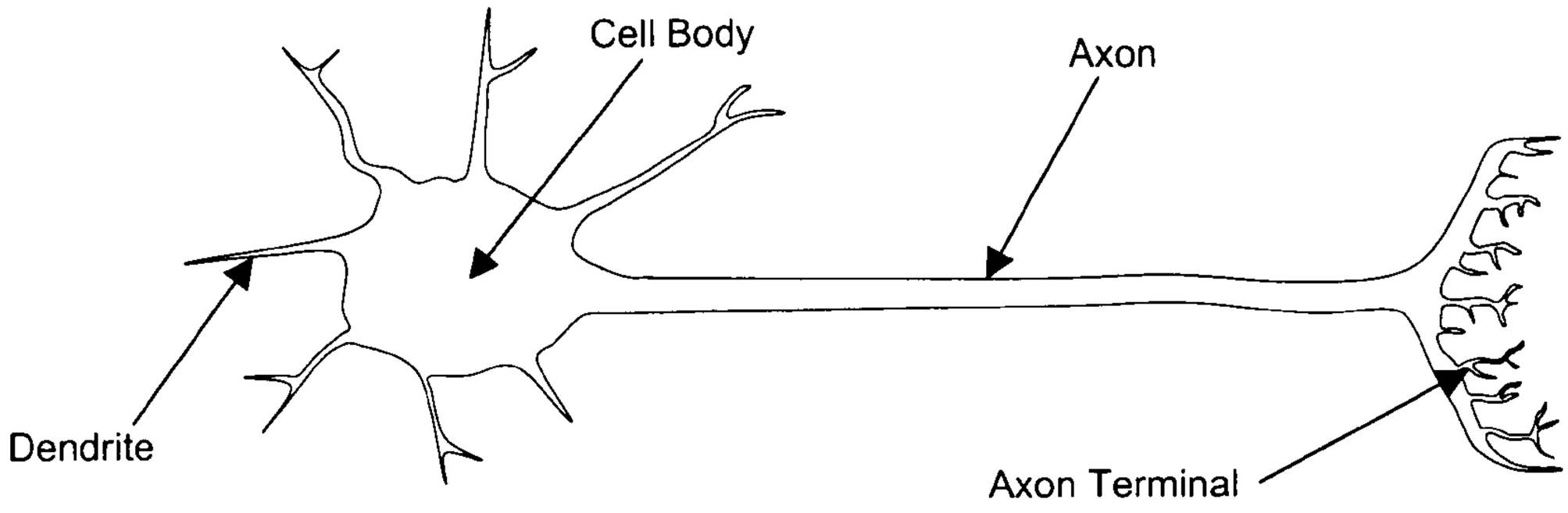

Figure 1.1 Structure of a typical neuron

The axon, or nerve fibre, is a much longer outgrowth from the cell body. Nerve fibres can be hundreds of millimetres in length, thus allowing the transfer of information over long distances within the body. Axons have an essentially cylindrical shape with a diameter in the range of 0.3-20 μm [4]. Many axons are partially covered by an insulating layer of myelin (Figure 1.2). The myelin sheath is formed when neighbouring cells wrap several times around the axon to create a layer of electrical insulation. The myelin layer is not uniform along the length of the axon and gaps in the insulating layer known as nodes of Ranvier occur at frequent intervals. The myelinated regions of the axon between nodes of Ranvier are known as internodes. The significance of myelin will be discussed in Section 1.1.3. A nerve is the collective name given to a group of nerve fibres and it is important to note the distinction between the terms 'nerve', 'nerve fibre' and 'neuron'.

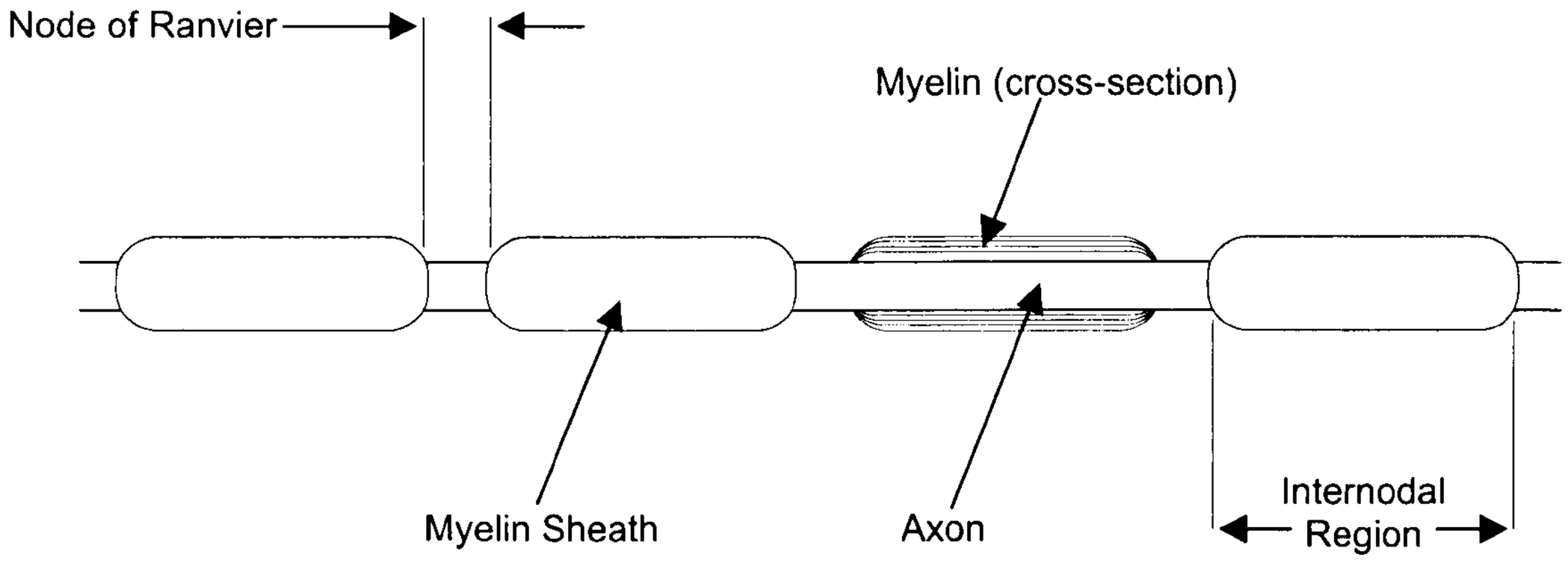

Figure 1.2 Schematic diagram of a myelinated axon

Axon terminals are a series of relatively short outgrowths at the end of the axon which are capable of releasing chemicals known as neurotransmitters. The axon terminals interface with the dendrites of other neurons via junctions known as synapses. A small gap, the synaptic cleft, exists between the axon terminal of one cell and the dendrite of another. Communication between neurons is achieved by the release of neurotransmitter into the synaptic cleft. A large number of neurons interconnected via synapses can be described as neural networks, which are the means of decision making and memory utilised by animals.

Like all animal cells, the nerve cell is enclosed by a cell membrane. This membrane separates the contents of the cell, particularly the intracellular fluid, from the extracellular fluid which surrounds the cell. The cell membrane acts as a selectively permeable barrier which regulates the internal composition of the cell, allowing the intracellular fluid to maintain a different composition to the extracellular fluid. This very important membrane property can be explained by

reference to the fluid-mosaic model of membrane structure shown in Figure 1.3 [1].

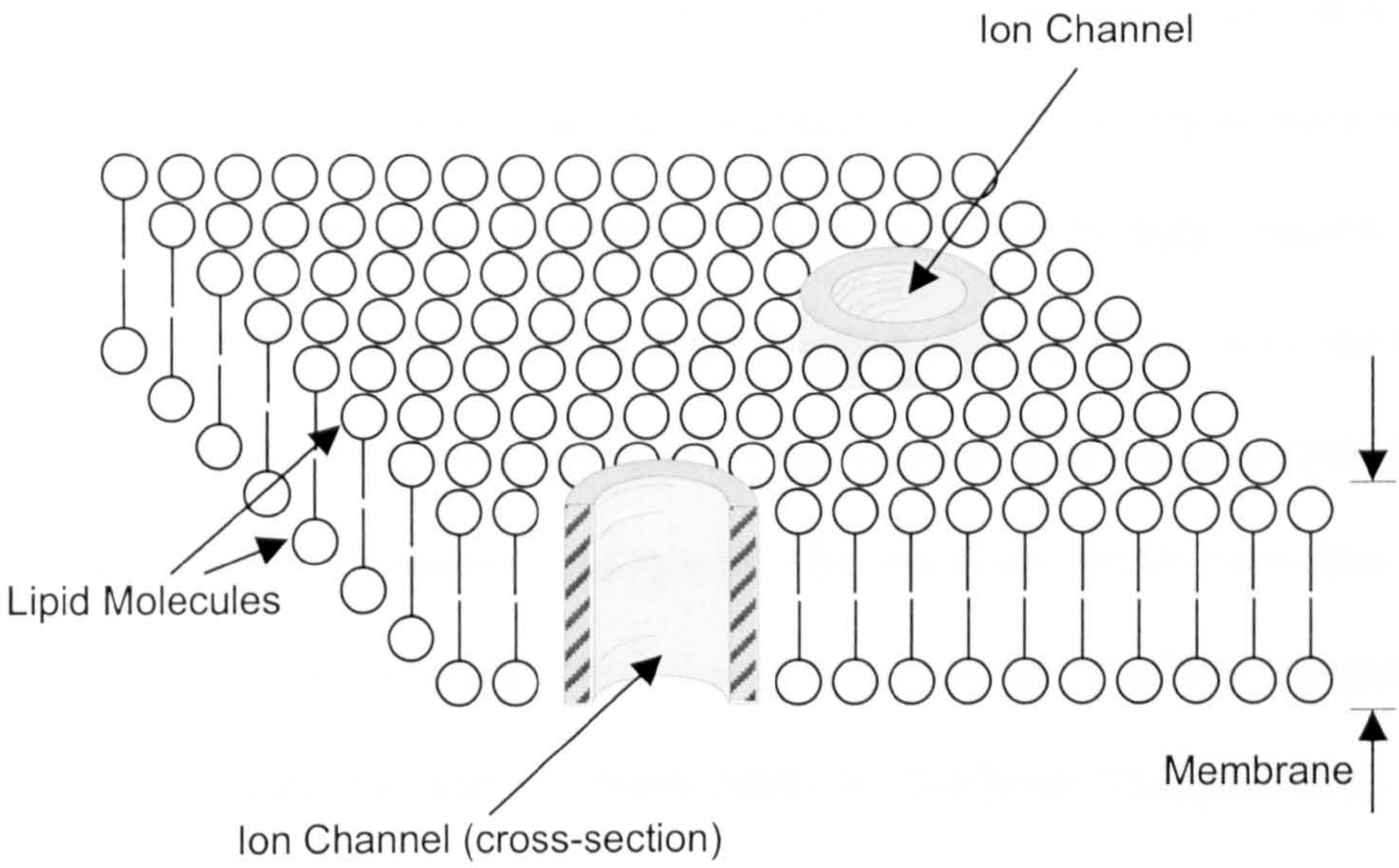

Figure 1.3 Fluid-mosaic model of membrane structure

The major part of the membrane's surface area is provided by a double layer (bilayer) of lipid molecules. An important property of all lipids is their insolubility in 'polar' solvents, such as water, whose molecules have no net charge but do have an uneven charge distribution. Similarly, polar molecules are insoluble in lipids as are ions, which are atoms or molecules with a net charge due to a surplus or deficit of electrons. However, nonpolar molecules are soluble in lipids. The intracellular and extracellular fluids contain a wide variety of solutes including: nonpolar molecules such as oxygen and carbon dioxide; polar molecules such as glucose; the ions of sodium, potassium and chlorine [1]. The nonpolar molecules, due to their solubility in the lipid membrane, can easily pass between the intracellular fluid and the extracellular fluid. Polar molecules

and ions are insoluble in the membrane and thus the membrane retains these solutes on one side of the membrane.

Despite their insolubility in the cell membrane, ions can traverse the membrane by passing through ion channels. Ion channels are formed by protein molecules which span the membrane to form a small aperture through which ions can pass. Ion channels often exhibit a high degree of specificity and only conduct one preferred species of ion. This specificity results from the diameter of the ion channel and from the electric charge on the proteins which form the channel. For example, sodium-specific channels are too small to allow the passage of larger ions whereas chloride channels repel all positively charged ions.

Some ion channels may exist in either an 'open' or 'closed' state, with this so-called channel gating occurring via changes to the shape of the channel proteins. In the closed state, the ion channel becomes impermeable to the passage of ions. Several factors can affect the gating of an ion channel. For example, the permeability of a voltage-gated channel is determined by the potential difference across the membrane. Application of a potential difference across a voltage-gated channel exerts a force on charged groups within the ion channel protein, causing the shape of the channel to distort and block the passage of ions.

1.1.2. Resting Potential of Neurons

It has been stated that the properties of the cell membrane allow the cell to maintain different intracellular and extracellular fluid compositions. Several ions are present in these fluids, including sodium (Na^+), potassium (K^+), calcium (Ca^{2+}), magnesium (Mg^{2+}), chloride (Cl^-) and bicarbonate (HCO_3^-). Sodium, potassium and chloride are the most abundant ions and typical concentrations of these ions are presented in Table 1.1 [2, 5].

	Intracellular Concentration (mM)	Extracellular Concentration (mM)
Potassium ion (K^+)	141.0	4.2
Sodium ion (Na^+)	10.0	142.0
Chloride ion (Cl^-)	4.3	103.0

Table 1.1 Intracellular and extracellular ion concentrations

It can be seen that the intracellular fluid contains a relative surplus of potassium ions and a relative deficit of chloride and sodium ions with respect to the extracellular fluid. A potential difference exists across the membrane as a result of this separation of ions. To explain this concept, first consider a situation in which the cell membrane is only permeable to potassium ions. Since there is an unequal concentration of potassium ions across the membrane, the potassium ions will diffuse down their concentration gradient, leaving the cell via ion channels in the cell membrane. However, this movement of ions creates a potential difference due to the separation of charge and leaves the intracellular

region with a slight negative charge. This potential difference attracts the positively charged potassium ions back into the cell.

This process of potassium ions leaving the cell due to a concentration gradient and entering the cell due to a potential difference occurs until a point is reached at which there is no net flow of ions across the membrane. The potential difference across the cell membrane when there is no potassium ion flux is known as the equilibrium potential (or Nernst potential) for potassium ions. The Nernst equation can be used to calculate the equilibrium potential, V_{eq}, for a particular ion of valence z with intracellular and extracellular concentrations of $[C]_i$ and $[C]_o$ respectively, at temperature T [1]:

$$V_{eq} = \frac{RT}{zF} ln \frac{[C]_o}{[C]_i} \tag{1.1}$$

Using the concentrations in Table 1.1, the equilibrium potential for potassium ions at body temperature (37°C) is –93.9 mV. A negative equilibrium potential signifies that the intracellular region is negative with respect to the extracellular fluid, which is assumed to be at zero potential. The same reasoning can be applied to sodium ions by assuming a membrane permeable only to sodium, for which the equilibrium potential can be calculated as +70.9 mV. A positive equilibrium potential signifies that the intracellular region is positive with respect to the extracellular region.

The membrane of a neuron is permeable to both sodium and potassium ions but with a much greater permeability to potassium ions than to sodium ions.

Therefore, potassium ions have a greater influence on the membrane potential than sodium ions. Hence the resting potential of the membrane, the potential at which there is no net movement of ions across the membrane, has a similar value to the potassium equilibrium potential. The exact value of the cell's resting potential can be calculated with the Goldman equation [1]:

$$V_r = \frac{RT}{F} ln \frac{P_k \cdot [K]_o + P_{Na} \cdot [Na]_o}{P_k \cdot [K]_i + P_{Na} \cdot [Na]_i} \quad (1.2)$$

Using the concentrations above, a sodium permeability constant (P_{Na}) of 1.78 x 10^{-9} cm s^{-1} and a potassium permeability constant (P_K) of 148 x 10^{-9} cm s^{-1} [5, 6], the resting potential is calculated as -84.8 mV. Since this resting potential is not at the equilibrium potential for either sodium or potassium ions, a net efflux of potassium ions and a net influx of sodium ions would be expected due to the concentration gradient across the cell, causing the membrane potential to decay towards zero. This situation is prevented by ion pumps (Na,K-ATPase pumps) which maintain the concentration gradients by actively transporting potassium ions into the cell whilst transporting sodium ions out of the neuron. Hence the concentration gradients and the resulting membrane potential can be maintained indefinitely.

Table 1.1 shows that there is a significant concentration of chloride ions in the extracellular fluid. In fact, these chloride ions have no effect on the resting potential of the neuron. This is because neurons have no chloride pumps and so the chloride concentration gradient is free to adjust until the equilibrium potential for chloride ions is equal to the neuron's resting potential. Since the

majority of chloride ions are in the extracellular fluid this suggests that they are not responsible for the neuron's net negative charge. The negative charge is largely created by a high intracellular concentration of negatively charged molecules such as proteins, which are unable to cross the membrane and thus create an intracellular surplus of negative charge.

1.1.3. Electrical Properties of Neurons

Certain factors can influence the potential difference between the intracellular and extracellular regions of the nerve cell and this property of neurons is utilised whenever a neuron transmits information. Long range communication is achieved by a voltage pulse, known as an action potential, which is transmitted along the axon.

Figure 1.4 shows the variations in membrane potential that occur during a typical action potential. Initially the membrane is at rest and the membrane potential is equal to the neuron's resting potential of approximately –85 mV. Since there is a potential difference and a separation of charge across the membrane, the membrane is described as polarised. At approximately 0.2 milliseconds, the membrane potential rapidly increases towards zero. The degree of charge separation across the membrane decreases, therefore this process is called depolarisation. For large nerve fibres, overshoot occurs and membrane potential becomes greater than zero due to a net intracellular surplus of positive charge. The phenomenon of overshoot does not occur in smaller neurons. At around 0.3 milliseconds, the membrane begins to repolarise and the membrane potential decreases towards its initial resting potential. The process of repolarisation is slower than depolarisation and the entire duration of the action potential is generally a few tenths of a millisecond.

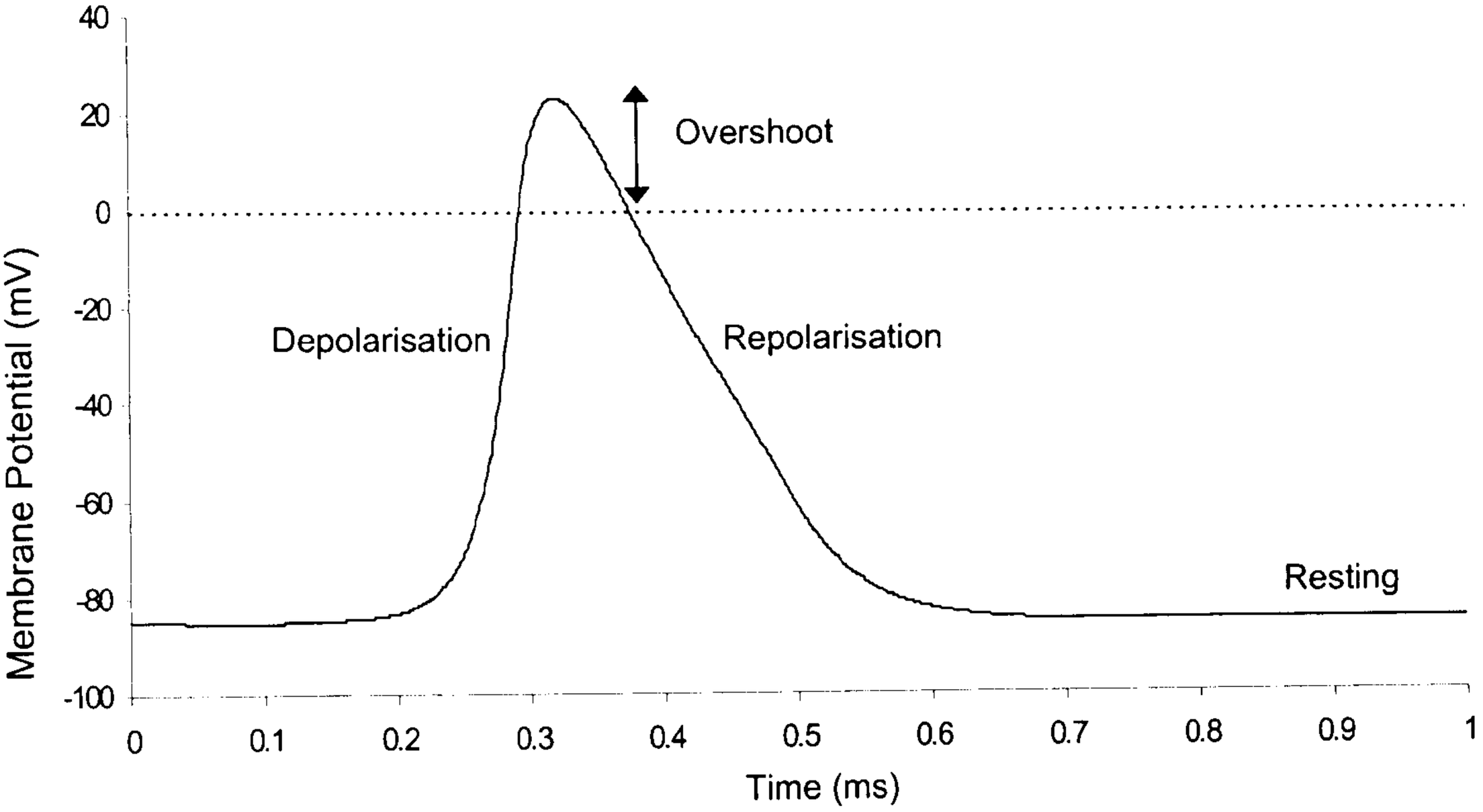

Figure 1.4 A typical action potential

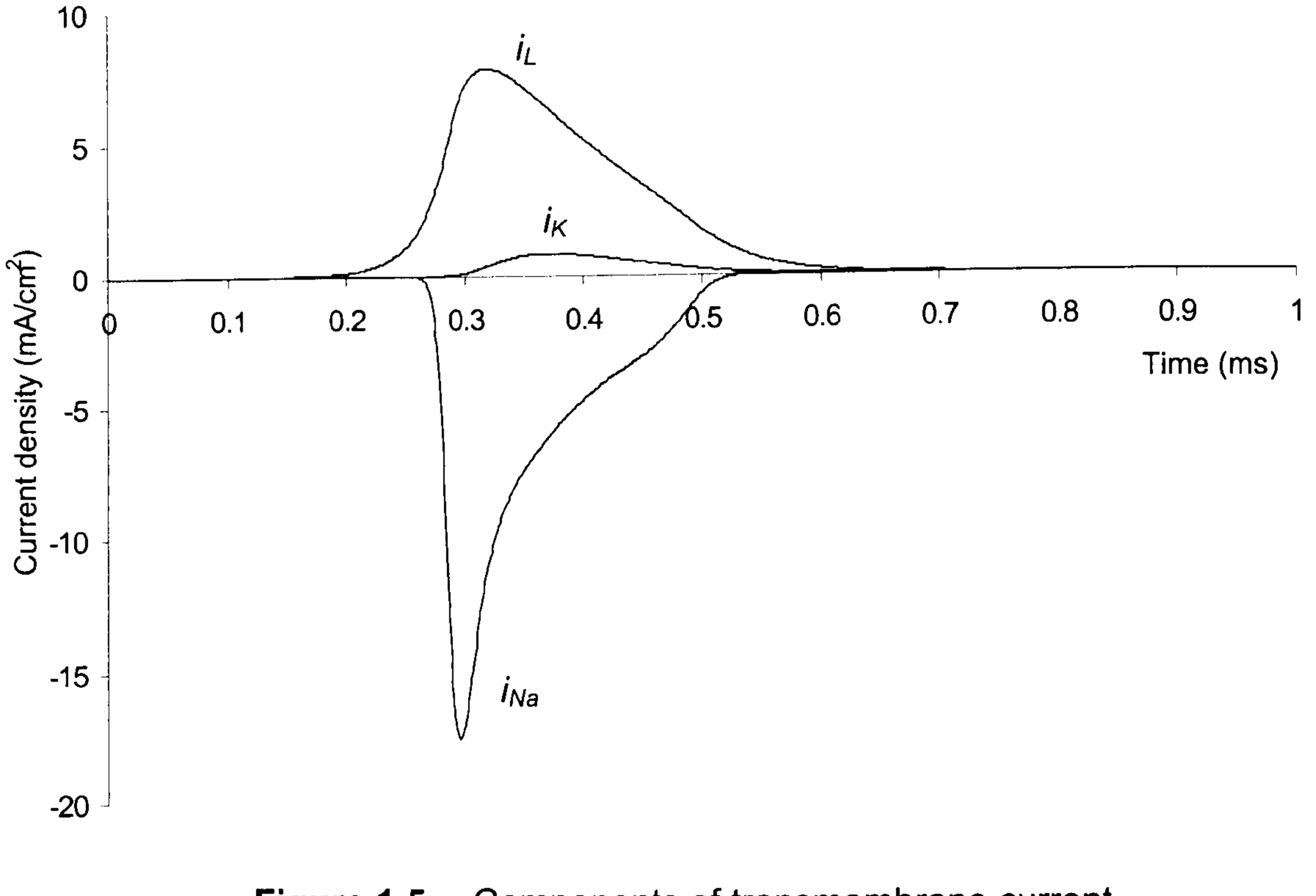

Figure 1.5 Components of transmembrane current

Action potentials result from rapid changes to the ionic permeabilities of the cell membrane. Membranes which are capable of generating action potentials are said to be excitable. Two varieties of voltage-gated ion channels are involved, voltage-gated sodium channels and voltage-gated potassium channels. When the membrane is at rest, both types of voltage-gated channel are in the 'closed' state and are impermeable to sodium and potassium ions. In addition to the voltage-gated channels, leakage channels are present which exist permanently in the 'open' state and are insensitive to voltage changes. Three components are involved in the generation of an action potential (Figure 1.5):

1. Sodium current, i_{Na} – A sufficiently large depolarisation of the membrane will cause the activation or opening of voltage-gated sodium channels. Activation of sodium channels increases the membrane's permeability to sodium ions, allowing extracellular sodium ions to diffuse down their concentration gradient into the neuron. This influx of positive charge reduces the potential difference across the nerve cell membrane, which results in further activation of voltage-gated sodium channels and an increased influx of sodium ions. This positive feedback cycle is summarised in Figure 1.6.

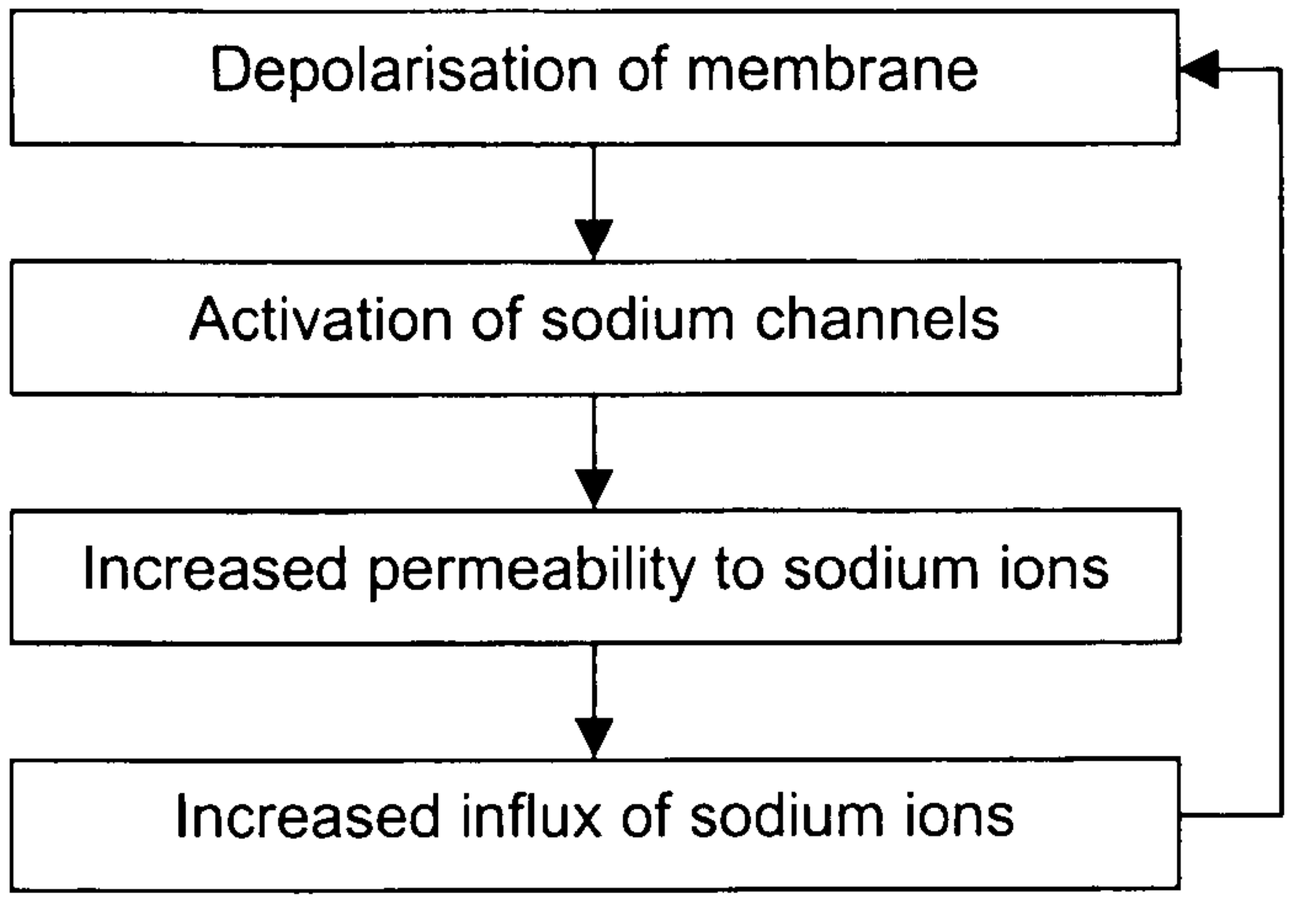

Figure 1.6 Positive feedback cycle for sodium ion permeability

The feedback cycle causes a rapid flow of sodium ions into the membrane which is represented by the sodium current, i_{Na}, plot in Figure 1.5. i_{Na} is given a negative magnitude because the flow of current (and hence positive ions) out of the membrane is considered to be the positive direction. Depolarisation of the membrane due to the influx of sodium ions continues until a membrane potential is reached at which the voltage-gated sodium channels begin to close and become deactivated. Deactivation of the sodium channels causes the membrane's permeability to sodium ions to decrease rapidly, which can be seen from the rapid decay of i_{Na}. The net effect of the activation and deactivation of sodium channels is to significantly depolarise the membrane, or even cause the overshoot seen in Figure 1.4.

2. Potassium current, i_K – Depolarisation of the cell membrane also causes activation of voltage-gated potassium channels. Activation of potassium channels increases the permeability of the membrane to potassium ions, allowing potassium ions to diffuse out of the cell. This efflux of potassium ions,

represented by the potassium current, i_K, in Figure 1.5 opposes the sodium current and serves to repolarise the cell. However, activation of potassium channels takes significantly more time than the activation of sodium channels, which can be seen by the relative timing of the peaks of i_K and i_{Na} in Figure 1.4. The slight delay in the onset of potassium channel activation allows the sodium current to achieve depolarisation of the membrane before the repolarisation process begins.

In non-mammalian nerve fibres the action potential can be almost entirely accounted for by sodium and potassium currents through voltage-gated channels, as demonstrated for squid axons by Hodgkin and Huxley [7] and for frog axons by Frankenhaeuser and Huxley [8]. Horáckova *et al.* [9] observed during experiments on rat axons that the potassium current is relatively insignificant in mammalian nerve fibres. Chiu *et al.* [10] (and later Schwarz and Eikhof [6]) accounted for the lack of voltage-gated potassium channels and the reduced potassium current in mammalian axons by demonstrating the importance of a third transmembrane current component, the leakage current:

3. Leakage current, i_L – As previously mentioned, leakage channels exist which are not voltage-gated and have a fixed conductivity. When the membrane is at rest, there is no net flow of current through the leakage channels. However, when the membrane is depolarised by an action potential, there is a net flow of positive charge into the neuron through leakage channels. This leakage current, represented by i_L in Figure 1.5, flows as a result of the membrane's deviation from resting potential. Since the leakage current is produced by the change in

membrane potential, the shape of the i_L plot is similar to the shape of the action potential. Leakage channels are described as unspecific since they are permeable to a variety of ion species. In mammalian nerve fibres, the leakage current is significantly greater than the potassium current and is therefore mostly responsible for repolarisation of the neuron.

An action potential may be initiated in many ways. Synaptic input to the neuron via the dendrites, or the action of receptor cells on afferent neurons may cause sufficient depolarisation of the axon to elicit an action potential. Alternatively, electrodes placed within the neuron or extracellular fluid can be used to produce an action potential. In order to successfully initiate an action potential, the membrane must be depolarised to a threshold voltage. Any stimulus which does not generate an action potential is described as sub-threshold whereas stimuli with magnitudes greater than threshold are described as supra-threshold.

The duration of the depolarising stimulus is an important factor in determining whether threshold is achieved or not [3]. Threshold depolarisation of the nerve fibre may be achieved by intense stimuli of short duration, or by weaker stimuli of longer duration. However, some stimuli may have insufficient strength to initiate an action potential, even when applied for an infinite duration. The inverse relationship between the magnitude and duration of threshold stimuli is illustrated in the strength-duration curve of Figure 1.7.

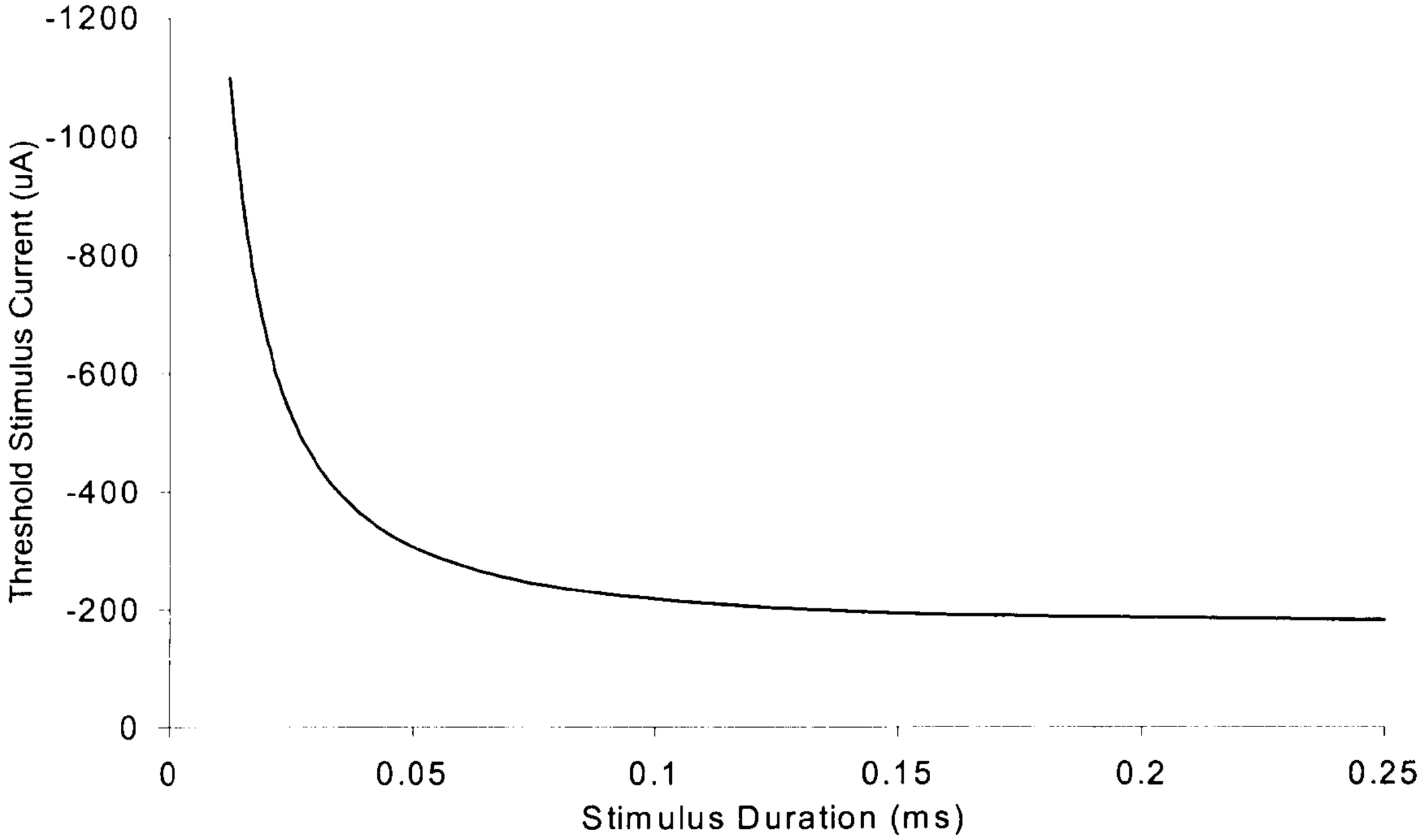

Figure 1.7 Strength-duration curve

In order to achieve long range communication via a nerve fibre, it is necessary for the action potential to propagate along the axon. The intracellular and extracellular fluids are electrolytes which act as reasonable conductors of electricity with resistivities of the order of 1 Ω m [5]. Their ability to conduct electricity arises from the presence of free ions in an aqueous solution, which act as the charge carriers when a voltage is applied. When an area of the membrane depolarises whilst generating an action potential, the potential difference between the depolarised area and adjacent regions of resting membrane causes current to flow through the intracellular fluid of the axon (the axoplasm). This localised current flow causes the depolarisation of adjacent regions of resting membrane, which will generate an action potential if depolarised to threshold. Therefore, the action potential propagates via the spread of depolarisation along the length of the axon.

An unmyelinated axon is excitable along its entire length and all regions of an unmyelinated fibre generate the propagating action potential. For a myelinated axon, the insulating myelin layer prevents the flow of ions across the membrane. Therefore, the unmyelinated nodes of Ranvier are the only regions of a myelinated axon to generate an action potential during propagation. This method of propagation, saltatory conduction, serves to increase the speed of propagation of action potentials since the presence of myelin prevents the flow of ions across the membrane and thus minimises charge loss from the axon. This allows a larger current to flow along the length of the axon which facilitates depolarisation at the node of Ranvier and permits the spread of depolarisation along the fibre to proceed at a greater speed. Additionally, since there is a reduced flow of ions across the cell membrane, less metabolic energy is expended by the sodium-potassium pumps in restoring and maintaining ionic concentration gradients. Conduction velocities for unmyelinated fibres are typically around 1 m s^{-1} and of the order of 10 m s^{-1} for myelinated axons [2, 3].

Following the generation of an action potential, the neuron experiences a period of reduced excitability known as the refractory period. The refractory period can be divided into two consecutive time intervals, known as the absolute and relative refractory periods. During the absolute refractory period, the neuron is unable to generate an action potential even when a large stimulus is applied. The absolute refractory period arises because voltage-gated sodium channels remain in an inactivated state for a short time after the membrane has returned to its resting potential, preventing the influx of sodium required to initiate an action potential. Typically around 0.4 ms [2], the absolute refractory period

places a fundamental limit upon the maximum rate of action potential generation. The relative refractory period follows the absolute refractory period and is the period of time during which an increased stimulus strength is required to generate an action potential. The relative refractory period occurs because some sodium channels are still inactivated whilst the potassium channels remain activated following repolarisation, thus impeding the net influx of positive charge required to cause threshold depolarisation. The duration of the relative refractory period is approximately four times that of the absolute refractory period [11, cited in 5].

The peak depolarisation achieved during an action potential is determined solely by ionic concentrations and the kinetics of membrane ion channels. The magnitude of all action potentials in any given nerve fibre is constant, regardless of the magnitudes of the stimuli which created them. This concept is known as the all-or-nothing principle. Therefore, the nerve is unable to communicate information regarding the magnitude of a stimulus through variations in the magnitude of the resulting action potential. Instead, stimulus strength is encoded by the frequency of a series of action potentials. If a supra-threshold depolarising stimulus is maintained following the generation of an action potential, further action potentials will be generated until the stimulus is removed. Since large stimuli can generate these repeated action potentials earlier in the relative refractory period than smaller stimuli, the interval between action potentials will be shorter for large stimuli than for small stimuli. Hence, large stimuli are represented by a high frequency series of action potentials, while smaller stimuli are represented by a lower frequency sequence of action

potentials. The number of action potentials generated is determined by both the magnitude and the duration of the depolarising stimulus.

1.2. Anaesthesia

Anaesthesia is a reversible state of reduced perception, in particular the perception of painful stimuli. Anaesthesia is induced by the administration of drugs and is commonly used to prevent physical discomfort to patients during surgical procedures. There are two classes of anaesthetic drugs, local anaesthetics and general anaesthetics, which differ in their effects and method of action.

Local anaesthetics act by preventing the propagation of action potentials in the peripheral nervous system [12, 13, 14]. Topical local anaesthetics are administered by application to areas on the surface of the body, such as the skin or mucous membranes. More commonly, a local anaesthetic drug is injected into the body in the vicinity of the target nerve, from where it diffuses into individual nerve fibres. Once inside the nerve fibre, the anaesthetic agent blocks sodium channels, either by binding with receptors in the channel or by physically blocking the pore. By blocking sodium channels, the influx of sodium ions necessary to depolarise the nerve fibre is prevented and the nerve fibre is unable to conduct action potentials. If the local anaesthetic drug acts upon a sensory nerve, the nerve is unable to communicate information to the brain which results in a reduced perception of stimuli.

In contrast, general anaesthetic drugs act upon the central nervous system [14]. General anaesthetics prevent the perception of stimuli by depressing brain function and inducing unconsciousness in the patient. However, the precise

method of action of general anaesthetic agents is not fully understood. General anaesthetic drugs may be administered via an intravenous injection or may be inhaled in a gaseous form.

Anaesthetic drugs have traditionally presented a significant risk to patients, with children and the elderly being most at risk from the undesirable side-effects of these drugs [14, 15]. General and local anaesthetics both carry the risk of inducing allergic reactions in patients. The administration of an injected local anaesthetic is often uncomfortable and large doses may cause injury. Local anaesthetic drugs also diffuse into the central nervous system, where they may cause undesirable side-effects including drowsiness, convulsions or cardiovascular effects. General anaesthetics are potentially hazardous since they depress brain function and can prevent important protective reflex actions. Depression of respiratory function and cardiac dysrhythmia are possible side-effects of some general anaesthetic drugs. Additionally, it takes considerable time for patients to recover from the effects of general anaesthesia and its use is often precluded in patients who are intoxicated, are taking other medicines or have recently eaten.

Due to the shortcomings and dangers of traditional anaesthetics, it is desirable to discover a non-invasive method of inducing anaesthesia in patients without the need for drugs. An ideal non-invasive anaesthetic technique would be safer than anaesthetic drugs and could be operated by unskilled staff. In contrast to anaesthetic drugs, an ideal method of non-invasive anaesthesia would provide an instant effect and have a short recovery time. By removing the need for a

skilled anaesthetist and minimising the time taken for patients to recover from the effects of anaesthesia, non-invasive anaesthesia could minimise the cost of minor surgery.

1.3. The Effects of Magnetic Fields on Biological Systems

The possible harmful effects on human health caused by exposure to electromagnetic fields is a topic which has recently been the subject of much media attention and public concern. Low frequency electric and magnetic fields, particularly those produced by power transmission lines, and radio frequency electromagnetic radiation, as generated by mobile telecommunications devices, have all been subject to scrutiny. There is a growing body of evidence which suggests that electromagnetic fields may have a diverse range of effects upon biological organisms, including an increased likelihood of cancer, neurological effects, and abnormal growth rate. This evidence is summarised in the review article by Azanza and del Moral [16] and in the EMF Working Group Report published by the National Institute of Environmental Health Sciences (part of the United States National Institutes of Health) [17].

The research in this thesis is focused upon the effects of magnetic fields on nerve function. Previous studies of the influence of magnetic fields on nerve function can be broadly divided into two categories: those that study the effects of static magnetic fields and studies of the effects of time-varying fields. The effects of static magnetic fields on nerve conduction are of particular relevance to this research.

1.3.1. Effects of Static Magnetic Fields on Nerve Function

Research into the influence of static magnetic fields on nerve function can be divided into three categories: theoretical studies, usually based upon a consideration of microscopic phenomena such as membrane structure or the motion of charge carriers in a magnetic field; laboratory studies of the effect of an applied magnetic field on the properties of nerves or isolated neurons, either *in vitro* or *in vivo*; or *in vivo* clinical studies, in which the ability of magnetism to produce pain relief is assessed. Laboratory studies generally examine well-defined and directly measurable properties of a single nerve or nerve fibre. In contrast, the results of clinical studies are based upon loosely defined criteria, such as a patient's perception of his/her pain. Furthermore, the biological system under consideration in clinical studies is vastly more complex, since any study which attempts to measure perception and sensation is indirectly influenced by the central nervous system.

1.3.1.1 *Theoretical Effects*

Several years before the effect of magnetic fields on nerve function became a popular field of research, Labes published a hypothetical mechanism of interaction between magnetic fields and biological systems [18]. The scope of Labes' article was not limited solely to the effects of magnetism on nerve fibres, but has been frequently cited by researchers to explain magnetically induced variations in nerve function. Labes noted research which had demonstrated that liquid crystals could be oriented by an applied magnetic field and reports that liquid crystalline material had been discovered in biological systems. He suggested that these biological liquid crystals may be oriented by the presence of a magnetic field, causing a change in the properties of the biological system. Labes hypothesised that by this mechanism an applied magnetic field of at least 0.1 T may effect charge transport, mass transport and reaction rate within an organism.

Liboff considered two theoretical methods by which an action potential in a nerve fibre may be affected by an applied magnetic field [19]. The first mechanism considered by Liboff was the Hall effect. The Hall effect describes the phenomenon where a voltage, the Hall voltage, is produced by a change in the direction of charge carrier motion under an applied magnetic field. Liboff estimated that a magnetic field of approximately 2.5×10^3 tesla would be required for the Hall voltage to be 1% of the amplitude of an action potential. Clearly, generation of such a strong magnetic field is not currently possible and it is doubtful that the small Hall voltage produced by a 2.5 kT field would have a

significant effect upon nerve function. Liboff also examined the inductive effect of a static magnetic field on current flow during the propagation of action potentials. He concluded that significant inductive effects would only occur if the distribution of current flow was considerably non-uniform over the circumference of the nerve fibre. Liboff calculated that an applied flux density of 0.26 T would result in a significant distortion to a perfectly asymmetric current flow, but much larger fields would be necessary to affect a realistic flow of current with a greater degree of symmetry.

Wikswo and Barach considered the possible effects of a distortion of ionic currents caused by the Lorentz force in the presence of a magnetic field [20]. They calculated that a 24 T applied magnetic field would result in a 10% deflection of ions, for typical nerve fibre parameters. However, this magnetic field estimate must be treated with caution because the researchers did not explain a mechanism by which this distortion in ion motion would cause a physiological effect. Wikswo and Barach's requirement of a 10% deflection of ion motion is highly arbitrary, therefore the magnetic field necessary to cause a measurable change in nerve function may differ considerably from their estimate of 24 tesla.

These theoretical considerations show a large variation in the estimates of magnetic field required to influence nerve cells. Labes suggested that significant physiological effects may occur in the presence of a relatively weak 0.1 T field, Wikswo and Barach estimate that 24 T may be necessary to affect nerve function, while Liboff considered that a field of at least 2.5 kT would be required

to influence the nerve via the Hall effect. The real merit of these theoretical estimates is to assist with the explanation of the experimentally observed effects of magnetism on nerve function.

1.3.1.2 Laboratory Studies

The earliest known investigation into the effect of magnetic fields on nerve function was reported in 1879 by McKendrick, who placed a frog's leg onto the insulated poles of a horseshoe electromagnet [21]. McKendrick observed that contraction of the muscles of the frog's leg, elicited by touching the sciatic nerve with copper wire, occurred normally when the axis of the nerve was perpendicular to the direction of the magnetic field. However, the excitability of the nerve was reduced when it was aligned parallel to the magnetic field and muscle contraction failed to occur as a result of nerve stimulation.

Schwarz performed several *in vitro* experiments upon lobster nerve in an applied field of 1.2 T. In his first set of experiments, Schwarz aligned the magnetic field in either a parallel or perpendicular direction with respect to the nerve [22]. The nerve was exposed to the magnetic field for a period of 20 to 30 minutes. Schwarz measured the conduction velocity of the compound action potentials which are produced by the summation of the individual action potentials in each of the many nerve fibres that constitute the nerve. He reported that the magnetic field had no significant effect upon the conduction velocity of compound action potentials. Schwarz compared his results to those of a similar study by Reno [23, cited in 22] in which a 1.16 T field had significantly reduced the conduction velocity of frog nerve. Schwarz suggested that his experiments may have failed to reproduce Reno's results due to inadequate temperature regulation, inhomogeneity of the applied magnetic field or because of structural differences between frog and lobster nerves.

In a second series of experiments, Schwarz performed voltage clamp experiments on a lobster giant axon [24]. As with the first set of experiments, the magnetic field was applied in two directions, either parallel or perpendicular to the nerve fibre. Neuron resting potential, action potential amplitude and membrane current during action potentials were found to be unaffected by the presence of the magnetic field.

Edelman *et al.* measured the amplitude of the compound action potential of frog nerves under an applied static magnetic field [25]. The researchers measured no change in compound action potential amplitude when magnetic fields with flux densities in the 0.1-0.7 T range were applied in a direction parallel to the nerve. However, Edelman *et al.* observed that the amplitude of compound action potentials slowly increased after 15-20 minutes of exposure to a similar magnetic field applied in a perpendicular direction. The compound action potential reached a stable maximum value after 45-60 minutes of exposure to the magnetic field. When the magnetic field was removed, the amplitude of compound action potentials gradually decreased but did not reach its original amplitude. One suggested explanation of this phenomenon was a decrease in the resistance of the fibres, causing an increased sodium current and resulting in more nerve fibres contributing to the compound action potential. Alternatively, Edelman *et al.* hypothesised that the threshold potential of the nerve fibres was reduced by exposure to the magnetic field, again resulting in an increased number of fibres contributing to the compound action potential.

Gaffey and Tenforde also conducted *in vitro* experiments on frog nerves [26]. In their first set of experiments they exposed the frog nerves to a 2.0 T magnetic field, aligned in either a parallel or perpendicular direction with respect to the nerve, for a four hour period. The researchers measured no significant effects upon the amplitude or conduction velocity of compound action potentials in the nerve. Additionally, they observed no change in the absolute or relative refractory periods of the nerve. In a second set of experiments, the excitation threshold of the frog nerve was found to be unaffected by exposure to a 1.0 T magnetic field aligned perpendicular to the axis of the nerve. Gaffey and Tenforde suggested that the effects of a static magnetic field on nerve function reported by Reno [23] and Edelman *et al.* [25] were experimental artefacts caused by inadequate temperature regulation.

Hong *et al.* observed the *in vivo* effects of static magnetic fields on rat nerves [27]. In this study, the researchers electrically stimulated the tail nerve of anaesthetised rats and measured the resulting compound muscle action potential (CMAP). Muscle fibres exhibit electrical excitability and, like nerve fibres, are able to produce action potentials. The CMAP results from the summation of action potentials produced by a number of individual fibres within the muscle. Analysis of the CMAP gives an indication of the properties of the nerve that innervates the muscle. In the first of their experiments, Hong *et al.* exposed rat's tails to magnetic fields of up to 1.2 T for 60 seconds. They measured no significant variations in amplitude of the CMAP or of the latency of onset of the CMAP resulting from exposure to the magnetic field. In a second experiment, the researchers applied submaximal stimuli to the tail nerve in

order to produce submaximal compound muscle action potentials. The tail nerve was exposed to magnetic fields of up to 1.2 T for 30 or 60 seconds. Hong *et al.* observed a significant increase in amplitude of the CMAP when the nerve was exposed to fields greater than 0.5 T for periods longer than 30 seconds. This infers that the excitability of the rat nerve was increased by exposure to a magnetic field.

Hong *et al.* explained the increased excitability of the nerve by reference to an earlier paper by Labes [18] in which it was suggested that molecules in biological membranes may be oriented in the presence of a magnetic field. This rotation is suggested to occur because the molecules possess diamagnetic anisotropy, which causes them to align with an applied magnetic field. Hong *et al.* speculated that rotation of the molecules causes an increase in membrane permeability and thus an increase in the excitability of nerve fibres.

Hong also performed a similar series of *in vivo* experiments upon human nerves [28]. He exposed human forearms and legs to 1 tesla magnetic fields for 15 seconds. Hong reported that the conduction velocity of action potentials was unaffected by exposure to the magnetic field. However, Hong observed a significant increase in the excitability of human nerves, indicated by an increase in the amplitude of submaximally evoked compound muscle action potentials. This supports the results of Hong *et al.*'s experiments on rat nerves [27]. As before, Hong suggested that the increase in nerve excitability resulted from the alignment of magnetically anisotropic molecules in nerve fibre membranes.

Azanza and del Moral published several papers on the effects of magnetism on snail neurons *in vitro*. They applied static magnetic fields of 0.116 and 0.26 T to snail nerve cells, and observed that exposure to the field hyperpolarised the membranes of the majority (86%) of neurons [29]. The excitability of these neurons was inhibited as a result of this membrane hyperpolarisation. However, a significant minority (14%) of neurons were excited by exposure to the magnetic field. No neurons were reported to be unaffected by the magnetism.

The researchers attributed the effects of the magnetic field to an increase in the concentration of free calcium ions in the intracellular fluid. The increase in intracellular calcium ion concentration activates Ca^{2+}-dependent-K^{+}-channels, allowing an influx of potassium ions which results in hyperpolarisation and inhibition of the nerve cell. Azanza and del Moral accounted for the excitation of some neurons by suggesting the magnetic field also causes in increase in the extracellular concentration of free calcium ions. These calcium ions then diffuse into the cell through nonspecific channels, causing depolarisation of the membrane and subsequent excitation of the neuron. A similar study by Azanza confirmed the results of the previous experiment [30].

Del Moral and Azanza proposed a model to explain the increase in intracellular calcium ion concentration caused by the exposure of neurons to a static magnetic field [31]. Using similar reasoning to that of Labes [18], they hypothesised that the lipid molecules that compose the neuron membrane are diamagnetically anisotropic. In a process they describe as 'cooperative superdiamagnetism', clusters of membrane lipids rotate in order to align themselves with an applied magnetic field. As a result of the physical motion of

lipid molecules, calcium ions bound to the lipid molecules experience increased electrostatic repulsive forces due to a reduced distance of separation from their nearest neighbours. If the repulsive forces are sufficiently large, calcium ions may be released into the intra- or extracellular solution from their binding sites on the lipids. The extracellular calcium ions can then diffuse into the nerve cell, further increasing the intracellular calcium concentration. Del Moral and Azanza estimated that a field of the order of 1.4 T is required to cause such an effect, a flux density comparable to the 0.26 T used in their experiments.

In another experiment by Azanza and del Moral, the frequency of action potentials in spontaneously firing snail neurons *in* vitro was recorded as the magnetic field was increased in the range 0.003-0.72 T [32]. They observed that an increase in the applied magnetic flux density resulted in a decrease in the firing frequency of the neurons. At a threshold of 0.57 T, spontaneous firing of the nerve cell ceased. The researchers considered that these observations were consistent with their model of increased intracellular calcium ion concentration in the presence of a magnetic field [31].

A further study of snail neurons *in vitro* by Azanza and del Moral involved measurement of the amplitude of action potentials as the flux density of an applied magnetic field was increased from 0-0.7 T [33]. Azanza and del Moral noted that the amplitude of the action potentials decreased as the applied flux density was increased over the course of the experiment. They explained this effect by suggesting that the Na,K-ATPase pump, which maintains the concentration gradients of sodium and potassium ions across the cell

membrane, has anisotropic diamagnetic properties. The researchers suggested that the Na,K-ATPase protein orientates under the magnetic field, in a similar way to their previous model of membrane lipid orientation [31]. Azanza and del Moral hypothesised that the efficiency of the protein in pumping sodium and potassium ions was reduced by the orientation, thus allowing the membrane concentration gradients to decrease over a period of time. The resulting equalisation of intra- and extracellular sodium ion concentrations caused the amplitude of action potential depolarisation, due to the influx of sodium ions, to decrease.

Balaban *et al.* also studied the effects of magnetic fields on the function of snail neurons *in vitro* [34]. The neurons were exposed to magnetic fields of 0.023, 0.12 or 0.2 T for 20 minute periods. In agreement with Azanza and del Moral [32], they observed a significant decrease in the firing frequency of spontaneously firing nerve cells. Furthermore, the input resistance of spontaneously firing neurons was found to be decreased by exposure to the magnetic field, while that of non-spontaneous neurons was found to increase. The researchers considered that the dependence of the change in input resistance on the type of neuron gave evidence of a genuine effect of the magnetic field. Balaban *et al.* reported that removing the perineuronal glia from the neurons removed the magnetic field's effect upon the input resistance of the neuron. Therefore, the researchers suggested that the mechanism by which the applied magnetic field influences nerve function is mediated by glial cells, although the precise mechanism of action was unknown.

Holcomb, McLean and colleagues performed a number of experiments upon cultured mouse sensory neurons *in vitro*. The researchers were testing the efficacy of a proprietary magnetic device, Magna Bloc, designed to provide pain relief by preventing the conduction of action potentials in nerve fibres [35]. This device consisted of four alternating magnetic poles with a maximum flux density of 10 mT. McLean *et al*. found that exposure to the magnetic device reversibly inhibited the propagation of action potentials in sensory neurons [36, 37]. The researchers also reported that a similar array of four alternating poles, but with much smaller physical dimensions and a flux density of 1 mT, induced a similar failure of action potentials. The resting potential and input resistance of the neurons were unaffected by the magnetic field. The effectiveness of these devices was found to reach a maximum after 200-250 seconds of exposure and nerve function returned to normal 400-600 seconds after the magnetic field was removed.

They compared the effectiveness of these devices to those of an array with four magnetic poles of the same polarity and 35 mT flux density; an array with two magnetic poles of alternating polarity and 28 mT peak flux density; and a single magnet of 88 mT flux density. McLean *et al.* reported that the array of four like poles reduced action potential propagation to a lesser extent than an array of four alternating poles, but the dipolar and monopolar arrays did not significantly reduce the firing of action potentials. The researchers concluded that the spatial gradient of the magnetic field, which was greatest for the arrays with four magnetic poles, was more important than the absolute value of the applied magnetic field [36, 37, 38].

McLean *et al.* suggested a number of possible explanations for the blockade of action potentials in an applied magnetic field, including conformational changes to voltage-gated sodium channels, a modulation of ion channel activity through changes to phosphorylation of the channels, altered lipoprotein interactions or the creation of interfering ionic flow patterns around the membrane [36, 37].

A summary of the results of experimental studies on the effects of static magnetic fields on nerve function is presented in Table 1.2. Although some research has concluded that magnetic fields have no observable influence on nerve cells, a considerable number of studies have presented convincing evidence to the contrary. A wide variety of effects on nerve function have been reported, occurring over a large range of applied magnetic flux densities from 1 millitesla to 2.0 tesla. Clearly, there is no consensus on the interaction between magnetic fields and the nervous system and this is an area worthy of further research.

Researcher	Biological System Studied	Applied Magnetic Flux Density (T)	Observed Effects
McKendrick, 1879, [21]	Frog nerve *in vitro*	Not specified	Reduced nerve excitability
Reno, 1969 [23]	Frog nerve *in vitro*	1.16	Reduced conduction velocity
Schwarz, 1978 [22]	Lobster nerve *in vitro*	1.2	No effects observed
Schwarz, 1979 [24]	Lobster giant axon *in vitro*	1.2	No effects observed
Edelman *et al.*, 1979 [25]	Frog nerve *in vitro*	0.1-0.7	Reduced amplitude of compound action potentials
Gaffey and Tenforde, 1983 [26]	Frog nerve *in vitro*	2.0	No effects observed
Hong *et al.*, 1986 [27]	Rat nerve *in vivo*	1.2	Increased nerve excitability
Hong, 1987 [28]	Human nerve *in vivo*	1.0	Increased nerve excitability
Azanza and del Moral, 1988 [29] Azanza, 1990 [30]	Snail neurons *in vitro*	0.116, 0.26	Majority of neurons hyperpolarised and excited; Remaining neurons inhibited
Balaban *et al.*, 1990 [34]	Snail neurons *in vitro*	0.023, 0.12, 0.2	Decrease in activity and input resistance of spontaneously firing neurons; Increase in input resistance of non-spontaneous neurons
McLean *et al.*, 1991 [36] McLean *et al.*, 1995 [37]	Mouse neurons *in vitro*	0.001 (quadrupolar array)	Blockade of action potentials
Azanza and del Moral, 1995 [32]	Snail neurons *in vitro*	0.57	Cessation of spontaneous activity
Azanza and del Moral, 1996 [33]	Snail neurons *in vitro*	0-0.7	Reduction in amplitude of action potentials

Table 1.2 Summary of laboratory studies of the effects of static magnetic fields on nerve function

1.3.1.3 *Clinical Studies*

One of the earliest clinical studies of the use of magnetism for pain relief was published by Hansen in 1938 [39]. Some of Hansen's experiments involved the application of a magnetic field directly to the site of the pain and show no direct evidence of an interaction between magnetism and the nervous system. However, patients suffering from sciatica reported pain relief when the poles of an electromagnet were moved along the course of the sciatic nerve and spinal column for a period of between two and fifteen minutes. Although the conditions of this trial were not carefully controlled, Hansen was convinced of the ability of magnetic fields to provide pain relief.

Possibly the most striking effect of an applied magnetic field on nerve function was reported by Becker in the autobiographical account of his career studying bioelectrical phenomena [40]. Becker exposed an entire salamander to a static magnetic field and measured its electroencephalogram (EEG) whilst increasing the applied flux density from zero to 0.3 tesla. In an applied magnetic field of 0.2 T, delta waves appeared in the EEG. Delta waves are low frequency, high amplitude fluctuations in brain activity which correspond to the deepest stages of sleep and are not normally measured during wakefulness [41]. Under an applied magnetic field of 0.3 T, the salamander's EEG was entirely composed of delta waves and the animal was reported to be "motionless and unresponsive to all stimuli." When the magnetic field was removed, the EEG returned to normal and the salamander quickly regained consciousness. Becker considered

this to be a discovery of "the best possible anaesthetic, allowing prompt recovery with no side effects."

Becker proposed that the magnetic field affected the salamander's nervous system by means of the Hall effect. Based on earlier research by Szent-Györgyi [42, cited in 40], Becker suggested that a semiconducting current exists in the nervous system in which charge is carried by the motion of electrons through long chains of protein molecules. Owing to their high mobility, these electrons experience a significant deflection in an applied magnetic field. Becker considered that deflection of the electrons stopped the semiconducting current, resulting in the loss of consciousness experienced by the salamander.

Despite the huge potential for clinical use of such a dramatic non-invasive anaesthetic effect, this experiment does not appear to have been published in any journals. Furthermore, no reports of independent research reproducing these experimental results were found in a literature search. Therefore, this report of a magnetically induced anaesthetic effect in salamanders must be viewed with some scepticism.

A randomised double-blind clinical trial by Vallbona *et al.* examined the use of a proprietary magnetic field device for pain relief [43]. The magnetic device, marketed as Bioflex magnets, consisted of permanent magnets with flux densities of 30 mT or 50 mT, arranged in concentric circles with alternating magnetic polarity. Vallbona *et al.* observed that application of the magnets over pain 'trigger-points' significantly reduced pain in patients suffering from

postpolio syndrome. The researchers could not explain the mechanism by which the magnetic field provided pain relief, but speculated that the effect may be due to a change in pain receptors, a change in the response of the central nervous system to pain perception or a release of enkephalins (neurotransmitters with an analgesic effect). Vallbona *et al.* did not comment on the possibility of a magnetic effect upon nerve excitability or the conduction of action potentials in afferent nerves.

Holcomb *et al.* [44] and Segal *et al.* [45] conducted clinical trials on the pain relieving ability of a different proprietary magnetic device, the Magna Bloc [35]. Magna Bloc is the quadrupolar magnetic device which was described in Section 1.3.1.2 and was demonstrated to reversibly reduce the propagation of action potentials by McLean *et al.* [36, 37]. In a randomised double-blind placebo-controlled crossover study, the magnetic field significantly reduced pain of the lower back and knee [44]. In a pilot study with no placebo control, Magna Bloc was found to significantly reduce arthritic pain of the knee [45].

Collacott *et al.* conducted a randomised double-blind, placebo-controlled crossover study on the effects of magnetism on low back pain [46]. The magnetic devices used in the study consisted of triangular magnetic poles of alternating polarity and 0.03 T flux density. The magnets were placed over the lower back for 6 hour periods over the course of 3 days. Collacott *et al.* reported that the magnets did not significantly reduce pain.

As in the laboratory experiments on the effects of static magnetic fields on isolated nerves and neurons, there is no consensus on the ability of magnetic fields to provide pain relief. However, there are sufficient reports of pain relief resulting from exposure to static magnetic fields to warrant further investigation.

1.3.2 Effects of Time-Varying Magnetic Fields on Nerve Function

The most popular area of research on the effects of time-varying magnetic fields on nerve function is the investigation of magnetic stimulation. Clinical practice of magnetic stimulation involves the use of a rapidly changing magnetic field to induce electric fields within the body. Faraday's law of electromagnetic induction [47] states that the electromotive force, E, induced in a conductor by a changing magnetic field is equal to the rate of change of magnetic flux, ϕ, with respect to time, t, i.e.:

$$E = -\frac{d\phi}{dt} \tag{1.3}$$

The electromagnets used in clinical magnetic stimulation typically generate a peak magnetic flux density of 2 tesla over a period of 100 microseconds [48]. The resulting induced electromotive force (EMF) causes ionic currents to flow within the body and action potentials are generated by nerve fibres if these currents are sufficient to cause a threshold depolarisation of nerve cell membranes. These nerves are said to be magnetically stimulated. The frequency of stimulating pulses ranges from 30 Hz to less than 1 Hz. The maximum stimulating frequency is limited by heating of the electromagnetic coil and the time taken to charge the large capacitors which are necessary to deliver large currents (~5 kA) through the coil.

The first research into the effects of induced currents in the nervous system appears to have been conducted by McKendrick in 1879 [21]. McKendrick used

an electromagnet to induce a current in a frog sciatic nerve *in vitro* and observed the contraction of the frog's leg muscles. Early observations were also made by d'Arsonval (in 1896) and Thompson (in 1910), who both reported visual disturbances when electromagnets were used to induce currents within the brain [49].

Research into the use of magnetic stimulation for clinical purposes was pioneered by Polson, Barker, Freeson and Jalinous, who published the first clinical results of stimulation of the peripheral [50] and central [51] nervous systems. Magnetic stimulation is commonly used as a painless, non-invasive tool for diagnostic purposes and for research into brain function [48]. Furthermore, there have been clinical studies of the use of magnetic stimulation for pain relief, which will be discussed in Section 1.3.2.1. The mechanism of magnetic stimulation is well understood and there is not the same quantity of conflicting experimental evidence as there is for the effects of static magnetic fields on the nervous system.

There are very few reports of the effects of time-varying magnetic fields on nerve function that are unrelated to the topic of magnetic stimulation. Ueno *et al.* studied the effects of magnetic fields in the 5 Hz – 20 kHz frequency range on lobster giant axons *in vitro* [52]. The researchers exposed the lobster nerve fibres to sinusoidal fields with flux densities of 0.1 – 1.2 T in directions either perpendicular or parallel to the axon for 5 second intervals. Ueno *et al.* reported that the refractory period of the nerve fibre and the amplitude, shape and conduction velocity of action potentials were unaffected by the magnetic field.

Azanza and del Moral observed the effects of a 50Hz sinusoidal field with flux density in the 1-15 mT range on snail neurons *in vitro* [53]. They reported that synchronous firing of action potentials was observed in some neurons when the applied flux density was approximately 7 mT. In a separate study, Azanza and Calvo examined the effect on snail neurons of varying the magnitude of an applied 50Hz magnetic field in the 1-15 mT range [54]. They reported that increasing the applied flux density caused either excitation or inhibition of the spontaneous activity of the neurons, with the response dependent upon the individual neuron being tested. In both experiments, it was suggested that this response was due to the activation of Ca^{2+}-dependent-K^{+}-channels, resulting from an increase in the intracellular concentration of calcium ions. The model to explain the release of calcium ions in an applied magnetic field was previously described in Section 1.3.1.2 and reference [31].

1.3.2.1 *Use of Magnetic Stimulation for Pain Relief*

Magnetic stimulation has gained popularity as a technique for diagnosis and research. There have also been clinical studies of the use of magnetic stimulation, either of the central or peripheral nervous systems, to provide pain relief. One such study is that conducted by Migita *et al.*, who reported the results of a trial of transcranial stimulation on two patients suffering from pain due to a central nervous system lesion [55]. The researchers observed that one patient received noticeable pain relief following exposure to 200 stimulating pulses (of unspecified frequency or magnitude), with the duration of this pain relief lasting for over an hour. In contrast, the second patient received no pain relief from magnetic stimulation.

Amassian *et al.* reported pain relief as a result of magnetic stimulation of the brain [56]. Muscle pain was induced by arresting circulation to the arms of five healthy volunteers. Ten stimulating pulses at 20 Hz were applied and four patients reported pain relief within a few seconds of stimulation. The pain recurred 30-35 seconds after stimulation had ceased. One patient did not experience pain relief.

In a larger clinical trial, Ellis investigated the analgesic effects of magnetic stimulation in ten patients suffering from chronic pain [57]. The site of the pain, rather than the brain, was stimulated with a 1.45 T field at a frequency of 10-45 Hz for a period of 10 minutes. A significant reduction in pain was reported, with pain relief lasting for 8-72 hours in most cases. Pain relief was experienced for

over four months by one patient. Ellis hypothesised that chronic pain was caused by the dysfunction of neural networks and that eddy currents produced by magnetic stimulation helped to restore their normal function.

1.4. References

1. Vander, A.J., Sherman, J.H. and Luciano, D.S.
   Human Physiology: The Mechanisms of Body Function, Sixth Edition.
   McGraw-Hill, 1994.
2. Guyton, A.C.
   Textbook of Medical Physiology, Sixth Edition.
   Saunders, 1981.
3. Aidley, D.J.
   The Physiology of Excitable Cells, Third Edition.
   Cambridge University Press, 1989, pp 48-53.
4. Reilly, J.P., Geddes, L.A. and Polk, C.
   Bioelectricity.
   (in The Electrical Engineering Handbook, Dorf, R.C. (Ed.))
   CRC Press, 1993, p. 2301-2341.
5. Frijns, J.H.M., Mooij, J. and ten Kate, J.H.
   A Quantitative Approach to Modelling Mammalian Myelinated Nerve Fibers for Electrical Prosthesis Design.
   IEEE Transactions on Biomedical Engineering, Vol. 41, 1994, pp. 556-566.
6. Schwarz, J.R. and Eikhof G.
   Na Currents and Action Potentials in Rat Myelinated Nerve Fibres at 20 and 37°C
   Pflügers Archiv, Vol. 409, 1987, pp. 569-577.
7. Hodgkin, A.L. and Huxley, A.F.
   A Quantitative Description of Membrane Current and its Application to Conduction and Excitation in Nerve.
   Journal of Physiology, Vol. 117, 1952, pp. 500-544.
8. Frankenhaeuser, B. and Huxley, A.F.
   The Action Potential in the Myelinated Nerve Fibre of *Xenopus Laevis* as Computed on the Basis of Voltage Clamp Data.
   Journal of Physiology, Vol. 171, 1964, pp. 302-315.

9. Horáckova, M., Nonner, W. and Stämpfli, R.
Action Potentials and Voltage Clamp Currents of Single Rat Ranvier Nodes.
Proceedings of the International Union of Physiological Sciences, Vol. 7, 1968, p. 198.

10. Chiu, S.Y., Ritchie, J.M., Rogart, R.B. and Stagg, D.
A Quantitative Description of Membrane Currents in Rabbit Myelinated Nerve.
Journal of Physiology, Vol. 292, 1979, pp. 149-166.

11. Paintal, A.S.
Conduction Properties of Normal Peripheral Mammalian Axons.
(in Physiology and Pathobiology of Axons, Waxman, S.G. (Ed.))
Raven Press, 1978, pp 131-144.

12. Tuckley, J.M.
The Pharmacology of Local Anaesthetic Agents.
Update in Anaesthesia, Issue 4, 1994.

13. Nogrady, T.
Medicinal Chemistry, Second Edition.
Oxford University Press, 1988.

14. Foster, R.W.
Basic Pharmacology, Third Edition.
Butterworth-Heinemann, 1991.

15. Ions, G.K.
A Device for Inducing Anaesthesia.
Patent Application PCT/GB98/01676, 1998.

16. Azanza, M.J. and del Moral, A.
Cell Membrane Biochemistry and Neurobiological Approach to Biomagnetism.
Progress in Neurobiology, Vol. 44, 1994, pp. 517-601.

17. Portier, C.J. and Wolfe, M.S. (Eds.)
Working Group Report - Assessment of Health Effects from Exposure to Power-Line Frequency Electric and Magnetic Fields.
National Institute of Environmental Health Sciences, NIH Publication No. 98-3981, 1998.

18. Labes, M.M.
A Possible Explanation for the Effect of Magnetic Fields on Biological Systems.
Nature, Vol. 211, 1966, p. 968

19. Liboff, R.L.
Neuromagnetic Thresholds.
Journal of Theoretical Biology, Vol. 83, 1980, pp. 427-436

20. Wikswo, J.P. and Barach, J.P.
An Estimate of the Steady Magnetic Field Strength Required to Influence Nerve Conduction.
IEEE Transactions on Biomedical Engineering, Vol. 27, 1980, pp. 722-623.

21. McKendrick, M.
Observations on the Influence of an Electromagnet on some of the Phenomena of a Nerve.
Journal of Anatomy, Vol. 13, 1879, pp. 218-223.

22. Schwarz, J.L.
Influence of a Constant Magnetic Field on Nervous Tissues: I. Nerve Conduction Velocity Studies.
IEEE Transactions on Biomedical Engineering, Vol. 25, 1978, pp. 467-473.

23. Reno, V.R.
Conduction Velocity in Nerve Exposed to a High Magnetic Field.
NASA Report NAMI-1089, 1969.

24. Schwarz, J.L.
Influence of a Constant Magnetic Field on Nervous Tissues: II. Voltage-Clamp Studies.
IEEE Transactions on Biomedical Engineering, Vol. 26, 1979, pp. 238-243.

25. Edelman, A., Teulon, J. and Puhalska, I.B.
Influence of the Magnetic Fields on Frog Sciatic Nerve.
Biochemical and Biophysical Research Communications, Vol. 91, 1979, pp. 118-122.

26. Gaffey, C.T. and Tenforde, T.S.
Bioelectric Properties of Frog Sciatic Nerves During Exposure to Stationary Magnetic Fields.
Radiation and Environmental Biophysics, Vol. 22, 1983. pp. 61-73.

27. Hong, C-Z., Harmon, B.S. and Yu, J.
Static Magnetic Field Influence on Rat Tail Nerve Function.
Archives of Physical Medicine and Rehabilitation, Vol. 67, 1986, pp. 746-749.

28. Hong, C-Z.
Static Magnetic Field Influence on Human Nerve Function.
Archives of Physical Medicine and Rehabilitation, Vol. 68, 1987, pp. 162-164.

29. Azanza, M.J. and del Moral, A.
Effects of Static Magnetic Fields on Isolated Neurons.
Journal de Physique, Vol. 49, 1988, pp. C8 2059-2060.

30. Azanza, M.J.
Characterization of Neuronal Membrane K^+ and Ca^{2+} Channels Operated Under Steady Magnetic Fields Exposure.
Journal of Magnetism and Magnetic Materials, Vol. 83, 1990, pp. 527-529.

31. del Moral, A. and Azanza, M.J.
Model for the Effect of Static Magnetic Fields on Isolated Neurons.
Journal of Magnetism and Magnetic Materials, Vol. 114, 1992, pp. 240-242.

32. Azanza, M.J. and del Moral, A.
Neuron Firing Frequency Dependence on the Static Magnetic Field Intensity.
Journal of Magnetism and Magnetic Materials, Vol. 140, 1995, pp. 1464-1465.

33. Azanza, M.J. and del Moral, A.
Isolated Neuron Amplitude Spike Decrease Under Static Magnetic Fields.
Journal of Magnetism and Magnetic Materials, Vol. 158, 1996, pp. 593-594.

34. Balaban, P.M., Bravarenko, N.I. and Kuznetzov, A.N.
Influence of a Stationary Magnetic Field on Bioelectric Properties of Snail Neurons.
Bioelectromagnetics, Vol. 11, 1990, pp. 13-25.

35. Holcomb, R.R.
Method and Apparatus for Suppressing Neuron Action Potential Firings.
US Patent Number 5312321.

36. McLean, M.J., Holcomb, R.R., Wamil, A.W. and Pickett, J.D.
Effects of Steady Magnetic Fields on Action Potentials of Sensory Neurons in Vitro.
Environmental Medicine, Vol. 8, 1991, pp. 36-45.

37. McLean, M.J., Holcomb, R.R., Wamil, A.W., Pickett, J.D. and Cavopol, A.V.
Blockade of Sensory Neuron Action Potentials by a Static Magnetic Field in the 10 mT Range.
Bioelectromagnetics, Vol. 16, 1995, pp. 20-32.

38. Cavopol, A.V., Wamil, A.W., Holcomb, R.R. and McLean, M.J.
Measurement and Analysis of Static Magnetic Fields which Block Action Potentials in Cultured Neurons.
Bioelectromagnetics, Vol. 16, 1995, pp. 197-206.

39. Hansen, K.M.
Some Observations with a View to Possible Influence of Magnetism Upon the Human Organism.
Acta Medica Scandinavica, Vol. 97, 1938, pp. 339-364.

40. Becker, R.O. and Selden, G.
The Body Electric.
Quill, 1985.

41. Purves, D., Augustine, G.J., Katz, L.C., LaMantia, A-S. and McNamara, J.O. (Eds.)
Neuroscience.
Sinauer Associates, 1997.

42. Szent-Györgyi, A.
Introduction to a Submolecular Biology.
Academic Press, 1960.

43. Vallbona, C., Hazlewood, C.F. and Jurida, G.
Response of Pain to Static Magnetic Fields in Postpolio Patients: A Double-Blind Pilot Study.
Archives of Physical Medicine and Rehabilitation, Vol. 78, 1997, pp. 1200-1203.

44. Holcomb, R.R., Parker, R.A. and Harrison, M.S.
Biomagnetics in the Treatment of Human Pain – Past, Present, Future.
Environmental Medicine, Vol. 8, 1991, pp. 24-30.

45. Segal, N., Houston, J., Fuchs, H., Holcomb, R. and McLean, M.J.
Efficacy of a Static Magnetic Device Against Knee Pain Associated with Inflammatory Arthritis.
Journal of Clinical Rheumatology, Vol. 5, 1999, pp. 302-305.

46. Collacott, E.A., Zimmerman, J.T., White, D.W. and Rindone, J.P.
Bipolar Permanent Magnets for the Treatment of Chronic Low Back Pain.
Journal of the American Medical Association, Vol. 283, 2000, pp. 1322-1325.

47. Duffin, W.J.
Electricity and Magnetism, Third Edition.
McGraw-Hill, 1980.

48. Barker, A.T.
Electricity, Magnetism and the Body: Some Uses and Abuses.
Journal of the Royal Society of Health, Vol. 114, 1994, pp. 91-97.

49. Barker, A.T.
Personal communication.

50. Polson, M.J.R., Barker, A.T. and Freeston, I.L.
Stimulation of Nerve Trunks with Time-Varying Magnetic Fields.
Medical & Biological Engineering & Computing, Vol. 20, 1982, pp. 243-244.

51. Barker, A.T., Jalinous, R. and Freeston, I.L.
Non-Invasive Magnetic Stimulation of Human Motor Cortex.
The Lancet, Vol. 1, 1985, pp. 1106-1107.

52. Ueno, S., Lövsund, P. and Åke Öberg, P.
Effect of Time-Varying Magnetic Fields on the Action Potential in Lobster Giant Axon.
Medical & Biological Engineering & Computing, Vol. 24, 1986, pp. 521-526.

53. Azanza, M.J. and del Moral, A.
ELF-Magnetic Field Induced Effects on the Bioelectric Activity of Single Neurone Cells.
Journal of Magnetism and Magnetic Materials, Vol.177, 1998, pp. 1451-1452.

54. Azanza, M.J. and Calvo, A.C.
Snail Neuron Bioelectric Activity Induced Under Static or Sinusoidal Magnetic Fields Reproduces Mammal Neuron Responses Under Transcranial Magnetic Stimulation.
Electro- and Magnetobiology, Vol. 19, 2000, pp. 303-319.

55. Migita, K., Uozumi, T., Arita, K. and Monden, S.
Transcranial Magnetic Coil Stimulation of Motor Cortex in Patients with Central Pain.
Neurosurgery, Vol. 36, 1995, pp. 1037-1039.

56. Amassian, V.E., Vergara, M., Somasundaram, M., Maccabee, P.J. and Cracco, R.Q.
Temporary Relief of Induced Pain by Repetitive Magnetic Stimulation of Human Parietal Lobe.
Journal of Physiology, Vol. 499, pp. P88-89.

57. Ellis, W.V.
Pain Control Using High-Intensity Pulsed Magnetic Stimulation.
Bioelectromagnetics, Vol. 14, 1993, pp. 553-556.

2. COMPUTER SIMULATION OF NERVE FIBRES

A computer simulation of a mammalian nerve fibre was developed to assist with the evaluation of possible methods of inducing non-invasive anaesthesia. Simulation provides a simple method to assess the feasibility of hypothetical techniques, before performing more complex and time-consuming *in vivo* or *in vitro* experimentation.

2.1. Axon Modelling

In 1976, McNeal [1] published the first model of a myelinated axon in the presence of an extracellular electric field. Although other, more anatomically detailed, models have since been developed, McNeal's model remains at the heart of much current research due to its simplicity and accuracy in predicting the excitation of real nerve fibres. Figure 2.1 shows the equivalent circuit for a myelinated axon, as developed by McNeal.

As suggested by Hodgkin and Huxley [2], the excitable membrane at the nodes of Ranvier (hereafter referred to simply as 'nodes') is represented by a parallel conductance and capacitance. The membrane conductance, G_m, represents the combined effect of the passage of ions across the membrane through voltage-gated sodium and potassium channels and leakage channels. The ionic current density (i.e. the ionic current per unit area) in the membrane conductance at node n is denoted by $i_{i,n}$.

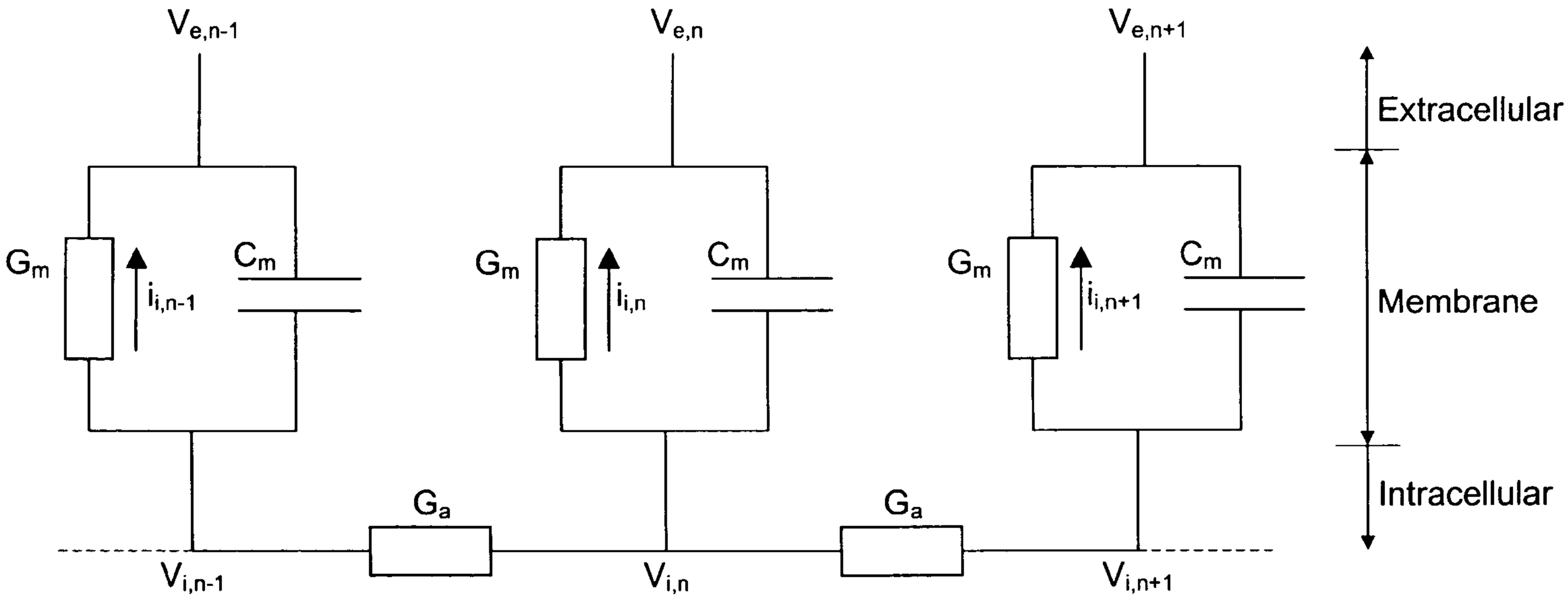

Figure 2.1 Equivalent circuit of an axon.

The membrane capacitance, C_m, represents the separation of ionic charge across the membrane. The lipid bilayer that constitutes the membrane is extremely thin, with a thickness of approximately 2 nm [3], and has a reasonably large capacitance per unit area of 2 $\mu F\ cm^{-2}$ [4]. The membrane capacitance for an axon of diameter *d*, with nodes of length *l* and capacitance per unit area c_m is calculated from:

$$C_m = c_m.\pi.d.l \qquad (2.1)$$

Each node is connected to two adjacent nodes by an internodal (axoplasmic) conductance, G_a, which represents the conductivity of the intracellular fluid. The internodal conductance for an axon of diameter *d*, internode length *L* (i.e. length of the myelinated region between adjacent nodes of Ranvier), with an intracellular medium of resistivity ρ_i is given by:

$$G_a = \frac{\pi d^2}{4\rho_i L} \qquad (2.2)$$

The intracellular potential at node *n* is denoted by $V_{i,n}$, whilst the extracellular potential at node *n* is indicated by $V_{e,n}$.

To analyse the equivalent circuit of the axon, consider the flow of currents into node *n*. The current at node *n* has three components: a capacitive component due to the accumulation of charge at the membrane surface, an ionic component due to the passage of ions through the membrane and an axial component due to conduction along the length of the fibre through the axoplasm. Kirchoff's current law, which states that there is no net current into any node, gives:

$$C_m \cdot \frac{d(V_{i,n} - V_{e,n})}{dt} + i_{i,n} + G_a(V_{i,n} - V_{i,n-1}) + G_a(V_{i,n} - V_{i,n+1}) = 0 \quad (2.3)$$

Capacitive component *Ionic component* *Axial component*

To simplify analysis, the 'reduced potential' at node n, V_n, is introduced. This is defined as the potential difference across the membrane minus the resting potential and is evaluated by:

$$V_n = V_{i,n} - V_{e,n} - V_r \quad (2.4)$$

Rearrangement of (2.4) yields:

$$V_{i,n} = V_n + V_r + V_{e,n} \quad (2.5)$$

Substituting (2.5) into (2.3) gives:

$$C_m \cdot \frac{d(V_n + V_r)}{dt} + i_{i,n} + G_a((V_n + V_r + V_{e,n}) - (V_{n-1} + V_r + V_{e,n-1})) + G_a((V_n + V_r + V_{e,n}) - (V_{n+1} + V_r + V_{e,n+1})) = 0 \quad (2.6)$$

which can be simplified to:

$$C_m \cdot \frac{dV_n}{dt} + i_{i,n} + G_a(-V_{n-1} + 2V_n - V_{n+1} - V_{e,n-1} + 2V_{e,n} - V_{e,n+1}) = 0 \quad (2.7)$$

Rearrangement of (2.7) results in:

$$\frac{dV_n}{dt} = \frac{G_a(V_{n-1} - 2V_n + V_{n+1} + V_{e,n-1} - 2V_{e,n} + V_{e,n+1}) - i_{i,n}}{C_m} \quad (2.8)$$

Equation (2.8) is the fundamental differential equation used in the modelling of axon stimulation.

The ionic transmembrane current is calculated via empirical equations, derived from 'voltage-clamp' or 'patch-clamp' experiments on axons *in vitro*, such as the Frankenhaeuser-Huxley equations for frog nerve fibres [4] as utilised by McNeal. However, the Frankenhaeuser-Huxley equations are unsuitable for the simulation of mammalian fibres for two reasons. Firstly, parameters in the Frankenhaeuser-Huxley equations were determined at a temperature of 20°C, a temperature significantly lower than human body temperature (37°C). Several of these parameters are strongly temperature dependant and although temperature compensation is possible for some parameters, the temperature disparity remains a source of error. Secondly, there is a significant difference in methods of membrane repolarisation for frog and mammalian axons. As previously mentioned, repolarisation following an action potential occurs in mammals via the passage of unspecific ions through leakage channels with a small contribution to repolarisation from the efflux of potassium ions. This contrasts with frog axons, which repolarise due to a large flow of potassium ions out of the cell and a relatively small leakage current. These fundamental dissimilarities suggest that a set of equations derived from experiments on mammalian nerve fibres are required for the accurate modelling of ionic currents in human nerve fibres.

Sweeney *et al.* [5] used the equations for rabbit nerves published by Chiu *et al.* [6] which, although requiring compensation for temperature due to their derivation at 14°C, do account for the relative importance of leakage currents. The Schwarz-Eikhof equations [7] for rat axons, utilised by Rattay *et al.* [8] and

Frijns *et al.* [9], account for both mammalian body temperature and the large leakage current which occurs during repolarisation.

The total ionic membrane current density, i_i, is the sum of the sodium current density, i_{Na}, potassium current density, i_K, and the leakage current density, i_L:

$$i_i = i_{Na} + i_K + i_L \tag{2.9}$$

The Schwarz-Eikhof equations describing the ionic current densities are:

$$i_{Na} = P'_{Na}\, m^3 h \frac{EF^2}{RT} \frac{[Na]_o - [Na]_i\, exp^{EF/RT}}{1 - exp^{EF/RT}} \tag{2.10}$$

$$i_K = P'_k\, n^2 \frac{EF^2}{RT} \frac{[K]_o - [K]_i\, exp^{EF/RT}}{1 - exp^{EF/RT}} \tag{2.11}$$

$$i_L = G_L(V_n - V_L) \tag{2.12}$$

where E, the membrane potential, is the potential difference across the membrane and is defined as:

$$E = V_{i,n} - V_{e,n} = V_n + V_r \tag{2.13}$$

The variable m is called the sodium activation parameter and represents the probability of a sodium channel being in the 'open' state. When considering an area of membrane which has several sodium channels, the sodium activation parameter represents the proportion of sodium channels that are activated. Hence, the sodium activation parameter has a value between zero and unity. Parameter h is known as the sodium inactivation parameter and the probability of the sodium channel being inactivated is (1 - h). The combined effect of parameters m and h determines the permeability of the membrane to sodium ions. Similarly, n is known as the potassium activation parameter and

represents the probability of activation of potassium channels. Potassium channels are unable to become inactivated and there is therefore no potassium inactivation parameter. The activation and inactivation parameters are described by the equations:

$$\frac{dm}{dt} = \alpha_m(1-m) + \beta_m \cdot m \tag{2.14}$$

$$\frac{dh}{dt} = \alpha_h(1-h) + \beta_h \cdot h \tag{2.15}$$

$$\frac{dn}{dt} = \alpha_n(1-n) + \beta_n \cdot n \tag{2.16}$$

where α_m, β_m, α_n, β_n, α_h and β_h are rate constants, calculated using the empirical equations:

$$\alpha_m = \frac{1.87(V-25.41)}{1-exp\left(\frac{25.41-V}{6.06}\right)} \qquad \beta_m = \frac{3.97(21-V)}{1-exp\left(\frac{V-21}{9.41}\right)} \tag{2.17}$$

$$\alpha_h = \frac{-0.55(V+27.74)}{1-exp\left(\frac{V+27.74}{9.06}\right)} \qquad \beta_h = \frac{22.6}{1+exp\left(\frac{56-V}{12.5}\right)} \tag{2.18}$$

$$\alpha_n = \frac{0.13(V-35)}{1-exp\left(\frac{35-V}{10}\right)} \qquad \beta_n = \frac{0.32(10-V)}{1-exp\left(\frac{V-10}{10}\right)} \tag{2.19}$$

For a resting membrane *dm/dt* is equal to zero, therefore the initial value of the sodium activation parameter, m_0, can be calculated using:

$$m_0 = \frac{\alpha_m}{\alpha_m + \beta_m} \tag{2.20}$$

Similar equations are used to evaluate h_0 and n_0.

Equations (2.10) and (2.11) show that the ion channel activation and inactivation parameters serve to adjust the membrane permeability constants from their maximum values of P'_{Na} and P'_K for sodium and potassium channels respectively, to the permeabilities observed at any given voltage, P_{Na} and P_K:

$$P_{Na} = P'_{Na} m^3 h \tag{2.21}$$

$$P_K = P'_K n^2 \tag{2.22}$$

Hence equation (1.2), the Goldman equation for the membrane resting potential can be restated in terms of the maximum permeabilities and the resting values of the activation and inactivation parameters:

$$V_r = \frac{RT}{F} ln \frac{P'_k n_0^2 \cdot [K]_o + P'_{Na} m_0^3 h_0 \cdot [Na]_o}{P'_k n_0^2 \cdot [K]_i + P'_{Na} m_0^3 h_0 \cdot [Na]_i} \tag{2.23}$$

In equation (2.12), the leakage channels are modelled by an ohmic conductance, G_L, and a leakage potential, V_L. The leakage conductance for an axon of diameter d, node length l and leakage conductance per unit area of g_L is calculated from:

$$G_L = g_L . \pi . d . l \tag{2.24}$$

V_L is adjusted to a value which gives no net transmembrane current when the membrane is in the resting state. Perturbations in the membrane potential cause variations in the potential difference across the leakage conductance, thus causing variations in the leakage current. There are no activation or inactivation parameters associated with leakage channels since leakage channels are not voltage-gated.

The ionic currents in every node of a real axon obey a set of differential equations such as the Frankenhaeuser-Huxley or Schwarz-Eikhof equations. McNeal approximated this situation by incorporating a single node, the so-called excitation node, which obeys the Frankenhaeuser-Huxley equations and modelling the membrane at all other nodes with an ohmic conductance. The excitation node was assumed to be the node which experiences the largest stimulus and this situation allows the determination of the threshold stimulus required to initiate an action potential. The limitation of this approximation is that the propagation of an action potential can not be simulated. This is because the large non-linear changes in membrane conductivity which occur during an action potential are not incorporated in nodes other than the excitation node, hence these nodes are unable to generate action potentials. Reilly *et al.* [10] published their 'spatially extended non-linear node' (SENN) model in which several adjacent nodes obey the Frankenhaeuser-Huxley equations, allowing the propagation of action potentials. The incorporation of several non-linear nodes in the SENN model requires significantly more computational effort than McNeal's original model.

McNeal used the symmetry of the equivalent circuit of Figure 2.1 to simplify the model of the nerve fibre, by assuming the applied extracellular electric field was symmetrical about the non-linear excitation node which was designated as node zero. The choice of a symmetrical extracellular field infers that each of the terms V_n, $V_{e,n}$ and $i_{i,n}$ are equal for nodes n and $-n$ (i.e. $V_n = V_{-n}$, $V_{e,n} = V_{e,-n}$ and $i_{i,n} = i_{i,-n}$). This simplification is particularly useful when several non-linear nodes are considered and almost halves the required computational effort. However, this

simplification is only appropriate for the consideration of simple configurations of stimulating electrodes that possess symmetry.

Another simplification employed by McNeal was to restrict the length of the model used. McNeal demonstrated that truncation of the model to just eleven nodes produces results accurate to better than 0.2 percent for a 1 ms stimulating pulse. Of these eleven nodes, only six require calculation since voltages and currents at the remaining five nodes can be derived from the symmetry about the excitation node.

The aim of McNeal's model was to determine the threshold stimulus required to initiate an action potential. The stimulus was assumed to be a point current source and the extracellular potential at node *n*, a distance of *r* metres from the current source in a homogeneous isotropic extracellular medium of resistivity ρ_e is calculated by:

$$V_{e,n} = \frac{\rho_e I}{4\pi r} \tag{2.25}$$

where *I* is the stimulus current. Current flow towards the electrode, and hence out of the neuron, is assumed to be positive and it is assumed that the presence of the fibre has no effect on the extracellular field. Although each node has a finite area, it is assumed that the extracellular potential is constant over the entire nodal area and the distance *r* is taken as the distance from the current source to the centre of the node in question. Complex electrode arrangements may be modelled by the superposition of point current sources.

McNeal assumed that the myelin sheath was a perfect insulator with zero capacitance, despite published research in which the resistivity and capacitance of myelin have been quantified as 290 MΩ mm and 1.6 pF mm^{-2} respectively in the case of frog axons [11]. The extra computational effort required to account for the resistance and capacitance of the myelin was considered by McNeal to be unjustified. Neglect of these parameters is a feature of most published work based upon the McNeal model.

Simulation of an unmyelinated nerve fibre is also possible by means of a slight variation on McNeal's model [8]. In the case of an unmyelinated axon, the parameters G_m, C_m and G_a refer to an element of length δx and the membrane is assumed to have a non-linear conductance along its entire length. The axon is simulated by consideration of these discrete elements and numerical convergence is achieved as the element length δx approaches zero. Since simulation of an unmyelinated fibre involves calculation of ionic currents for a large number of small membrane elements, simulation of a given length of unmyelinated fibre requires considerably more computational effort than for the same length of myelinated fibre.

2.2. Development of a Simulated Nerve Fibre

McNeal's model of a nerve fibre in an extracellular electric field was used as the basis for the computer simulation of an axon. A multiple non-linear node model was developed, with the Schwarz-Eikhof equations [7] describing the ionic current at every node. A model with a large number of non-linear nodes allows the propagation of action potentials along the length of the axon and, whilst requiring more computational effort, prevents inaccuracies arising from the approximation of nodes by an ohmic conductance.

Since Schwarz and Eikhof did not provide all the parameters necessary for simulation, the parameters were adjusted as suggested by Frijns *et al.* [9]. Schwarz and Eikhof published the absolute values of ionic permeabilities, P_K and P_{Na}, and leakage conductance, G_L, without stating the diameters of the fibres used. Frijns *et al.* estimated the fibre diameter from the conduction velocities of the action potentials presented by Schwarz and Eikhof and converted the ionic permeabilities and leakage conductances into the appropriate values for a unit area of membrane. Frijns *et al.* corrected the internodal resistivity, ρ_i, to a realistic value for 37°C since Schwarz and Eikhof only published the value of this parameter at 20°C. The experiments of Schwarz and Eikhof were performed in an extracellular medium composed of Ringer's solution, therefore Frijns *et al.* substituted the typical mammalian extracellular ionic concentrations published by Guyton [12].

McNeal and Frijns *et al.* made several assumptions regarding the geometry of nerve fibres in order to simulate fibres of arbitrary diameters. Following Goldman and Albus [13], it was assumed that the ratio of axon diameter (the diameter of the axon's membrane) to fibre diameter (the external diameter of the myelin sheath) was 0.7. As suggested by Hursh [14] and Dodge and Frankenhaeuser [15], the ratio of internodal length to fibre diameter was assumed to be 100. These geometric relations allow parameters for a unit area of membrane or unit fibre diameter to be converted to an absolute value for a fibre of given diameter. Each node of Ranvier was assumed to have a constant length of 1 μm for all fibre diameters. The independence of node length upon fibre diameter was reported by Dodge and Frankenhaeuser [15] and infers that the area of the node of Ranvier is proportional to the fibre diameter.

Additionally, Frijns *et al.* calculated the resting potential of the membrane using the Goldman equation (equation (2.23)), to reflect the actual values of ion concentrations and membrane permeabilities used in the simulation. In previously published models of nerve fibres, the axon was assumed to have a fixed resting potential of 70-80 mV regardless of the actual ionic compositions or membrane properties used elsewhere in the simulation.

The simulation which was implemented is largely based on the so-called SEF model published by Frijns *et al.* The ionic concentrations used in the simulation are presented in Table 1.1 (Section 1.1.2), whilst other simulation parameters are summarised in Table 2.1.

Parameter	Value	Unit
Membrane capacitance per unit area (c_m)	2	$\mu F\ cm^{-2}$
Leakage conductance per unit area (g_L)	72.8	$mS\ cm^{-2}$
Maximum value of potassium permeability constant (P'_K)	2×10^{-4}	$cm\ s^{-1}$
Maximum value of sodium permeability constant (P'_{Na})	51.5×10^{-4}	$cm\ s^{-1}$
Absolute Temperature (T)	310.15	K
Resistivity of intracellular medium (ρ_i)	0.3	$k\Omega\ cm$
Resistivity of extracellular medium (ρ_e)	0.07	$k\Omega\ cm$

Table 2.1 Simulation parameters

The most important difference between the simulation presented here and the models of McNeal and Frijns *et al.* is that this simulation uses an asymmetrical fibre model. Previous models of nerve fibres assume the stimulus to be symmetrical about the excitation node, thus allowing a significant reduction in the computational effort required since the calculation of ionic currents is only necessary for half of the nerve fibre. However, it was considered to be undesirable to restrict this simulation to the consideration of symmetrical stimuli. Therefore intracellular and extracellular voltages and the resulting currents are calculated for each of the nodes in the simulation. This situation significantly increases the flexibility of the model, allowing the simulation of arbitrary electrode arrangements at the expense of an almost twofold increase in computational effort.

The number of nodes to be simulated was dependent upon the stimulus under investigation and was chosen to be sufficiently large so that the effect of the boundary conditions could be neglected. For a model composed of z nodes, the

boundary nodes will be nodes zero and (z - 1). Boundary conditions of zero extracellular potential and zero reduced potential were applied at these nodes, i.e.:

$$V_{e,n} = 0 \qquad \text{for } n = 0 \text{ and } n = (z - 1) \tag{2.26}$$

$$V_n = 0 \qquad \text{for } n = 0 \text{ and } n = (z - 1) \tag{2.27}$$

This infers that the intracellular potential is equal to the resting potential at the boundary nodes. Since the resting potential is constant, the intracellular potential is also constant. Therefore, the boundary nodes are permanently maintained at the resting potential and are unable to generate action potentials. The presence of these boundary conditions will introduce inaccuracies since, from equation (2.8), the values of $V_{e,n}$ and V_n affect the rate of change of the reduced potential at the adjacent nodes. In practice, this causes the magnitude of propagated action potentials to decrease as the boundary node is approached. The length of the simulated axon was adjusted so that the presence of the boundary nodes had negligible effect upon sites of interest along the axon, such as the node where the action potential is initiated.

Numerical evaluation of equation (2.8) was achieved with a first-order method with a fixed step size. It was demonstrated that a step size of 0.1 μs produced sufficiently accurate results.

The simulation software was written in C, allowing portability of the code between various hardware platforms and operating systems. The software allowed the graphical display and animation of membrane potentials.

2.3 Discussion

The computer simulation of a nerve fibre has been demonstrated as a useful tool with which the feasibility of the hypothetical techniques of non-invasive anaesthesia proposed in Chapters 3 and 4 can be predicted. Since the simulation is based on data for rat neurons, it does not provide a truly accurate description of the human axon. The Schwarz-Eikhof equations for rat axons do account for several properties of human nerve fibres such as the relative importance of the leakage current during repolarisation and human body temperature of 37°C. Frankenhaeuser and Huxley's equations describing the ionic currents in frog axons have been frequently used to predict human nerve function, despite not accounting accurately for either leakage currents or body temperature. Similarly, the equations for rabbit axons published by Chiu *et al.* have been applied to the human nervous system yet do not account accurately for body temperature. Although the use of the Schwarz-Eikhof equations to model human neurons is not without precedent [9], the dissimilarities between human and rat nerve fibres remain a source of inaccuracy.

Eight years after the publication of his equations for rat neurons, Schwarz, together with Reid and Bostock [16], published a series of empirical equations which describe the ionic membrane currents in human nerve fibres. These equations show that the ion channel kinetics in human and rat axons are reasonably similar, although human potassium currents were shown to consist of three components, namely a 'slow' component and two 'fast' components. The resultant effect of the two fast potassium components is similar to that of

the single potassium component found in rat nerve fibres and has a relatively small effect in comparison to the sodium and leakage currents. The slow component of the potassium current has little effect other than to limit the rate at which action potentials are generated when the nerve is exposed to prolonged stimuli. A limitation of the human equations published by Schwarz *et al.* is their derivation at 20°C. Therefore, simulation of a human nerve fibre at body temperature will require temperature compensation of some parameters, which will introduce a source of inaccuracy into the simulation.

Schwarz *et al.* did not provide values for all the parameters required for simulation. This situation was addressed by Wesselink *et al.* [17] who published estimates for these absent parameters. However, Wesselink's paper was published after the simulation based on the Schwarz-Eikhof equations had been developed and used for some time. Therefore it was decided to continue using a simulation based on rat axons. This decision is partially justified by the uncertainty regarding the effects of temperature compensation on Schwarz *et al.*'s equations for human nerve fibres.

The popularity of McNeal's model for the simulation of nerve fibres appears undiminished, despite the publication of 'distributed parameter' models which incorporate a greater level of anatomical detail, such as that of Halter and Clark [18]. The complexity of distributed parameter models requires a great deal computational effort, therefore most current research utilises models based on that of McNeal. This precedent was followed, hence the computer simulation which was developed for this research is also based on McNeal's model.

A source of inaccuracy in the implementation of the simulation arises from the use of a first-order method, Euler's method, in the numerical solution of differential equations. Despite its computational simplicity, Euler's method is inaccurate in comparison to higher order methods for any given step size [19]. However, when used with a sufficiently small step size, the computational accuracy of Euler's method is adequate for the purposes of this simulation.

In conclusion, although all known methods by which human nerve fibres can be modelled have inherent limitations, the simulation which has been developed provides a useful means by which the properties of nerve fibres can be studied. The simulation accounts for many of the properties of real human axons and allows the evaluation of non-invasive anaesthesia techniques to a reasonable level of accuracy without the need for *in vivo* testing.

2.4 References

1. McNeal, D.R.
   Analysis of a Model for Excitation of Myelinated Nerve.
   IEEE Transactions on Biomedical Engineering, Vol. 23, 1976, pp. 329-337.
2. Hodgkin, A.L. and Huxley, A.F.
   A Quantitative Description of Membrane Current and its Application to Conduction and Excitation in Nerve.
   Journal of Physiology, Vol. 117, 1952, pp. 500-544.
3. Hille, B.
   Ionic Channels of Excitable Membranes, Second Edition.
   Sinauer Associates Inc., 1992.
4. Frankenhaeuser, B. and Huxley, A.F.
   The Action Potential in the Myelinated Nerve Fibre of *Xenopus Laevis* as Computed on the Basis of Voltage Clamp Data
   Journal of Physiology, Vol. 171, 1964, pp. 302-315.
5. Sweeney, J.D., Mortimer, J.T. and Durand, D.
   Modelling of Mammalian Myelinated Nerve for Functional Neuromuscular Stimulation
   IEEE 9th Annual International Conference of the Engineering in Medicine and Biology Society, 1987, pp. 1577-1578
6. Chiu, S.Y., Ritchie, J.M., Rogart, R.B. and Stagg, D.
   A Quantitative Description of Membrane Currents in Rabbit Myelinated Nerve
   Journal of Physiology, Vol. 292, 1979, pp. 149-166.
7. Schwarz, J.R. and Eikhof G.
   Na Currents and Action Potentials in Rat Myelinated Nerve Fibres at 20 and 37°C
   Pflügers Archiv, Vol. 409, 1987, pp. 569-577.

8. Rattay, F. and Aberham, M.
Modelling Axon Membranes for Functional Electrical Stimulation
IEEE Transactions on Biomedical Engineering, Vol. 40, 1993, pp. 1201-1209.

9. Frijns, J.H.M., Mooij, J. and ten Kate, J.H.
A Quantitative Approach to Modelling Mammalian Myelinated Nerve Fibers for Electrical Prosthesis Design
IEEE Transactions on Biomedical Engineering, Vol. 41, 1994, pp. 556-566.

10. Reilly, J.P., Freeman, V.T. and Larkin, W.D.
Sensory Effects of Transient Electrical Stimulation: Evaluation with a Neuroelectrical Model
IEEE Transactions on Biomedical Engineering, Vol. 32, 1985, pp. 1001-1011.

11. Tasaki, I.
New Measurements of the Capacity and the Resistance of the Myelin Sheath and the Nodal Membrane of the Isolated Frog Nerve Fiber
American Journal of Physiology, Vol. 181, 1955, p. 639.

12. Guyton, A.C.
Textbook of Medical Physiology, Sixth Edition.
Saunders, 1981.

13. Goldman, L. and Albus, J.S.
Computation of Impulse Conduction in Myelinated Fibres: Theoretical Basis of the Velocity-Diameter Relation.
Biophysical Journal, Vol. 8, 1968, p. 596.

14. Hursh, J.B.
Conduction Velocity and Diameter of Nerve.
American Journal of Physiology, Vol. 127, 1939, p.131.

15. Dodge, F.A. and Frankenhaeuser, B.
Sodium Currents in the Myelinated Nerve Fibre of *Xenopus Laevis* Investigated with the Voltage Clamp Technique.
Journal of Physiology, Vol. 148, 1959, p. 188-200.

16. Schwarz, J.R., Reid, G. and Bostock, H.
Action Potentials and Membrane Currents in the Human Node of Ranvier.
Pflügers Archiv, Vol. 430, 1995, pp. 283-292.

17. Wesselink, W.A., Holsheimer, J. and Boom, H.B.K.
A Model of the Electrical Behaviour of Myelinated Sensory Nerve Fibres Based on Human Data.
Medical and Biological Engineering and Computing, Vol. 37, 1999, pp.228-235.

18. Halter, J.A. and Clark, J.W.
A Distributed-Parameter Model of the Myelinated Nerve Fibre.
Journal of Theoretical Biology, Vol. 148, 1991, pp.345-382.

19. Press, W.H., Teukolsky, S.A., Vetterling, W.T. and Flannery, B.P.
Numerical Recipes in C.
Cambridge University Press, 1992.

3. NON-INVASIVE ANAESTHESIA BY A ROTATING MAGNETIC FIELD

Two hypothetical methods by which non-invasive anaesthesia may be achieved were investigated. The first non-invasive anaesthetic technique, described in this chapter, was proposed and patented by an orthopaedic surgeon and had received backing from companies within the healthcare industry. The research group was invited to evaluate the electrical engineering aspects of this technique and to refine the system in order to produce the desired non-invasive anaesthetic effect. This project proved to be the starting point for the larger body of research documented in this thesis.

3.1 Blocking of Action Potentials with an Extracellular Electric Field

The application of an extracellular electric field to prevent the conduction of action potentials in nerves has been the subject of much research. A variety of methods in which electrical stimuli, applied by electrodes placed in the extracellular region, may be used to block action potentials have been investigated. Unfortunately, a perfectly safe technique has yet to be discovered. DC blocking stimuli cause bodily tissue to be electrolysed whilst the application of AC stimuli, where the frequencies used are generally in the range of 2-20 kHz, has been shown to cause damage to the nerve due to hyperactivity [1]. The requirement to place stimulating electrodes within the body is particularly undesirable and makes these techniques unsuitable in many clinical situations.

One way in which the conduction of action potentials along a nerve may be prevented is to hyperpolarise its constituent nerve fibres. In the hyperpolarised state, the intracellular region of a nerve cell contains more negative charge than when in the resting state and thus the membrane potential of a hyperpolarised neuron is more negative than the neuron's resting potential. The result of hyperpolarisation is that a stimulus of greater magnitude is required to produce threshold depolarisation of the nerve fibre. Since the amplitude of action potentials is determined solely by ionic concentrations and ion channel gating kinetics, the amplitude of action potentials in any particular nerve fibre is unable to vary. Therefore, propagating action potentials are unable to cause a threshold depolarisation of the hyperpolarised regions of the nerve fibre. Thus, the excitation of adjacent areas of membrane which is essential to allow the action potential to propagate is prevented and action potentials attempting to propagate through the hyperpolarised region are blocked.

The aim of the hypothetical non-invasive anaesthesia technique considered in this chapter is to block action potentials by hyperpolarising a small region of a nerve fibre via the use of a rotating magnetic field.

3.2. Use of a Rotating Magnetic Field to Hyperpolarise Nerve Fibres

The mechanism by which it is was hypothesised that an anaesthetic effect could be produced, as explained in the patent application [2], is presented in this chapter. At this point, no judgements will be made regarding the feasibility of the technique.

The proposed apparatus for producing hyperpolarisation of nerve fibres is illustrated in Figure 3.1. The apparatus consists of two cylindrical permanent magnets, aligned so that the north pole of one magnet faces the south pole of the other. The two magnets share a common axis and are able to rotate in the same direction and with the same angular velocity about this axis. Rotation is achieved by an electric motor connected to a drive shaft on each magnet. A small separation exists between the magnets into which a conductor, potentially a nerve fibre within a limb, can be placed. This conductor is positioned so that its axis intersects the axis of the magnets perpendicularly.

For the sake of argument, it is assumed that rotation of the magnets causes rotation of the magnetic field. The validity of this assumption is addressed in Section 3.5.

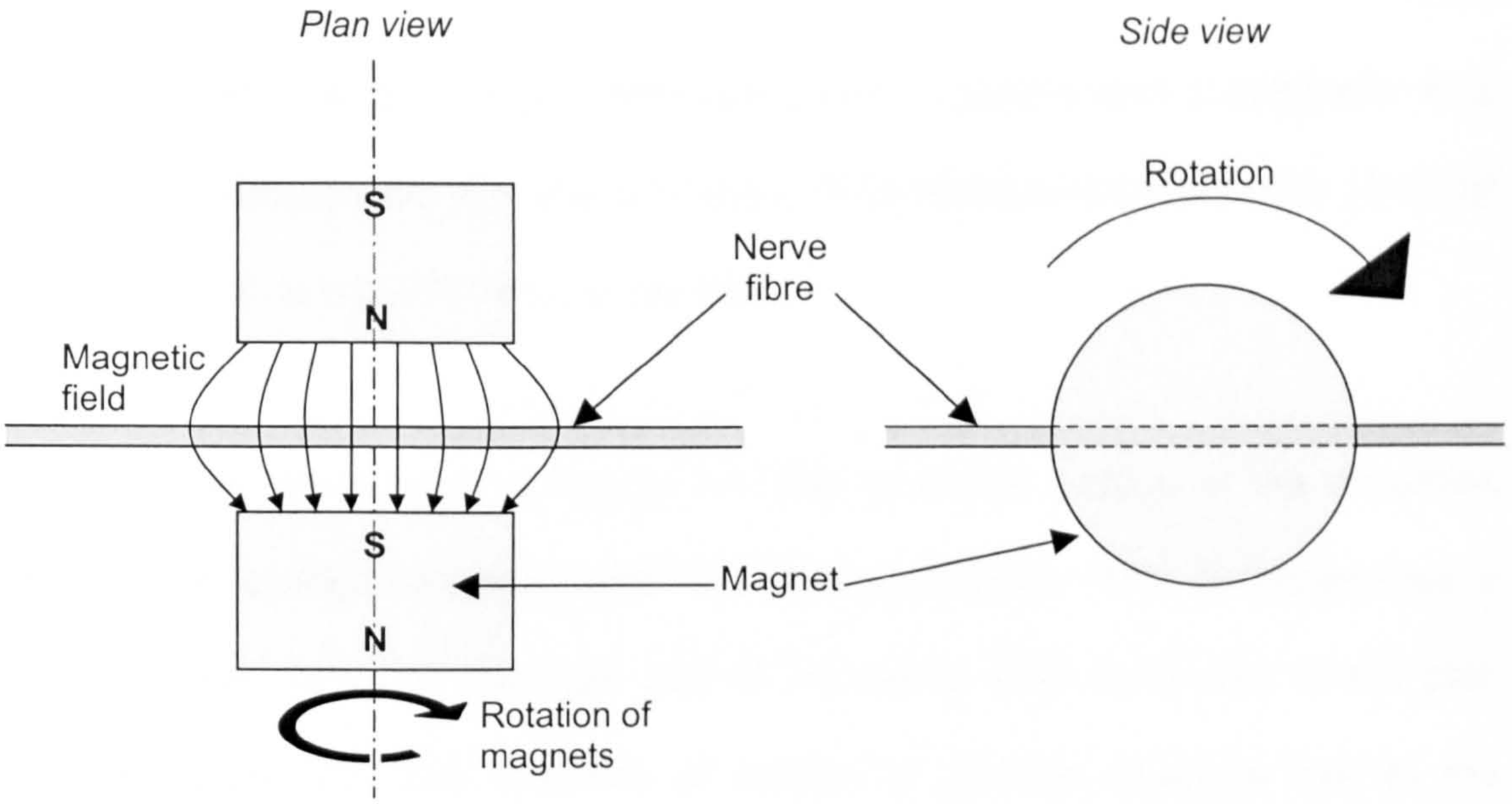

Figure 3.1 Schematic diagram of rotating magnet apparatus

A charge carrier of charge Q moving with velocity $\boldsymbol{v}$ relative to a stationary magnetic field of flux density $\boldsymbol{B}$ experiences a force $\boldsymbol{F}$, the Lorentz force, which is calculated from [3]:

$$\boldsymbol{F} = Q\boldsymbol{v} \times \boldsymbol{B} \tag{3.1}$$

However, in the case where a magnetic field is moving with velocity $\boldsymbol{v}_M$ relative to a stationary charge, the Lorentz force is given by:

$$\boldsymbol{F} = -Q\boldsymbol{v}_M \times \boldsymbol{B} \tag{3.2}$$

The effect of this force is to cause a motion of charge carriers in the direction perpendicular to the vectors $\boldsymbol{v}_M$ and $\boldsymbol{B}$. By definition, the electric field $\boldsymbol{E}$ at a point in space where a charge Q experiences a force $\boldsymbol{F}$ is given by [3]:

$$\boldsymbol{E} = \frac{\boldsymbol{F}}{Q} \tag{3.3}$$

Therefore, equation (3.2) may be substituted into (3.3) to yield:

$$\boldsymbol{E} = -\boldsymbol{v}_M \times \boldsymbol{B} \tag{3.4}$$

In other words, relative motion between charge carriers and a magnetic field induces an electric field $\boldsymbol{E}$ in the conductor. This phenomenon is put to practical use in equipment for electricity generation.

For the apparatus shown in Figure 3.1, the rotational motion of the magnetic field causes charge carriers within the limb and nerve fibre to experience a Lorentz force. Consider the right half of the nerve fibre illustrated in the plan view of Figure 3.1. The direction of motion of positive charges due to the Lorentz force may be calculated by solving equation (3.2), or rather more easily by using Fleming's right hand rule. At any instant, the direction of motion of the right hand side of the magnet as it intersects the nerve fibre is into the plane of the paper. Therefore the direction of motion of the nerve fibre relative to that of the magnet is out of the paper. The magnetic field is directed downwards from the north pole of the upper magnet to the south pole of the lower magnet. Thus, Fleming's right hand rule indicates that positive charge will move towards the right hand side of the page. By similar reasoning, positive charge in the left hand side of the nerve fibre will experience a force directed towards the left of the page. Additionally, charge motion in the nerve fibre will be accompanied by a corresponding movement of positive charge in the extracellular fluid surrounding the nerve fibre, which also experiences a Lorentz force directed radially outwards from the axis of the magnet. In electrolytic conductors, such as the intracellular and extracellular fluids, charge is carried by both positive and negative ions. Negative ions will experience a Lorentz force in a direction

opposite to that of positive ions, causing a movement of anions towards the axis of the magnet. The motion of ions in the intracellular and extracellular electrolytes was hypothesised to result in the axial distribution of charge shown in Figure 3.2.

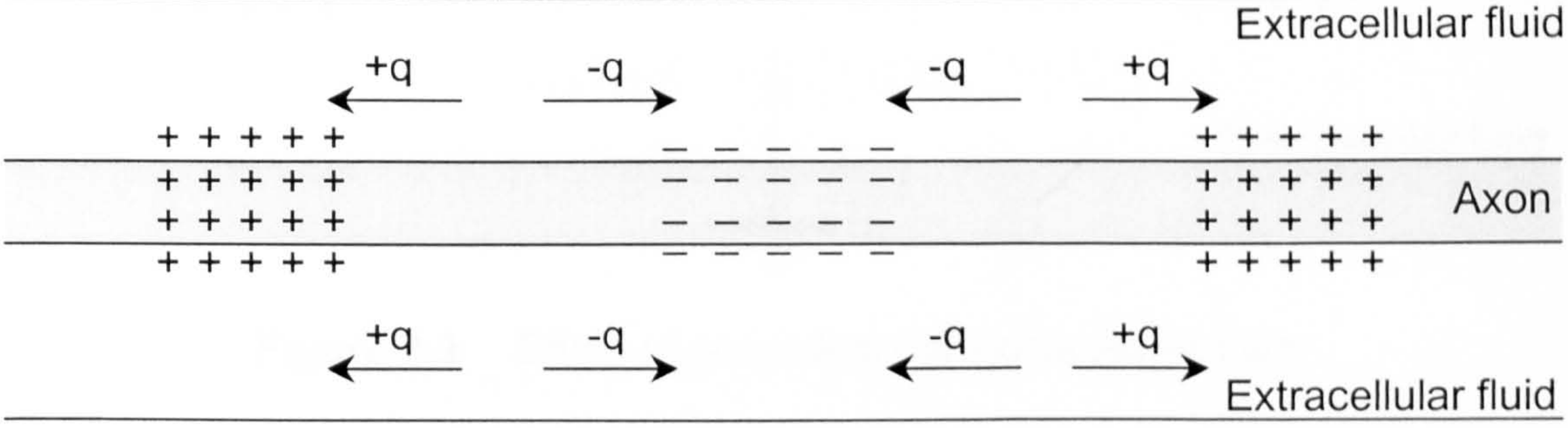

Figure 3.2 Resulting charge distribution

It was hypothesised that if the extracellular fluid was connected to earth potential at its intersection with the axis of the magnets, electrostatic repulsion between the high density of negative ions in this region would cause the movement of extracellular anions towards ground, where they will be discharged. This will cause hyperpolarisation of the axon, since the intracellular fluid will possess a large net negative charge with respect to the extracellular fluid, as shown in Figure 3.3. It was assumed that any reduction in hyperpolarisation of the nerve fibre that may be caused by an efflux of intracellular negative charge would be negligible, since the majority of intracellular negative charge is accounted for by large ions which are unable to cross the membrane. By maintaining the rotation of the magnetic field, and thus preventing the movement of cations towards the site of hyperpolarisation at the

axis of the magnets, the possibility of hyperpolarisation being reduced by an influx of positive charge was also considered to be negligible.

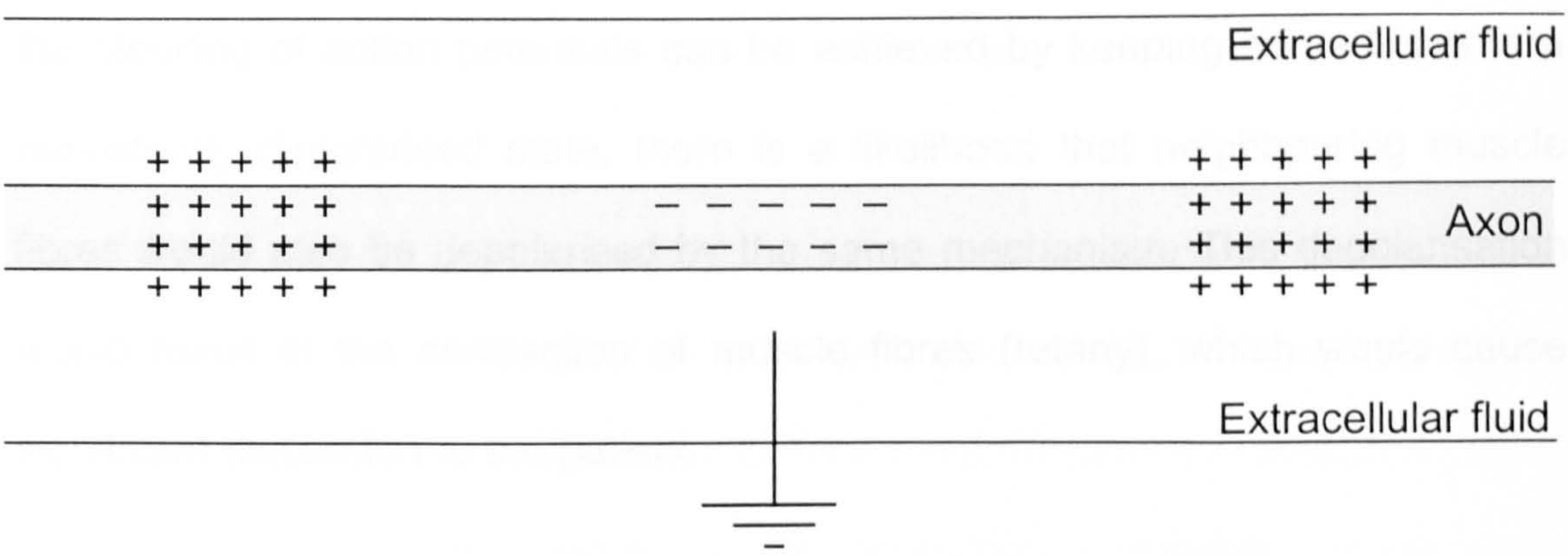

Figure 3.3 Effect of grounding the extracellular fluid

In practice, non-invasive grounding of the extracellular fluid may be difficult to achieve due to the high resistance of the skin which is typically in the range of 1-2 MΩ [4]. Therefore, a large potential difference will exist across the skin, limiting the quantity of negative ions that will be discharged. However, electrode jelly as used on ECG electrodes can significantly reduce the resistance of the electrode/skin interface to a few thousand ohms.

It was hypothesised that the propagation of action potentials would be prevented if a sufficient hyperpolarisation of nerve fibres is achieved by this apparatus. By blocking the conduction of action potentials, this apparatus may be able to produce a non-invasive anaesthetic effect.

If the direction of rotation of the magnets were to be reversed, the direction of the Lorentz force on charge carriers would also be reversed. Therefore, positive

ions would move towards the axis of the magnets while negative ions would move towards the circumference of the magnets. In this situation, grounding of the extracellular fluid would result in the depolarisation of nerve fibres. Although the blocking of action potentials can be achieved by keeping nerve fibres in a persistently depolarised state, there is a likelihood that neighbouring muscle fibres would also be depolarised by the same mechanism. This depolarisation would result in the contraction of muscle fibres (tetany), which would cause significant discomfort to the patient.

To evaluate the feasibility of this hypothetical technique of non-invasive anaesthesia, a computer simulation to assess the effectiveness of blocking action potential conduction by hyperpolarisation of nerve fibres was performed, as well as a series of experiments involving rotating permanent magnets.

3.3. Computer Simulation of Action Potential Blocking by Hyperpolarisation

The computer simulation of Chapter 2 was adapted to estimate the level of hyperpolarisation necessary to prevent the conduction of action potentials in nerve fibres. The McNeal model [5], upon which the computer simulation was based, is intended to simulate the excitation of a nerve fibre due an applied extracellular electric field. Therefore, the computer simulation cannot completely account for the axial variations in intracellular potential which were hypothesised to result from the rotating magnetic field. However, an extracellular electric field distribution was developed to approximate the effect of the magnetic field.

The linear velocity v of a point at a distance r from the axis of a magnet rotating with angular velocity ω is given by:

$$v = r\omega \tag{3.5}$$

By substituting (3.5) into (3.4), the magnitude of the electric field E produced by the rotating magnet at that point can be calculated from:

$$E = r\omega B \tag{3.6}$$

The voltage V at a point r is obtained by integration of equation (3.6) with respect to radial distance:

$$V = \tfrac{1}{2} r^2 \omega B \tag{3.7}$$

Thus both the induced intracellular and extracellular potentials are proportional to the angular velocity of the rotating magnets and the magnetic flux density.

Furthermore, the voltage at any point within the magnetic field is proportional to the square of the distance from that point to the axis of the magnet. The variation of intracellular and extracellular potential with respect to distance from the axis of the magnet is illustrated in Figure 3.4. In Figure 3.4, the axis of the rotating magnets occurs at a distance of zero. At the axis of the magnets, the intracellular and extracellular potentials are both negative with respect to the rest of the body due to the accumulation of negative charge. As distance from the axis of the magnets increases, voltage also increases due to the movement of positive charge towards the circumference of the magnets.

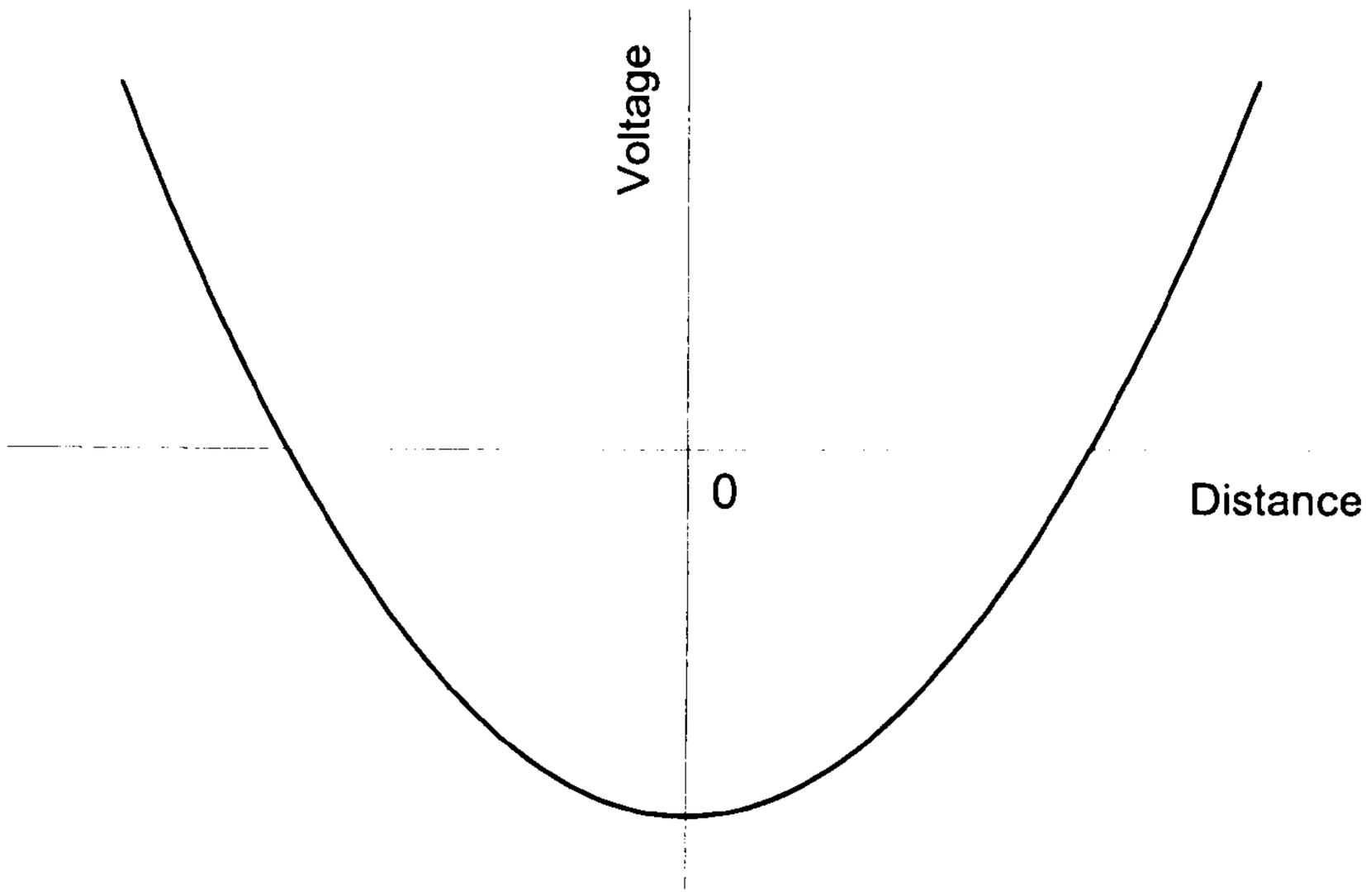

Figure 3.4 Variation of intracellular and extracellular potential with distance from axis of rotating magnets

Grounding of the extracellular fluid was expected to cause the extracellular potential to differ from that shown in Figure 3.4. In the mechanism of the non-invasive anaesthesia technique, it was hypothesised that the movement of negative ions towards ground would cause the extracellular potential to become more positive at the point at which the extracellular fluid is connected to earth. Due to the finite resistance of the extracellular electrolyte and the skin/ground electrode interface, the extracellular potential would not be equal to earth potential. Calculation of the distribution of charge in the extracellular fluid is non-trivial, since it is dependent on the resistance of the many different conducting paths through the complex volume conductor of the patient's limb. However, the intracellular potential will be unaffected by the grounding of the extracellular fluid and will have an axial distribution similar to that shown in Figure 3.4.

A possible distribution of membrane potential along the axis of a nerve fibre is shown in Figure 3.5. Three points along the axis of the nerve are defined in Figure 3.5. Points A and C are at a position corresponding to the circumference of the rotating magnets, while point B corresponds to the axis of the magnet. It is assumed that the magnetic field is zero at radial distances greater than points A and C. The membrane potential at point B, defined as the difference between intracellular and extracellular potentials, is more negative than the resting potential V_r due to the accumulation of intracellular negative charge and the absence of extracellular negative charge caused by the grounding of the extracellular fluid. At points A and C, membrane potential is equal to the membrane resting potential if the accumulation of positive charge is assumed to

be equal in the intracellular and extracellular media. Membrane potential at intermediate points between A, B and C is determined by the properties of the extracellular volume conductor and Figure 3.5 attempts only to show an estimate of how it may be distributed.

The hyperpolarising extracellular potential was modelled by a voltage distribution as shown in Figure 3.6. At points A and C, the applied extracellular voltage is zero. The maximum applied extracellular potential is at point B and there is a linear variation in potential between points A and B and between points B and C. The membrane potential which results from this applied extracellular voltage distribution is shown in Figure 3.7. Comparison of Figures 3.5 and 3.7 shows that the peak hyperpolarisation of the membrane occurs in the central region of both voltage distributions. The most significant difference between these two distributions of membrane potential is that the simulated membrane potential of Figure 3.7 exhibits two depolarised regions at distances corresponding to points A and C of Figure 3.4. The depolarised regions are a consequence of applying a hyperpolarising extracellular voltage and it is not possible to apply an extracellular potential which entirely eliminates these regions of depolarisation [6]. However, the extracellular voltage profile shown in Figure 3.6 minimises the spatial extent of the depolarised regions and thus prevents these regions from blocking the conduction of action potentials.

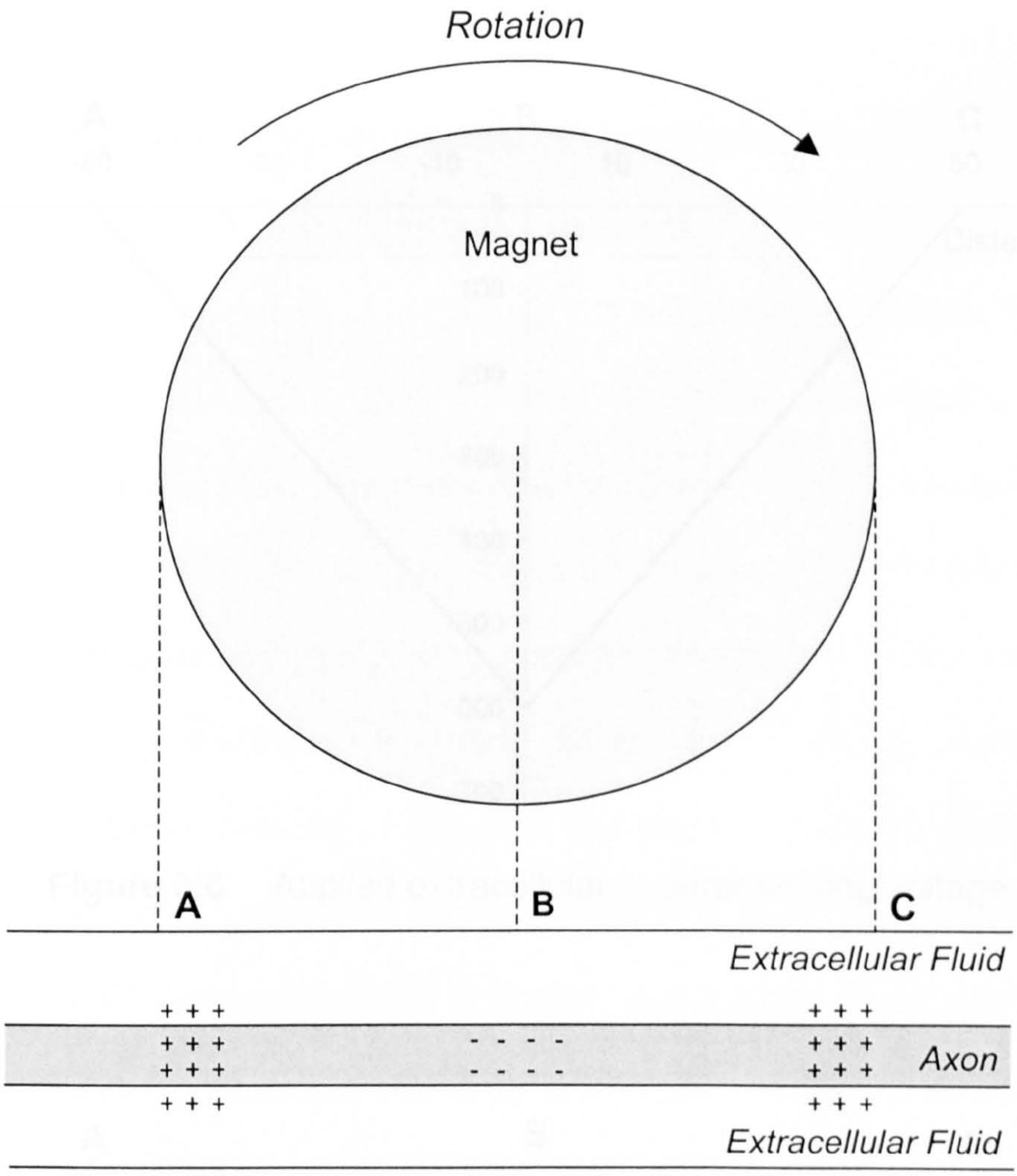

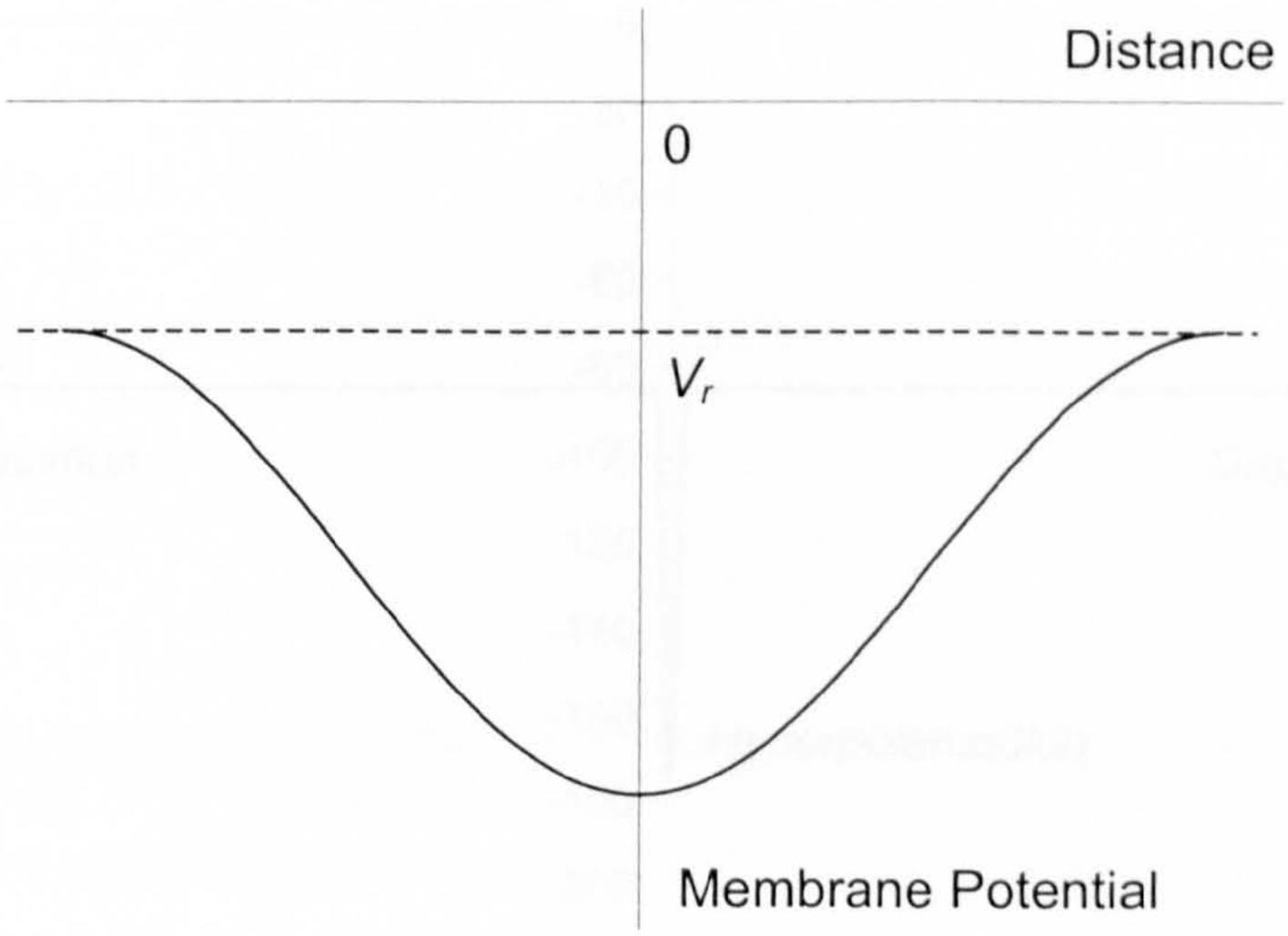

Figure 3.5 Possible distribution of membrane potential due to rotating magnetic field

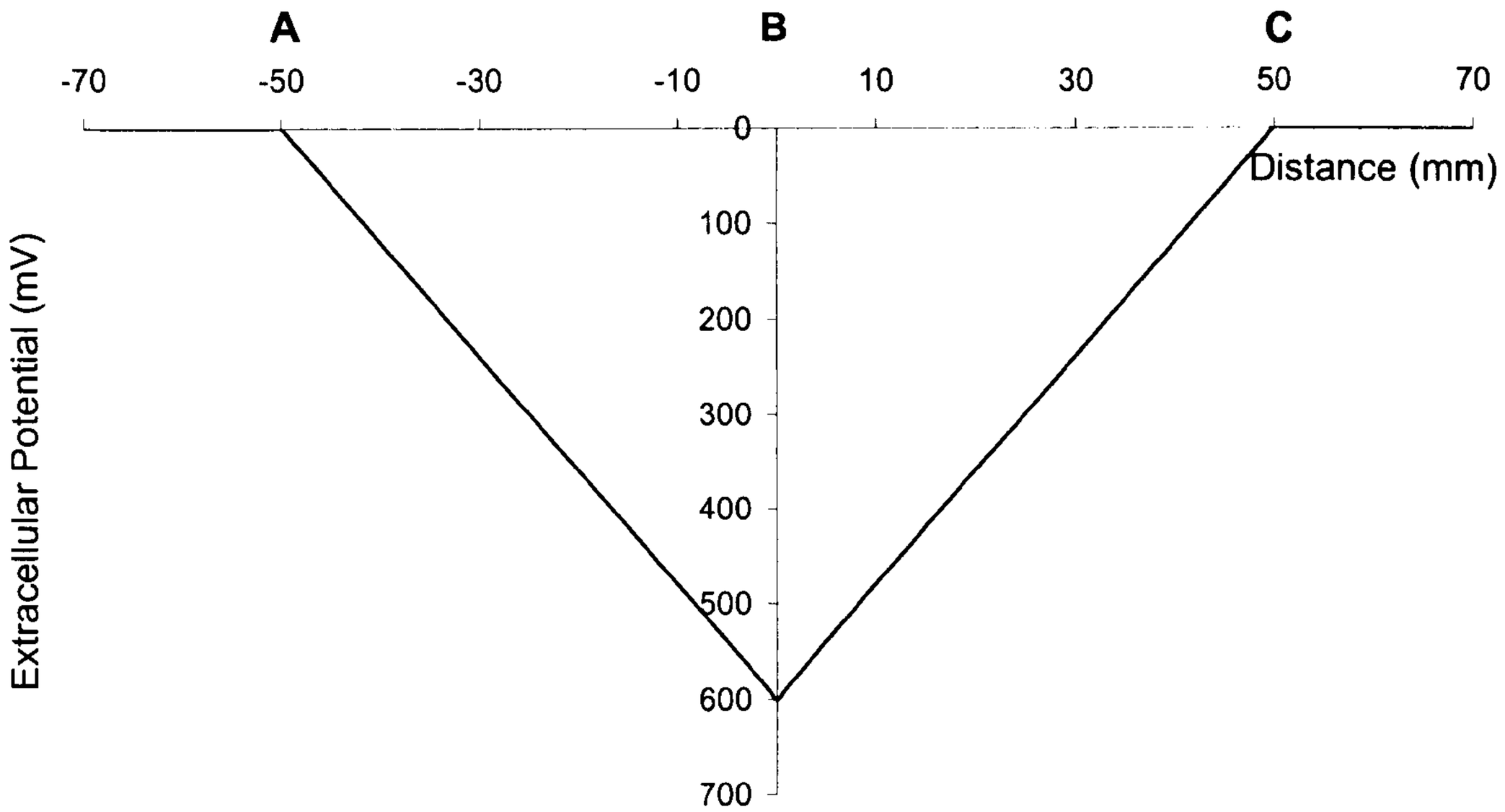

Figure 3.6 Applied extracellular hyperpolarising voltage

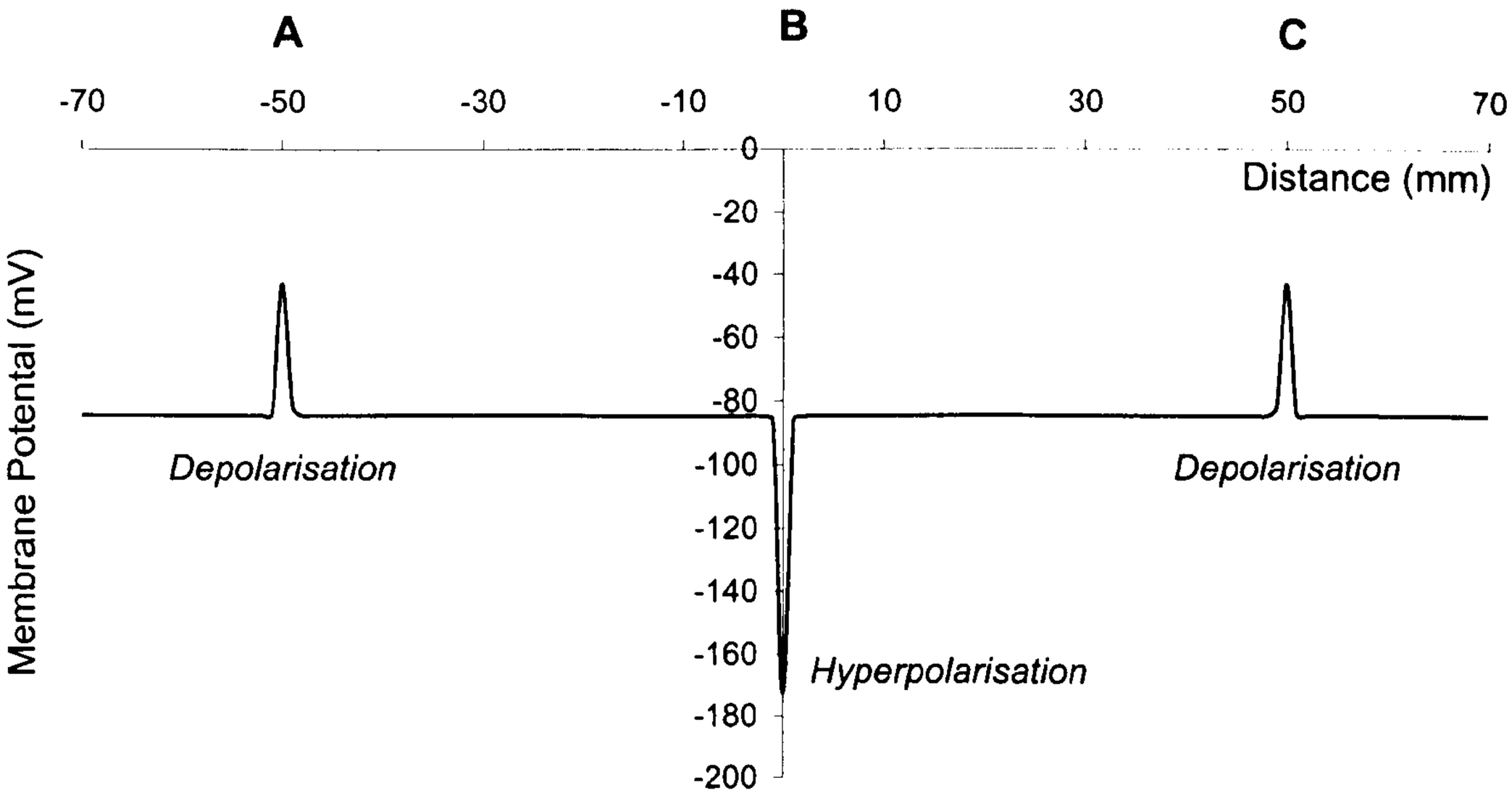

Figure 3.7 Membrane potential due to applied extracellular voltage

3.3.1. Method of Computer Simulation

The nerve fibres that carry information regarding painful stimuli are typically unmyelinated or myelinated fibres with diameters in the range of 1-4 μm [7]. Furthermore, it was established in Section 2.2 that the length of the myelinated internodal region between adjacent nodes of Ranvier is proportional to the diameter of the nerve fibre. Therefore, the simulation of either an unmyelinated fibre or a myelinated fibre of small diameter involves the calculation of non-linear ionic conductances at a greater number of simulated nodes than for the same length of a larger diameter fibre. To minimise computational requirements, it was decided to simulate the effect of hyperpolarisation upon large diameter nerve fibres and to extrapolate these results to ascertain the effects on nerve fibres of smaller diameter. Simulations were performed for nerve fibres with diameters in the 10-20 μm range, which corresponds to the diameters of large afferent fibres such as those carrying information from receptors on muscle spindles [7]. Since the model of a myelinated nerve fibre also assumes that the length of the node of Ranvier has a fixed length of 1 μm, the decision to simulate larger nerve fibres also avoids any inconsistencies which may arise if the nodal length is comparable to fibre diameter.

An extracellular electric field with an axial distribution of the form shown in Figure 3.6 was used to produce hyperpolarisation of the simulated nerve fibre. In all simulations, the length of the region experiencing an extracellular field (AC in Figure 3.6) was chosen to be 10 cm, which is equal to the diameter of the magnets of the experimental apparatus described in Section 3.4. A 10 cm

length of nerve fibre corresponds to 50 simulated nodes of a 20 μm fibre, or 100 nodes of a 10 μm fibre. To prevent errors due to the effect of the boundary conditions (equations (2.26) and (2.27)) on a finite length of fibre, a length of fibre consisting of at least twice the minimum necessary number of nodes was simulated. Hence, 101 nodes of a 20 μm fibre and 201 nodes of a 10 μm fibre were simulated. It was estimated that the error due to limiting the length of the simulated nerve fibre to twice the minimum number of nodes was less than 1% in the case of a 20 μm fibre.

To assess whether the applied hyperpolarisation was sufficient to block action potentials, an action potential was elicited by a depolarising current pulse of 0.1 ms duration situated a distance of five nodes from the boundary. The amplitude of this current pulse was 110% of the threshold amplitude for a fibre of a given diameter. In some cases, the depolarised regions that were created as a side-effect of the applied hyperpolarisation were sufficient to elicit an action potential. To minimise the effect of the refractory period associated with these action potentials on the conduction properties of the nerve fibre, the current pulse was produced 5 seconds after the application of the hyperpolarising stimulus. The error due to refractoriness was estimated to be less than 1% for a fibre of 20 μm diameter.

Simulated action potential voltage waveforms were observed using the graphical interface of the simulation software. Action potentials that did not propagate past the end of the hyperpolarised region were judged to be blocked. By an iterative process, the peak magnitude of the applied hyperpolarising

voltage was adjusted until the threshold value necessary to block the conduction of action potentials was determined.

3.3.2 Results of Computer Simulation

The threshold peak applied hyperpolarising voltage necessary to block action potentials and the membrane potential at the centre of the depolarised region are presented in Table 3.1.

Fibre diameter (μm)	Threshold peak applied hyperpolarising voltage (mV)	Threshold membrane potential at centre of hyperpolarised region (mV)
10.0	-1176	-127
12.5	-940	-127
15.0	-785	-127
17.5	-675	-127
20.0	-591	-127

Table 3.1 Threshold applied hyperpolarising voltages and membrane potentials

The variation of the threshold applied hyperpolarising voltage with fibre diameter, extrapolated to include fibres of smaller diameters, is plotted in Figure 3.8. This graph shows that there is an inverse relationship between the applied hyperpolarising voltage and nerve fibre diameter. For small fibres of less than 4 μm diameter, such as those carrying information from pain receptors, it is estimated that applied voltages in excess of approximately 2 volts are necessary to cause threshold hyperpolarisation.

Despite the inverse relationship between the threshold applied hyperpolarising voltage and nerve fibre diameter, it is interesting to note that the threshold membrane potential at the centre of the hyperpolarised region has a value of

–127 mV and is independent of fibre diameter. Therefore, a hyperpolarisation of –127 mV is sufficient to prevent the conduction of action potentials in fibres of all diameters, including the small diameter fibres that carry pain information and were not simulated here.

Figure 3.8 Variation of threshold applied hyperpolarising voltage with nerve fibre diameter

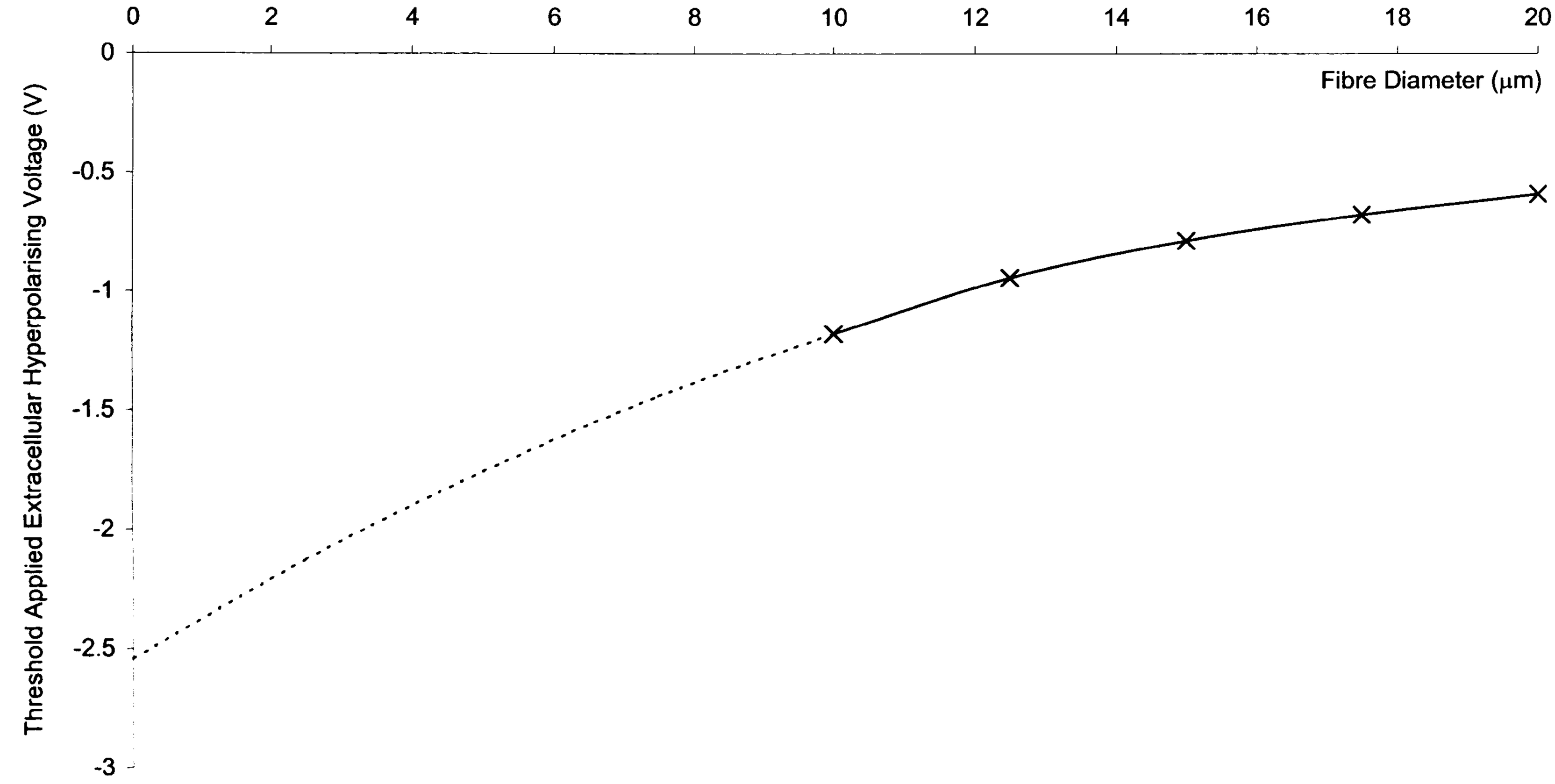

3.4. Experiments with Rotating Magnets

To test the hypothesis that a rotating magnetic field can produce an anaesthetic effect, a series of experiments with rotating permanent magnets, including an *in vivo* experiment, were conducted.

3.4.1. Apparatus

An experimental apparatus of the form shown in Figure 3.1 was constructed. The apparatus consisted of two cylindrical permanent magnets, positioned so that opposite magnetic poles faced each other. These magnets each had a diameter of 10 cm and a relatively uniform flux density of 0.4 Tesla over the entire area of their pole faces. The magnets were made from an electrically conducting material. The separation of the two magnets was adjustable, allowing conductors with a wide range of diameters to be placed into the gap between the magnets. At its largest extent, this gap was sufficient for a human forearm to be placed between the magnets.

The magnets were able to rotate in the same direction and with the same angular speed about their common axis by means of a gearing mechanism. Rotation was achieved by a three-phase motor with a power of 4 kW per phase. An electronic controller allowed the speed of rotation to be adjusted between zero and in excess of 2000 revolutions per minute.

An technical drawing of the apparatus is presented in Figure A1 (Appendix 1).

3.4.2. Experimental Method

Three experiments were performed with the rotating magnet apparatus. The first two experiments were designed to assess the feasibility of inducing a potential difference along the axis of a conductor placed between the poles of the rotating magnets. The final experiment was an *in vivo* experiment to test the hypothesis that the spinning magnetic field can produce an anaesthetic effect by preventing the conduction of action potentials in nerve fibres.

(a) The potential difference between the axis and circumference of the magnets was measured by placing the probes of a digital voltmeter (Fluke 73 Series III) directly onto the magnet, as shown in Figure 3.9. When the magnets were rotated, the voltmeter probes were held in a stationary position whilst maintaining contact with the pole face of the magnet, thus acting as a simple form of commutator. The radial voltage was measured when the magnets were stationary and when rotating at 2000 revolutions per minute.

(b) A length of copper wire was placed in the centre of the gap between the magnets, as illustrated in Figure 3.10. The wire was positioned so that its centre intersected the axis of the magnets. The potential difference between the centre and end of the wire was measured with the digital voltmeter while the magnets were rotated at an angular speed of 2000 revolutions per minute.

(c) The index finger of a human volunteer was positioned in the gap between the stationary magnets. The finger was connected to earth at its intersection

with the axis of the magnets by means of an EEG electrode placed on the skin. A repetitive mechanical stimulus was applied to the fingertip and the volunteer was asked to report any changes in his perception of the stimulus as the speed of rotation of the magnets was increased to 2000 revolutions per minute.

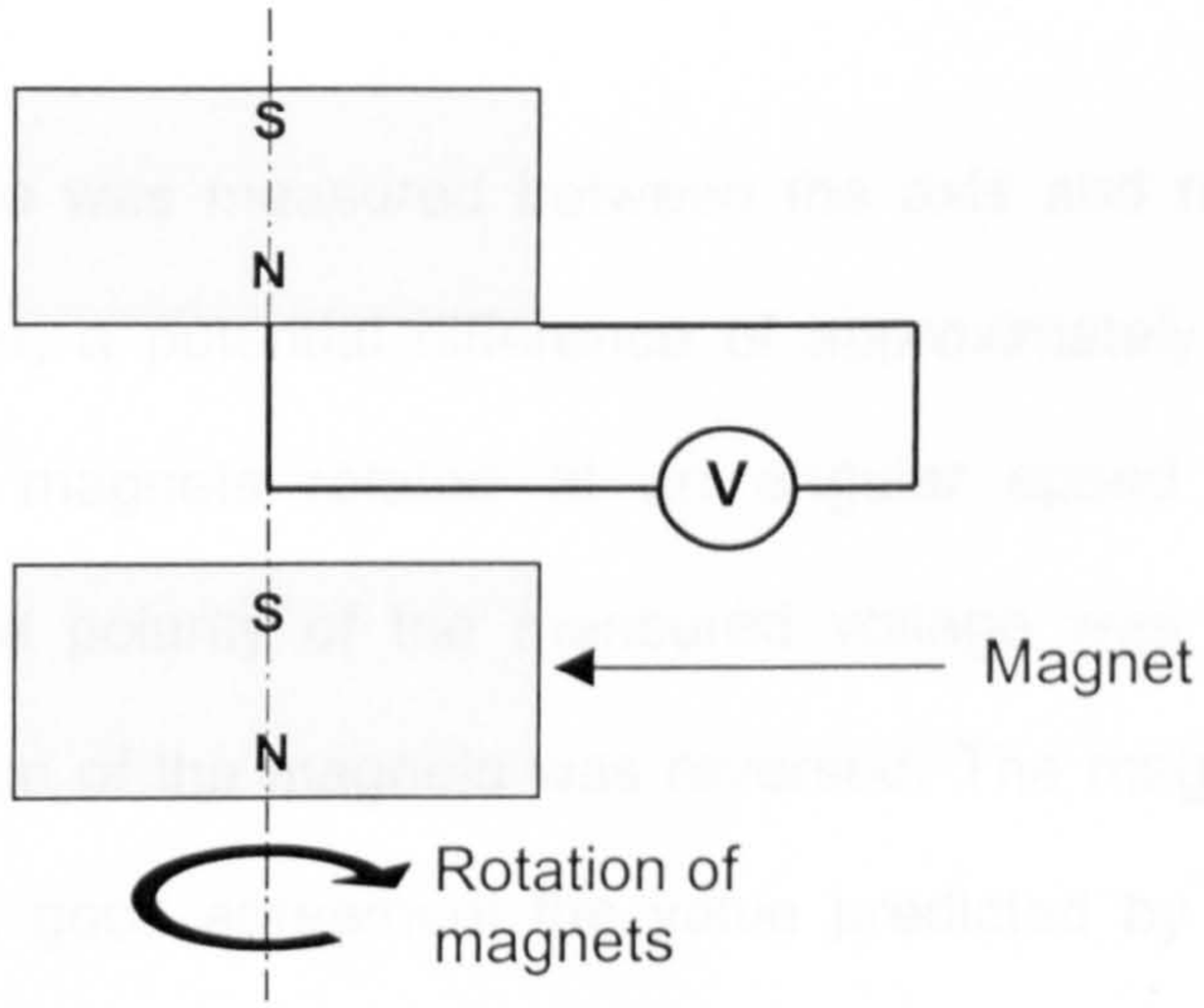

Figure 3.9 Measurement of an EMF between the axis and circumference of a rotating magnet

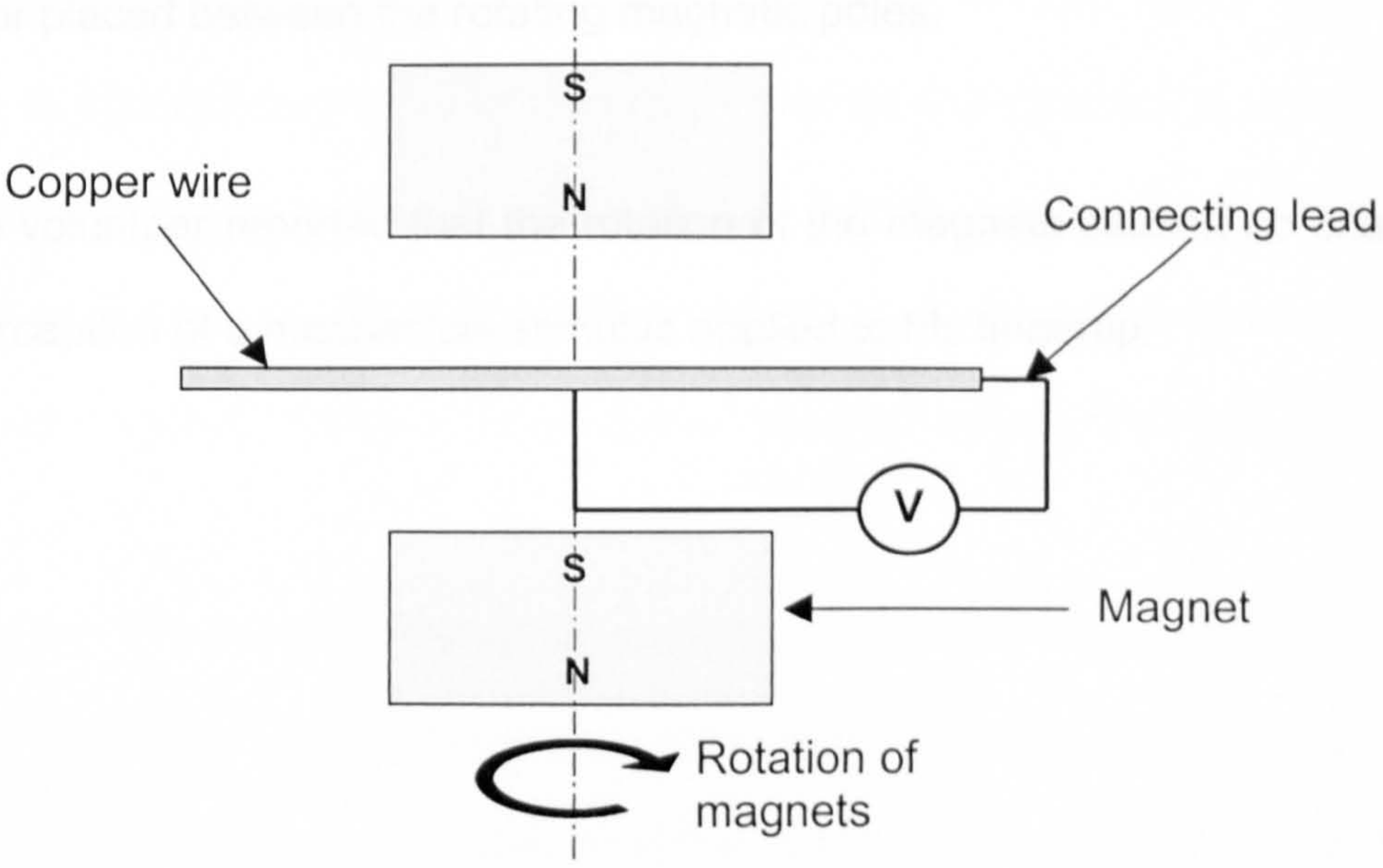

Figure 3.10 Measurement of an EMF in a conductor placed between rotating magnetic poles

3.4.3. Results

(a) No potential difference was measured between the axis and rim of the stationary magnet. However, a potential difference of approximately 100 mV was measured when the magnets rotated at an angular speed of 2000 revolutions per minute. The polarity of the measured voltage was reversed when the direction of rotation of the magnets was reversed. The magnitude of the measured voltage is in good agreement the value predicted by equation (3.7).

(b) No potential difference was measured between the centre and end of a conductor placed between the rotating magnetic poles.

(c) The volunteer reported that the rotation of the magnets caused no change in his perception of a mechanical stimulus applied to his fingertip.

3.5. Discussion

The computer simulation demonstrated that the conduction of action potentials can be prevented by the hyperpolarisation of nerve fibres. For the applied hyperpolarising voltage distribution used in this simulation, blocking of action potentials was achieved when the membrane potential was reduced to –127 mV. This represents an additional polarisation of approximately 42 mV beyond the membrane resting potential of –84.8 mV.

Creating a hyperpolarisation of 42 mV by any non-invasive method will be difficult to achieve in practice. To produce this additional potential difference between the intracellular and extracellular regions of the nerve fibre, an increase in intracellular negative charge as well as the discharge of negative ions in the extracellular fluid is necessary. It will be argued later within this section that it is impossible to achieve either a significant redistribution of intracellular charge or a flow of ions between the extracellular fluid and ground.

It is likely that the axial distribution of membrane and extracellular potentials will affect the threshold hyperpolarisation necessary to block the conduction of action potentials. It has been shown that the threshold stimulus amplitude for a nerve fibre stimulated by an extracellular electric field is determined by the second derivative of the extracellular voltage with respect to the distance along the axis of the fibre (i.e. d^2V/dx^2) [8]. It is probable that the threshold depolarisation will also exhibit some dependence upon the spatial characteristics of the intracellular and extracellular potentials. Thus, it may be

possible to optimise the size and position of the grounding electrode or to use rotating magnets with a non-uniform magnetic field to minimise the threshold membrane hyperpolarisation. However, it can be shown that the use of a rotating magnetic field to produce hyperpolarisation of nerve fibres is not feasible for other, more fundamental, reasons.

In Section 3.2 it was argued that charge carriers within a moving magnetic field experience a Lorentz force, which causes positive and negative ions to move in opposite directions. However, the hypothetical method of non-invasive anaesthesia failed to take into account that, in an open circuit with no steady state current flow, this redistribution of charge causes ions to experience a net electrostatic force. The electrostatic force opposes the Lorentz force and attempts to restore the original distribution of charge along the axis of the nerve fibre. In equilibrium, the condition that charge carriers experience no net force must always be satisfied at every point within the system. Therefore, the system will achieve equilibrium when the electrostatic force is equal and opposite to the Lorentz force.

The effect of the Lorentz force is to cause charge carriers to move by a very small distance, before a significant electrostatic force develops and opposes further carrier motion. Although there is some movement of ions, the formation of an electrostatic force prevents the large redistribution of charge along the axis of the nerve fibre that would be necessary for non-invasive anaesthesia. Furthermore, no net electric field is produced along the nerve fibre by the rotating magnets, since the electric field induced by the Lorentz force is

opposed by an equal electric field due to the electrostatic force. Hence, the axial distribution of voltage suggested in equation (3.7) is not induced by rotation of the magnets.

To illustrate that the rotating magnetic field has no significant effect on the distribution of ions within the nerve fibre and extracellular fluid, the distance moved by ions due to the Lorentz force may be estimated. In the absence of an applied force, the sum of the electrostatic forces exerted on any particular ion by the ions that surround it is equal to zero in order to satisfy the condition that ions experience no net force. However, the motion of ions due to the Lorentz force results in a change in the magnitude of the electrostatic force acting upon each ion. The system reaches equilibrium when the net electrostatic force created by the redistribution of charge is equal and opposite to the Lorentz force.

The electrostatic force between two charges Q_1 and Q_2, separated by a distance x in a medium of relative permittivity ε_r is calculated from [9]:

$$F_E = \frac{Q_1 Q_2}{4\pi\varepsilon_0\varepsilon_r x^2} \tag{3.8}$$

where ε_0 is the permittivity of free space and has a value of 8.854×10^{-12} F m^{-1}. For the purposes of this simple estimate, the relative permeability of the extracellular fluid is assumed to be 80, the value for pure water.

Although ions move randomly throughout the intracellular and extracellular electrolytes, the calculation is simplified by assuming ions to be located in a

cubic lattice prior to the application of the Lorentz force. This assumption allows the interionic distance x_0 (measured in nanometres) to be calculated from the equation [10]:

$$x_0 = 0.95c^{-1/3} \tag{3.9}$$

where c is the ionic concentration measured in moles per litre. To further simplify the calculation, the extracellular medium is approximated by 0.1 M sodium chloride solution, which corresponds to an interionic distance of 1.62 nm.

The redistribution of ions due to the Lorentz force is shown in Figure 3.11, where ions near the axis of the rotating magnets are assumed to move by a small distance δ_a, while ions at the circumference of the magnet move by distance δ_c. Ions located directly on the axis of the magnets or beyond the magnets' circumference are assumed to experience no motion. Since, from equations (3.2) and (3.5), the magnitude of the Lorentz force acting upon an ion is proportional to its distance from the axis of the magnets, δ_a is expected to be greater than δ_c.

It is not feasible to find an analytical expression for δ_a and δ_c due to the large numbers of interionic forces that must be taken into account and the complexity of the three-dimensional lattice of ions. Therefore, δ_a and δ_c were calculated numerically by an iterative process, such that the ions denoted by grey shading in Figure 3.11 experienced no net force. For the spinning magnet apparatus described in Section 3.4.1 with a flux density of 0.4 tesla, diameter of 10 cm and rotating at 2000 revolutions per minute, δ_a and δ_c are calculated as 5×10^{-15} m

and 2×10^{-7} m respectively. These values are insignificant in comparison to the length of the nerve fibre, and the distance moved by ions at the proposed site of hyperpolarisation is small even in comparison to the length of a node of Ranvier. Therefore, the distance moved by ions is of insufficient magnitude to cause the large axial redistribution of charge that would be required to hyperpolarise the nerve fibre.

The hypothetical mechanism of non-invasive anaesthesia also assumed that negative charge from the extracellular fluid would flow to earth when a grounded electrode was connected to the skin in the rotating magnetic field, causing the distribution of charge shown in Figure 3.3. However, it can be argued that the rotating magnetic field will not cause charge carriers to move towards ground. Consider a negatively charged ion at the centre of the extracellular fluid in Figure 3.2. In equilibrium, this ion will be acted upon by a Lorentz force and by an equal electrostatic force in the opposite direction. The electrostatic force is caused solely by the separation of negative charge at the centre of the extracellular fluid and positive charge in the peripheral regions. If the negatively charged ion under consideration were to move towards earth, as assumed by the hypothetical method of non-invasive anaesthesia, this would entail a further separation of charge and would therefore increase the electrostatic force acting upon the ion. This increase in the electrostatic force opposes any motion of the ion towards ground and thus prevents the discharge of anions required to induce the anaesthetic effect.

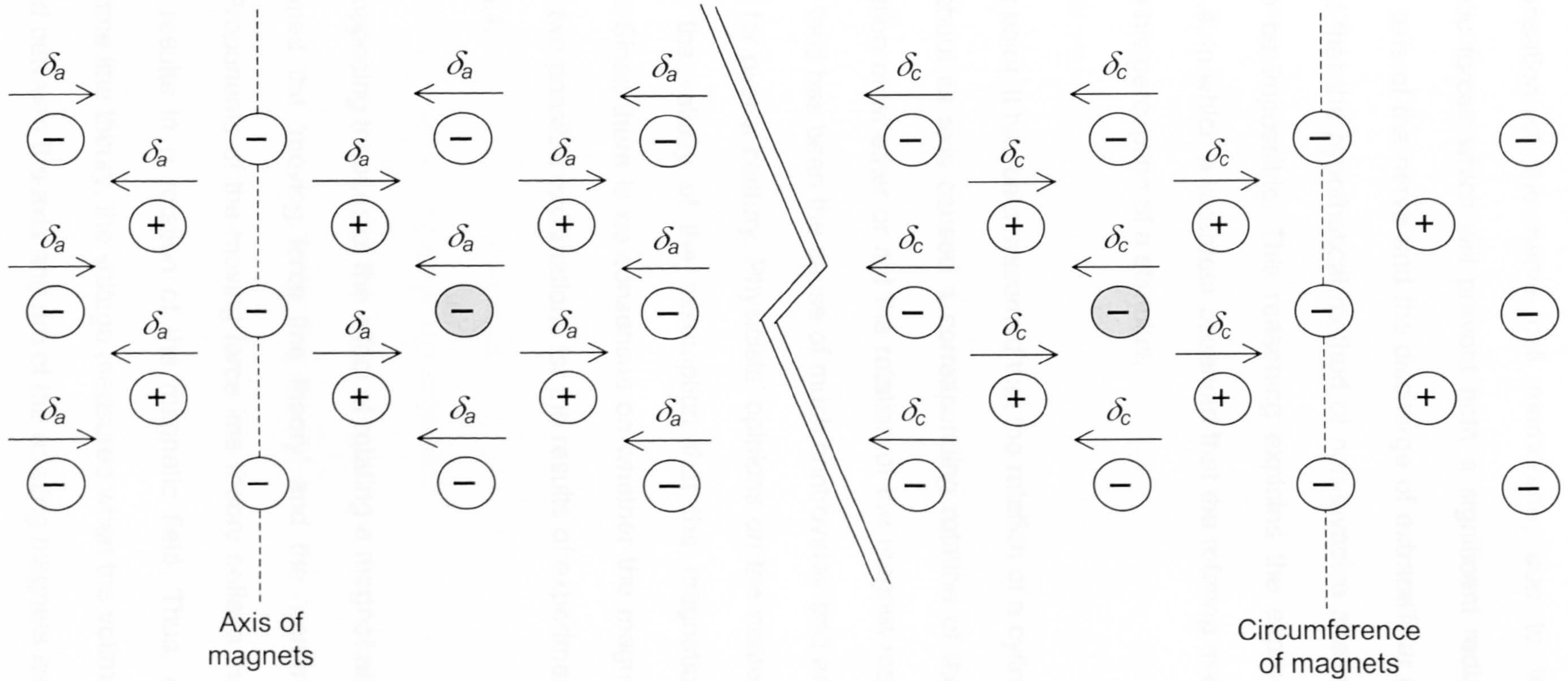

Figure 3.11 Calculation of ion motion due to a rotating magnetic field

Therefore, the proposed method of non-invasive anaesthesia is unable to cause hyperpolarisation of the nerve cell membrane, due to the existence of electrostatic forces which will prevent both a significant redistribution of ions along the axis of the nerve and the discharge of extracellular anions. It can be concluded that the hypothetical method of non-invasive anaesthesia has been proved to be impossible. This reasoning explains the experimental result of Section 3.4, in which a volunteer observed that the rotating magnets caused no change in his perception of a stimulus.

Up to this point, it has been assumed that the rotation of a cylindrical permanent magnet about its axis caused a corresponding rotation of the magnetic field. The question of whether or not the rotation of the magnet results in a rotating magnetic field has been the cause of much controversy and argument between scientists for over a century. Physicists' opinions on the matter are still divided and thus the validity of the assumption that the magnetic field rotates is uncertain. Since there is no consensus on whether the magnetic field rotates, there are two possible explanations for the results of experiments *(a)* and *(b)* of Section 3.4.

The two opposing theories of the effect of rotating a magnet about its axis have been named the 'moving force line theory' and the 'non-moving force line theory'. Proponents of the moving force line theory believe that rotation of the magnets results in a rotation of the magnetic field. Thus, according to the moving force line theory, the voltage measured when the voltmeter probes were connected between the axis and rim of the rotating magnets as shown in Figure

3.9 was induced by magnetic flux in the rotating magnetic field cutting the stationary measuring circuit. This situation is commonly described by stating that the seat of the electromotive force is in the measuring circuit.

Conversely, the non-moving force line theory states that the magnetic field remains stationary when the magnets are rotated. According to the non-moving force line theory, the voltage measured in the experiment of Figure 3.10 is due to the stationary magnetic flux being cut by the moving conducting material that constitutes the magnet. Proponents of the non-moving force line theory argue that the measuring circuit plays no role, other than as a means by which to measure the voltage that is induced in the magnets. In this case, the seat of the electromotive force is in the rotating magnets.

Similarly, there are also two possible explanations for the absence of a measured voltage when a conductor was placed between the rotating magnets as illustrated in Figure 3.10. According to the non-moving force line theory, there is no cutting of magnetic flux because there is no relative motion between the stationary magnetic field and the stationary conductor, hence no electromotive force is induced in the conductor. The moving force line theory suggests that although EMFs are induced within the conductor, their direction is such that no net EMF is induced in the circuit. As illustrated in Figure 3.12, according to the moving force line theory an EMF is induced in the copper wire. However, the connecting leads of the voltmeter are also cut by flux from the rotating magnets and thus an EMF is induced therein. The EMF induced within the copper wire is equal and opposite to that in the connecting leads and no net

electromotive force is measured in this circuit. Therefore, the results of this experiment are consistent with both the non-moving and moving force line theories.

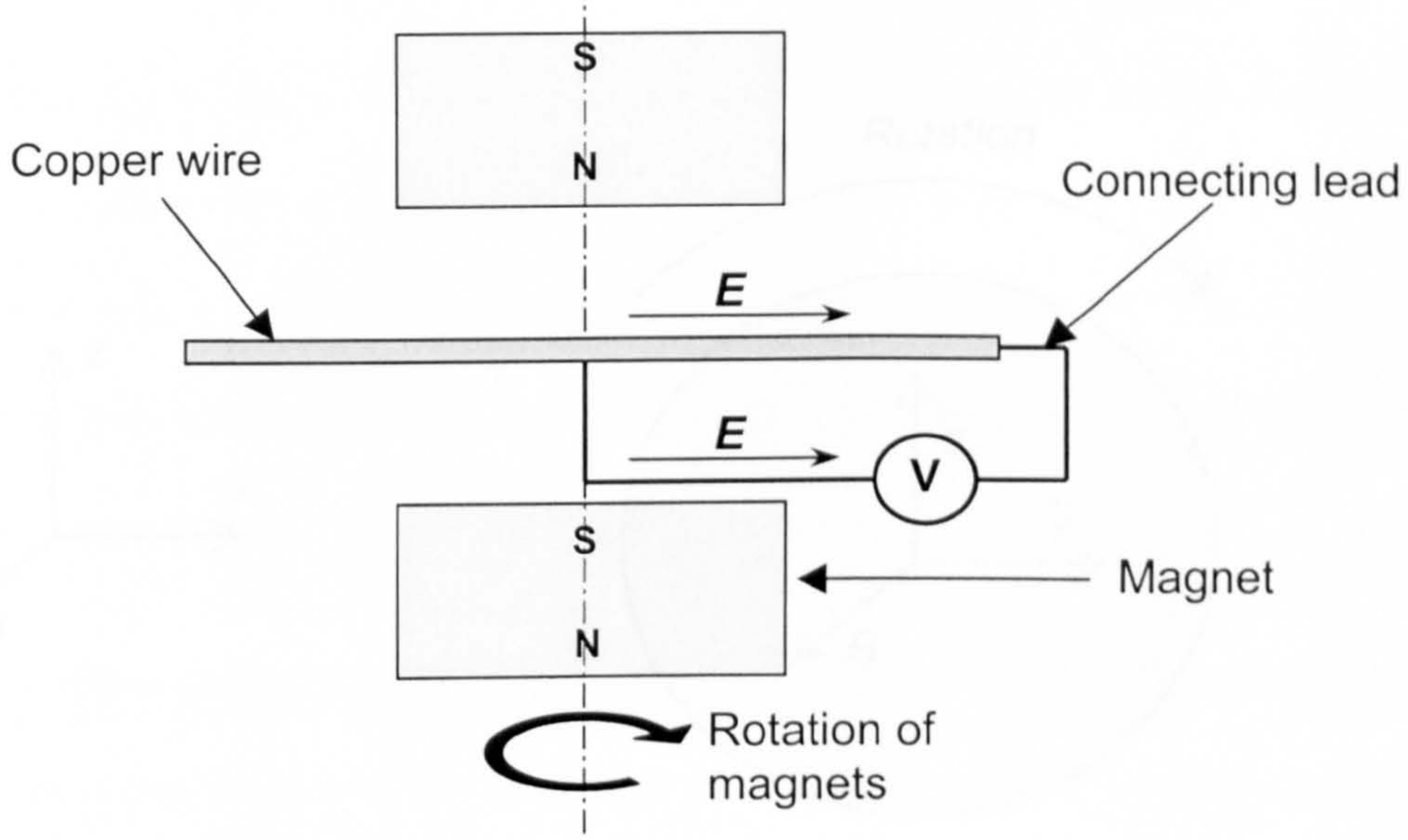

Figure 3.12 Cancellation of induced EMFs in a closed loop within a rotating magnetic field

The results of these experiments according to the moving force line theory may be expressed mathematically. Consider a simplified situation in which a cylindrical permanent magnet is rotating about the origin of a Cartesian coordinate system as shown in Figure 3.13. The magnet is assumed to have a uniform magnetic flux density of magnitude B that exists only in a direction parallel to the x axis and to rotate with angular frequency ω in the yz plane. The flux density $\boldsymbol{B}$ and velocity $\boldsymbol{v}_M$ of the magnetic field can be expressed in vector notation as:

$$\boldsymbol{B} = B\boldsymbol{i} \tag{3.10}$$

and

$$\boldsymbol{v}_M = \omega \bar{z}\,\boldsymbol{j} - \omega \bar{y}\,\boldsymbol{k} \tag{3.11}$$

where $\boldsymbol{i}$, $\boldsymbol{j}$ and $\boldsymbol{k}$ are unit vectors in the x, y and z directions respectively. $\bar{y}$ and $\bar{z}$ are displacements from the origin along the y and z axes respectively.

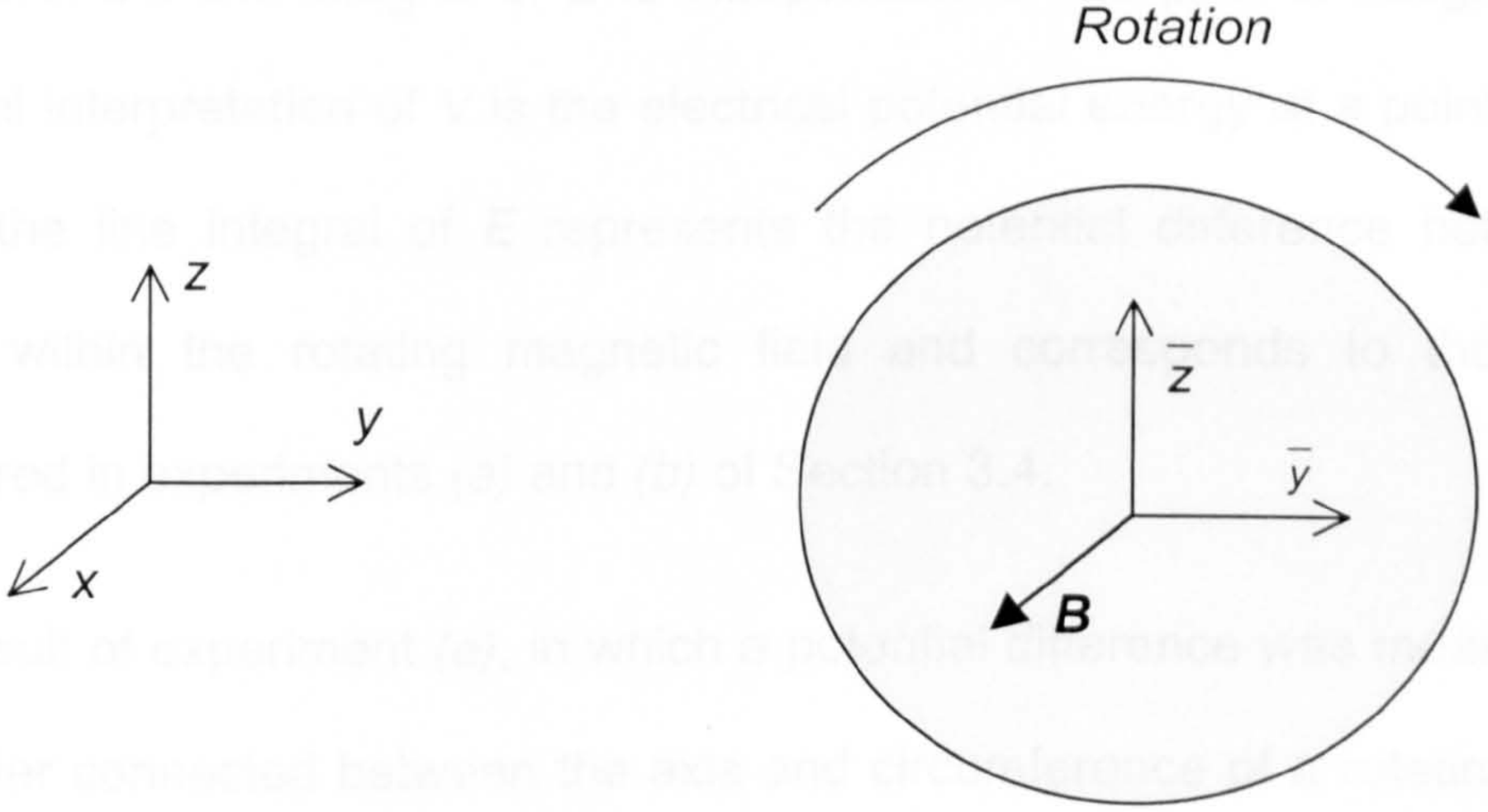

Figure 3.13 Generalised rotating magnet system

The electric field $\boldsymbol{E}$ at any point is:

$$\boldsymbol{E} = -\boldsymbol{v}_M \times \boldsymbol{B} = \omega\, \bar{y}\, B\, \boldsymbol{j} + \omega\, \bar{z}\, B\, \boldsymbol{k} \tag{3.12}$$

The line integral of the electric field between two points is independent of the path of integration if the vector $\boldsymbol{E}$ is the gradient of some scalar function, V [11]. If the integral is independent of path, the line integral of $\boldsymbol{E}$ between two points is evaluated as the difference of the values of V at those points, i.e.

$$\int_B^A \boldsymbol{E}(l)\, dl = V(A) - V(B) \tag{3.13}$$

where the line integral is calculated over path l, which has endpoints A and B.

Inspection of equation (3.12) reveals that ***E*** is the gradient of a scalar function V, where:

$$V = \tfrac{1}{2}\omega B(\bar{y}^2 + \bar{z}^2) \tag{3.14}$$

Therefore, the line integral of ***E*** is independent of the path of integration. The physical interpretation of V is the electrical potential energy at a point in space. Thus, the line integral of ***E*** represents the potential difference between two points within the rotating magnetic field and corresponds to the voltages measured in experiments *(a)* and *(b)* of Section 3.4.

The result of experiment *(a)*, in which a potential difference was measured by a voltmeter connected between the axis and circumference of a rotating magnet, is confirmed by evaluation of equation (3.13). If the magnetic field is assumed to rotate with the permanent magnets, only those charge carriers which experience motion relative to the magnetic field are acted upon by the Lorentz force. Therefore, an EMF is induced in the path of the stationary measuring circuit, which exists between the origin of the coordinate system at the centre of the magnet and a point r on the circumference of the magnet. The magnitude of the induced EMF is calculated as:

$$\int_0^r \boldsymbol{E}(l)\, dl = \tfrac{1}{2} r^2 \omega B \tag{3.15}$$

Equation (3.15) is equivalent to equation (3.7) and agrees with the experimental observation that a finite potential difference was measured by a voltmeter placed across a rotating magnet.

In experiment *(b)*, no potential difference was measured by a stationary voltmeter connected across a stationary conductor placed between the rotating magnets. In this case, a complete circuit is cut by magnetic flux and an EMF is induced in all parts of the circuit. Therefore, the voltmeter measures the line integral of the electric field around a closed path, in which the starting point, *s*, of the path is identical to its endpoint *e*. Evaluation of equation (3.13) yields:

$$\int_s^e \boldsymbol{E}(l)\, dl = V(e) - V(s) \tag{3.16}$$

Since points *e* and *s* are identical,

$$V(e) = V(s) \tag{3.17}$$

Therefore:

$$\int_s^e \boldsymbol{E}(l)\, dl = 0 \tag{3.18}$$

Equation (3.18) confirms the absence of a measured potential difference in experiment *(b)*.

Although solving the puzzle of the moving force line theory is beyond the scope of this thesis, it is of interest to briefly review the history of the problem. The first experiments upon a magnet rotating about its axis were performed in 1851 by Michael Faraday [12]. Faraday measured the current produced between the edge and axis of a permanent bar magnet when either the magnet, the measuring circuit or both the magnet and measuring circuit were rotated. He observed a flow of current when the magnets rotated with respect to the stationary measuring circuit and when the measuring circuit rotated with respect to the stationary magnets. In the case of the simultaneous rotation of both the current and the measuring circuit, no current flow was measured. Faraday

suggested that his experiments were unable to distinguish whether the seat of the EMF was in the conductor or in the measuring circuit.

In the early part of the twentieth century, there was a prolonged and heated scientific debate on this topic between Kennard and Barnett. Kennard performed experiments with a rotating steel bar inside a stationary solenoid and concluded that he had disproved the moving force line theory [13]. Barnett refuted this conclusion and suggested that Kennard's experiments were incapable of distinguishing between the two hypotheses [14]. Despite publishing many papers on this subject and generating much interest within the scientific community, neither of these scientists was able to conclusively prove or disprove the moving force line theory.

At around the same time as the discourse between Kennard and Barnett, Pegram performed experiments upon a rotating solenoid and was confident that he had disproved the moving force line theory [15]. However, in 1975 Djuric claimed that one of Pegram's results was erroneous [16]. Djuric also agreed with Barnett's opinion that Kennard's experiments were inconclusive. In 1963, Das Gupta experimented upon permanent magnets and concluded that rotation of the magnets did not result in rotation of the magnetic field [17]. However, a recent paper by Kelly [18] in which the author claimed to have proved the moving force line theory demonstrates that this is still a controversial topic, even 150 years after Faraday reported the first experiments.

Clearly, because of the divided opinion of scientists on the subject of rotating magnetic fields, it is impossible to state with certainty that the rotating magnets in the non-invasive anaesthesia apparatus will have any effect upon ions within a patient's nerve fibres. However, it has already been argued that, if the moving force line theory is correct, the rotating magnetic field would be unable to produce the hyperpolarisation of the nerve cell necessary for non-invasive anaesthesia. Alternatively, if the non-moving force line theory is correct, then charge carriers would not experience the Lorentz force that is required by the hypothetical mechanism of non-invasive anaesthesia, since there is no relative motion between the magnetic field and charge carriers. Therefore, the question of whether or not the moving force line theory is correct has no bearing on the conclusion that an anaesthetic effect cannot be produced by the use of a rotating magnetic field.

3.6. References

1. Andrews, B.J. and Kooi, B.B.J.
   Localized Electrical Nerve Blocking.
   18th Annual International Conference of the IEEE Engineering in Medicine and Biology Society, 1996, pp. 347-348.
2. Ions, G.K.
   A Device for Inducing Anaesthesia.
   Patent Application PCT/GB98/01676, 1998.
3. Duffin, W.J.
   Electricity and Magnetism, Third Edition.
   McGraw-Hill, 1980.
4. Ferris, C.D.
   Electric Shock.
   (in The Electronics Handbook, Whitaker, J.C. (Ed.))
   CRC Press/IEEE Press, 1996, pp. 2197-2203
5. McNeal, D.R.
   Analysis of a Model for Excitation of a Myelinated Nerve.
   IEEE Transactions on Biomedical Engineering, Vol. 23, 1976, pp. 329-337.
6. Barr, R.C.
   Basic Electrophysiology.
   (in The Biomedical Engineering Handbook, Bronzino, J.D. (Ed.))
   CRC Press/IEEE Press, 1995, pp. 101-118.
7. Aidley, D.J.
   The Physiology of Excitable Cells, Third Edition.
   Cambridge University Press, 1989.
8. Rattay, F.
   Analysis of Models for External Simulation of Axons.
   IEEE Transactions on Biomedical Engineering, Vol. 33, 1986, pp. 974-977.

9. Carter, R.G.

Electromagnetism for Electronic Engineers, Second Edition.

Chapman & Hall, 1992.

10. Pethig, R.

Dielectric and Electronic Properties of Biological Materials.

Wiley, 1979.

11. Kreyszig, E.

Advanced Engineering Mathematics, Seventh Edition.

Wiley, 1993.

12. Faraday, M.

Faraday's Diary (Martin, T. (Ed.))

Bell, 1934, Vol. V, pp. 392-411.

13. Kennard, E.H.

Unipolar Induction.

Philosophical Magazine, Vol. 23, 1912, pp. 937-941.

14. Barnett, S.J.

On Electromagnetic Induction.

Physical Review, Vol.2, 1913, pp. 323-326.

15. Pegram, G.B.

Unipolar Induction and Electron Theory.

Physical Review, Vol. 10, 1917, pp. 591-600.

16. Djuric, J.

Spinning Magnetic Fields.

Journal of Applied Physics, Vol. 46, 1975, pp. 679-688.

17. Das Gupta, A.K.

Unipolar Machines. Association of the Magnetic Field with the Field-Producing Magnet.

American Journal of Physics, Vol. 32, 1963, pp. 428-430.

18. Kelly, A.G.

Experiments on Unipolar Induction.

Physics Essays, Vol. 12, 1999, pp. 372-382.

4. NON-INVASIVE ANAESTHESIA BY A STATIC AXIAL MAGNETIC FIELD

Another method by which it was hypothesised that non-invasive anaesthesia may be achieved was to use a magnetic field directed along the axis of the nerve. It was expected that a sufficiently strong magnetic field could affect the motion of sodium ions entering a nerve fibre during the depolarisation stage of an action potential, and this disruption of the influx of sodium ions may prevent the transmission of pain signals along the nerve fibre.

4.1. Effect of a Magnetic Field on the Motion of a Charged Particle

When a magnetic field $\boldsymbol{B}$, is applied orthogonally to the direction of motion of a particle of mass m, charge Q and velocity $\boldsymbol{v}$, the particle experiences a Lorentz force in a direction perpendicular to that of both the particle motion and the magnetic field:

$$\boldsymbol{F} = Q(\boldsymbol{v} \times \boldsymbol{B}) \qquad (3.1)$$

For any particle moving in a circular path of radius r, the centripetal force which acts in a direction perpendicular to the particle's direction of motion is calculated from the equation:

$$F = \frac{mv^2}{r} \qquad (4.1)$$

Equating (3.1) and (4.1) and rearranging gives:

$$r = \frac{mv}{QB} \tag{4.2}$$

That is, the force due to the magnetic field causes the charged particle to move in a circular path and the radius of this path is known as the Larmor radius (Figure 4.1). Equation (4.2) demonstrates that the Larmor radius is proportional to the particle velocity and is inversely proportional to the flux density of the magnetic field and the charge/mass ratio of the particle.

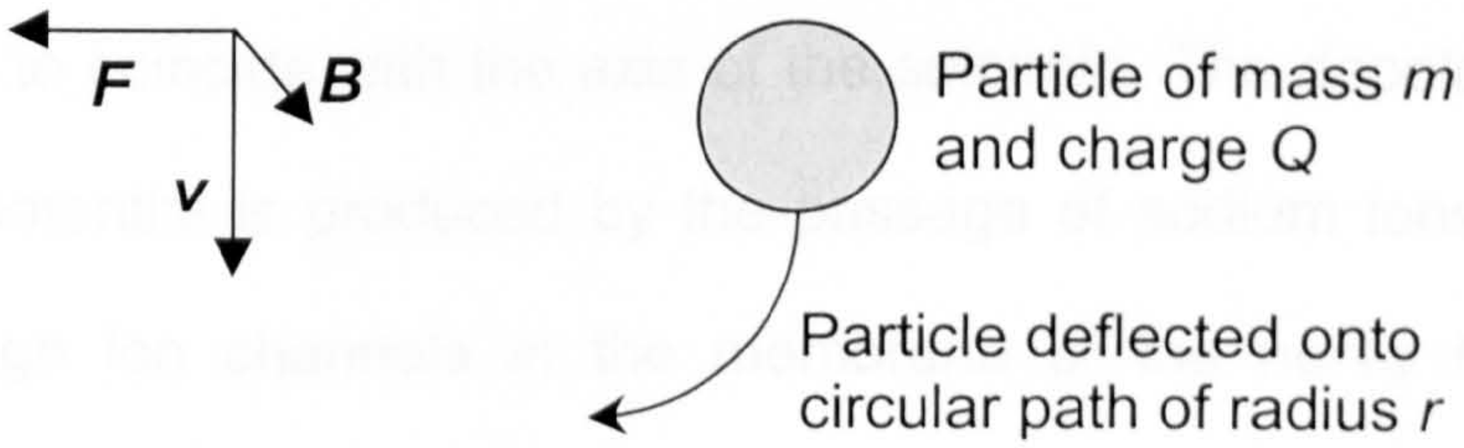

Figure 4.1 Effect of a magnetic field on the motion of a charged particle

4.2. Use of a Static Axial Magnetic Field to Block the Conduction of Action Potentials

It was hypothesised that a static magnetic field aligned along the axis of a nerve fibre could disrupt the propagation of action potentials and thus provide a non-invasive anaesthetic effect. Figure 4.2 shows the suggested implementation of this idea, in which a nerve fibre is placed within the centre of a cylindrical solenoid. The nerve fibre can be part of a peripheral nerve within a limb or part of the central nervous system within the spinal cord. A magnetic field will be created when a current is passed through the solenoid and in the central region of a sufficiently long solenoid the direction of this magnetic field can be considered to coincide with the axis of the solenoid. The depolarising phase of an action potential is produced by the passage of sodium ions into the nerve fibre, through ion channels in the membrane of the nerve fibre. If the ion channels are considered to be aligned in a radial direction (perpendicular to the axis of the nerve fibre), then it can be seen that all sodium ions entering the nerve fibre move in a direction perpendicular to the magnetic field (Figure 4.3).

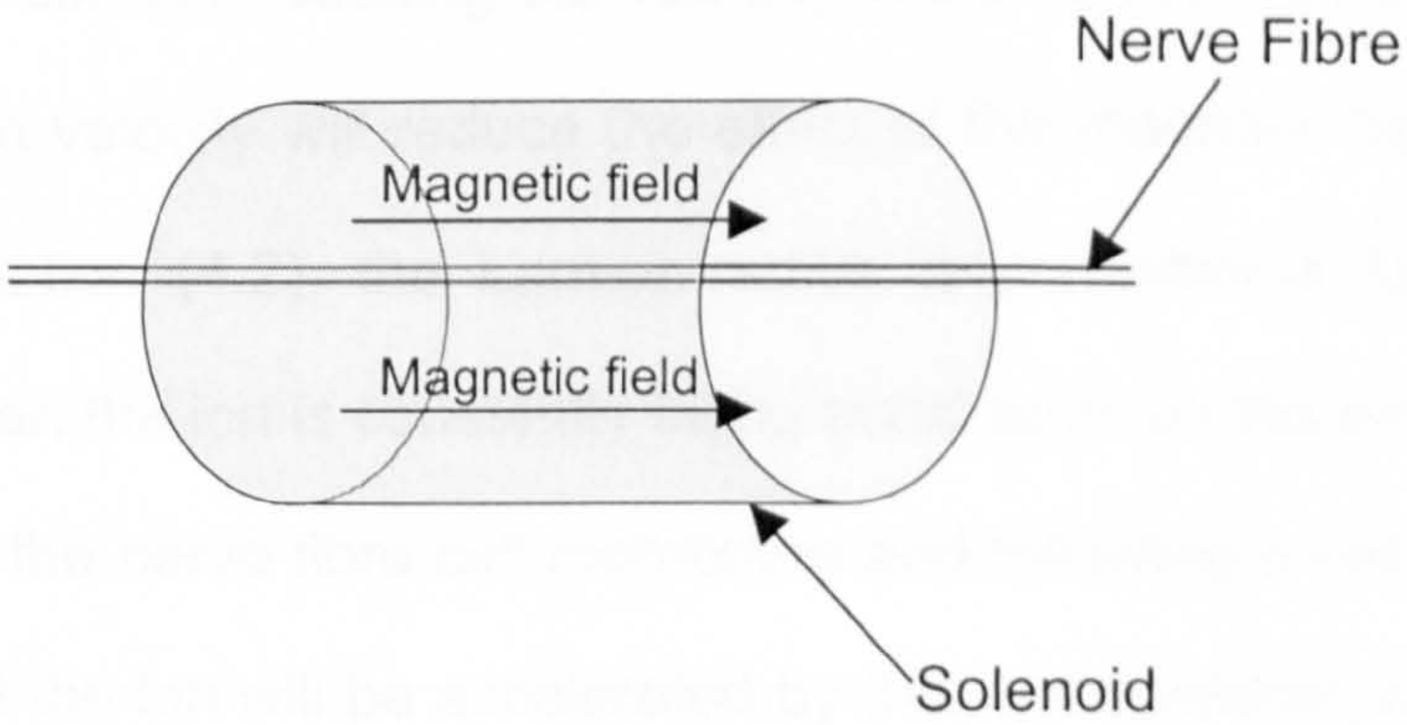

Figure 4.2 Nerve fibre within a solenoid

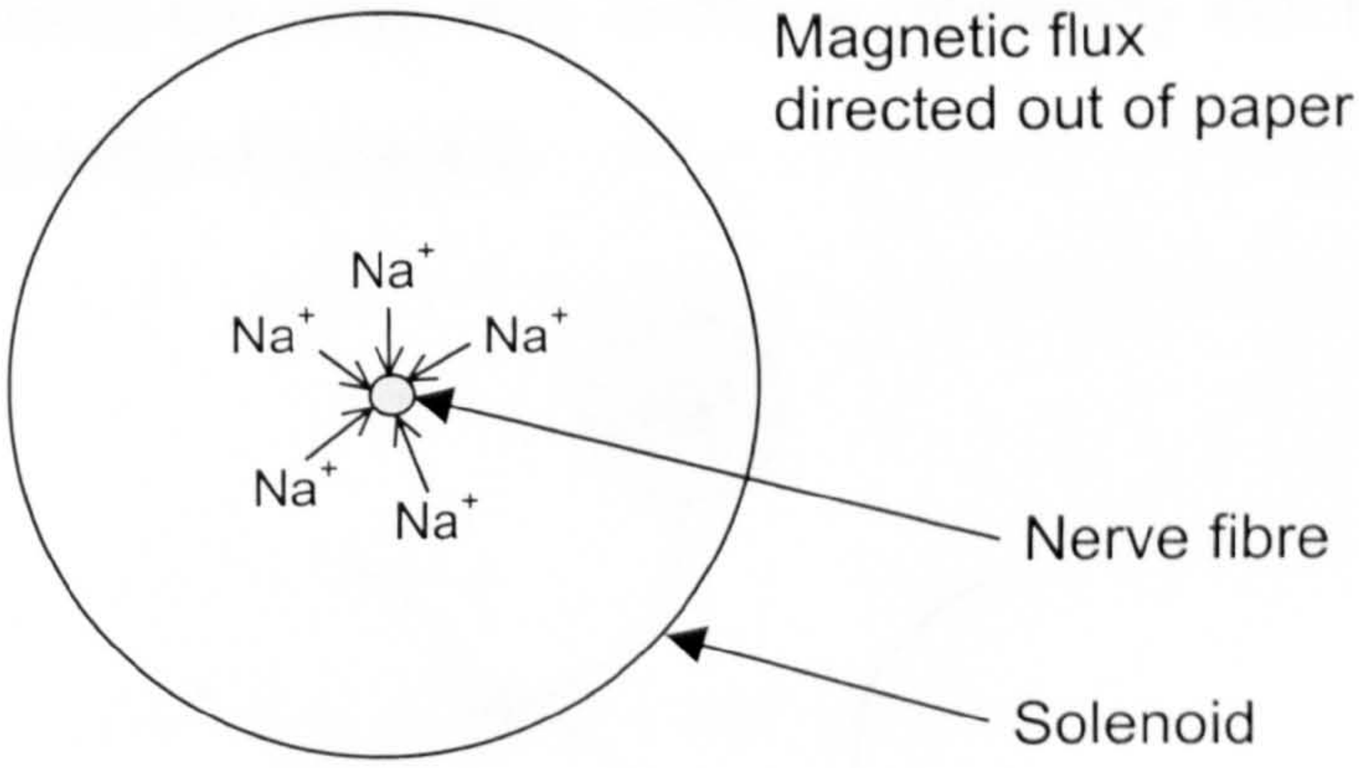

Figure 4.3 Influx of sodium ions into a nerve fibre

The arrangement illustrated in Figures 4.2 and 4.3 ensures that the magnetic field is approximately perpendicular to the direction of all sodium ions entering the nerve fibre, therefore the magnetic field should deflect the motion of sodium ions and cause them to follow a circular path as described in Section 4.1. If the flux density of the magnetic field is sufficiently large then it is hypothesised that the deflection of the sodium ions will cause the ions to collide with the walls of the ion channel. It is assumed that collisions between sodium ions and the ion channel are inelastic, meaning that a loss of momentum and kinetic energy results from the collision, causing the velocity of the sodium ion to be reduced. This reduction in velocity will reduce the effect of the magnetic field on the ion since from equation (4.2), the Larmor radius is proportional to the particle velocity. However, the ion is constantly being acted upon by the electrochemical gradient across the nerve fibre cell membrane and following a collision with the ion channel wall the ion will be accelerated by this electrochemical gradient. As the velocity of the ion increases, the deflecting effect of the magnetic field will also increase and cause the ion to collide again with the ion channel wall and

lose velocity. It is therefore hypothesised that the magnetic field will cause the sodium ions entering the nerve fibre to collide repeatedly with the walls of the ion channel as shown in Figure 4.4.

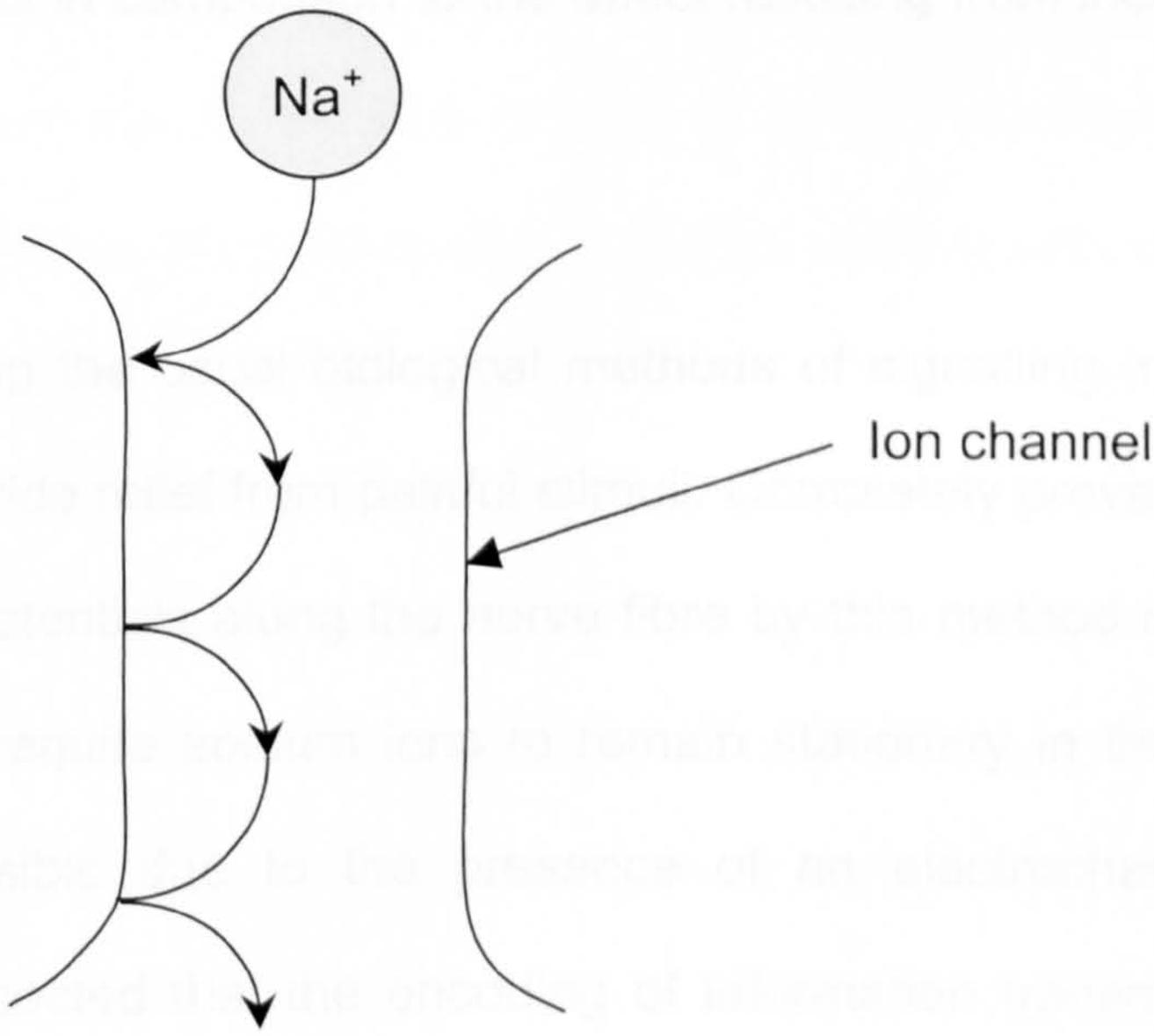

Figure 4.4 Sodium ion colliding repeatedly with the ion channel in an applied magnetic field

The feasibility of this method of inducing non-invasive anaesthesia depends upon the unproven assumption that the effect of the magnetic field will significantly retard the passage of sodium ions into the nerve cell, disrupting the generation of action potentials. The amount by which the rate of influx of sodium ions is reduced is dependent upon the extent to which collisions between sodium ions and the ion channels are inelastic. If these collisions are perfectly inelastic then sodium ions will be briefly reduced to zero velocity (until the electrochemical gradient causes acceleration of the ions) and it is expected that depolarisation of the nerve fibre will be significantly disrupted by the magnetic field. If collisions were perfectly elastic, the velocity of sodium ions would not be

reduced by the collisions and the only effect of the magnetic field would be to cause the ions to follow a longer (circular) path into the nerve fibre. Although this may have a minor effect in preventing the generation of action potentials, this effect is likely to be small in comparison to the effect resulting from inelastic collisions.

It is assumed that disrupting the usual biological methods of signalling in this way will be sufficient to provide relief from painful stimuli. Completely preventing the propagation of action potentials along the nerve fibre by this method is not possible, since this would require sodium ions to remain stationary in the ion channel which is not possible due to the presence of an electrochemical gradient. However, it is expected that the encoding of information transmitted along a nerve fibre will be sensitive to these disruptions in action potentials. Therefore, even if action potentials are propagated by the nerve fibre, it is hypothesised that this disruption to the normal form of pain signals may be sufficient to prevent the brain from interpreting these signals correctly.

As an estimate of the feasibility of this technique, some typical parameters were substituted into equation (4.2). To simplify the calculation, the ion channel is assumed to be a perfect cylinder with a smooth uncharged interior. The cylinder has a diameter of 0.73 nm [1] and length equal to the thickness of the nerve cell membrane (2.3 nm [1]). A hydrated sodium ion has a diameter comparable to that of the ion channel (0.48 nm [2]), therefore if the centre of a hydrated sodium ion is imagined to coincide with the axis of the ion channel when it enters the channel, a deflection of only 0.125 nm in the radial direction will

cause a collision with the ion channel. If the centre of the sodium ion is imagined to travel in a circular arc between the axis of the ion channel at the extracellular end and a position 0.125 nm away from the axis at the intracellular end (Figure 4.5), this corresponds to a Larmor radius of 21.2 nm. The sodium ion is estimated to travel into the nerve fibre at 9.54 m s^{-1} [3], although this estimation is very subjective since no data on the velocity of sodium ions during action potentials was found in a search of literature. The mass of the hydrated sodium ion is estimated to be 1.27×10^{-25} kg (based upon an atomic mass of 3.82×10^{-27} kg and a hydration number of 3 [2]) and the charge on the ion is 1.6×10^{-19} coulomb. Substitution of these values into equation (4.2) suggests that a magnetic field of 356 Tesla is required to cause a single collision between a sodium ion and the ion channel. Although generating such a large magnetic field is unfeasible, the uncertainty in the estimated ionic velocity means that the reliability of this estimate of the required magnetic field is also questionable. Therefore, it was decided to continue investigating this concept as a method of non-invasive anaesthesia.

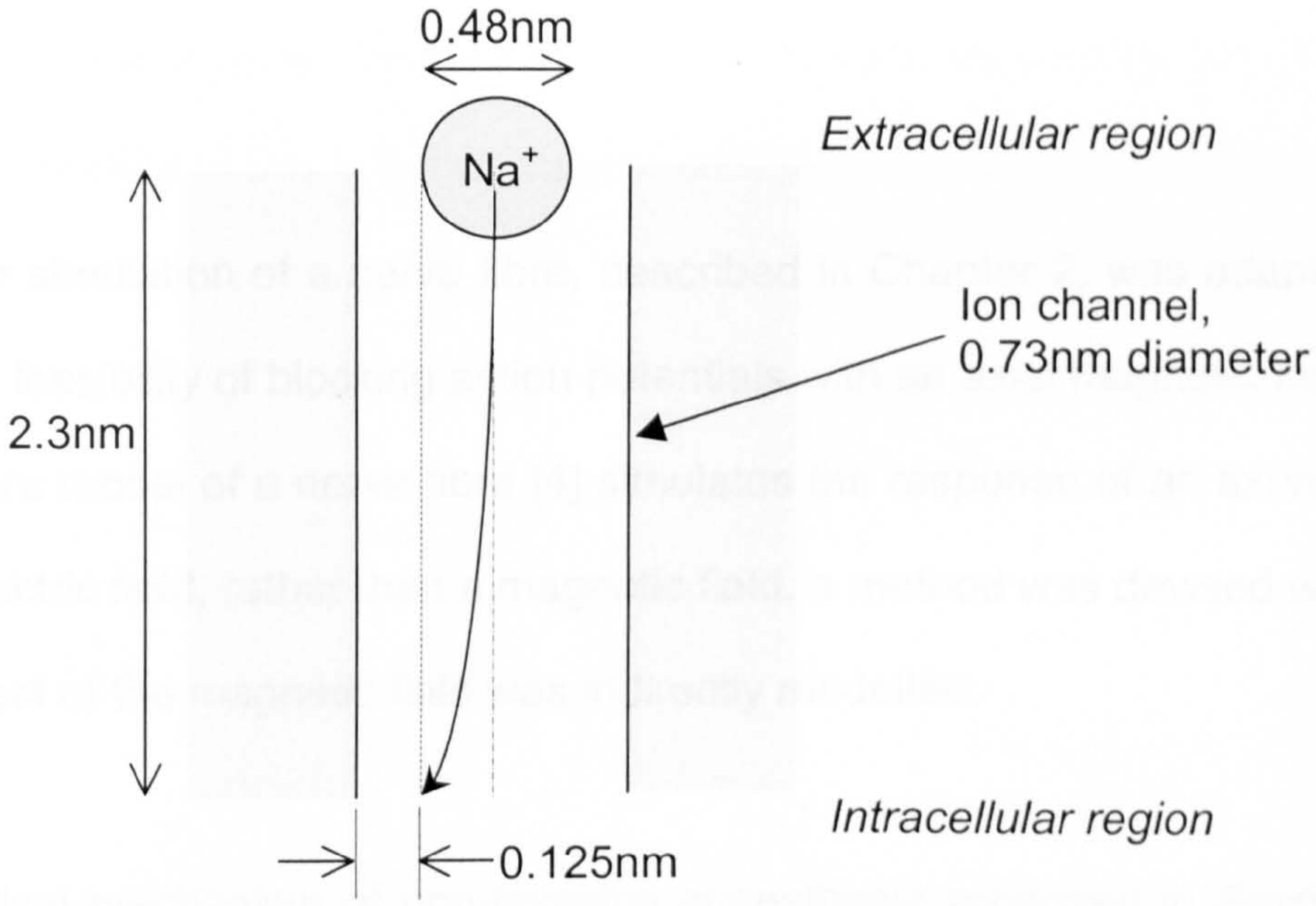

Figure 4.5 Estimate of Larmor radius required to cause a collision

4.3. Computer Simulation of the Effect of an Axial Magnetic Field on a Nerve Fibre

The computer simulation of a nerve fibre, described in Chapter 2, was adapted to assess the feasibility of blocking action potentials with an axial magnetic field. Since McNeal's model of a nerve fibre [4] simulates the response of an axon to an applied electric field, rather than a magnetic field, a method was devised with which the effect of the magnetic field was indirectly modelled.

The hypothetical mechanism of non-invasive anaesthesia proposed in Section 4.2 is expected to reduce the rate of influx of sodium ions during the depolarising phase of the action potential. The transmembrane sodium current, which is responsible for depolarisation of the nerve cell and the resulting propagation of action potentials, is expressed as a function of intracellular and extracellular sodium ion concentrations in equation (2.10). Therefore, the reduced sodium current caused by the effect of the magnetic field on sodium ions may be approximated by a reduction in the value of the extracellular sodium ion concentration parameter, $[Na]_o$, in equation (2.10).

This approach is justified by the experiments of Hodgkin and Katz [5], which demonstrated that a reduction in extracellular sodium ion concentration caused a reversible decrease in the amplitude of action potentials in squid axons. Hodgkin and Katz also showed that the generation of action potentials could be prevented by a substantial reduction in the concentration of sodium ions in the extracellular fluid. The computer simulation is in agreement with these

experimental observations. Therefore, simulating a reduction in the extracellular sodium ion concentration is considered to be a suitable method by which to examine the feasibility of this hypothetical non-invasive anaesthesia technique.

4.3.1. Method of Computer Simulation

Afferent nerve fibres carrying information about painful stimuli are either unmyelinated or myelinated fibres with diameters in the range of 1-4 μm [6]. Due to the significant computational effort required to simulate these fibres, the simulation was simplified by adopting the method developed in Section 3.3. With this method, larger fibres with diameters in the 10-20 μm range were simulated and these results were extrapolated to predict the effects of an applied magnetic field on smaller diameter sensory fibres.

The effect of an applied magnetic field on sodium ion influx was modelled by a reduction in the concentration of extracellular sodium ions at several nodes in the centre of the simulated nerve fibre. Extracellular sodium ion concentration was reduced by the same amount at each of the nodes in the affected region. Using the same method as the simulation of Section 3.3, a depolarising current pulse of 0.1 ms duration and 110% of threshold amplitude was used to elicit an action potential in the simulated axon. Action potentials that did not propagate beyond the region of depleted extracellular sodium ion concentration were considered to be blocked. By an iterative process, the concentration of extracellular sodium ions was reduced until the threshold concentration of sodium ions necessary to prevent the propagation of action potentials was determined.

To determine the dependence of the anaesthetic effect upon the length of nerve fibre on which the magnetic field acts, the number of nodes experiencing a

depleted sodium ion concentration was varied. For fibres of 10, 15 and 20 μm diameter, the threshold extracellular sodium ion concentration was calculated when the length of the region of depleted ion concentration was varied between 1 and 49 nodes. To minimise errors resulting from the effect of the boundary conditions (equations (2.26) and (2.27)) on a finite length of nerve fibre, the number of nodes comprising the simulated nerve fibre was at least twice the length of the region of reduced sodium ion concentration. The resulting error was estimated to be less than 1% for a 20 μm nerve fibre.

4.3.2. Results of Computer Simulation

The threshold extracellular sodium ion concentrations necessary to prevent the propagation of action potentials along the simulated nerve fibre are presented in Table 4.1. The tabulated values are the maximum extracellular concentration of sodium ions that cause action potentials to be blocked, expressed as a percentage of the normal physiological concentration of 142.0 mM (Table 1.1). Table 4.1 shows that the threshold concentration is independent of nerve fibre diameter when an equal number of nodes experience a depleted extracellular sodium ion concentration.

Number of Affected Nodes	Threshold Extracellular Sodium Ion Concentration (as percentage of physiological concentration)		
	10 μm fibre	15 μm fibre	20 μm fibre
1	Not Blocked	Not Blocked	Not Blocked
3	23.5	23.5	23.5
5	30.3	30.3	30.3
9	34.0	34.0	34.0
19	35.8	35.8	35.8
25	36.1	36.1	36.1
37	36.3	36.3	36.3
49	36.3	36.3	36.3

Table 4.1 Threshold extracellular sodium ion concentrations required to prevent propagation of action potentials

The relationship between threshold concentration and the number of affected nodes is illustrated graphically in Figure 4.6. Action potentials were not blocked when a single node experienced reduced extracellular sodium ion concentration, even when the concentration was reduced to less than 0.1 % of

the normal physiological level. As the number of affected nodes is increased, the threshold extracellular sodium ion concentration increases up to a limiting value of 36.3 % of physiological concentration. When more than ~37 nodes are affected, the threshold extracellular sodium ion concentration necessary to block action potentials is always 36.3 % of physiological concentration and increasing the number of affected nodes has no further effect on threshold concentration.

Although the threshold extracellular concentration is independent of fibre diameter when equal numbers of nodes experience reduced sodium ion concentration, the threshold concentration is dependent upon fibre diameter when equal lengths of nerve fibre are considered. In Section 2.2 it was assumed that the length of the myelinated region between adjacent nodes of Ranvier is proportional to nerve fibre diameter. Therefore, small diameter nerve fibres possess a greater number of nodes per unit length than larger fibres. When a fixed length of nerve experiences a reduction in extracellular sodium ion concentration, the threshold concentration is greater for small diameter nerve fibres than for fibres of greater diameter since fewer nodes of the larger fibre are affected. In Table 4.2, the simulation results are expressed in terms of the length of nerve fibre that must be affected by a given reduction in extracellular sodium ion concentration in order to prevent the propagation of action potentials for fibres of 10, 15 and 20 μm diameter. The results of Table 4.2 are presented in Figure 4.7, which illustrates that a reduction in extracellular sodium ion concentration blocks action potentials more readily for small diameter nerve fibres than for fibres of larger diameter.

Extracellular Sodium Ion Concentration (%)	Length of Nerve Fibre Affected (mm)		
	10 μm fibre	15 μm fibre	20 μm fibre
23.5	2	3	4
30.3	4	6	8
34.0	8	12	16
35.8	18	27	36
36.1	24	36	48
36.3	36	54	72

Table 4.2 Relationship between threshold extracellular sodium ion concentration and length of affected region

Figure 4.6 Dependence of threshold reduction in extracellular sodium ion concentration upon length of region of depleted ion concentration

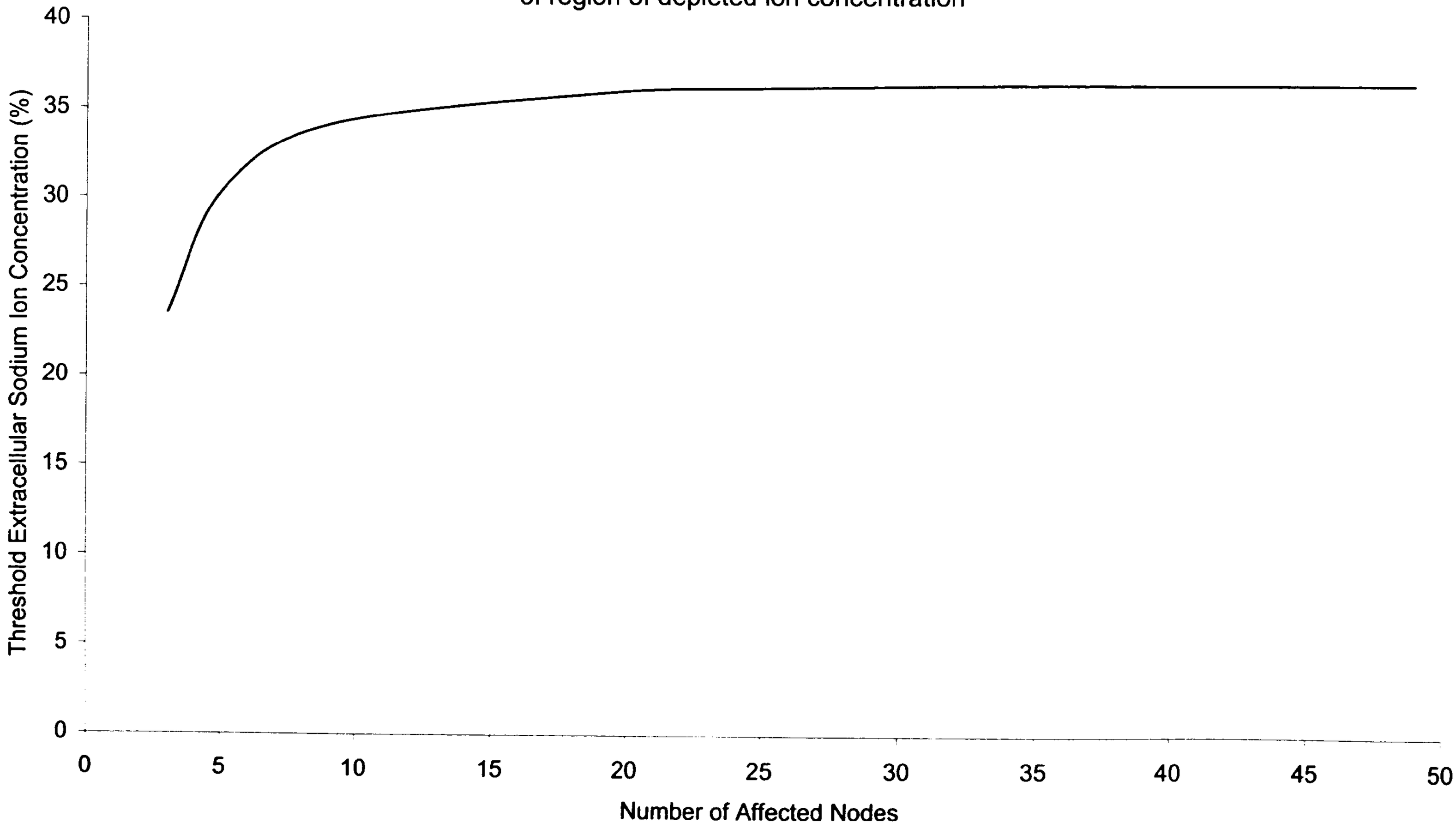

Figure 4.7 Dependence of threshold extracellular ion concentration upon length of affected region

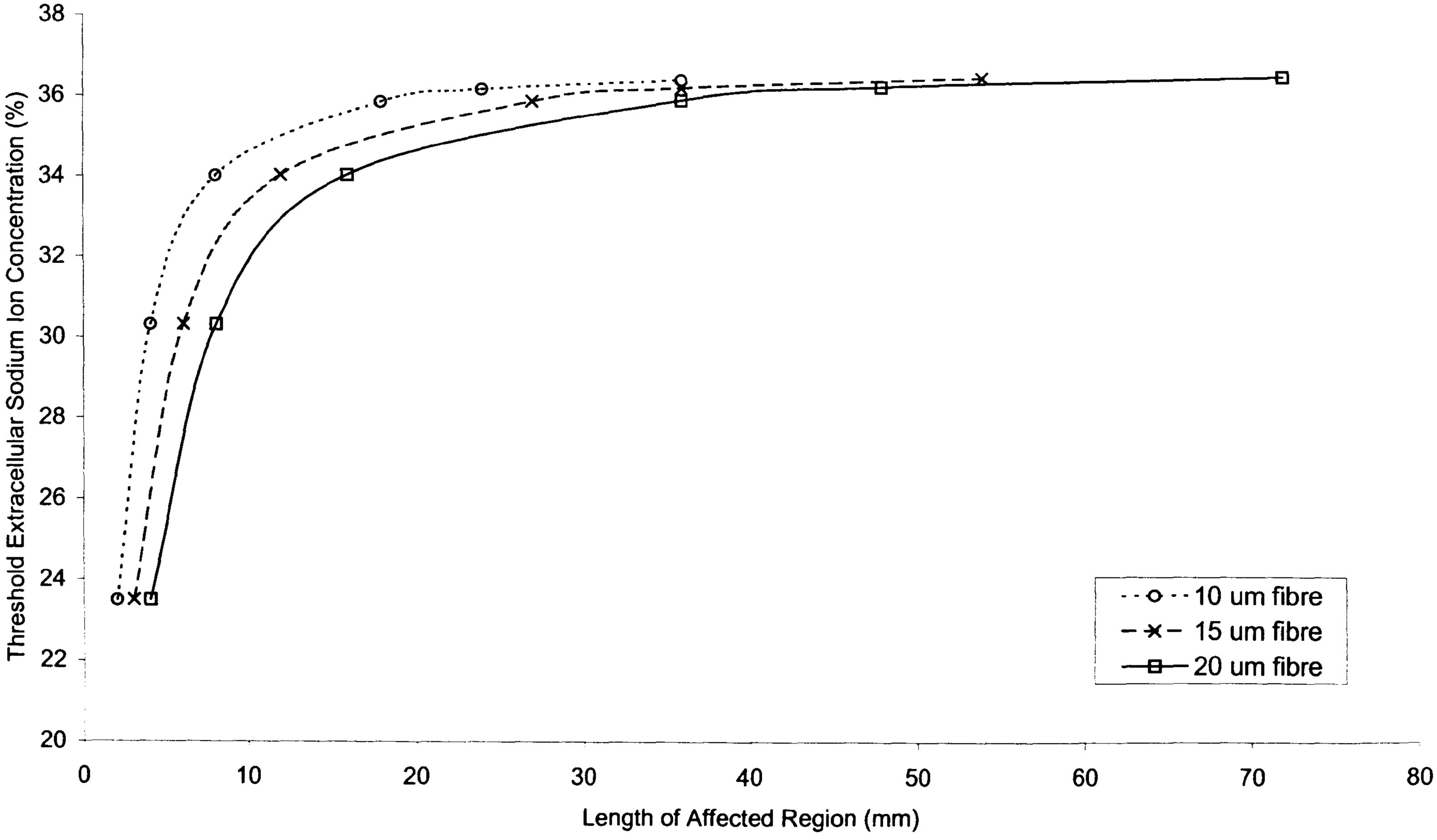

4.3.3. Discussion

The computer simulation suggests that the propagation of action potentials may be prevented by reducing the influx of sodium ions into a depolarising nerve fibre. To demonstrate that action potentials are blocked by a reduction in transmembrane sodium current, the ionic transmembrane currents during blocked and propagated action potentials are plotted in Figure 4.8. This graph compares the ionic current densities for a propagated action potential (black traces) to those of an action potential which was blocked by a reduction in the extracellular sodium ion concentration (grey traces). Figure 4.8 shows that reducing the concentration of sodium ions in the extracellular fluid greatly reduces the amplitude of the sodium current, i_{Na}, thus preventing depolarisation of the nerve cell during action potential propagation. The leakage current, i_L, is also noticeably attenuated by the reduction in sodium ion concentration. Since the leakage current is proportional to the membrane potential, the reduction in leakage current indicates that the amplitude of action potentials is diminished by the change in extracellular sodium ion concentration.

The simulation demonstrated that the maximum values of threshold extracellular sodium ion concentration occur when a large number of nodes of Ranvier experience depleted sodium ion concentration. Furthermore, the propagation of action potentials was unaffected when a reduced concentration of extracellular sodium ions was only present at a single node. The reason for the dependence of threshold concentration upon the length of nerve fibre affected is illustrated in Figure 4.9, which compares the intracellular currents

between two adjacent nodes during propagated and blocked action potentials. The propagated and blocked action potentials were simulated for nerve fibres for which the extracellular sodium ion concentration was reduced to 36.3 % of the normal physiological level across a length of 19 and 39 nodes respectively. Figure 4.9 shows that the amplitude of the intracellular current decreases when more nodes experience reduced extracellular sodium ion concentration. As noted in Section 1.1.3, the intracellular current is of vital importance to the conduction of action potentials since it allows the depolarisation of the nerve cell membrane at one node of Ranvier to cause a depolarisation at adjacent nodes. In the situation where only one node experiences depleted extracellular sodium ion concentration, the intracellular current enables the propagation of action potentials despite the fact that one node is unable to depolarise because of a greatly reduced transmembrane sodium current. However, the intracellular current is dependent upon transmembrane sodium currents and its magnitude is attenuated when several nodes experience reduced extracellular sodium ion concentration. Therefore, reducing the extracellular concentration of sodium ions at several nodes blocks action potentials by reducing the magnitude of intracellular currents and thus prevents the depolarisation of adjacent nodes of Ranvier.

The amount by which the extracellular sodium ion concentration must be reduced in order to prevent the propagation of action potentials is minimised when a large length of nerve fibre is affected. Therefore, the magnetic flux density necessary to cause an anaesthetic effect may be minimised by applying the magnetic field to a large axial region of the nerve fibre. However, this

observation is unlikely to be of much practical benefit. Table 4.2 shows that there is an inverse relationship between nerve fibre diameter and the limiting value of the threshold extracellular sodium ion concentration of 36.3%. For a fibre of 10 μm diameter, the limiting value of the threshold sodium ion concentration is reached when a 3.6 centimetre length of nerve fibre is affected. The limiting value of extracellular concentration will be achieved with a much shorter affected region of less than 1.5 cm for the small fibres of 1-4 μm diameter which carry information regarding painful stimuli. Since any electromagnet with a sufficiently large diameter to incorporate a human limb (as shown in Figure 4.2) is likely to exert its peak field over an axial region greater than 1.5 cm, it is not expected that a novel electromagnet design will be required to ensure that sodium influx is subjected to a magnetic field over a maximal number of nodes.

Although the computer simulation has demonstrated that action potentials may be blocked by reducing the influx of sodium ions into the nerve fibre, this does not infer that an anaesthetic effect will be produced by a magnetic field aligned with the axis of the nerve. The unproven assumption of inelastic collisions between sodium ions and the walls of the ion channels is crucial to the hypothetical mechanism of non-invasive anaesthesia described in this chapter. If collisions between sodium ions and the ion channel are highly elastic and there is a negligible loss of kinetic energy associated with these collisions, it is unlikely that an anaesthetic effect will arise. Furthermore, the feasibility of inducing an anaesthetic effect will be highly dependent upon the velocity of sodium ions within the ion channel. Equation (4.2) implies that the magnetic

field necessary to produce circular motion of sodium ions with any given Larmor radius is proportional to ion velocity. Therefore, it may not be possible to generate a sufficiently strong static magnetic field to cause collisions between sodium ions and ion channels if ionic velocities are greater than a few metres per second. However, the encouraging results of this simulation suggest that further experiments to measure the effect of magnetic fields on the flow of sodium ions through membranes are worthwhile.

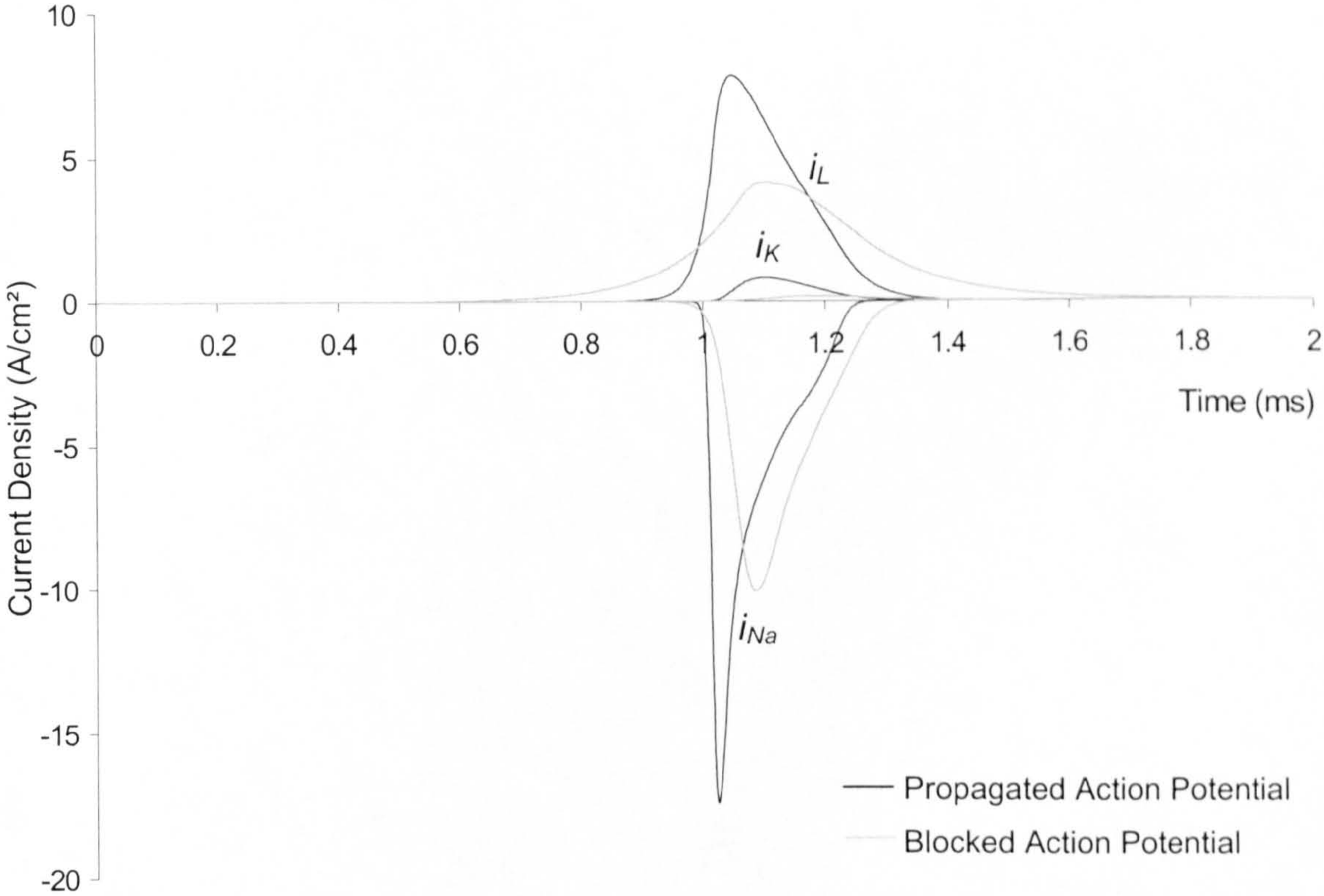

Figure 4.8 Ionic membrane currents during propagated and blocked action potentials

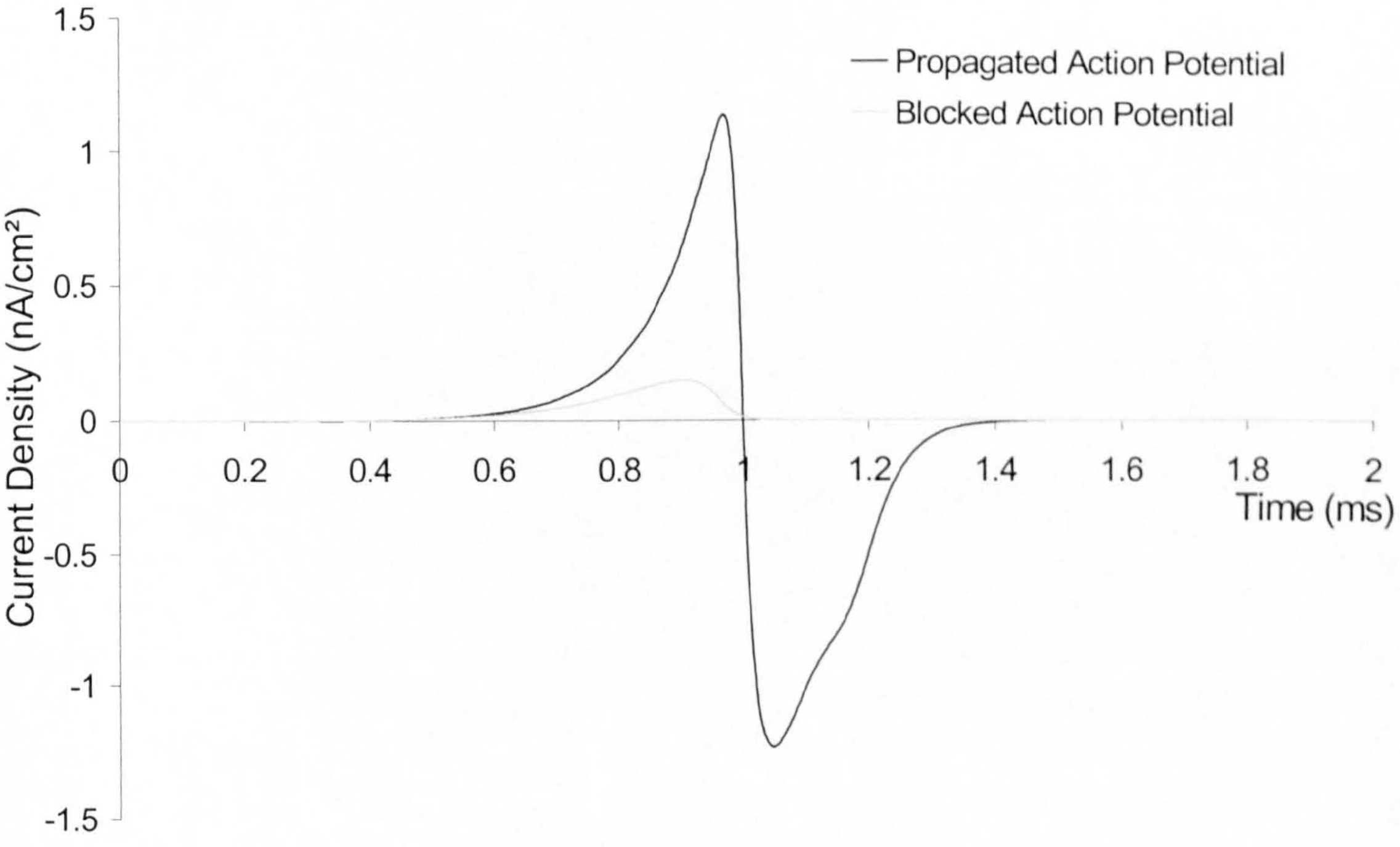

Figure 4.9 Intracellular currents during propagated and blocked action potentials

4.4. References

1. Hille, B.
   Ionic Channels of Excitable Membranes, Second Edition.
   Sinauer Associates Inc., 1992.
2. Moore, W.J.
   Physical Chemistry, 5th Edition.
   Prentice-Hall, 1972, pp. 430-431
3. Skerra, A. and Brickmann J.
   Simulation of Voltage-Driven Hydrated Cation Transport Through Narrow Transmembrane Channels
   Biophysical Journal, Vol. 51, 1987, pp. 977-983.
4. McNeal, D.R.
   Analysis of a Model for Excitation of a Myelinated Nerve.
   IEEE Transactions on Biomedical Engineering, Vol. 23, 1976, pp. 329-337.
5. Hodgkin, A.L. and Katz, B.
   The Effect of Sodium Ions on the Electrical Activity of the Giant Axon of the Squid.
   Journal of Physiology, Vol. 108, 1949, pp.37-77.
6. Aidley, D.J.
   The Physiology of Excitable Cells, Third Edition.
   Cambridge University Press, 1989.

5. EXPERIMENTAL APPARATUS TO SIMULATE THE EFFECT OF A STATIC AXIAL MAGNETIC FIELD ON A NERVE FIBRE

In order to qualitatively assess the feasibility of using a magnetic field aligned with the axis of a nerve fibre as a means of non-invasive anaesthesia, a series of experiments were devised by which the biological system can be modelled with an artificial (non-biological) system. In this chapter, the experimental apparatus common to all of these experiments is described.

5.1. Artificial Membranes

There are many difficulties associated with conducting experiments to determine the effect of a magnetic field on biological membranes. *In vivo* experiments may be unsuitable since the complexity of an entire organism can make small effects caused by the magnetic field difficult to detect and establishing a correlation between the applied magnetic field and any resulting effect on the test organism may present a substantial challenge. *In vitro* experiments on biological membranes also present significant difficulties. Biological membranes deteriorate soon after removal from the living organism, which makes long-term experimentation on a single membrane impossible. Although a series of experiments could be performed on a number of similar membrane samples, differences between the membrane samples may lead to a lack of consistency between experiments. Furthermore, the practical difficulties of experimentation on biological membranes in an engineering department without the experience or specialised facilities necessary for biological research

implied that experiments on biological membranes, either *in vivo* or *in vitro*, were not feasible.

A solution to the practical obstacles presented by experimentation on biological membranes is to use artificial membranes. Studies of the effect of cyclotron resonance on membranes [1, 2], caused by the combination of a static magnetic field with an ac electric field, have used gramicidin channels to model the ion channels of biological membranes. Gramicidin is an antibiotic which causes porous channels to form in layers of lipid [3], thus approximating the real membrane structure as described in Section 1.1. Gramicidin channels have dimensions similar to those of biological ion channels with a length and diameter of 2.5 nm and 0.4 nm respectively, compared to the values of 2.3 nm and 0.73 nm for biological channels that were suggested in Section 4.2.

Gramicidin channels exhibit some of the properties of biological membranes. Gramicidin channels are permeable only to cations which allows the formation of membrane potentials across the lipid membrane. For example, if a lipid membrane with gramicidin channels separates sodium chloride solution from pure water, the positively charged sodium ions are able to diffuse through the channels into the pure water. However, the selectivity of the gramicidin channel prevents the negatively charged chloride ions from permeating the membrane. Hence, the passage of sodium ions creates a potential difference across the membrane which opposes the diffusion gradient. The system will reach equilibrium when the effect of the potential difference is equal and opposite to

the effect of the concentration gradient and this potential difference can be calculated from equation (1.1), the Nernst equation.

Another property of gramicidin channels is that the pores have a limited lifetime. Gramicidin channels tend to form within the lipid membrane and then break down after a time period in the range of 30 milliseconds to 60 seconds. The lifetime of the gramicidin channel is determined by lipids that form the membrane and by the solutions which are separated by the membrane. The maximum current that can pass through a gramicidin channel is limited by the breakdown of the membrane which occurs when a large electric field is applied across the membrane. Typically, the lipid membrane can pass a maximum current of 30 pA under an applied potential of 300 mV [3].

The transient nature of gramicidin channels and the need to create a new membrane after each experiment were considered as factors which may adversely affect the repeatability of experiments involving gramicidin channels. Furthermore, the upper limit on the current that may be passed through the channel precludes certain experiments on gramicidin channels. For these reasons, gramicidin channels were considered unsuitable for these experiments.

The nerve cell membrane was modelled by a cation exchange membrane. A cation exchange membrane is a porous polymer sheet with negatively charged groups attached to the polymer structure [4]. These negatively charged groups repel anions, thus providing cation selectivity by allowing only positively charged

ions to permeate the porous structure of the membrane. The porous structure of a sample of cation exchange membrane can be seen from the scanning electron microscope images of Figures 5.1 and 5.2. Figure 5.1 shows the membrane at twenty thousand times magnification and reveals that the membrane surface contains many randomly distributed pores. Most pores have an approximately circular cross-section, with diameters varying from under 30 nm to over 200 nm. As an estimate of the pore area per unit area of membrane, the number of pores in Figure 5.1 was counted and the diameter of each pore was measured. The section of membrane shown in Figure 5.1 has an area of 2.3×10^{-11} m^2, and contains approximately one hundred pores with a mean diameter of approximately 90 nm. From these measurements, it was estimated that pores account for 3.5 per cent of the total membrane area. However, a different area of membrane viewed at 4300 times magnification (Figure 5.2) reveals that certain regions of the cation exchange membrane contain no pores. It can be seen that the central membrane region in Figure 5.2 contains a large density of pores, but the regions on either side of this contain very few pores. These non-porous regions are a normal feature of the cation exchange membrane and are considered to be negligible in comparison to the much larger porous regions.

A potential difference can be developed across the ion exchange membrane in a similar way to that in which the resting potential of a nerve cell is developed (Section 1.1.2). As for gramicidin channels, if a cation exchange membrane separates sodium chloride solution from pure water, positively charged sodium ions are able to diffuse across the membrane into the pure water whilst the

selectivity of the membrane prevents negatively charged chloride ions from diffusing across the membrane. Equilibrium will be reached when the membrane potential is equal to the Nernst potential for sodium ions.

The magnetic flux density required to cause a collision between a sodium ion and the pore walls of the cation exchange membrane can be estimated from equation (4.2). The manufacturer's data for the cation exchange membrane states that the thickness of the membrane and therefore the length of the pores is in the range of 0.11-0.15 mm. Assuming a perfectly cylindrical pore with an average length of 0.13 mm and the previously measured average pore diameter of 90 nm, the maximum possible Larmor radius which will result in a single collision between a sodium ion and the pore wall is calculated to be 0.19 m. Using the values of ion velocity (9.54 m s^{-1}) and mass of a hydrated sodium ion (1.27×10^{-25} kg) which were used in the similar calculation of Section 4.2, the minimum flux density required to cause a collision is estimated as 40.6×10^{-6} T. This estimate of the applied magnetic field is several orders of magnitude less than that calculated previously for a biological ion channel, due to the much smaller channel diameter/length ratio of the pores of the cation exchange membrane. Therefore, it was expected that the flow of sodium ions through the pores of this artificial membrane would have a greater sensitivity to the effects of an applied magnetic field than in the case of a biological membrane, which would be of great benefit in assessing the feasibility of using an axially aligned magnetic field as a means of anaesthesia.

Artificial membranes such as the cation exchange membrane provide a practical means by which transmembrane ion fluxes may be studied. Since these membranes are significantly different to biological membranes, experiments with artificial membranes are not able to prove or disprove the effect of a magnetic field on real nerve fibres. However, evidence collected from experiments on cation exchange membranes allows more accurate predictions to be made of the effect of magnetism on nerve fibres, whilst removing many of the practical difficulties associated with experimentation on biological membranes.

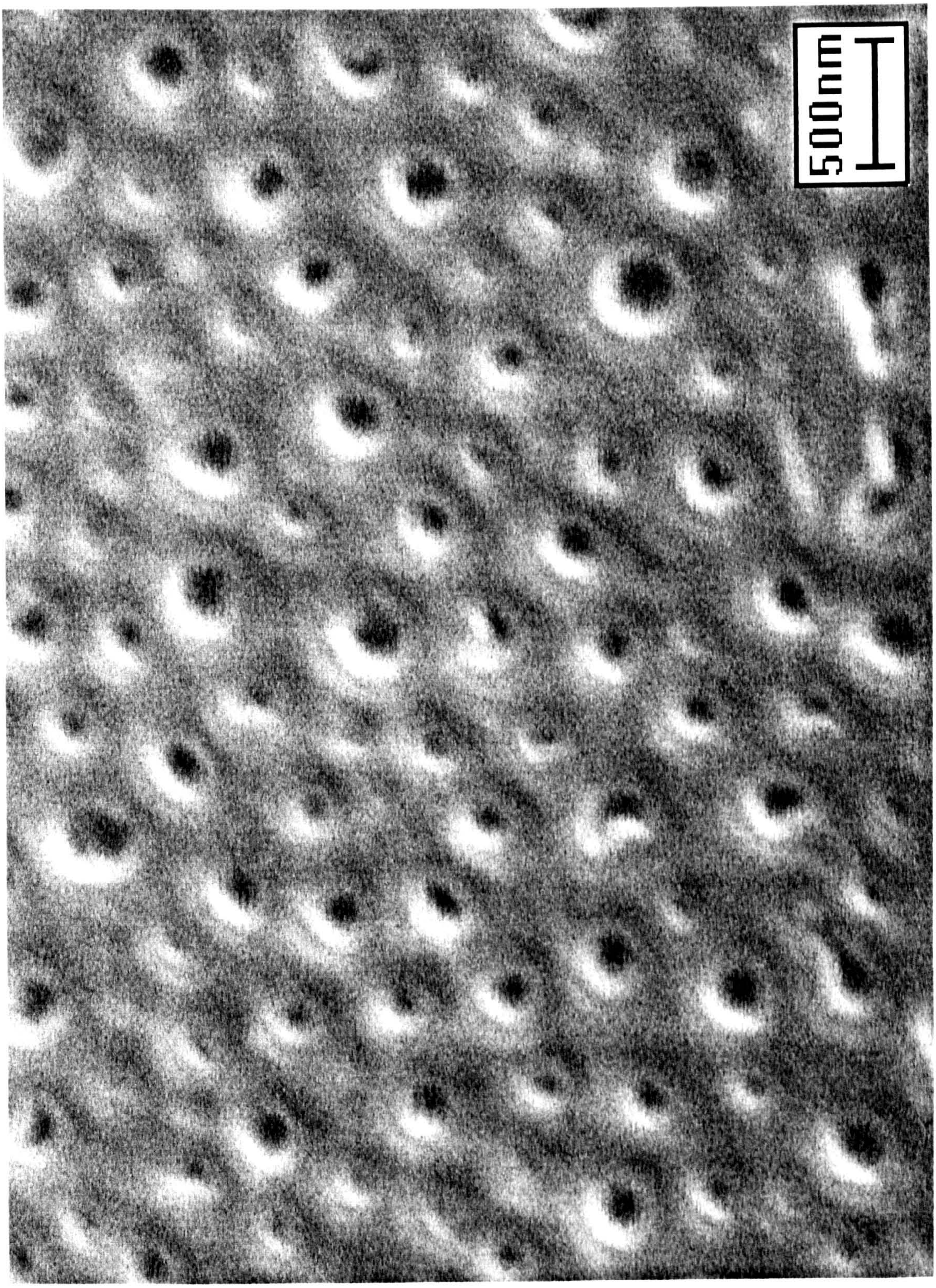

Figure 5.1 Scanning electron microscope image of cation exchange membrane (20000x magnification)

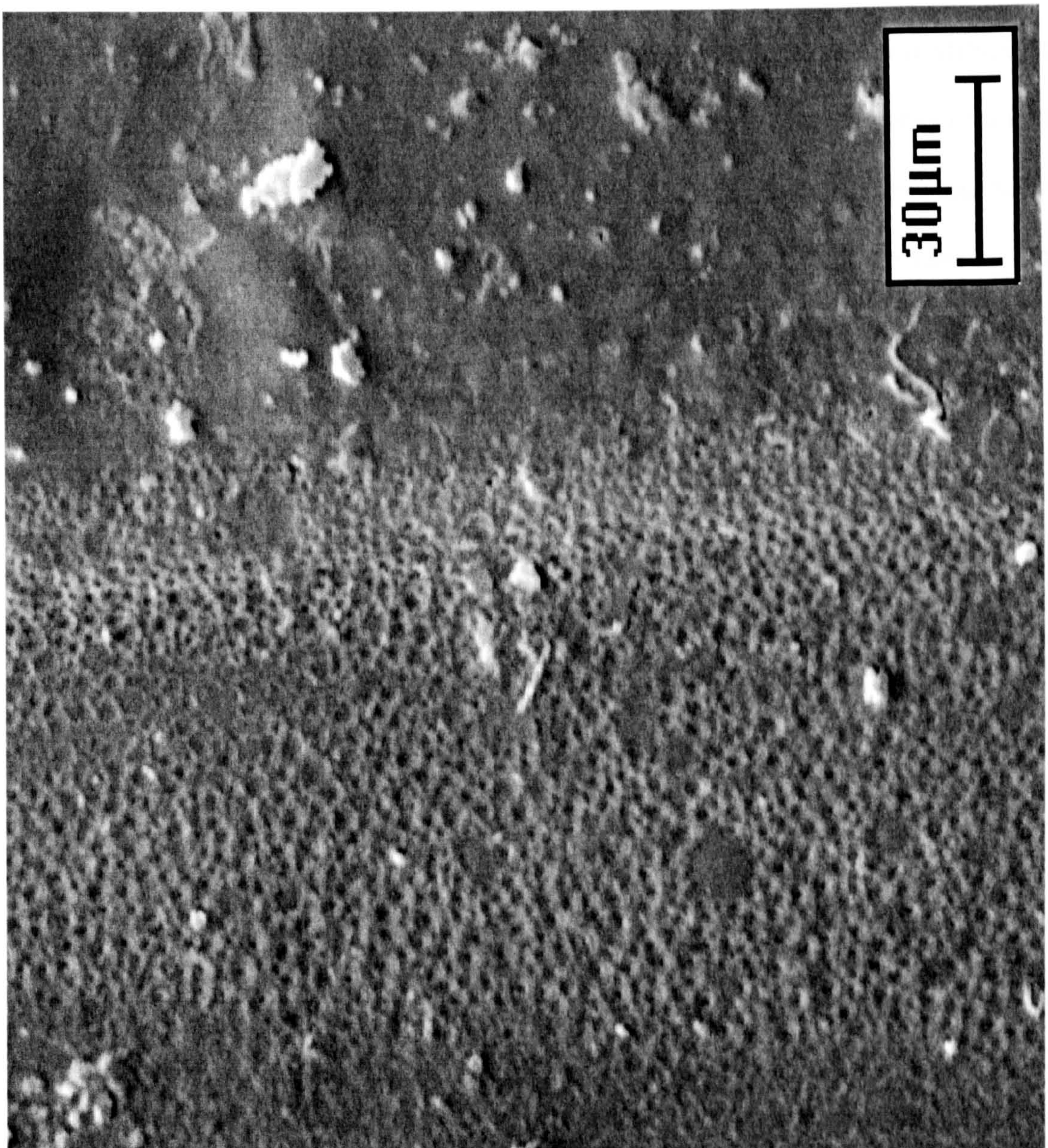

Figure 5.2 Scanning electron microscope image of cation exchange membrane (4300x magnification)

5.2. Measurement of Membrane Potential

In these experiments, an Ussing chamber was designed to mount a sample of cation exchange membrane between two ionic solutions. The Ussing chamber apparatus was originally devised by Ussing and Zerahn to measure the active transport of sodium ions through a biological membrane [5]. However, the apparatus is also suitable for measuring ion flux through an artificial ion exchange membrane. A schematic diagram of an Ussing chamber and the apparatus used to measure membrane potential is shown in Figure 5.3.

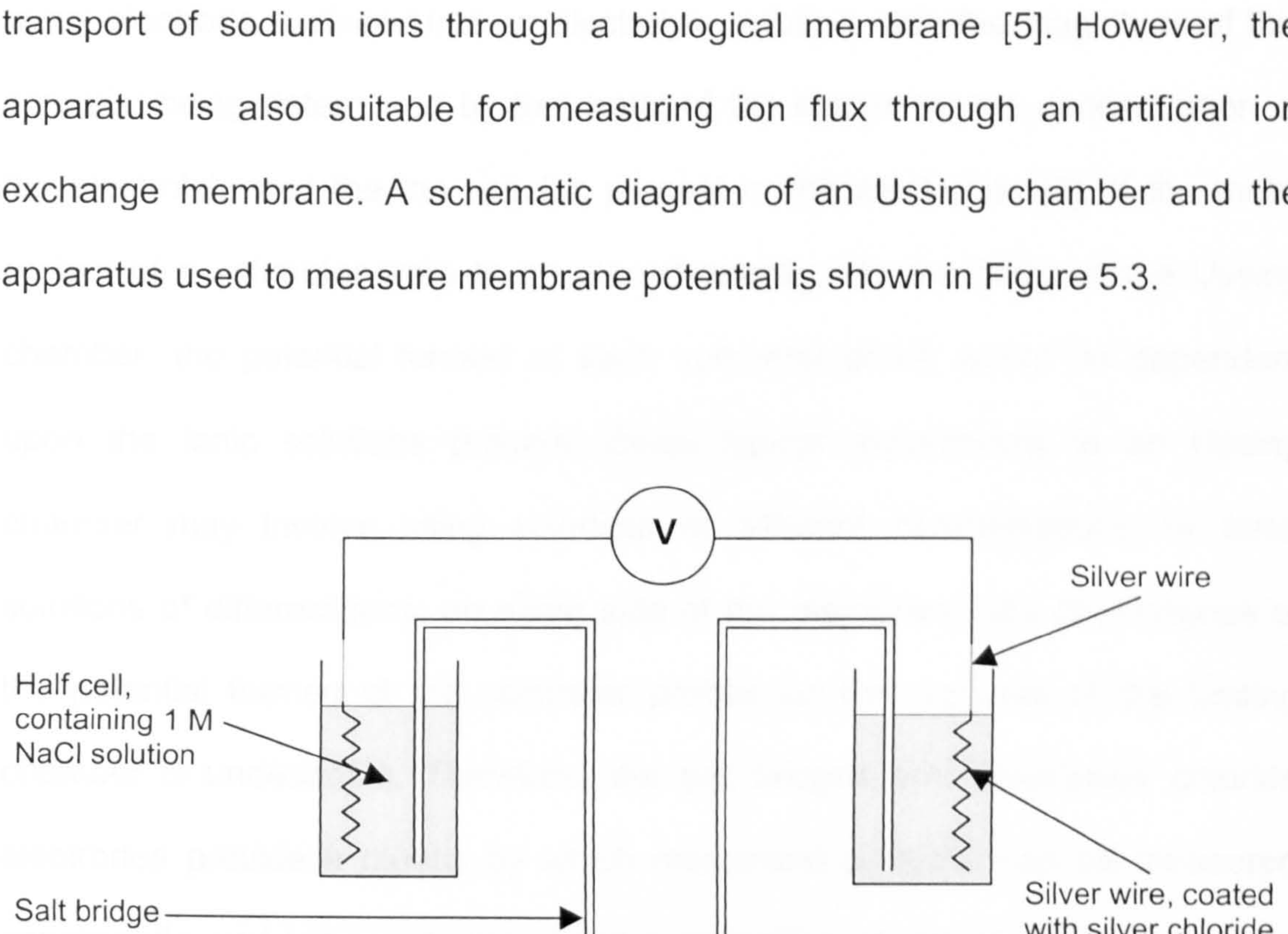

Figure 5.3 Cross section of apparatus

The potential difference across the membrane was measured using salt bridges and a pair of silver/silver chloride half cells which were connected to either a digital voltmeter or a data logger. The purpose of the salt bridges and half cells is to act as an inert electrical connection between the electrolyte baths and the voltage measurement equipment. An electromotive force is formed whenever a metal electrode is placed into an electrolyte solution, with the magnitude of this potential being determined by the metal of the electrode, the concentration of the electrolyte and the ion species present in the electrolyte [6]. If the metal probes of a voltmeter were to be placed directly into the baths of the Ussing chamber, the potential formed at each voltmeter probe would be dependent upon the ionic solutions present. Since typical experiments in an Ussing chamber may involve using solutions of different concentrations, or even solutions of different ions, on either side of the membrane, the dependence of the potential formed at the voltmeter probes on the contents of the Ussing chamber is undesirable. Therefore, the salt bridges and silver/silver chloride electrodes provide a means by which membrane potential can be measured consistently and independently of the composition of the electrolyte solutions present in the Ussing chamber.

The salt bridges were made by dissolving agar (to act as a gelling agent) in 1 M sodium chloride solution, which was then drawn into thin, flexible PVC tubing with a syringe. A potential difference, known as the liquid junction potential, is formed whenever two liquids of different concentration or different ionic content are placed in contact with each other. Since a salt bridge is essentially a solution of sodium chloride, a liquid junction potential will be formed at each of

its ends where it makes contact with the electrolytes in the half cells and the Ussing chamber. However, because such a concentrated solution of sodium chloride is used to make the salt bridge, it can be shown that the liquid junction potentials are almost independent of the concentration of the other solutions [6]. Furthermore, the directions of the liquid junction potentials at each end of the salt bridge oppose each other, such that the net DC offset introduced into voltage measurements by the salt bridges is negligible. The salt bridges were used to connect the sodium chloride solutions in the Ussing chamber to the half cells.

The silver/silver chloride half cells provide an interface between the sodium chloride solution of the salt bridges and the metal electrodes of the voltage measurement equipment. The half cells each consisted of a silver/silver chloride electrode in 1 M sodium chloride solution. Although a potential difference is formed at the interface between the silver/silver chloride electrode and the sodium chloride solution, an equal voltage is formed at each of the two electrodes since both are contact with 1 M sodium chloride solution. The manner in which the half cells are connected in the measuring circuit ensures that the half cell potentials oppose each other, thus the DC offset to voltage measurements caused by the half cells is negligible. In combination with the salt bridges, the silver/silver chloride half cells provide an inert means by which to measure membrane potentials in the Ussing chamber.

The silver/silver chloride electrodes were made by dipping one end of a piece of silver wire in household bleach in order to produce a surface layer of silver

chloride at the end of the wire. The silver wire used was of 0.5 mm diameter and 99.9% purity and was wound into a helical shape to increase the surface area of the electrode. The half cells were made by placing the silver/silver chloride electrodes into a plastic jar and 1 M sodium chloride solution was added until the level of the sodium chloride solution in the half cells was just insufficient to cover the silver chloride coated tip of the wire, thus ensuring that pure silver was not in contact with the sodium chloride solution.

Technical drawings of the Ussing chamber designed for these experiments are presented in Figures A2 and A3 (Appendix 1). This Ussing chamber consisted of two separate baths, each of approximately 10ml capacity and connected by a hole of 12 mm diameter. The cation exchange membrane was placed over the interconnecting hole and then the baths were clamped together so that the connection between the baths was watertight. The Ussing chamber contained a variety of holes to allow electrodes and salt bridges to be placed into the solutions, as well as two cut out sections near the membrane where magnetic pole pieces could be placed in order to maximise the magnetic field in the region of the membrane.

5.3. Magnetic Field

Permanent magnets were used to test the effect of a magnetic field upon the passage of sodium ions through the cation exchange membrane. Permanent magnets were chosen in preference to electromagnets since they allow large static magnetic fields to be produced in the region of the membrane without the need for the complex power electronics or cooling required by strong electromagnets.

Two magnetic field strengths were used in these experiments. The magnitude of the magnetic flux density in the region of the membrane was measured with a fluxmeter (Electronica DC Fluxmeter, Manchester Lasers Limited), by placing the fluxmeter probe into the interconnecting region of the two baths of the empty Ussing chamber. When taking measurements of the magnetic field, the fluxmeter probe was oriented so that the magnitude of the magnetic flux density in a direction within the plane of the membrane and perpendicular to the axis of the ion channels was measured. Rotating the plane of the fluxmeter probe through 90 degrees gave a measured flux density of approximately zero, confirming that magnetic flux density vector is almost exclusively in a direction perpendicular to the pole faces of each magnet.

The magnets used in the steady state experiments described in Chapter 6 produced a magnetic flux density of 0.1 tesla. This magnetic field strength was demonstrated as being sufficient to produce measurable results, but was small enough to allow the magnets to be manipulated easily.

For the transient response experiments of Chapter 8, stronger permanent magnets were used in order to maximise any possible effect of the magnets on the flow of ions. To further increase the magnetic flux density in the region of the membrane, ferrite pole pieces were placed into the cut out sections of the Ussing chamber described in Section 5.2. The resulting flux density was measured as approximately 0.29 tesla.

5.4. References

1. Wang, K.W. and Hladky, S.B.
   The Effects of Low Frequency, Low Amplitude Magnetic Fields on Gramicidin Channels
   British Journal of Pharmacology, Vol. 108, No. SS, 1993, p. P224
2. Wang, K.W. and Hladky, S.B.
   Absence of Effects of Low-Frequency, Low-Amplitude Magnetic Fields on the Properties of Gramicidin A Channels
   Biophysical Journal, Vol. 67, 1994, pp. 1473-1483
3. Hille, B.
   Ionic Cannels of Excitable Membranes, Second Edition
   Sinauer Associates Inc., 1992
4. BDH
   Ion Exchange Membranes
   Sheet No. 1035PP/1.0/0676
5. Ussing, H.H. and Zerahn, K.
   Active Transport of Sodium as the Source of Electric Current in the Short-circuited Isolated Frog Skin.
   Acta Physiologica Scandinavica, Vol. 23, 1951, pp. 110-127.
6. Atkins, P.W.
   Physical Chemistry, Fourth Edition
   Oxford University Press, 1990.

6. EFFECT OF A MAGNETIC FIELD ON STEADY STATE SODIUM ION FLUX

The first experiment to test the hypothesis that an applied magnetic field can affect the flux of ions through a membrane observed the effect of a magnetic field on the steady flow of sodium ions produced when a constant current was passed through sodium chloride solution and a sample of cation exchange membrane.

6.1. Experimental Method

The Ussing chamber was set up as shown in Figure 5.3. A digital multimeter (Thurlby 1905a) was connected across the two baths of the Ussing Chamber, via salt bridges and silver/silver chloride half cells. 10 ml of 0.1 M sodium chloride solution was added to one bath of the Ussing chamber and 10 ml of water was added to the other bath, causing the formation of a membrane potential of approximately 130 mV. In order to produce a concentration gradient of sodium ions across the membrane that was similar to that in found in nerve fibres, 0.1 M sodium chloride solution was added to the water-filled bath until the membrane potential was reduced to approximately 70 mV. This value of membrane potential is similar to the equilibrium potential for sodium ions that was calculated in Section 1.1.2.

A current source (Keithley Model 220 Programmable Current Source) was connected across the baths via electrodes made from platinum wire (0.5 mm

diameter, 99.99+% purity). The platinum electrodes provided an inert low resistance interface between the current source and electrolyte, allowing large currents to be passed through the membrane for prolonged periods of time without degradation of the electrode. A DC current of sufficient magnitude to reduce the membrane potential to zero was passed through the membrane. Thus, the flow of sodium ions that causes depolarisation of the neuron during the generation of an action potential is modelled by a constant current through the ion exchange membrane. The effect of the magnetic field upon the sodium current may be observed by measuring the potential difference across the membrane.

Figure 6.1 illustrates the polarities in which the equipment was connected for all steady state experiments.

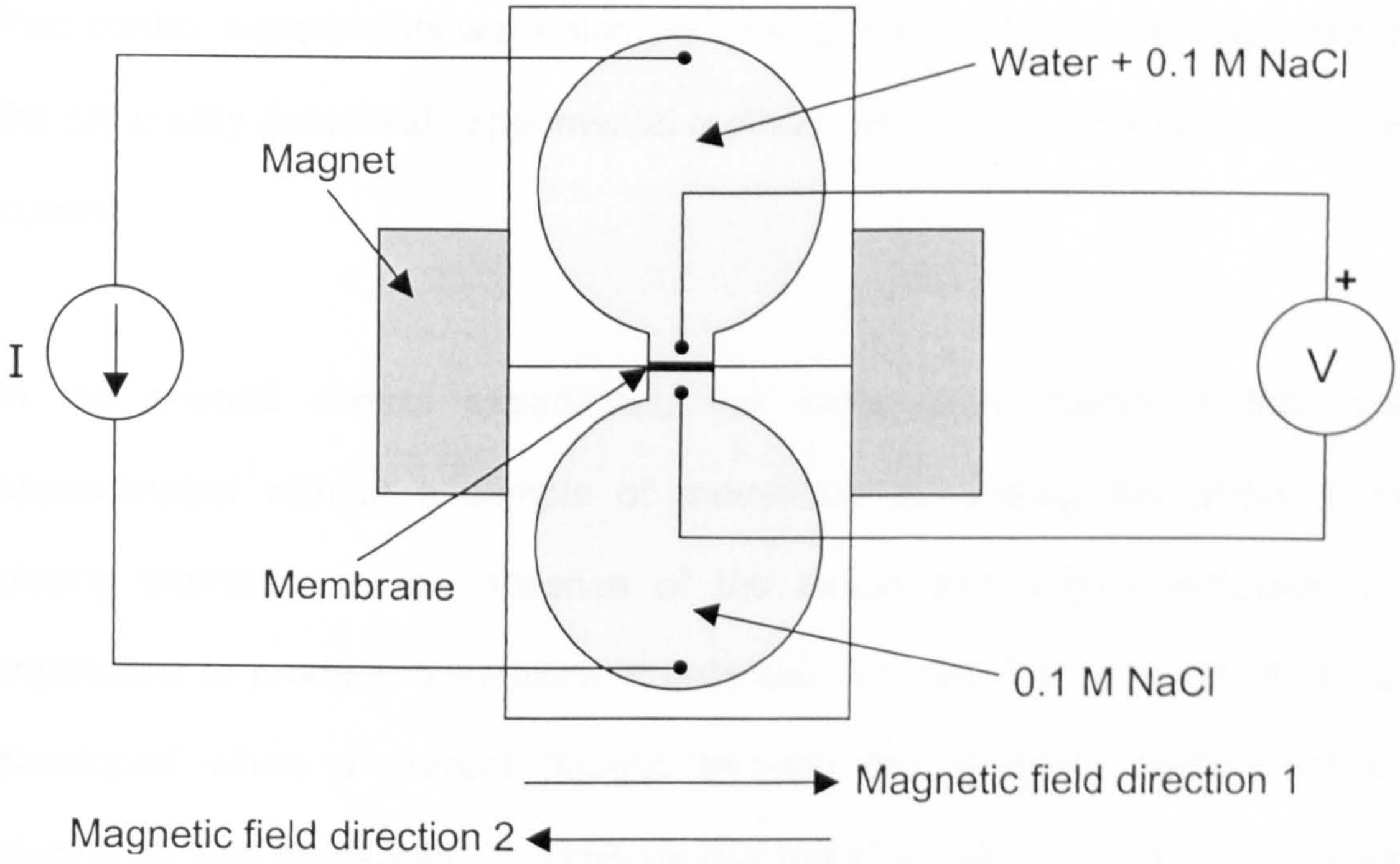

Figure 6.1. Apparatus for steady state experiment (plan view)

Once the membrane potential had achieved a reasonably stable value of approximately zero volts in an applied current, permanent magnets were positioned on either side of the Ussing chamber. The magnetic field was applied in either of two antiparallel directions, referred to as directions 1 and 2 as indicated in Figure 6.1, for 165 second periods. The periods in the presence of an applied magnetic field were alternated with 165 second 'control' periods in the absence of a magnetic field. These control periods allowed the response of the system to the removal of the magnetic field to be observed. Additionally, extra 165 second control periods were included in the experimental regime, with the direction of the applied magnetic field or the inclusion of an extra control period chosen randomly. Measurements of membrane potential were taken by the digital multimeter with a sampling frequency of 3 Hz and were logged to a personal computer.

Two control experiments were also performed. For the first control experiment, the previously described experimental method was repeated but with no applied current.

In the second control experiment, the same experimental method was approximated without a sample of membrane separating the baths of the Ussing chamber. In the absence of the cation exchange membrane it is impossible to produce a membrane potential. Instead, the potential difference developed when a current passes through the resistive medium of the electrolyte was measured. To produce this potential difference, a 3 mA current was applied to 20 ml of 0.1 M sodium chloride solution in the Ussing Chamber

as shown in Figure 6.2. The polarities of the current source and voltmeter were identical to those of previous experiments. The potential difference was measured between two points in the solution, corresponding to the positions at which membrane potential was previously measured, while the magnetic exposure regime was repeated. The ends of the salt bridges were placed near the centre of the interconnecting channel between the baths of the Ussing chamber, separated by a distance of approximately 5 mm along the axis of the channel.

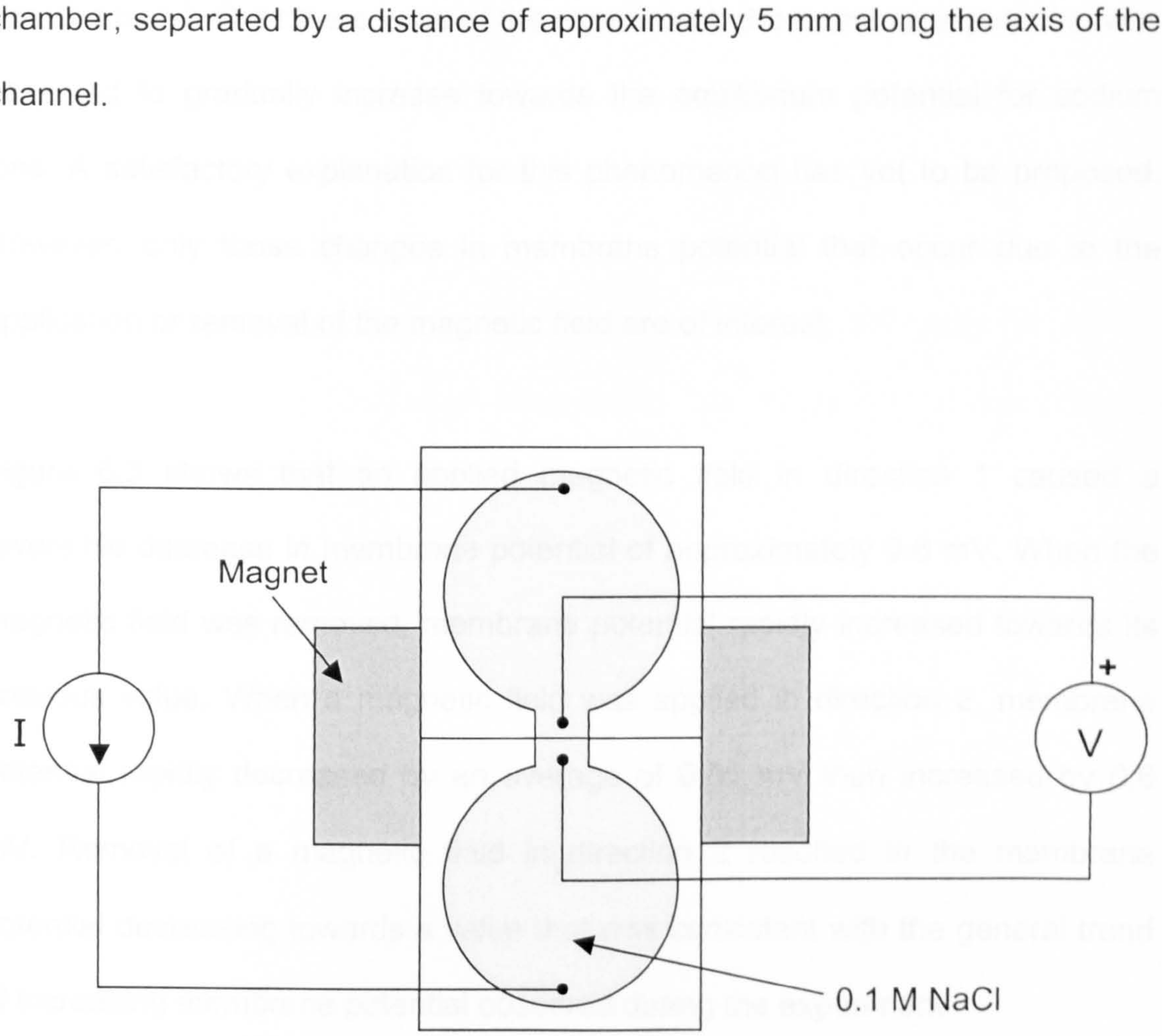

Figure 6.2. Apparatus for control experiment (plan view)

6.2. Results

The effect of an applied magnetic field on membrane potential is illustrated in the graph of voltage against time (Figure 6.3). Periods in which a magnetic field was applied in direction 1 and direction 2 are denoted in Figure 6.3 by "1" and "2" respectively, while control periods in the absence of a magnetic field are denoted by "-". Over the course of the experiment, the membrane potential was observed to gradually increase towards the equilibrium potential for sodium ions. A satisfactory explanation for this phenomenon has yet to be proposed. However, only those changes in membrane potential that occur due to the application or removal of the magnetic field are of interest.

Figure 6.3 shows that an applied magnetic field in direction 1 caused a reversible decrease in membrane potential of approximately 0.6 mV. When the magnetic field was removed, membrane potential rapidly increased towards its previous value. When a magnetic field was applied in direction 2, membrane potential rapidly decreased by an average of 0.05 mV then increased by 0.6 mV. Removal of a magnetic field in direction 2 resulted in the membrane potential decreasing towards a value that was consistent with the general trend of increasing membrane potential observed during the experiment.

In the first control experiment, transient changes in membrane potential were observed upon application and removal of the magnetic field in the absence of an applied current (Figure 6.4). These variations in membrane potential disappeared within 10 seconds of the magnets becoming stationary. The

magnetic field did not cause long-term changes in membrane potential, such as those seen in Figure 6.3.

A typical set of results from the second control experiment is presented in Figure 6.5. It should be noted that the voltage measurements are negative since the voltmeter is reverse biased, having been maintained in the same polarity as for the previous experiments. An applied magnetic field in direction 1 causes an average reversible decrease of 4.7 mV in the potential difference measured between two points in the electrolyte. However, since all voltage measurements are negative, a magnetic field in direction 1 results in an increase in the magnitude of the potential difference. Conversely, an applied magnetic field in direction 2 causes a reversible decrease in the magnitude of the potential difference, by approximately 4.2 mV.

Figure 6.3 Effect of magnetic field on membrane potential (constant current)

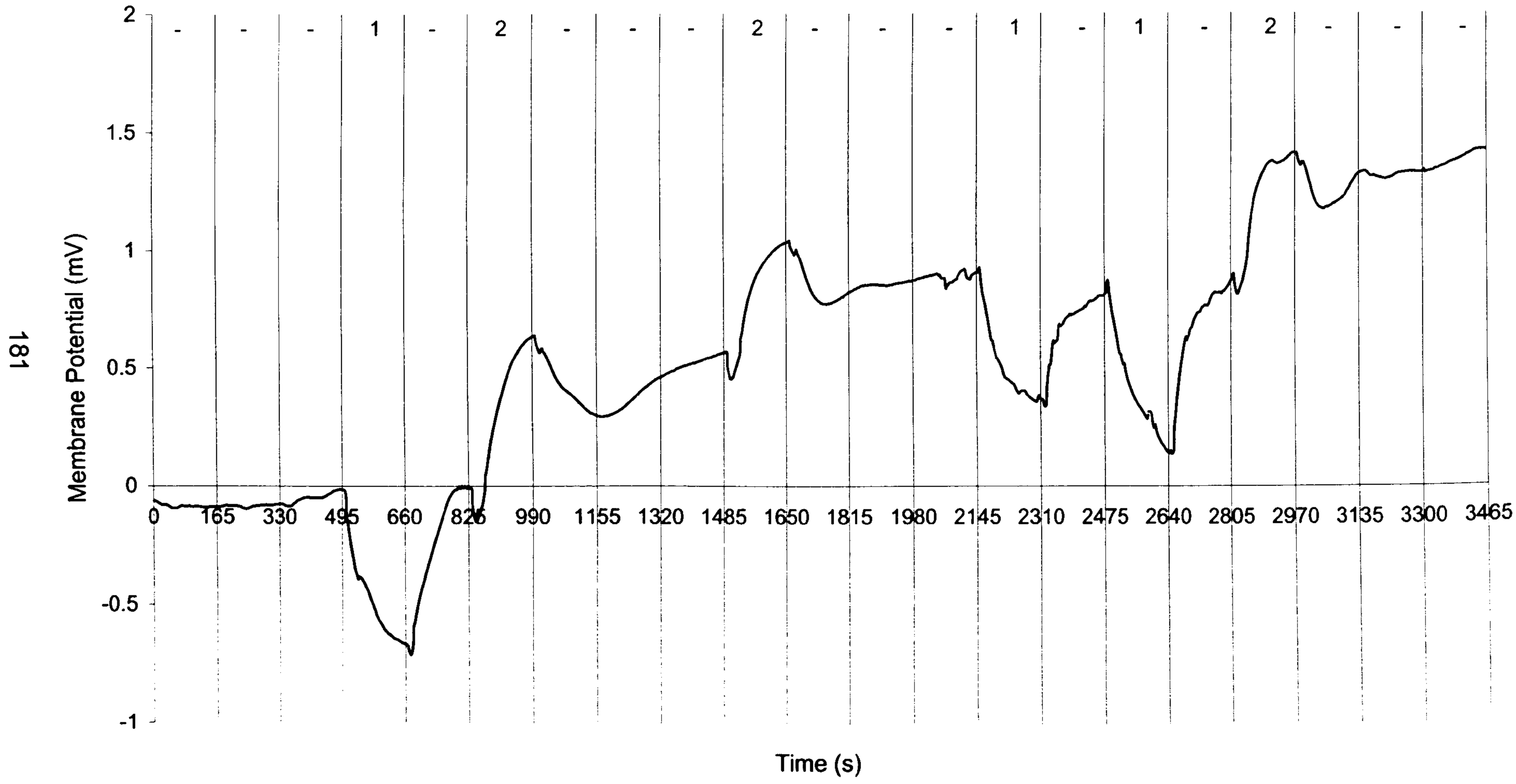

Figure 6.4 Effect of magnetic field on membrane potential in the absence of an applied current

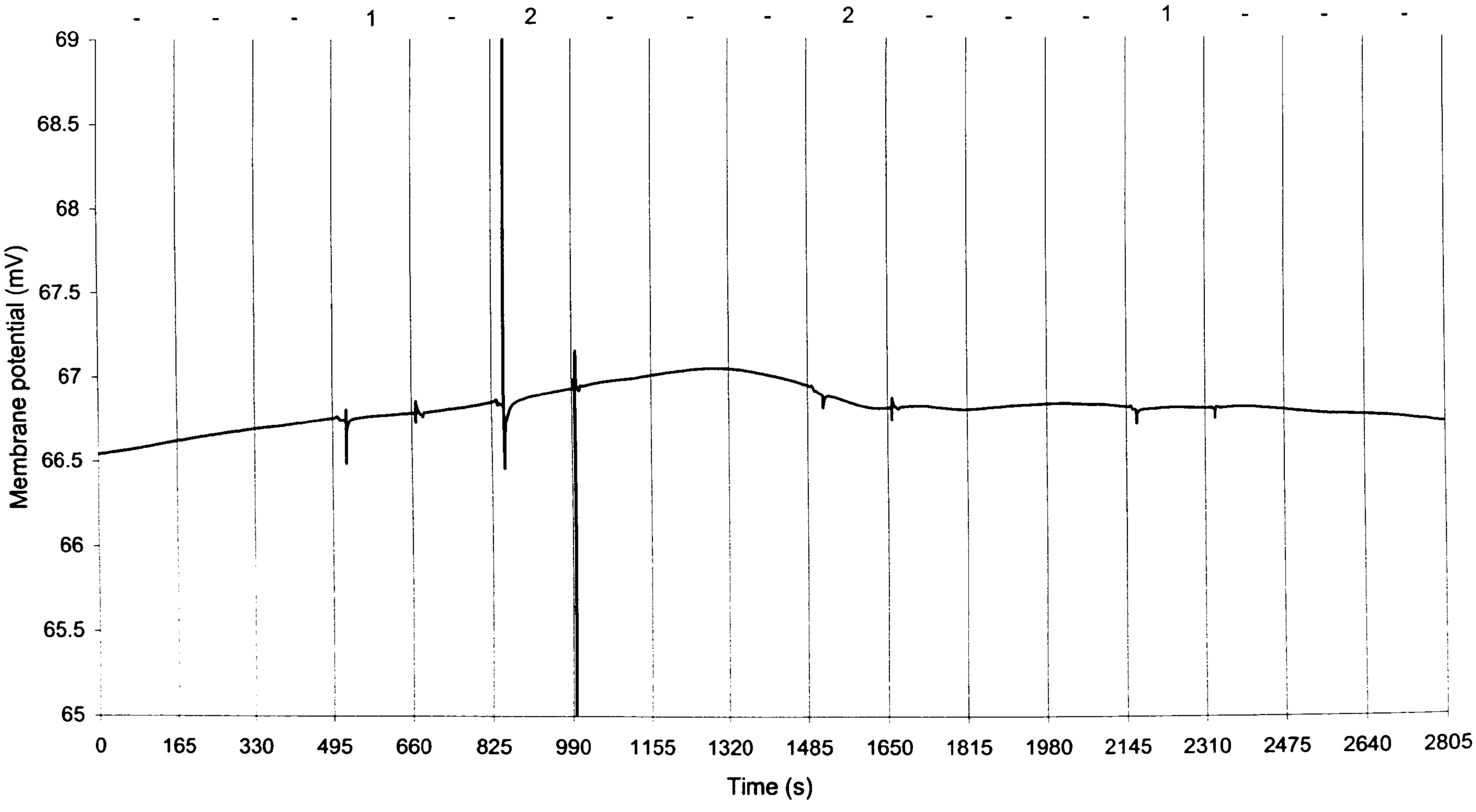

Figure 6.5 Effect of potential difference in electrolyte (constant current)

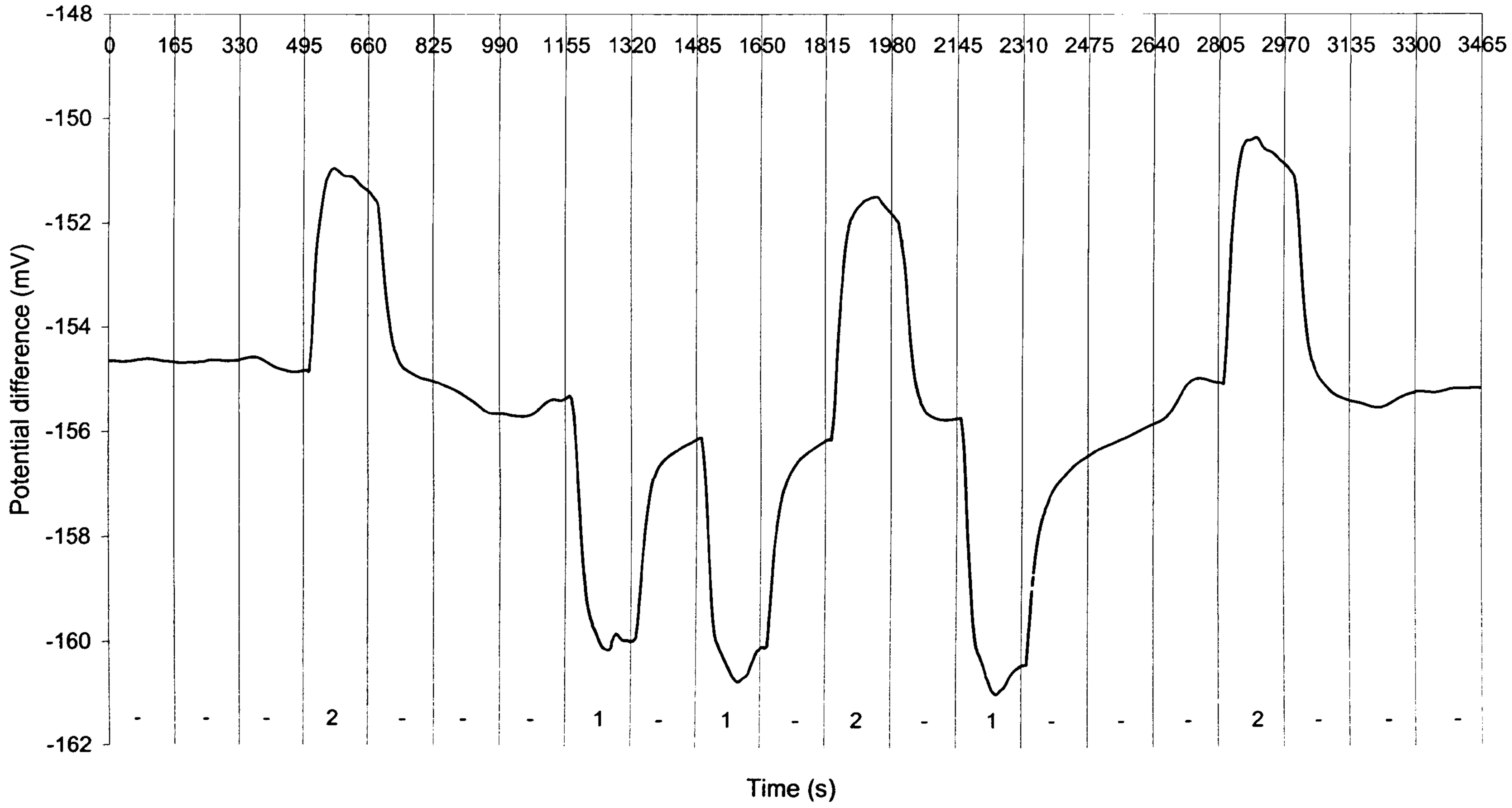

6.3. Discussion

The dependence of the change in membrane potential upon the direction of the applied magnetic field is inconsistent with the expected effect which was predicted in Chapter 4. It was expected that an applied magnetic field would cause sodium ions to collide with the pores of the cation exchange membrane and thus impede the flow of current through the membrane. According to equation (3.1), the direction of the Lorentz force experienced by sodium ions is dependent upon the direction of the applied magnetic field. However, since the pores of the cation exchange membrane are assumed to have rotational symmetry about their axes, it was predicted that collisions between sodium ions and pores would occur regardless of the direction of the applied magnetic field and the resulting Lorentz force. Hence, any change in membrane potential was expected to be independent of the direction in which the magnetic field was applied. This prediction is contradicted by the results presented in Figure 6.3, which show that the change in membrane potential was dependent upon the direction of the applied magnetic field.

The experimental situation may be described with the aid of the equivalent circuit proposed in Figure 6.6. As suggested by Hodgkin and Huxley [1], the membrane is represented by an ideal voltage source in series with a resistance. The EMF of the voltage source, V_r, is equal to the membrane resting potential which results from the separation of sodium chloride solutions of different concentrations across the membrane. The internal resistance of the membrane is represented by a resistance of R ohms, which incorporates the resistivity of

the electrolyte and the resistance to current flow caused by interaction between ions and the pores. With no applied current, the potential difference measured across the membrane is equal to the resting potential. However, an applied current *I* causes a potential difference of magnitude *IR* to develop across the internal resistance of the membrane. The current in the experiments of Section 6.1 was applied in the direction shown in Figure 6.6, such that the direction of the potential difference across the membrane resistance opposes the EMF resulting from the separation of ions across the membrane. The measured membrane potential V_{mem} is equal to:

$$V_{mem} = V_r - IR \tag{6.1}$$

Therefore, when the membrane potential was reduced to zero in these experiments, the applied current was of a sufficient magnitude that the potential difference across the internal resistance was equal and opposite to the membrane resting potential.

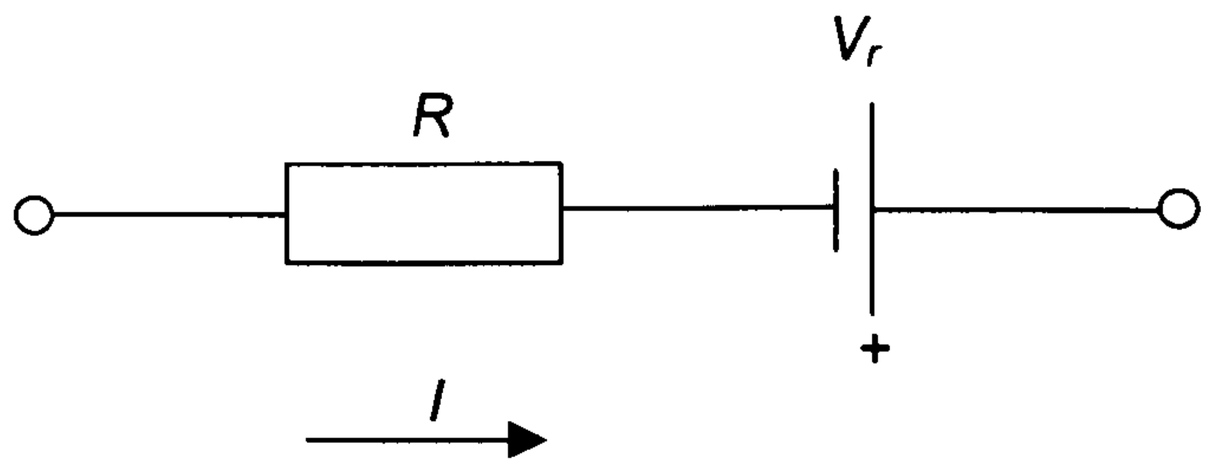

Figure 6.6 Equivalent circuit of membrane

It was expected that an applied magnetic field would impede the flow of sodium ions through the membrane, resulting in an apparent increase in the internal

resistance of the membrane. Since current in the membrane was constant due to the use of a current source, the magnitude of the potential difference across the internal resistance (*IR*) was expected to increase. Therefore, it was predicted from equation (6.1) that membrane potential would decrease, regardless of the direction of the applied magnetic field. However, Figure 6.3 shows that membrane potential decreases only in the presence of a magnetic field in direction 1, while a magnetic field in direction 2 caused membrane potential to increase. Thus, while a magnetic field in direction 1 caused the predicted increase in the internal resistance of the membrane, a field in the opposite direction caused an apparent decrease in resistance. These results provide evidence to suggest that the hypothetical mechanism of collisions between sodium ions and the cation exchange membranes did not occur in these experiments.

For the control experiment conducted in the absence of a membrane, an applied magnetic field produced an unexpected change in the potential difference developed across the resistive medium of the electrolyte. Figure 6.5 illustrates that the magnitude of the potential difference between two salt bridges placed within sodium chloride solution is increased by a magnetic field in direction 1 and is reduced by a magnetic field in direction 2. These results are in agreement with those in the presence of a membrane, in which a magnetic field in direction 1 increased the potential difference across the internal resistance of the membrane and a magnetic field in direction 2 reduced the voltage across the internal resistance. The similarity of these results suggests that the same mechanism of interaction between sodium chloride solution and a

magnetic field may occur in both the presence and absence of a membrane. Therefore, this control experiment provides additional evidence that the measured changes in membrane potential were not caused by collisions between sodium ions and pores.

It is considered that the experimental observations were not caused by an experimental artefact. Transient changes in potential difference may be caused by electromagnetic induction in the electrolyte and connecting wires during the application or removal of a magnetic field. However, the results of the control experiment conducted in the absence of an applied current (Figure 6.4) demonstrate that these induced voltages last for only a few seconds. This contrasts to the results of Figures 6.3 and 6.5, which demonstrate a long-term effect of the magnetic field upon potential difference in the sodium chloride solution. Therefore, the unexpected effect of the magnetic field cannot be attributed to electromagnetic induction. This control experiment also allows the possibility of a magnetically mediated change in the membrane resting potential V_r to be discounted.

The repeatability of these experiments indicates that the magnetic field has a direct effect upon sodium chloride solution. Additionally, the control experiment in which the membrane resting potential was unaffected by a magnetic field in the absence of an applied current, suggests that a flow of current is necessary for this phenomenon to occur. Although these experiments have not demonstrated the feasibility of the hypothetical mechanism of non-invasive anaesthesia, they do provide evidence of an interaction between sodium

chloride solution and an applied magnetic field. Further investigation of this novel phenomenon was considered to be worthwhile, since an improved understanding of the effect of magnetism upon these common physiological ions may allow other non-invasive anaesthesia techniques to be devised. Therefore, Chapter 7 is concerned with a further investigation of this phenomenon.

The unexpected results reported in this chapter do not give satisfactory evidence to prove or disprove the hypothetical method of non-invasive anaesthesia proposed in Chapter 4. Therefore, an alternative method to assess the feasibility of the non-invasive anaesthesia technique is considered in Chapter 8.

6.4 References

1. Hodgkin, A.L. and Huxley, A.F.
   A Quantitative Description of Membrane Current and its Application to Conduction and Excitation in Nerve.
   Journal of Physiology, Vol. 117, 1952, pp. 500-544.

7. EFFECT OF A MAGNETIC FIELD ON THE ELECTROLYSIS OF SODIUM CHLORIDE SOLUTION

The experiments of Chapter 6 demonstrated an unexpected interaction between sodium chloride solution and an applied magnetic field. Therefore, further experiments were conducted to fully document this phenomenon and to suggest possible explanations for the observed results.

7.1 Experimental Method

A great number of experiments were performed to attempt to explain the experimental results of Chapter 6. A subset of these experiments, referred to as experiments *(a)*-*(f)* for convenience, are described in this chapter.

(a) The apparatus was set up as illustrated in Figure 7.1. This apparatus and method was similar to that previously described in greater detail in Section 6.1, except for the inclusion of an additional multimeter (Thurlby 1905a) which was connected across the current source to measure the voltage applied to the electrolyte. In the absence of an applied current, the membrane potential was approximately 70 mV. A current of 1 mA was passed through the sodium chloride solution. This current is much larger than that required to reduce the membrane potential to zero volts, but increases the voltage applied across the solution by the current source and thus facilitates the observation of variations in the supply voltage. The potential difference across the current source was

recorded as magnetic fields were applied in the regime described in Section 6.1.

(b) The membrane was removed from the apparatus of experiment *(a)* and the Ussing chamber was filled with 20 ml of 0.1 M sodium chloride solution (Figure 7.2). The experimental method was similar to that of the second control experiment described in Section 6.1. A current of 3 mA was passed through the electrolyte, while the response of the voltage across the current source to magnetic fields, applied in the usual regime, was recorded.

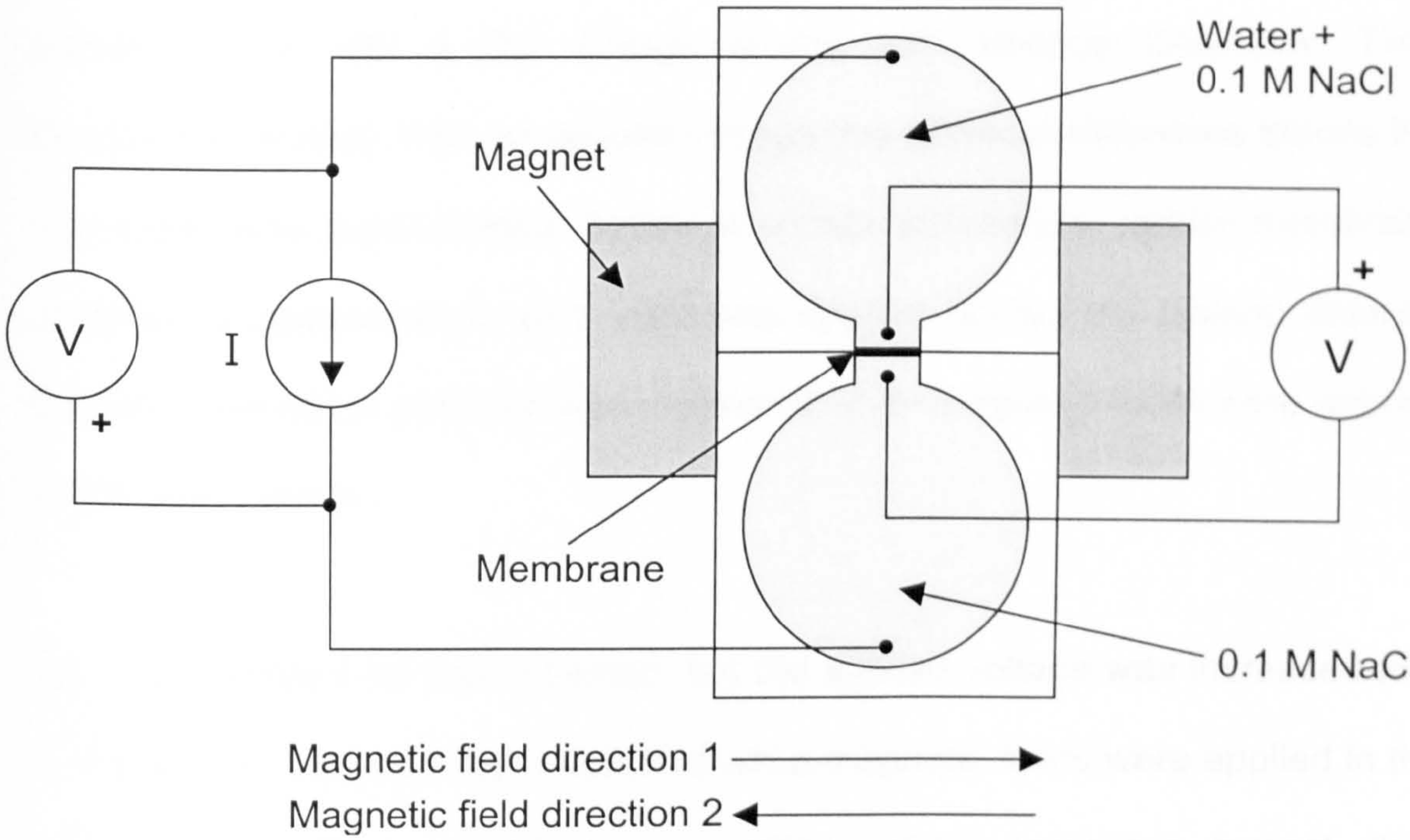

Figure 7.1. Apparatus for experiment *(a)*

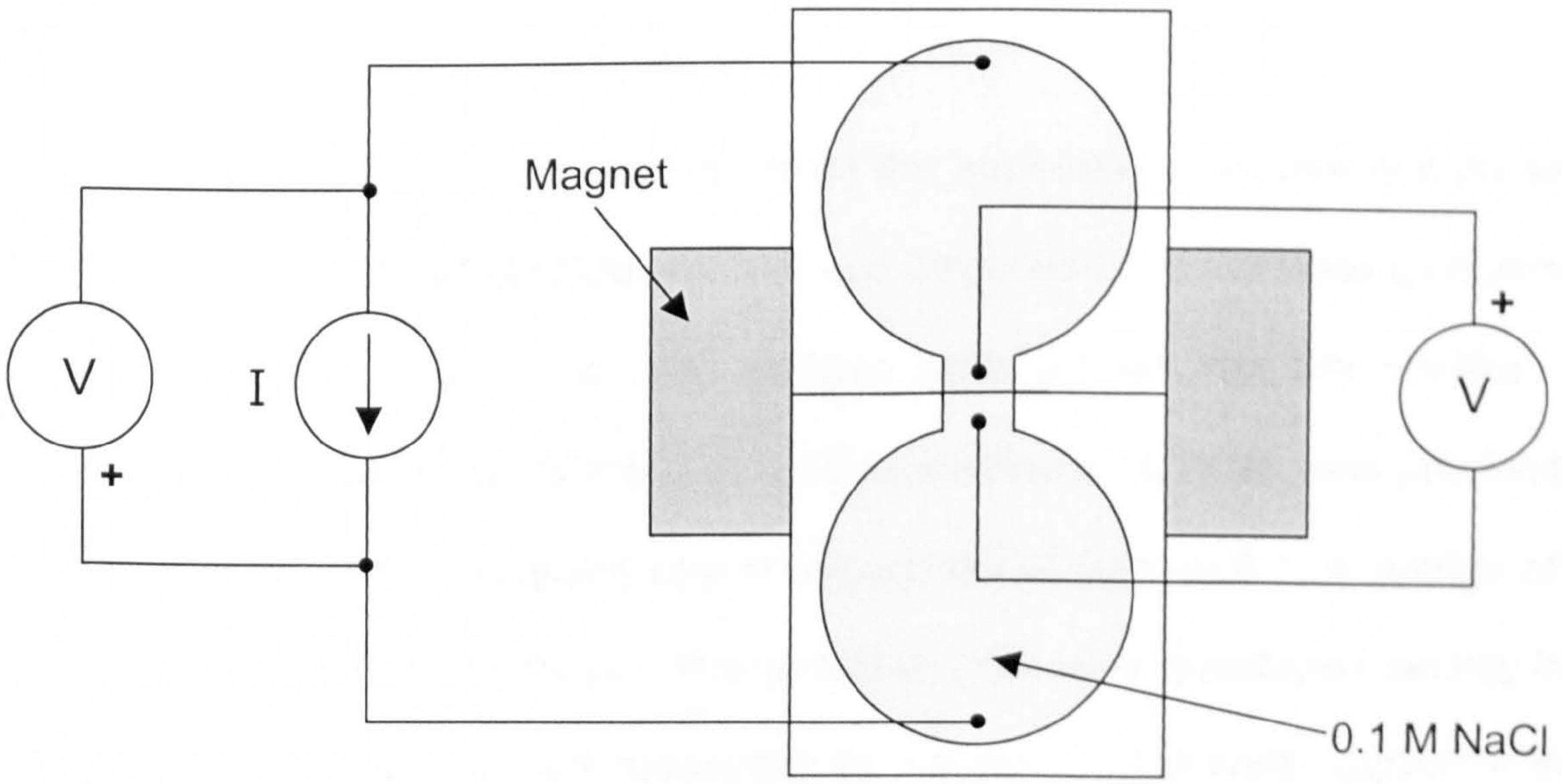

Figure 7.2. Apparatus for experiment *(b)*

(c) The apparatus was set up as shown in Figure 7.3. The apparatus and method are similar to those of Section 6.1, except for the substitution of the current source with a DC voltage source (DC Voltage Calibrator, Time Electronics Limited). With no applied voltage, the potential difference across the membrane was approximately 70 mV. A voltage sufficient to reduce membrane potential to approximately zero volts was applied across the sodium chloride solution. Membrane potential was measured while magnetic fields were applied in the usual regime.

(d) Experiment *(c)* was repeated, but the applied voltage was increased to 4 V. Current in the circuit was measured while magnetic fields were applied in the usual regime. The use of a larger applied voltage increases current, thus facilitating the observation of variations in current which result from an applied magnetic field.

(e) The membrane was removed from the apparatus of experiment *(c)* and 20 ml of 0.1 M sodium chloride solution was dispensed into the Ussing chamber as illustrated in Figure 7.4. Salt bridges were placed into the solution in positions corresponding to those at which membrane potential was previously measured, as with the second control experiment of Section 6.1. A voltage of 4 V was applied to the solution. The potential difference developed across the electrolyte and current were measured as magnetic fields were applied in the usual regime.

(f) A DC voltage of 4 V was applied across sodium chloride solution using the apparatus of Figure 7.4. To observe the effect of prolonged magnetic exposure, the current in the electrolyte was measured when magnetic fields were applied in directions 1 and 2 for one hour periods. The polarity of the applied voltage was then reversed and the experiment was repeated.

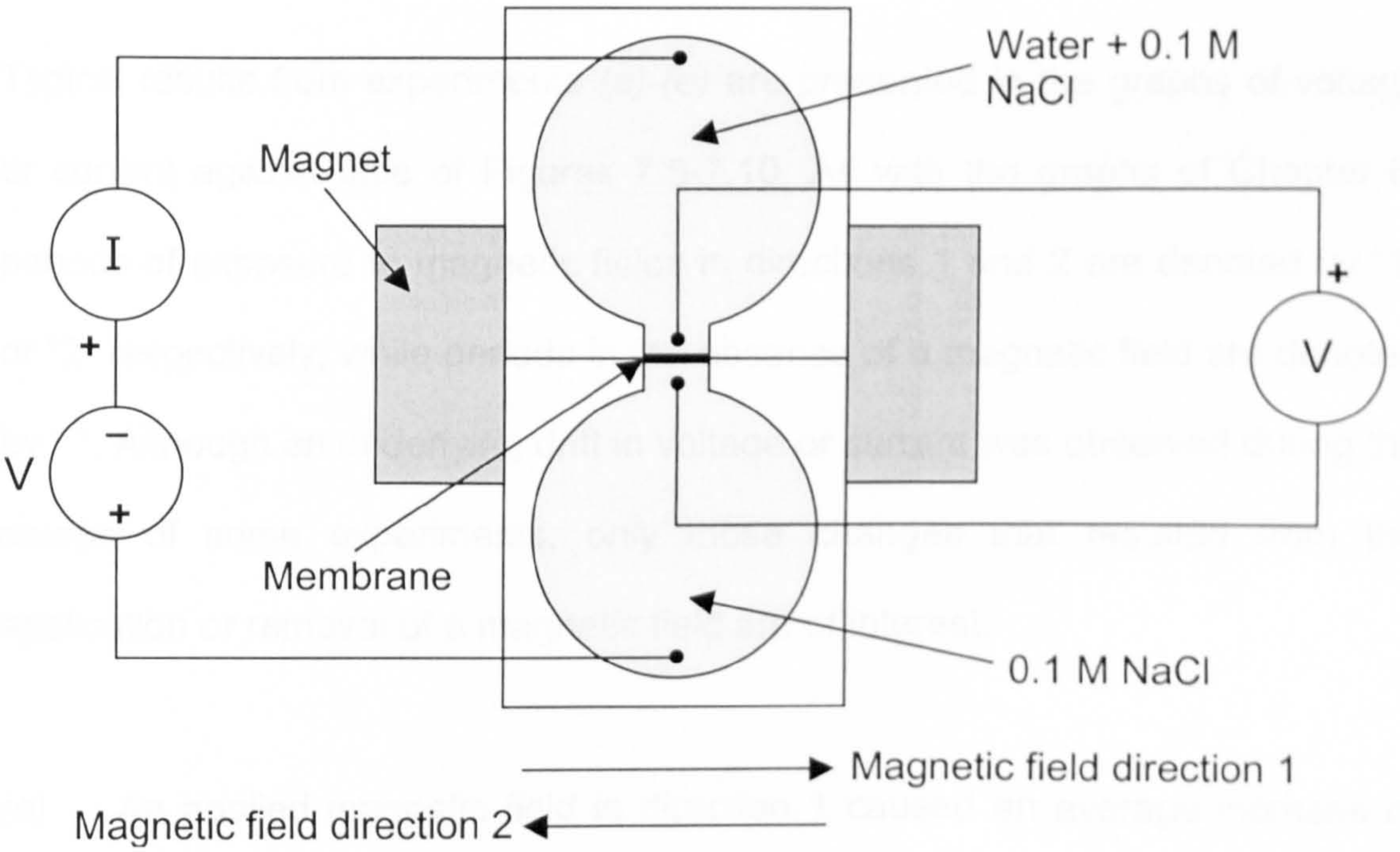

Figure 7.3. Apparatus for experiments *(c)* and *(d)*

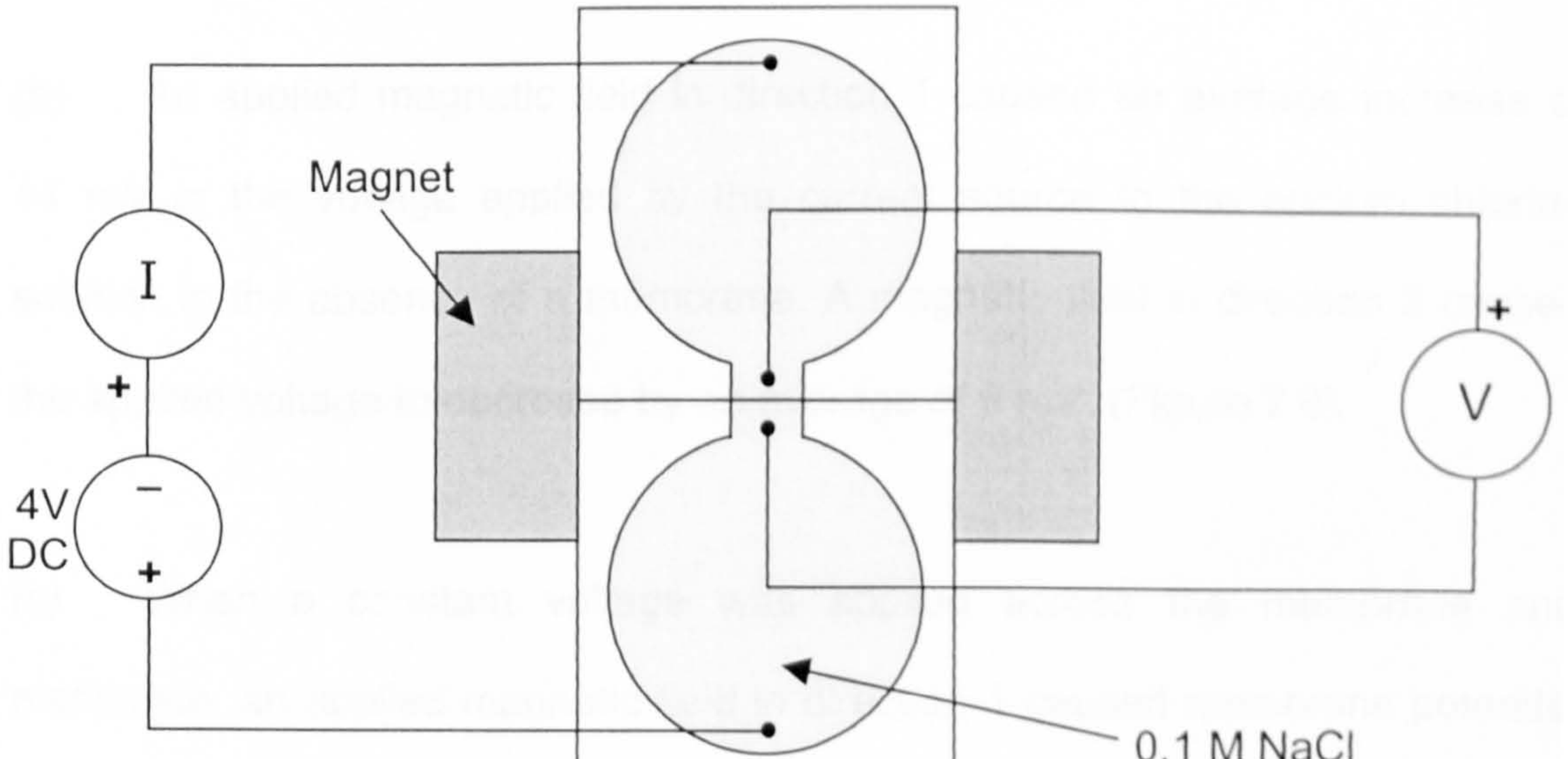

Figure 7.4. Apparatus for experiments *(e)* and *(f)*

7.2 Results

Typical results from experiments *(a)-(e)* are presented in the graphs of voltage or current against time of Figures 7.5-7.10. As with the graphs of Chapter 6, periods of exposure to magnetic fields in directions 1 and 2 are denoted by "1" or "2" respectively, while periods in the absence of a magnetic field are denoted by "-". Although an underlying drift in voltage or current was observed during the course of some experiments, only those changes that resulted from the application or removal of a magnetic field are of interest.

(a) An applied magnetic field in direction 1 caused an average increase of 17 mV in the voltage supplied by the current source to the sodium chloride solution and membrane, while a magnetic field in direction 2 caused an average 15 mV reduction in voltage. (Figure 7.5)

(b) An applied magnetic field in direction 1 caused an average increase of 14 mV in the voltage applied by the current source to the sodium chloride solution in the absence of a membrane. A magnetic field in direction 2 caused the applied voltage to decrease by an average of 6 mV. (Figure 7.6)

(c) When a constant voltage was applied across the membrane and electrolyte, an applied magnetic field in direction 1 caused membrane potential to decrease by an average of 0.3 mV (Figure 7.7). However, membrane potential showed a tendency to increase towards its previous value after 2 minutes of exposure to the magnetic field. The effect of a magnetic field in

direction 2 is less pronounced than for the other experiments presented here. Membrane potential rapidly decreased by approximately 0.1 mV following the application of a magnetic field in direction 2, but then rapidly increased to a value slightly greater than that before magnetic exposure. This trend, particularly the observation of a rapid consecutive decrease then increase in membrane potential, is similar to that when a magnetic field in direction 2 was applied when a constant current was passed through the membrane (Figure 6.3). It is therefore considered that the magnetic field in direction 2 increases membrane potential.

(d) A magnetic field in direction 1 caused the current supplied to the electrolyte and membrane by the voltage source to decrease by an average of 27 μA. An applied magnetic field in direction 2 caused current to increase by an average of 29 μA. (Figure 7.8)

(e) When a constant voltage was applied across sodium chloride solution in the absence of a membrane, a magnetic field in direction 1 caused the magnitude of the potential difference between two salt bridges in the electrolyte to increase by an average of 2 mV. Application of a magnetic field in the opposite direction caused the magnitude of the potential difference between the salt bridges to decrease by an average of 2 mV (Figure 7.9.) A magnetic field in direction 1 caused an average decrease of 17 μA in the current supplied by the voltage source. An applied magnetic field in direction 2 caused current to increase by an average of 17 μA (Figure 7.10).

The results of experiments *(a)-(e)*, together with those of Chapter 6, are summarised in Table 7.1. This summary of results clearly shows that the effect of a magnetic field in direction 1 is always opposite to that for a magnetic field in direction 2.

Experiment	Effect of applied magnetic field	
	Direction 1	Direction 2
Membrane potential (constant current)	Decreases	Increases
Applied voltage in presence of membrane (constant current)	Increases	Decreases
Membrane potential (constant voltage)	Decreases	Increases
Applied current in presence of membrane (constant voltage)	Decreases	Increases
Potential difference across bulk electrolyte (constant current)	Increases	Decreases
Applied voltage in absence of membrane (constant current)	Increases	Decreases
Potential difference across bulk electrolyte (constant voltage)	Increases	Decreases
Applied current in absence of membrane (constant voltage)	Decreases	Increases

Table 7.1 Summary of experimental results

Figure 7.5 Effect of magnetic field on applied voltage (constant current)

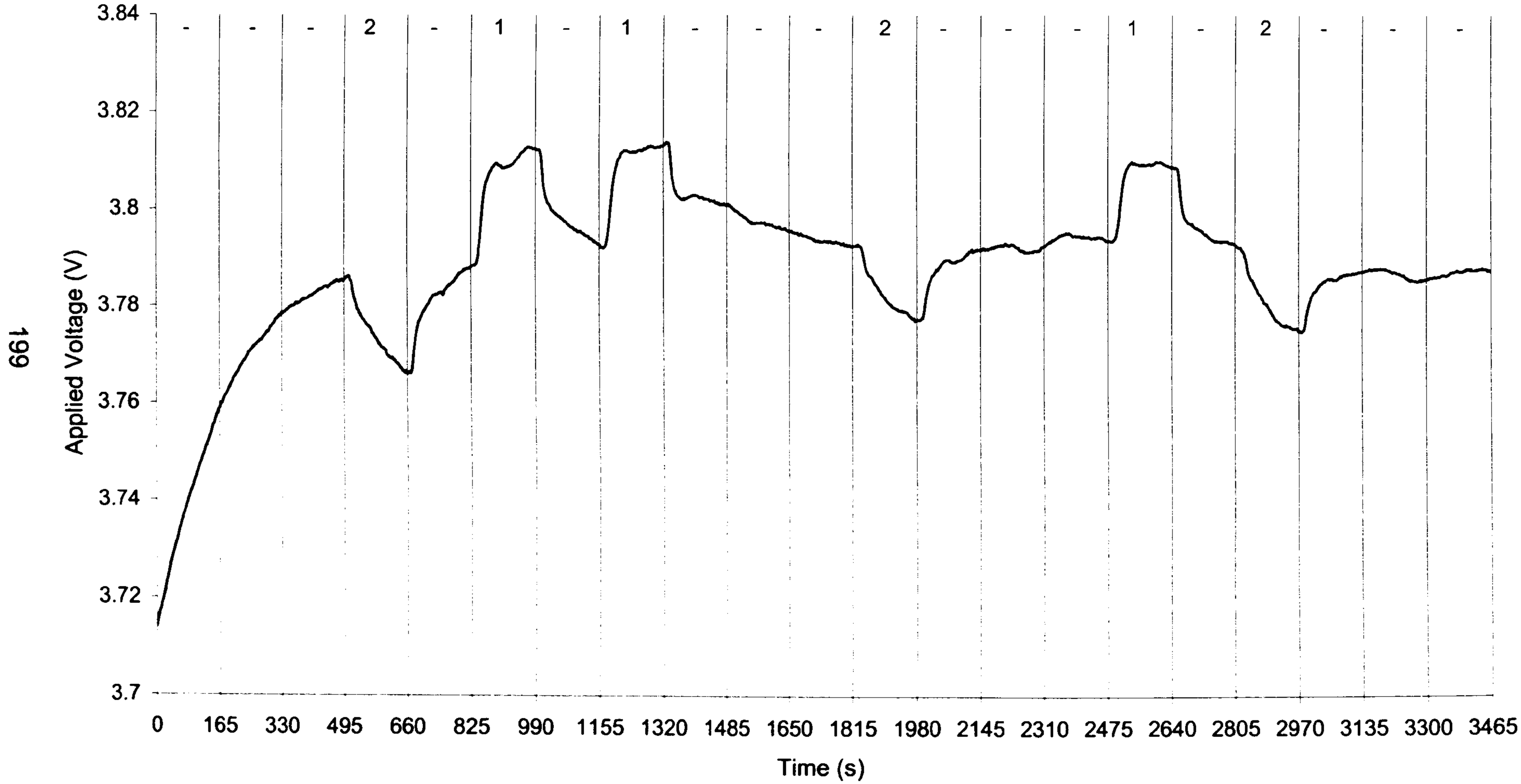

Figure 7.6 Effect of magnetic field on applied voltage in absence of a membrane (constant current)

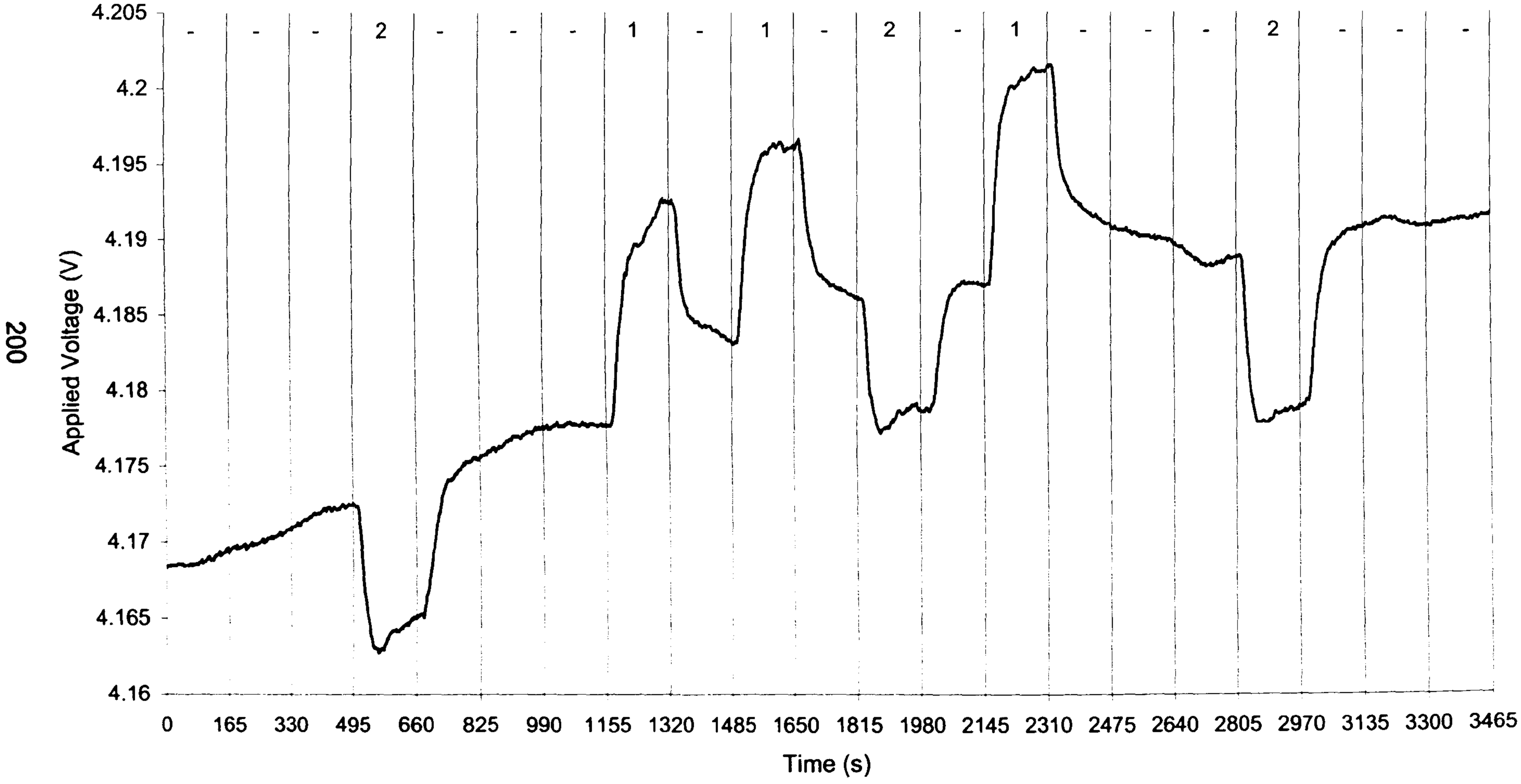

Figure 7.7 Effect of magnetic field on membrane potential (constant voltage)

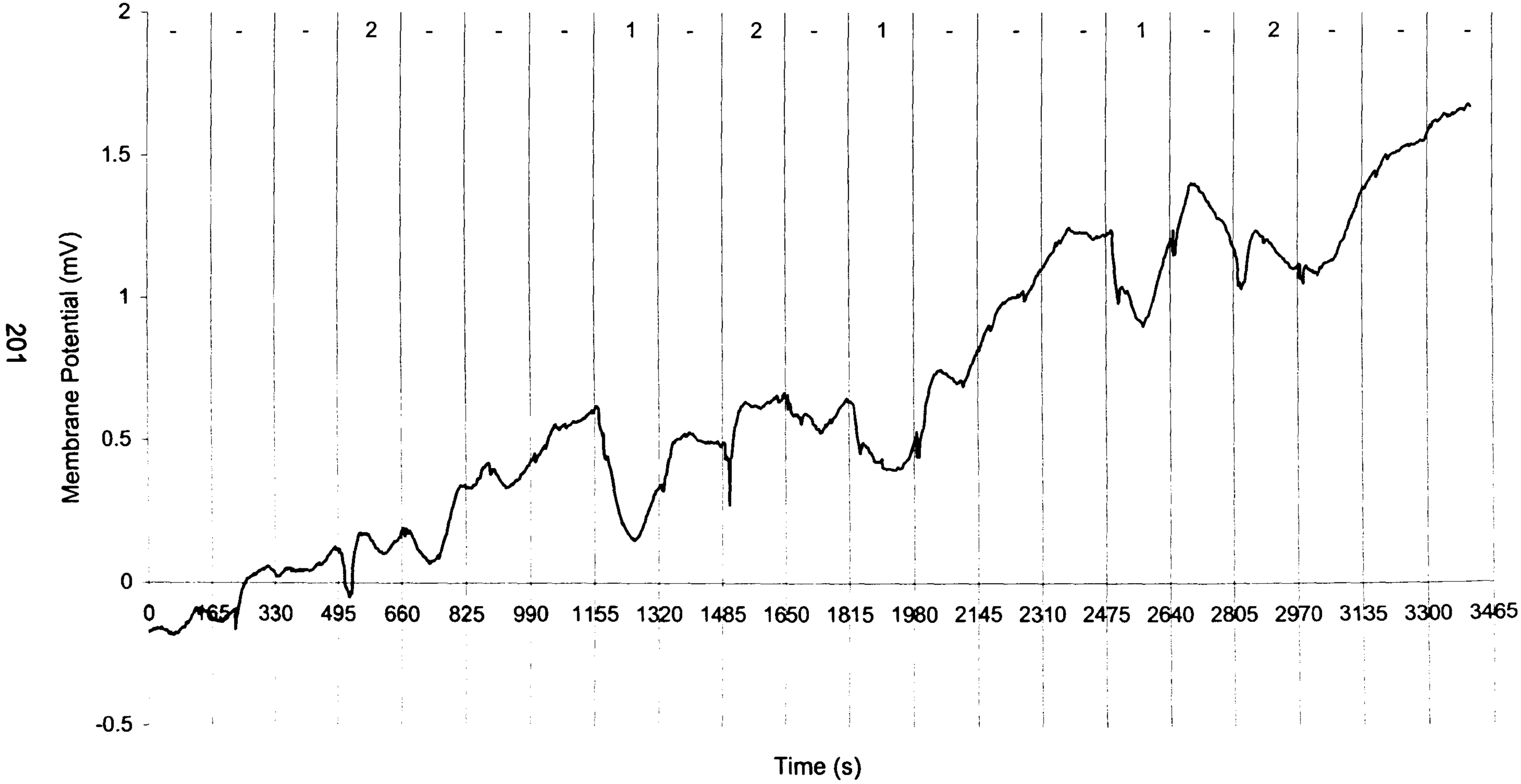

Figure 7.8 Effect of magnetic field on applied current (constant voltage)

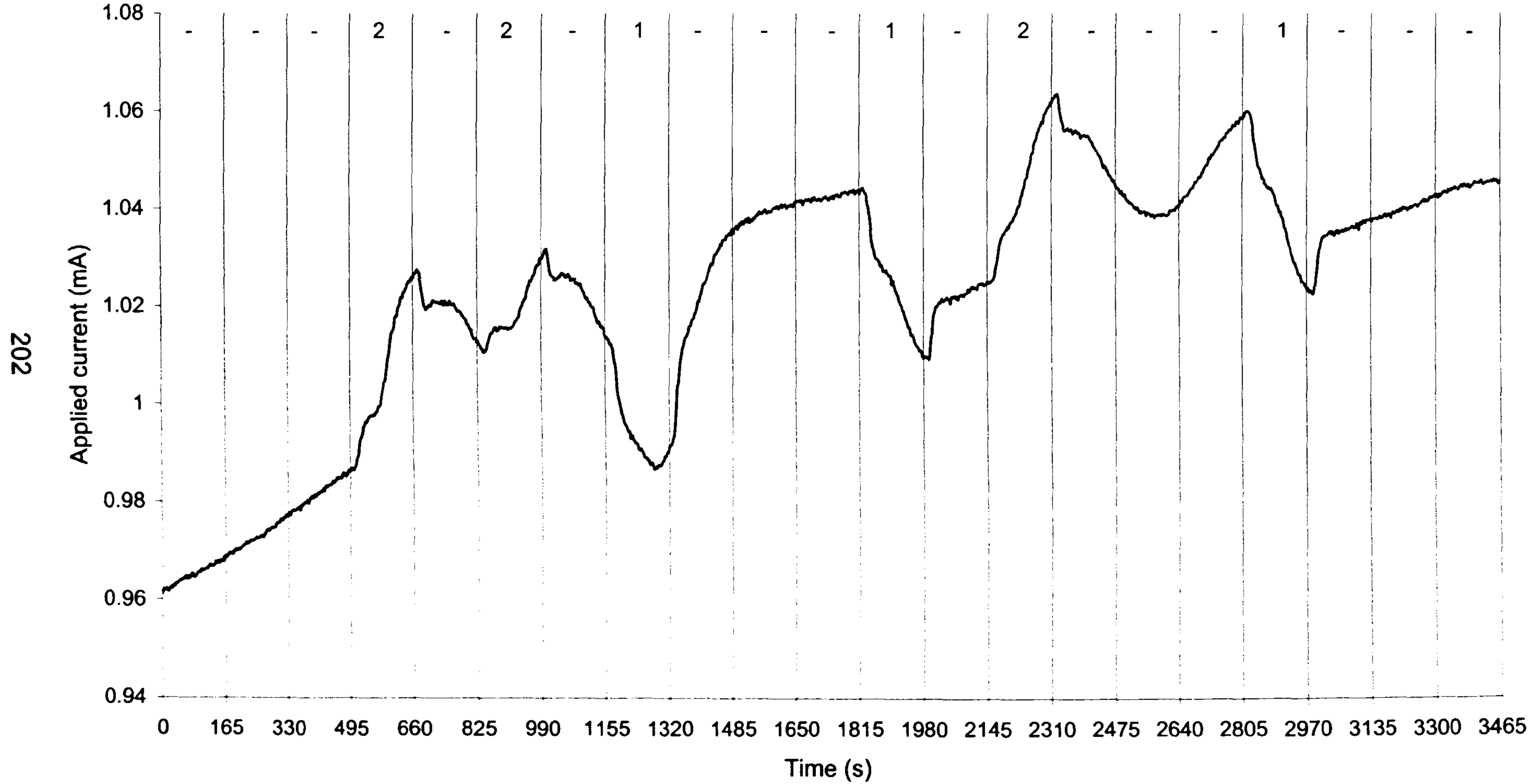

Figure 7.9 Effect of magnetic field on potential difference in electrolyte (constant voltage)

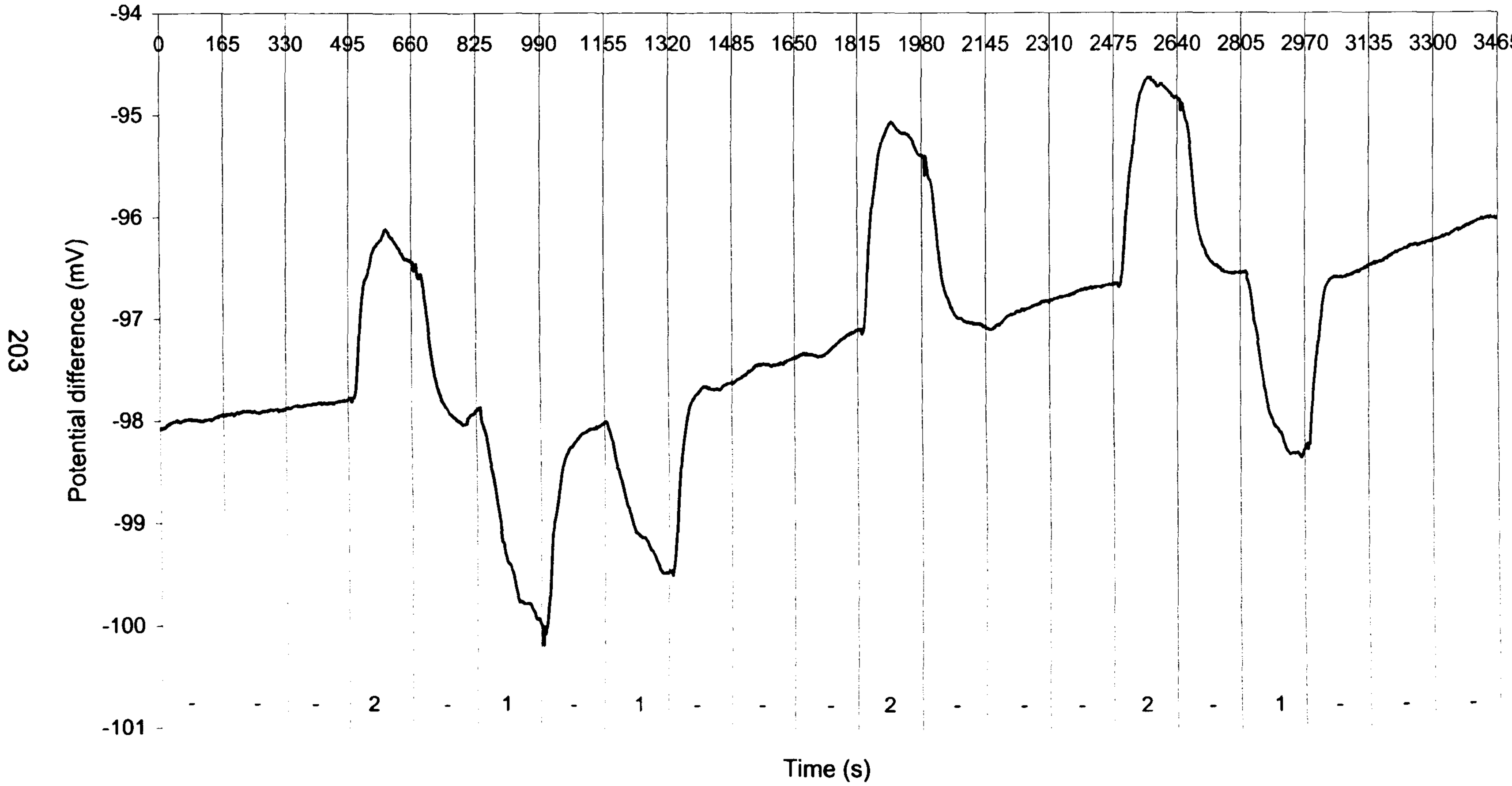

Figure 7.10 Effect of magnetic field on applied current in absence of a membrane (constant voltage)

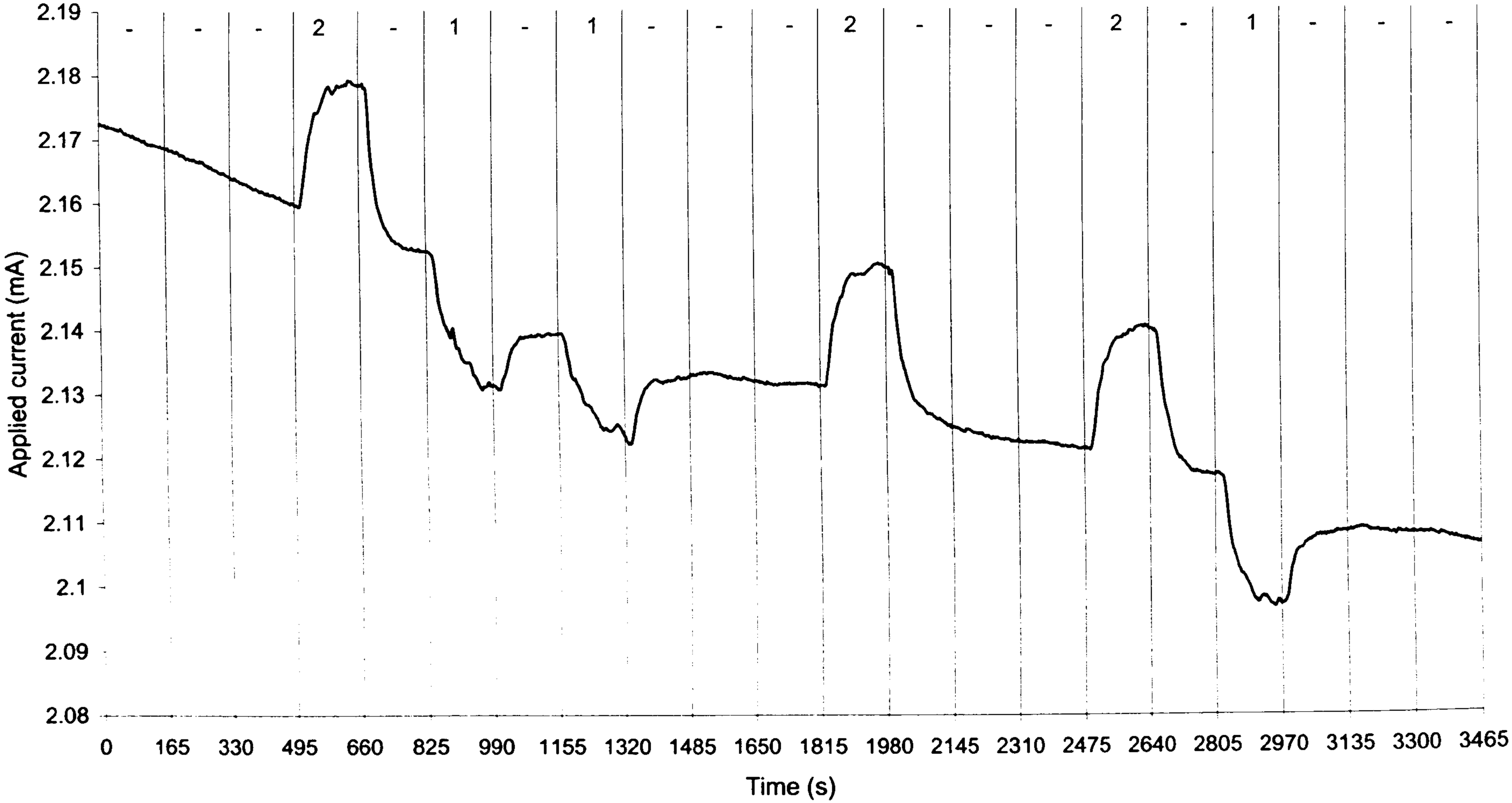

(f) Figures 7.11 and 7.12 illustrate the long term effects of an applied magnetic field on the current supplied to 0.1 M sodium chloride solution by the voltage source. When the applied voltage was in the direction indicated in Figure 7.4, an applied magnetic field in direction 1 caused a rapid rise in current as shown in Figure 7.11. After approximately 2 minutes of magnetic exposure and when current had increased by 50 μA, a small decrease in current was observed. However, current began to rise again after a further 90 seconds. The maximum increase in current of approximately 220 μA was achieved after approximately 30 minutes of magnetic exposure, which was followed by a small decrease in current. When the magnetic field was removed, current sharply decreased by 70 μA. After this sharp decrease, there was a rapid 30 μA increase in current which was followed by a slow decrease in current.

When a magnetic field was applied in direction 2, there was a rapid 160 μA decrease in current. A slight increase in current occurred approximately 2 minutes after the magnetic field was applied, followed by a steady decrease in current over the rest of the experiment. Removal of the magnetic field caused a sharp increase in current. However, the tendency for the current to return to its value in the presence of a magnetic field, observed when the field was applied in direction 1, did not occur with a magnetic field in the opposite direction.

The effect of a magnetic field on current when the polarity of the applied voltage was reversed is shown in Figure 7.12. When the applied voltage was reversed, the response of the system to a magnetic field in any given direction was similar to that which was previously observed with the original voltage polarity and a

magnetic field applied in the opposite direction. In other words, the effect of a magnetic field in direction 1 in Figure 7.12 is similar to that for a magnetic field in direction 2 shown in Figure 7.11; the graph obtained with a magnetic field in direction 2 as shown in Figure 7.12 bears many similarities to that for a magnetic field in direction 1 in Figure 7.12.

Figure 7.11 Effect of prolonged magnetic exposure on applied current

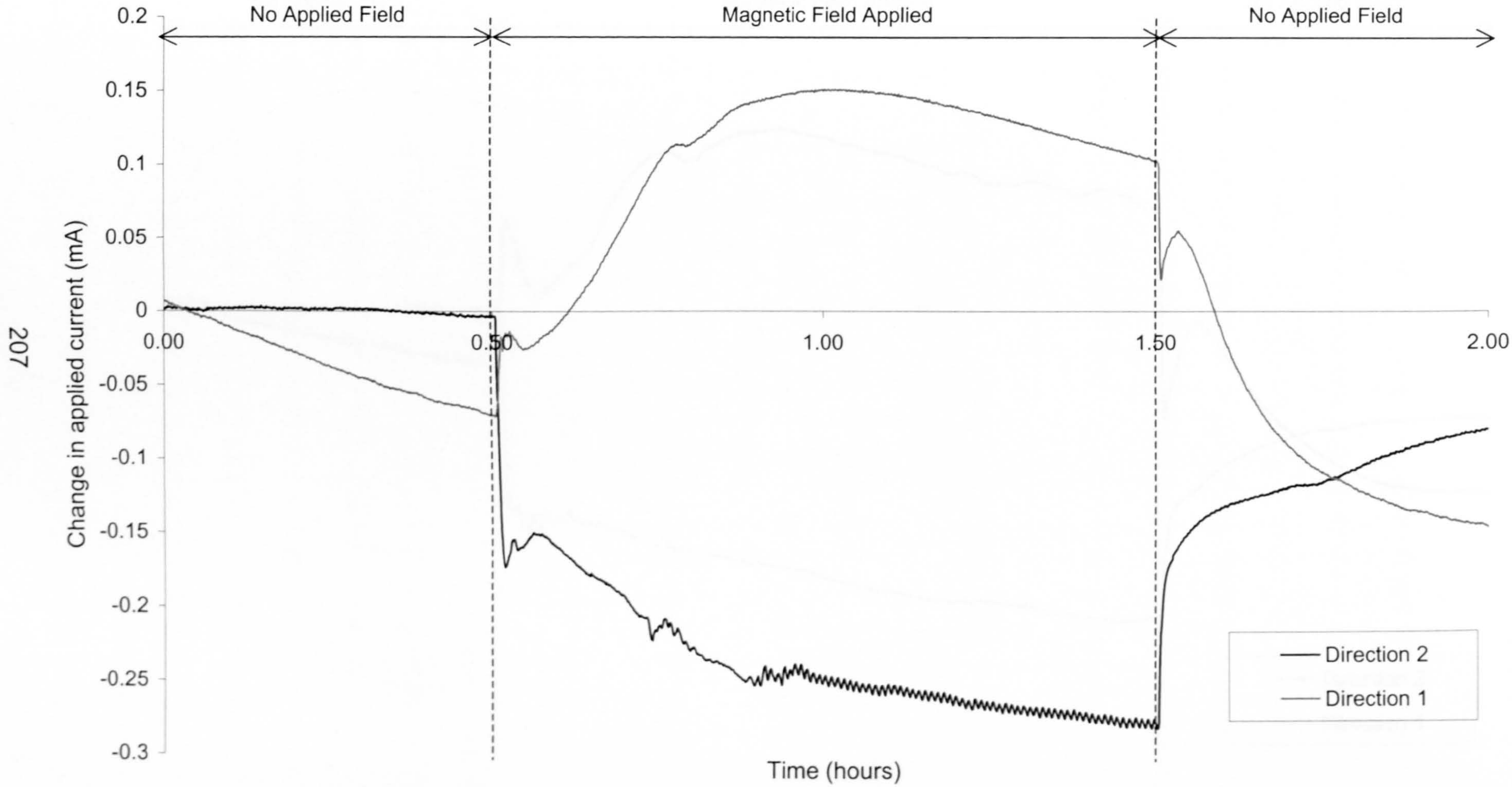

Figure 7.12 Effect of prolonged magnetic exposure on applied current (reversed current direction)

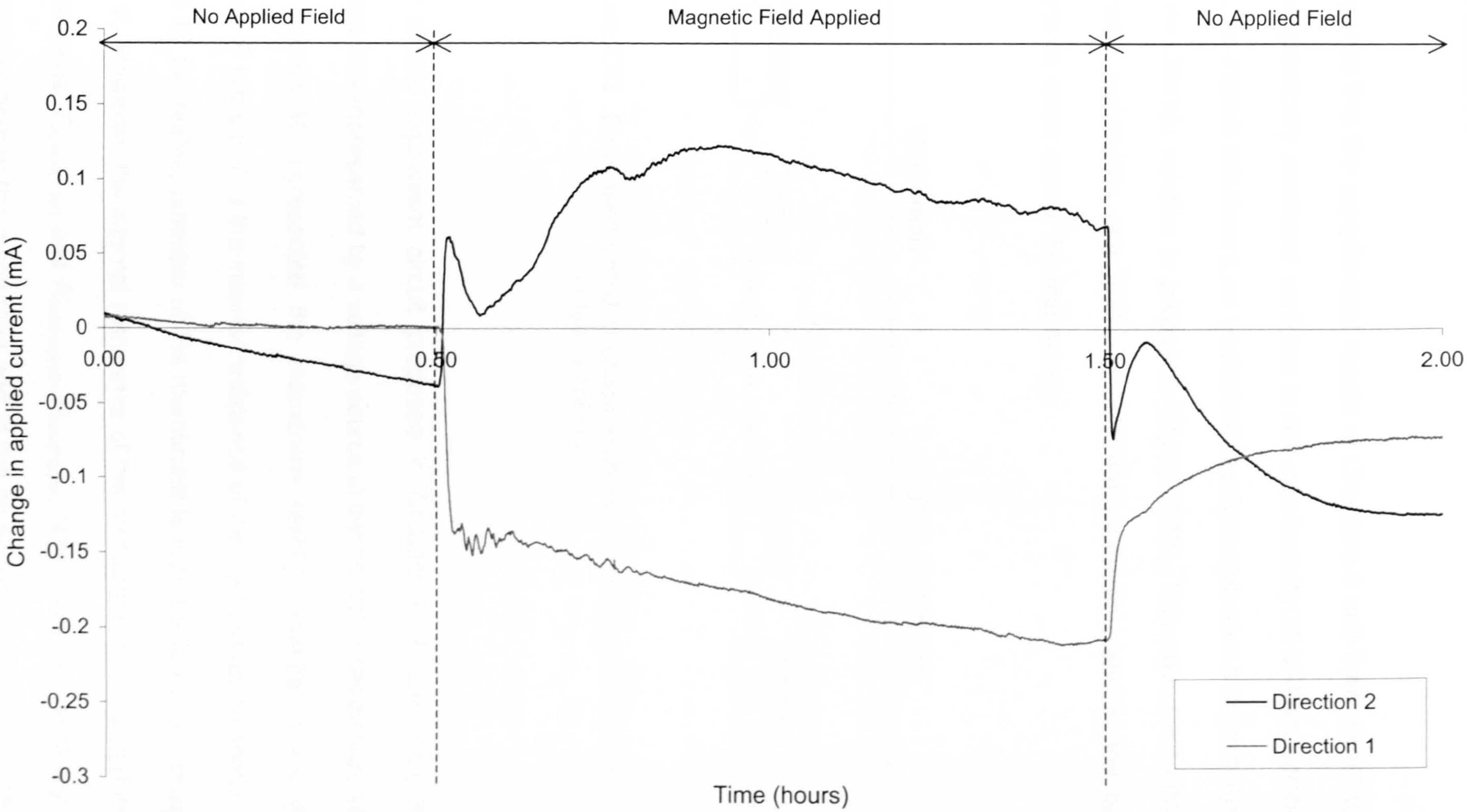

7.3 Discussion

It is proposed that the experimental results of Chapters 6 and 7 are consistent with a magnetically mediated variation in the conductivity of sodium chloride solution. To explain this theory, an equivalent circuit to represent the electrolysis of sodium chloride solution is proposed (Figure 7.13). This equivalent circuit incorporates resistivities and EMFs in both the membrane and in the bulk electrolyte on either side of the membrane.

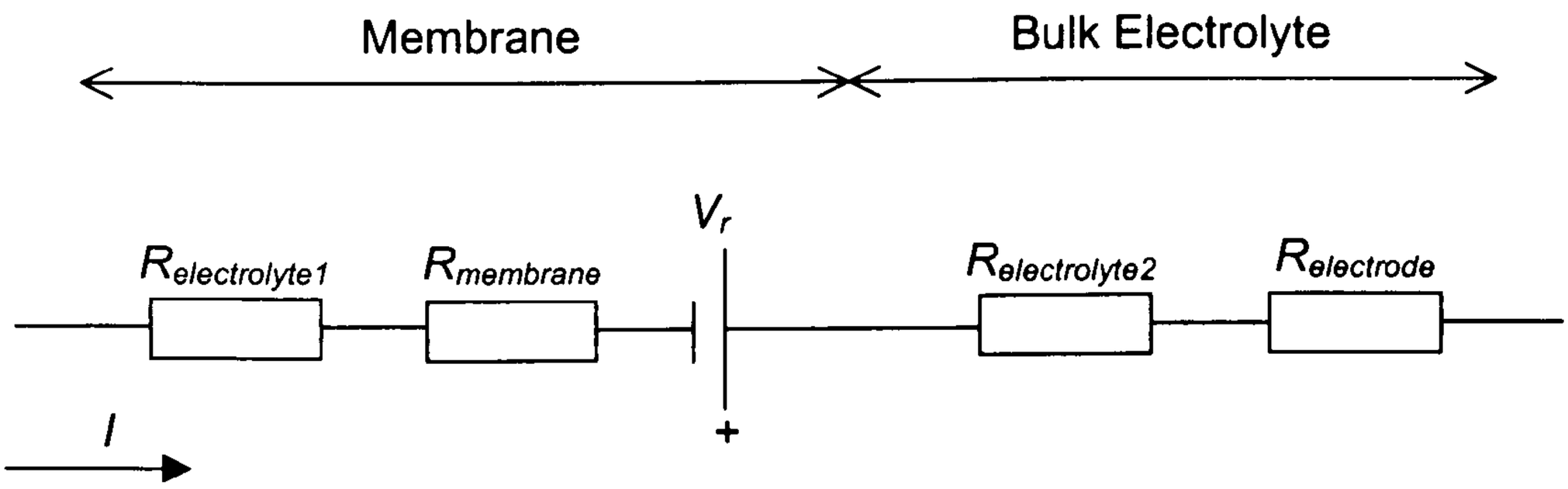

Figure 7.13 Equivalent circuit of cation exchange membrane in sodium chloride solution

For the simple equivalent circuit proposed in Chapter 6 (Figure 6.6), the membrane was represented by a voltage source in series with a resistance. The voltage source V_r represented the membrane resting potential, while the resistance R represented the internal resistance of the membrane. Similarly, in Figure 7.13 the resting potential of the membrane is represented by a voltage source, V_r. However, the internal resistance of the membrane is separated into two resistances, $R_{electrolyte1}$ and $R_{membrane}$. $R_{electrolyte1}$ represents the resistivity of the electrolyte, both in the membrane and in the small regions of bulk solution

that separate the salt bridges from the membrane. $R_{membrane}$ represents the tendency of the membrane to impede the flow of ions, which may occur due to the limited cross-sectional area available for ions to cross the membrane or due to electrostatic attraction between ions and the pores (described further in Section 8.3). The resistance of the membrane may be as much as ten times that of an equivalent volume of electrolyte [1]. Measurements of membrane potential V_{mem} correspond to the net potential difference across V_r , $R_{electrolyte1}$ and $R_{membrane}$, i.e.

$$V_{mem} = V_r - I(R_{electrolyte1} + R_{membrane}) \quad (7.1)$$

The resistance of the bulk electrolyte is considered to have two components, $R_{electrolyte2}$ and $R_{electrode}$. $R_{electrolyte2}$ represents the resistance of the sodium chloride solution in each of the baths of the Ussing Chamber, excluding the electrolyte in the region of the membrane that is already represented by $R_{electrolyte1}$, and is considered to be an ohmic resistance. $R_{electrode}$ is the resistance of the interface between the platinum electrodes and the sodium chloride solution. $R_{electrode}$ may be influenced by a number of factors including the formation of gas bubbles on the electrode which increase the resistance of the electrode/electrolyte interface. EMFs which form at the interfaces of each electrode and the electrolyte are neglected since these EMFs oppose each other and are assumed to have no net effect. The total resistance of the bulk electrolyte is non-linear as demonstrated by Figure 7.14, in which the apparatus of Figure 7.4 was used to measure the current in 0.1 M sodium chloride solution for a range of applied voltages, from which the resistance of the solution was calculated. Figure 7.14 shows an inverse relationship between resistance and

applied voltage and the majority of this non-linearity is assumed to result from the properties of the electrode/electrolyte interface.

It is proposed that when current flow is in the direction indicated in Figures 7.1-7.4, a magnetic field in direction 1 causes an increase in the resistivity of the electrolyte. In other words, the magnitude of the resistances $R_{electrolyte1}$ and $R_{electrolyte2}$ in the equivalent circuit are increased when a magnetic field is applied in direction 1. Conversely, a magnetic field in direction 2 causes the resistivity of the sodium chloride to decrease and thus causes $R_{electrolyte1}$ and $R_{electrolyte2}$ to decrease. The experimental results summarised in Table 7.1 for a magnetic field in direction 1 will be considered on an individual basis, to demonstrate their consistency with the theory that the resistivity of sodium chloride solution is affected by a magnetic field. Similar reasoning may be used to explain the results observed with a magnetic field in direction 2.

For the experiment in which a constant current was passed through the cation exchange membrane, a magnetic field applied in direction 1 caused membrane potential to decrease while the applied voltage across the membrane and electrolyte increased. Since current is constant, equation (7.1) implies that a decrease in membrane resting potential or an increase in either of the two resistances, $R_{electrolyte1}$ and $R_{membrane}$, could cause the potential difference across the membrane to decrease. The first control experiment performed in Chapter 6 suggested that the resting potential of the membrane is unaffected by an applied magnetic field. Therefore, either of the two resistances in the equivalent circuit must have increased to provide the observed decrease in membrane

potential. Similarly, an increase in the total resistance of the equivalent circuit of Figure 7.13 would explain the increase in the voltage supplied by the current source. There is evidence to suggest that the resistance of the electrode/electrolyte interface may be affected by an applied magnetic field, via magnetohydrodynamic effects which affect the rate of mass transport at the electrodes [2]. However, the only consistent explanation for both observations is that the resistivity of the electrolyte increased, and thus resistances $R_{electrolyte1}$ and $R_{electrolyte2}$ increased, due to the applied magnetic field in direction 1.

It was observed that both membrane potential and current decreased when a magnetic field was applied in direction 1 during the experiment in which a voltage was applied across the cation exchange membrane and electrolyte. Assuming that $R_{electrode}$ and $R_{membrane}$ remain constant, an increase in $R_{electrolyte1}$ would cause membrane potential to decrease since a greater proportion of the voltage applied to the potential divider network of Figure 7.13 would exist across $R_{electrolyte1}$. Similarly, an increase in the total resistance of the circuit due to an increase in $R_{electrolyte1}$ and $R_{electrolyte2}$ would cause a reduction in current, for a constant applied voltage.

For those experiments conducted without a membrane, the simplified equivalent circuit of Figure 7.15 may be used to analyse the effect of the magnets. While $R_{electrode}$ and $R_{electrolyte2}$ have the same interpretation as in the equivalent circuit of Figure 7.13, $R_{electrolyte1}$ now represents the resistance of the small quantity of electrolyte that separates the two salt bridges placed in the solution.

Figure 7.14 Total resistance of sodium chloride solution and platinum electrodes as a function of applied voltage

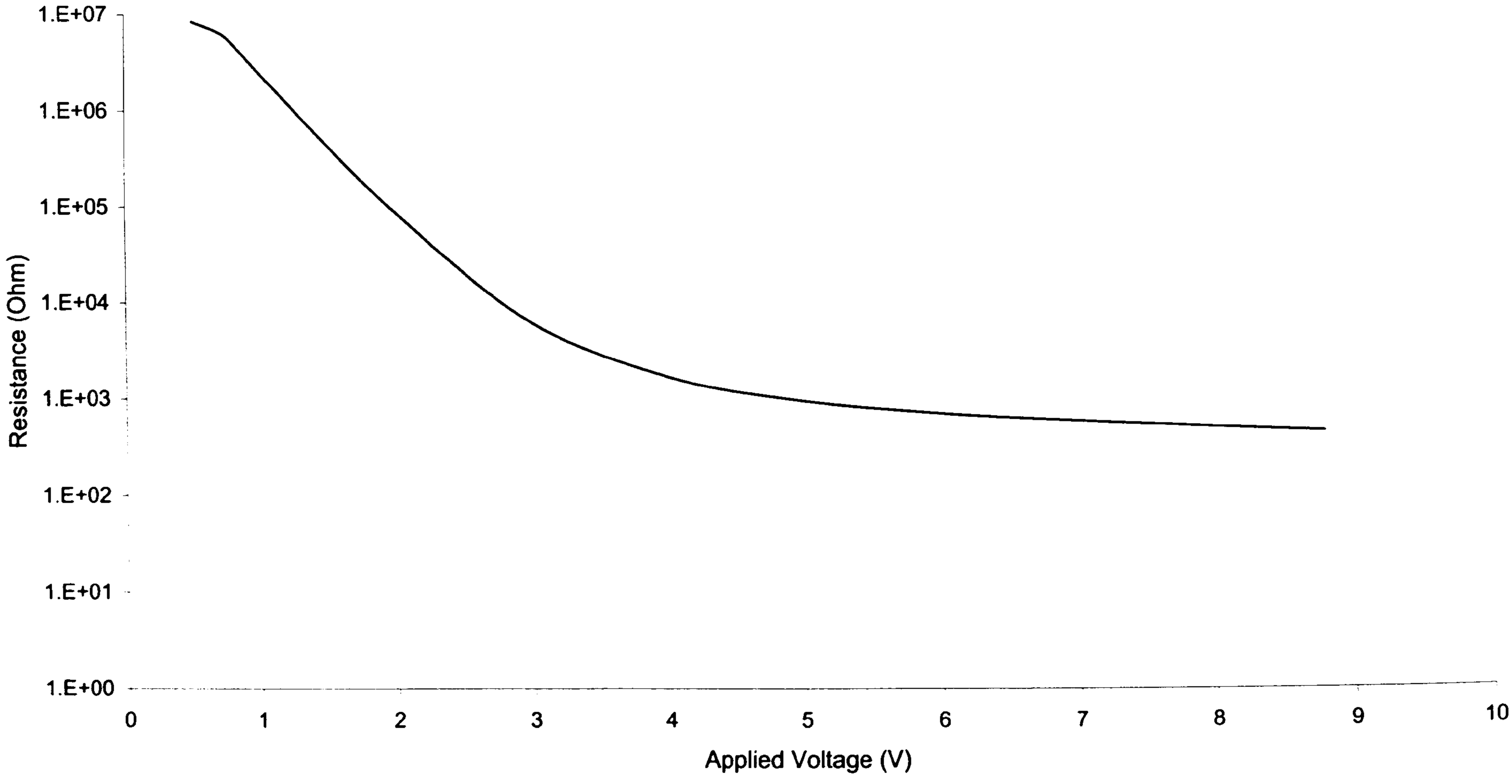

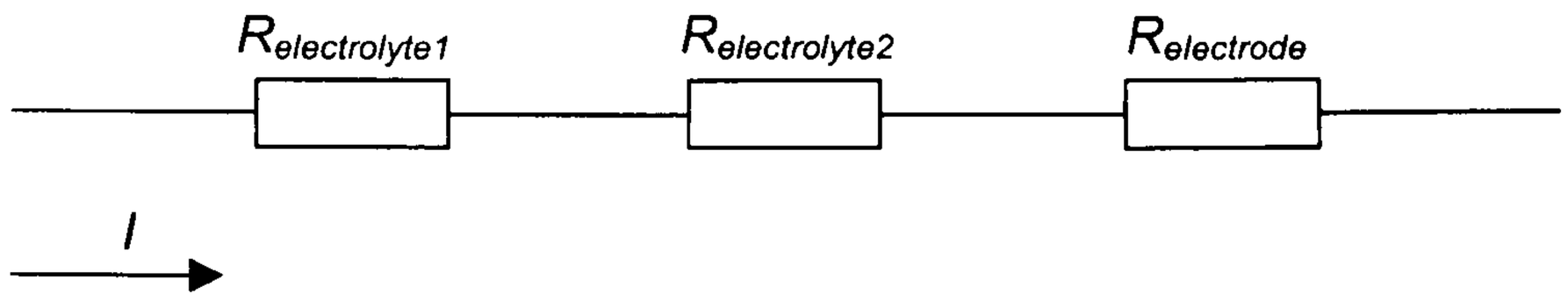

Figure 7.15 Equivalent circuit for electrolysis of sodium chloride solution

For the experiment in which a constant current was passed through sodium chloride solution in the absence of a membrane, the potential difference between two salt bridges placed in the electrolyte and the total voltage supplied to the circuit were observed to increase when a magnetic field was applied in direction 1. Since current in the circuit is constant, an increase in the resistivity of the electrolyte is the only possible explanation for the measured increase in the potential difference between the salt bridges, according to the equivalent circuit and Ohm's law. Therefore, this experimental observation is the most compelling reason to suggest that the resistivity of sodium chloride solution is affected by an applied magnetic field. An increase in the total resistance of the equivalent circuit, caused by an increase in electrolyte resistivity, would also explain the increase in the voltage supplied by the current source.

When a constant voltage was applied to sodium chloride solution in the absence of a membrane, a magnetic field in direction 1 caused the potential difference between two salt bridges placed in the electrolyte to increase, while current decreased. If $R_{electrolyte1}$ and $R_{electrolyte2}$ are assumed to increase by a

constant factor while $R_{electrode}$ remains constant, the voltage across $R_{electrolyte1}$ in the potential divider network of Figure 7.15 would increase. Therefore, an increase in electrolyte resistance would cause the observed increase in the potential difference between the salt bridges. Since applied voltage was constant, the decrease in current can be explained by an increase in the total resistance of the equivalent circuit, caused by an increase in the resistivity of the electrolyte and the magnitudes of $R_{electrolyte1}$ and $R_{electrolyte2}$.

It is believed that a magnetically mediated variation in the resistivity of sodium chloride solution provides the simplest explanation that is consistent with all experimental results. However, the mechanism by which a magnetic field might affect the conductivity of the electrolyte is unknown. It is intriguing that the sign of the change in conductivity appears to be dependent on the directions of both current flow and the applied magnetic field, as shown in Figures 7.11 and 7.12. The only known observation of a variation in the conductivity of an electrolyte due to a magnetic field was published by Ayrapetyan *et al.* [3], who reported that the conductivity of concentrated ($>10^{-4}$ M) calcium chloride solution decreased when exposed to a magnetic field of 27 mT. The conductivity of dilute (10^{-5} M) calcium chloride solution was reported to increase when exposed to the same magnetic field. However, the researchers stated that the conductivities of sodium and potassium chloride solutions were unaffected by an applied magnetic field. Ayrapetyan *et al.* suggested that the magnetic field affected conductivity by changing the hydration of calcium ions.

Ayrapetyan *et al.*'s experimental method consisted of exposing the electrolytes to magnetic fields for 2 minute periods, followed by measurement of solution conductivity. Conductivity measurements were taken outside the magnetic field using a specialised conductivity meter which passed currents of less than 1 nA. This contrasts with the experimental method used in these experiments, in which the magnetic field was applied to a solution carrying large currents in excess of 100 μA. The disparity between the experimental methods may explain why Ayrapetyan *et al.* observed no change in the conductivity of sodium chloride solution.

There is a large body of evidence to suggest that an applied magnetic field may have a direct effect on the properties of water or solutions. Many of these studies report that exposure to a magnetic field has an effect on the structure of water molecules or ions in solution. Changes in the structure of pure water [4] and water with a high mineral content [5]; changes in the structure of the water of hydration surrounding ions [6, 7]; changes in the structure of water and ions adsorbed on the surface of colloid particles [8, 9]; stabilisation of the water structure at the surface of an ionic solution [10] or around a fluorescent molecule [11]; and changes in the structure of water molecules in glucose solution [12] due to the presence of a magnetic field are among the structural effects that have been reported. A so-called "memory effect" has been reported in some of these publications, for example [6-11, 13], in which the magnetic effects may still be observed for up to a week after exposing water to a magnetic field, although the mechanism for this is unclear. Other reported effects of magnetism upon water and solutions include an increase in the

viscosity of both water and sodium chloride solution [14] and the appropriately named "Moses effect", in which the surface of water can be seen to part in the presence of magnetic fields with strong horizontal gradients [15].

Clearly, many phenomena arising from the interaction between water and a magnetic field have been reported although the mechanism of many of these effects has yet to be determined. While mankind's knowledge of the effects of magnetism upon water and ionic solutions remains incomplete, it is possible that the phenomenon described in this chapter may relate to one of those described in [4-12] or be due to some other, previously undiscovered, effect.

Since the sign of the observed phenomenon is dependent upon the direction of the applied magnetic field and the direction of current flow, the possibility that the effect was caused by the Lorentz force acting upon ions was considered. The effect of the Lorentz force would be to cause a redistribution of charge, producing a Hall voltage in a direction perpendicular to the directions of current and magnetic field. It was hypothesised that by affecting the spatial voltage distribution within the Ussing chamber, the formation of a Hall voltage may explain some of the observed results. The magnitude of the Hall voltage V_H in a conductor of thickness D and Hall coefficient R_H, measured in a direction perpendicular to a current I and a magnetic field of flux density B is calculated from [16]:

$$V_H = \frac{R_H I B}{d} \qquad (7.2)$$

It has been suggested that a suitable method to calculate the Hall coefficient for a solution containing two ion species is [17, cited in 2]:

$$R_H = \frac{\mu_+^2 \Gamma_+ - \mu_-^2 \Gamma_-}{F \eta_0 (\mu_+ + \mu_-)^2} \qquad (7.3)$$

where μ_+ and μ_- are the mobilities of the cation and anion respectively, Γ_+ and Γ_- are dimensionless coefficients for the cation and anion respectively and η_0 is the concentration of the electrolyte. The mobilities of sodium and chloride ions in aqueous solution at 298.15 K are 5.19×10^{-8} and 7.91×10^{-8} m^2 s^{-1} V^{-1} respectively [18]. The value of Γ_+ for sodium ions at 279.66 K is given in reference [2] as 8866.3. In the absence of a tabulated value of Γ_- for chloride ions, the value for bromide ions of 5486.4 is used. The Hall coefficient for a 0.1 M solution of sodium chloride is estimated from equation (7.3) to be -6.3×10^{-5} m^3 C^{-1}. Substituting this value of the Hall coefficient into equation (7.2), using parameters similar to those of the experiments of Section 7.1 (I = 5 mA, B = 0.1 T, d = 1 cm), the Hall voltage is calculated to be approximately 3 μV.

However, for a system in which the magnetic field and current flow are in mutually perpendicular directions in the horizontal plane, the Hall voltage would exist along the vertical axis. Although the direction of current flow and magnetic field were unlikely to be perpendicular in these experiments due to the irregular shape of the Ussing chambers and the use of cylindrical electrodes, the largest component of the Hall voltage would still be expected to occur in the vertical direction. The small magnitude of the Hall voltage predicted for these experimental conditions, together with the realisation that the Hall voltage would exist in a different axis to that in which the effect was measured, suggest that

the Hall effect is not responsible for the phenomenon observed in these experiments.

The exact cause of the experimental results reported in Chapters 6 and 7 remains unknown, although the results are consistent with a magnetically mediated change in the conductivity of sodium chloride solution. It is likely that the observed changes in membrane potential due to an applied magnetic field are not caused by collisions between sodium ions and the pores for the reasons already discussed in Section 6.3. Therefore, this phenomenon appears to be unlikely to contribute to the hypothetical method of non-invasive anaesthesia suggested in Chapter 4. Furthermore, large applied currents of the order of 100 μA are required to produce a measurable effect on membrane potential, several orders of magnitude greater than the membrane currents in nerve fibres (Figure 1.5). It therefore seems unlikely that the observed phenomenon could be utilised to induce a non-invasive anaesthetic effect.

7.4 References

1. Hart, A.B. and Womack, G.J.
   Fuel Cells: Theory and Application.
   Chapman and Hall, 1967.
2. Fahidy, T.Z.
   Magnetoelectrolysis.
   Reviews of Applied Electrochemistry, 13, 1983, pp. 553-563.
3. Ayrapetyan, S.N., Grigorian, K.V., Avanesian, A.S and Stamboltsian, K.V.
   Magnetic Fields Alter Electrical Properties of Solutions and Their Physiological Effects.
   Bioelectromagnetics, Vol. 15, 1994, pp. 133-142.
4. Rai, S., Singh, U.P. and Singh, A.K.
   X-Ray Determination of Magnetically Treated Liquid Water Structures.
   Electro- and Magnetobiology, Vol. 14, 1995, pp. 23-30.
5. Kronenberg, K.J.
   Experimental Evidence for Effects of Magnetic Fields on Moving Water.
   IEEE Transactions on Magnetics, Vol. 21, 1985, pp. 2059-2061.
6. Higashitani, K. and Oshitani, J.
   Magnetic Effects on Thickness of Adsorbed Layer in Aqueous Solutions Evaluated Directly by Atomic Force Microscope.
   Journal of Colloid and Interface Science, Vol. 204, 1998, pp. 363-368.
7. Oshitani, J., Yamada, D., Miyahara, M. and Higashitani, K.
   Magnetic Effect on Ion-Exchange Kinetics.
   Journal of Colloid and Interface Science, Vol. 210, 1998, pp. 1-7.
8. Higashitani, K., Okuhara, K. and Hatade, S.
   Effects of Magnetic Fields on Stability of Nonmagnetic Ultrafine Colloidal Particles.
   Journal of Colloid and Interface Science, Vol. 152, 1992, pp. 125-131.

9. Higashitani, K., Iseri, H., Okuhara, K., Kage, A. and Hatade, S.
Magnetic Effects on Zeta Potential and Diffusivity of Nonmagnetic Colloidal Particles.
Journal of Colloid and Interface Science, Vol. 172, 1995, pp. 383-388.

10. Oshitani, J., Uehara, R. and Higashitani, K.
Magnetic Effects on Electrolyte Solutions in Pulse and Alternating Fields.
Journal of Colloid and Interface Science, Vol. 209, 1999, pp. 374-379.

11. Higashitani, K., Oshitani, J. and Ohmura, N.
Effects of Magnetic Field on Water Investigated with Fluorescent Probes.
Colloids and Surfaces A: Physicochemical and Engineering Aspects, Vol. 109, 1996, pp. 167-173.

12. Iwasaka, M., and Ueno, S.
Structure of Water Molecules Under 14T Magnetic Field.
Journal of Applied Physics, Vol. 83, 1998, pp. 6459-6461.

13. Colic, M. and Morse, D.
The Elusive Mechanism of the Magnetic "Memory" of Water.
Colloids and Surfaces A: Physicochemical and Engineering Aspects, Vol. 154, 1999, pp. 167-174.

14. Viswat, E., Hermans, J.F. and Beenakker, J.J.M.
Experiments on the Influence of Magnetic Fields on the Viscosity of Water and a Water-NaCl Solution.
Physics of Fluids, Vol. 25, 1982, pp. 1794-1796.

15. Ueno, S. and Iwasaka, M.
Properties of Diamagnetic Fluid in High Gradient Magnetic Fields.
Journal of Applied Physics, Vol. 75, 1994, p. 7177-7179.

16. Callister, W.D.
Materials Science and Engineering: An Introduction, 3rd Edition.
Wiley, 1994.

17. Olivier, A.
Thesis Doctorat d'Etat.
Rheims, 1979.

18. Moore, W.J.
Physical Chemistry, 5th Edition.
Prentice-Hall, 1972.

8. EFFECT OF A MAGNETIC FIELD ON TRANSIENT SODIUM ION FLUX

The steady state experiments of Chapters 6 and 7 provided no evidence to suggest that it would be possible to produce a non-invasive anaesthetic effect with a magnetic field aligned along the axis of a nerve fibre. However, these experiments were considered to be too different to the physiological mechanism of action potential propagation in a nerve fibre to allow the feasibility of the hypothetical method of non-invasive anaesthesia to be predicted confidently.

To appreciate how the experimental method may be improved, consider the movements of sodium ions during an action potential as described in Section 1.1. In the resting neuron there is a high extracellular concentration of sodium ions and a low intracellular concentration of sodium ions. This concentration gradient, in combination with those of other ion species, produces the membrane resting potential. Furthermore, all voltage-gated sodium channels are closed when the membrane is in the resting state, rendering the membrane impermeable to sodium ions. Voltage-gated sodium channels open during the depolarisation phase of the action potential, allowing sodium ions to diffuse down their concentration gradient and into the nerve cell. This diffusion of sodium ions into the nerve fibre causes the membrane potential to increase towards zero.

Therefore, a more useful experimental model should measure the effect, if any, of an applied magnetic field on the diffusion of sodium ions due to a

concentration gradient across a membrane. This contrasts to the previous experiments which examined the effect of a magnetic field on the drift of sodium ions across the membrane, where the ionic drift resulted from a substantial applied current through the membrane.

An experimental method was developed by which the diffusion of sodium ions through the cation exchange membrane could be indirectly observed by measuring the formation of the potential difference that results from the sudden creation of a concentration gradient across the membrane. With this method, formation of the membrane potential takes place over a period of several seconds, allowing the rate of formation to be measured with reasonable repeatability and accuracy.

8.1. Experimental Method

The apparatus is illustrated in Figure 8.1. A sample of cation exchange membrane was placed between the baths of the Ussing chamber, with care being taken to ensure that the membrane was placed in the same position and with the same orientation for each experimental run. This was a precautionary measure to ensure that the same porous area was used in each experiment and thus prevent the possibility of inconsistencies arising from the non-uniform distribution of pores as seen in Figure 5.2

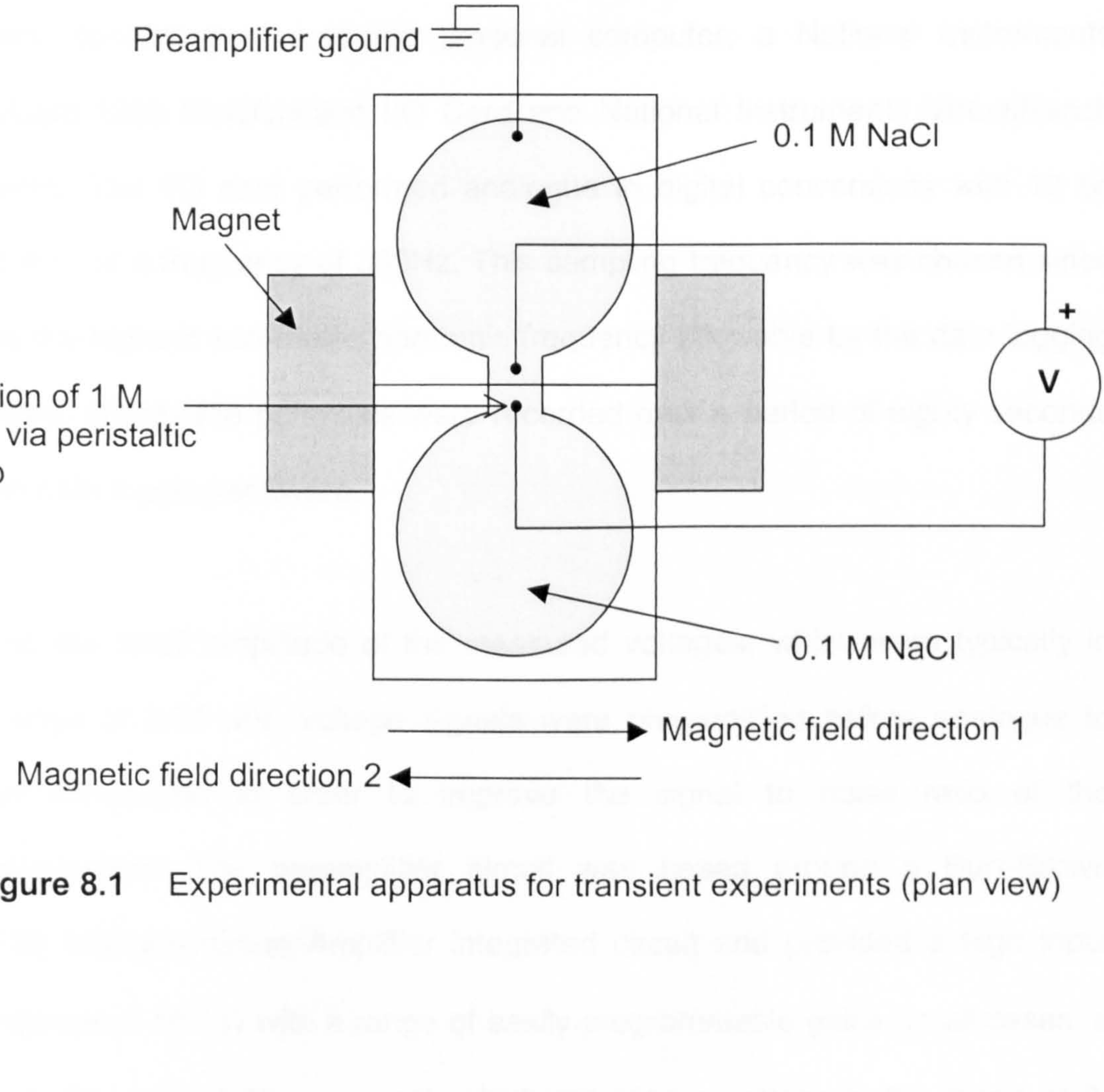

Figure 8.1 Experimental apparatus for transient experiments (plan view)

Each fluid bath was filled with 10 ml of 0.1 M sodium chloride solution. To ensure a consistent initial membrane potential of zero volts for each experiment, an electrical connection was made between the two fluid baths using an inert electrically conducting polymer. This discharges any membrane potential which may develop due to slight differences in concentrations of the solutions in each bath, which may be caused by the presence of residual ions from previous experiments in the pores of the membrane. The short circuit between the baths was removed once the membrane potential had reached zero volts.

Membrane potentials were measured using a computer-based data logging system, consisting of a laptop personal computer, a National Instruments DAQCard-1200 Multifunction I/O Card and National Instruments VirtualBench software. The I/O card performed analogue to digital conversions with 12 bit resolution at a frequency of 333Hz. This sampling frequency was chosen since it was the highest non-mains harmonic frequency allowable by the data logging software. Membrane potentials were recorded over a period of eighty seconds by the data logging software.

Due to the small amplitude of the measured voltages, which were typically in the range of 0-70 mV, voltage signals were preamplified before analogue to digital conversion in order to improve the signal to noise ratio of the measurements. The preamplifier circuit was based around a Burr-Brown INA102 Instrumentation Amplifier integrated circuit and provided a high input impedance of 10^{10} Ω with a range of easily programmable gains. In all cases, a preamplifier gain of 10 was used, which provided a voltage in the range of 0-

700 mV to the analogue to digital converter. To provide a constant reference voltage for the preamplifier, one of the fluid baths was connected to the ground of the preamplifier circuit. This connection was made by placing a piece of tinned copper wire directly into the Ussing chamber. A salt bridge, as described in Section 5.2, was placed into each of the baths of the Ussing chamber. The salt bridges were connected to the inputs of the preamplifier via silver/silver chloride half-cells.

To create a concentration gradient across the membrane, 1 M sodium chloride solution was added into one bath of the Ussing chamber by a peristaltic pump. Addition of the more concentrated solution increases the net concentration of the sodium chloride solution on one side of the membrane, thus forming a membrane potential. Excess solution, resulting from the increase in the total volume of solution within the bath, was able to drain from the bath through the overflow holes (Figures A2 and A3, Appendix 1). The peristaltic pump delivered sodium chloride solution into the vicinity of the membrane at a constant rate of 0.2 millilitres per second. The pump was started manually, five seconds after the logging of membrane potentials was initiated.

After each experimental run, the Ussing chamber and cation exchange membrane were rinsed thoroughly with deionised water to minimise the risk of contamination from residual ions from previous experiments. Contamination may affect the ionic content of the solutions in the current experimental run and cause inconsistencies between experimental runs.

Two series of experiments were performed. The initial series of experiments consisted of fifty experimental runs with no applied magnetic field and fifty runs with an applied field in direction 1 as indicated in Figure 8.1. The magnetic field was produced by permanent magnets and ferrite pole pieces were used to concentrate the magnetic flux in the region of the membrane. The applied magnetic flux density in the region of the membrane was measured as 0.29 T (Section 5.3).

To reduce the effect of systematic errors, experiments in the presence or absence of an applied magnetic field were performed in a random order. For example, deterioration of the sodium chloride solutions or degradation of the structure of the membrane may contribute to a drift in the rate of formation of membrane potential over the course of the experiments. Random selection of the order in which experiments are performed randomly distributes variations in uncontrolled experimental parameters between the results with and without an applied magnetic field, thus preventing the measurement of misleading artificial differences between these two sets of results [1, 2]. A random order was selected by a computer, such that the set of one hundred experimental runs consisted of an equal number of runs in the presence and absence of an applied magnetic field.

The first set of experiments revealed an unexpected difference in mean membrane potential, rather than a difference in the rate of formation of membrane potential, between experimental runs conducted with and without an applied magnetic field. Figure 8.4 (Section 8.3) shows that in the 10-30 seconds

time interval the mean value of membrane potential with an applied magnetic field is noticeably greater than that in the absence of a magnetic field.

To try to determine the reason for this unexpected result, the dependence of the mean value of membrane potential upon the direction of the applied magnetic field was examined. The hypothetical mechanism which produces collisions between sodium ions and the walls of the membrane pores should be independent of the direction of the applied magnetic field. Therefore, if this mechanism was responsible for the measured difference in means then applying a magnetic field in the reverse direction should also cause an increase in the mean membrane potential. However, if the difference in mean membrane potential is caused by some other previously unconsidered mechanism then this mechanism may exhibit a dependence upon the direction of the applied magnetic field.

In order to distinguish between these two possible mechanisms, a second set of experiments in which a magnetic field was applied in two antiparallel directions was performed. The two directions of the applied magnetic field, namely directions 1 and 2, are indicated in Figure 8.1. A total of 99 experimental runs were performed, with an equal number of runs for each of these three magnetic field regimes. As before, the order of the experimental runs was chosen randomly by computer.

8.1.1. Calculation of the Rate of Formation of Membrane Potential

The rate of formation of membrane potential is equivalent to the gradient of a graph of membrane potential against time. As an example of typical results produced by this experimental method, Figure 8.3 (Section 8.2) shows the voltage against time graphs of fifty experimental runs in the absence of an applied magnetic field. During the 15-30 second time interval in Figure 8.2, it is apparent that the gradients of the graphs are similar. However, although the shapes and gradients of the graphs are similar during this time interval, the graphs of voltage against time appear to be slightly "offset" along the time axis. Although the times taken for the voltage to increase from, for example, forty to fifty millivolts are comparable for each experimental run, the time at which this voltage transition starts to occur is noticeably different in each case. In view of this, it is more meaningful to compare the gradients of the graphs as the voltage increases between two values, rather than comparing the gradients over any particular time interval.

Gradients were calculated over voltage ranges where the graphs for each experimental run show the greatest level of consistency. For the example of Figure 8.3, the period when membrane potential increases from 3 mV to 18 mV is suitable for the calculation of gradients of the voltage against time graphs. Similarly, the 37 mV to 50 mV interval is also sufficiently consistent to make the calculation of gradients worthwhile. Conversely, the variances of both the membrane potential and the gradient of the membrane potential were noticeably greater during the 18 mV to 37 mV interval than at any other point

during the experimental runs. Gradients were not calculated in intervals which exhibited large variances.

The rate of formation of membrane potential was calculated by dividing the difference between two reference voltages by the time taken for the membrane potential to cross these reference voltages. Linear interpolation was used to estimate the time at which the membrane potential was equal to the reference potential, if the membrane potential crossed the reference voltage between sample points. Due to noise on the measured membrane potentials, the time at which the membrane potential crosses the reference voltage is not always clear. Figure 8.2 shows the typical form of a membrane potential measured in the presence of noise. Noise causes the measured values of membrane potential to cross the reference voltage, V_{ref}, at two times, t_1 and t_2. When calculating gradients for noisy readings similar to this, the membrane potential was judged to cross V_{ref} at the midpoint of the two crossings of V_{ref}, i.e. $\frac{1}{2}(t_1 + t_2)$.

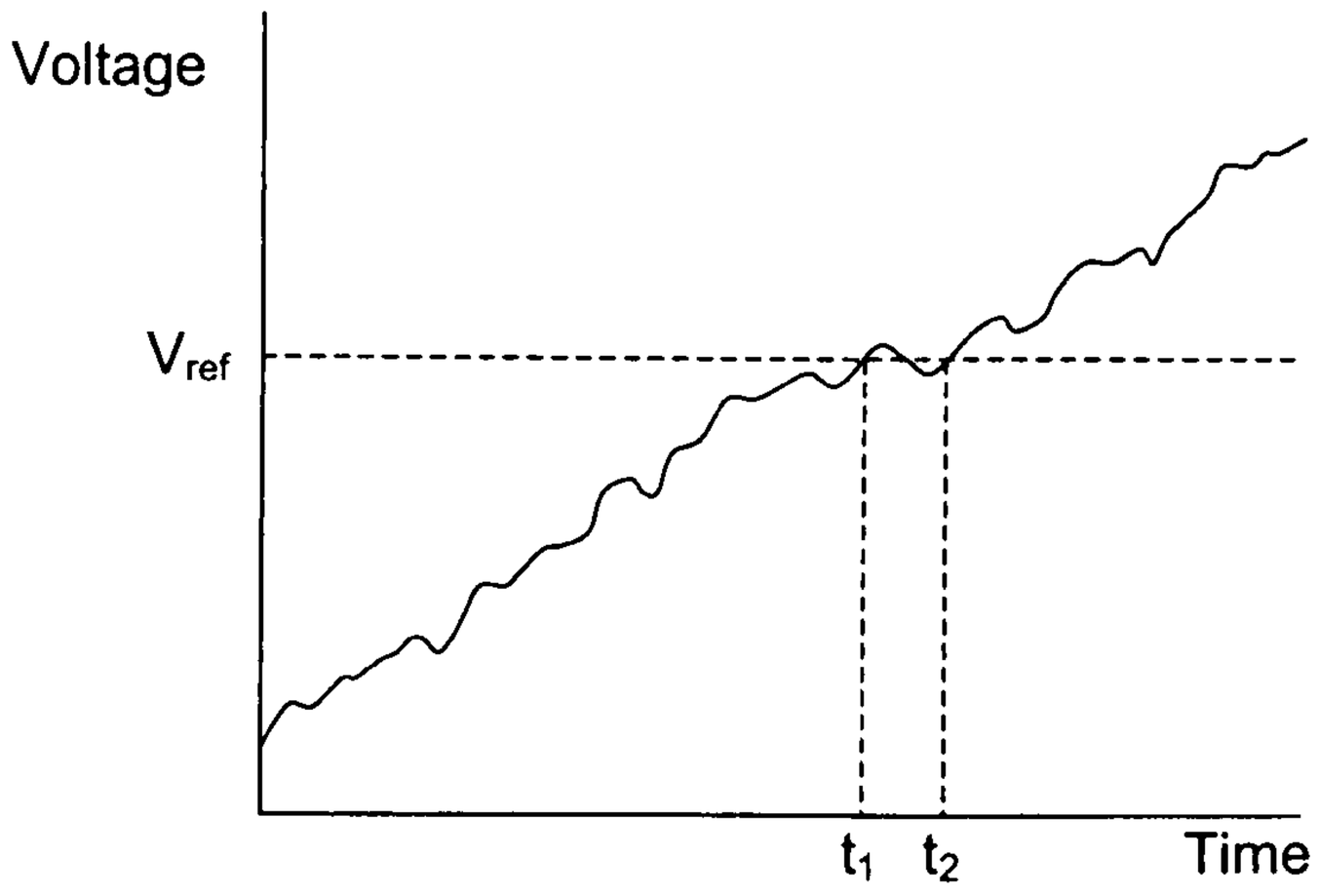

Figure 8.2 Calculation of rate of formation of membrane potential in the presence of noise

8.1.2. Statistical Methods

To determine whether the applied magnetic field has an effect on the rate of formation of membrane potential, the differences between the mean gradients in the presence and absence of a magnetic field were tested for statistical significance. The *t*-test for distributions with unequal variances was chosen as a suitable statistical test for this purpose [3]. In this test, the significance of the difference between the means of two distributions is measured by the statistic *t*, which is calculated from [4]:

$$t = \frac{\overline{x_1} - \overline{x_2}}{\sqrt{\frac{Var(x_1)}{N_1} + \frac{Var(x_2)}{N_2}}} \tag{8.1}$$

where x_1 and x_2 are the two samples of interest (e.g. gradients with and without magnets respectively), $\overline{x}$ denotes the mean value of sample x, $Var(x)$ denotes the variance of sample x and N_x is the size of sample x (i.e. the number of observations).

The statistic t is distributed with Student's t-distribution with ν degrees of freedom, where ν is calculated from [4]:

$$\nu = \frac{\left(\frac{Var(x_1)}{N_1} + \frac{Var(x_2)}{N_2}\right)^2}{\frac{\left(\frac{Var(x_1)}{N_1}\right)^2}{N_1 - 1} + \frac{\left(\frac{Var(x_2)}{N_2}\right)^2}{N_2 - 1}} \tag{8.2}$$

The significance levels of the difference between the means of samples x_1 and x_2 were calculated by substituting the calculated values of t and ν into the algorithm published in reference [4]. The significance level p represents the probability that the two samples were drawn from the same population. A low significance level, such as $p < 0.05$, suggests that the observed differences between the mean values of x_1 and x_2 were caused by a real effect of the magnets upon the experimental system [5].

The *t*-test for distributions with unequal variances was also used to test the significance of the difference between mean membrane potentials. The second series of experiments involved three applied magnetic field regimes: without an applied field; with an applied magnetic field in direction 1; and with an applied magnetic field in direction 2. Since this *t*-test can only compare the differences between two sample means, three *t*-tests were necessary to compare every possible pairing of magnetic field configurations in this series of experiments.

8.2. Results

To illustrate the consistency of the results obtained by this experimental method, Figure 8.3 is a graph of voltage against time showing the results of individual experimental runs. These measurements were made in the absence of an applied magnetic field, during the first set of experiments. The corresponding results in the presence of an applied magnetic field during the first set of experiments are shown in Figure A4 (Appendix 2). To improve the signal to noise ratio of the measurements and thus clarify the presentation of the results, each data series was manipulated by a digital filter algorithm. The filter algorithm consisted of a bandstop filter with cut-off frequencies of 48Hz and 52Hz, to remove the mains frequency noise component, and a 10-point averaging function. The averaging function acts as a low-pass filter, removing higher frequency noise components at the expense of an effective reduction in sampling frequency from 333 Hz to 33 Hz. Filtering of the data was done for the sole purpose of facilitating the visual identification of the general trends in the graphs presented in this section.

The similarity of many features in the voltage against time graphs for each of the individual experimental runs shown in Figure 8.3 is noteworthy. It can be seen that the initial voltage before addition of sodium chloride solution has a consistent value of approximately zero volts and formation of the membrane potential starts to occur at approximately seven seconds in every experimental run. The final values of membrane potential reached after forty seconds also show a reasonable level of agreement.

The results from each of the experimental runs are consistent over two regions of these voltage against time graphs. These consistent regions occur when the membrane potential is increasing from 3 mV to 18 mV and from 37 mV to 50 mV. Therefore, these two regions were considered to be suitable for statistical analysis of the gradients of the graphs of voltage against time. The *t*-test for unequal variances was used to calculate the significance level of the difference between mean gradients in the presence and absence of a magnetic field, as described previously. The mean rates of formation of membrane potential, calculated as the membrane potential increases from 3 mV to 18 mV and from 37 mV to 50 mV, together with the significance levels of the differences between the mean rates of formation of membrane potential, are presented in Table 8.1. The high significance levels ($p > 0.6$) indicate that the rate of formation of membrane potential is unaffected by an applied magnetic field.

Voltage range (mV)	Mean rate of formation of membrane potential ($mV\ s^{-1}$) ± standard error of mean		Significance level of difference between means
	Without applied field	With applied field	
3-18	9.54 ± 0.07	9.31 ± 0.14	0.814
37-50	1.73 ± 0.25	1.70 ± 0.13	0.603

Table 8.1 Mean rates of formation of membrane potential and significance level of difference between means for first series of experiments

An unexpected, yet potentially interesting, result is observed when the mean values of membrane potential, rather than the mean values of the gradients, are calculated. Figure 8.4 is a comparison of the mean values of membrane potential measured in the presence and absence of an applied magnetic field.

The standard error of the mean is shown on this figure at evenly spaced intervals. The repeatability of the experimental method is demonstrated by the close agreement between the mean membrane potentials during the initial increase in membrane potential between seven and nine seconds and the equilibrium value of the membrane potential after thirty-five seconds. However, the difference in the values of mean membrane potential during the 10-30 second time period is of particular interest.

It was expected that the application of a magnetic field would cause a decrease in the rate of formation of membrane potential, but not the apparent increase in mean membrane potential that can be seen in Figure 8.4. The significance of the difference between the mean values of membrane potential at each point in time was calculated using the *t*-test for unequal variances, as described previously. The significance levels of the difference between sample means are plotted in Figure 8.5 and the mean membrane potentials are also plotted for reference. To clarify the visual presentation of the graph of significance levels, the *t*-test was performed upon data processed by the bandstop and low-pass filter algorithms described previously. During the initial seven seconds the differences between sample means exhibit a wide range of significance levels from $p > 0.99$ to $p < 0.01$. However, this period is prior to the formation of the membrane potential and is not of interest. As the membrane potential starts to form the difference between the mean membrane potentials is not particularly significant ($p > 0.2$), but does become increasingly significant over the next ten seconds. At approximately 20 seconds, the difference between sample means is very significant ($p < 0.02$). After 25 seconds, when the membrane potentials

are approaching the equilibrium value, the difference between the mean membrane potentials becomes less significant. When the equilibrium membrane potential is established the difference between sample means is insignificant ($p > 0.6$). The second set of experiments was conducted because the low significance levels observed at around 20 seconds gave reason to believe that the phenomenon of the difference between means was worthy of further investigation.

Figure 8.3 Membrane potentials measured in the absence of an applied magnetic field during first series of experiments

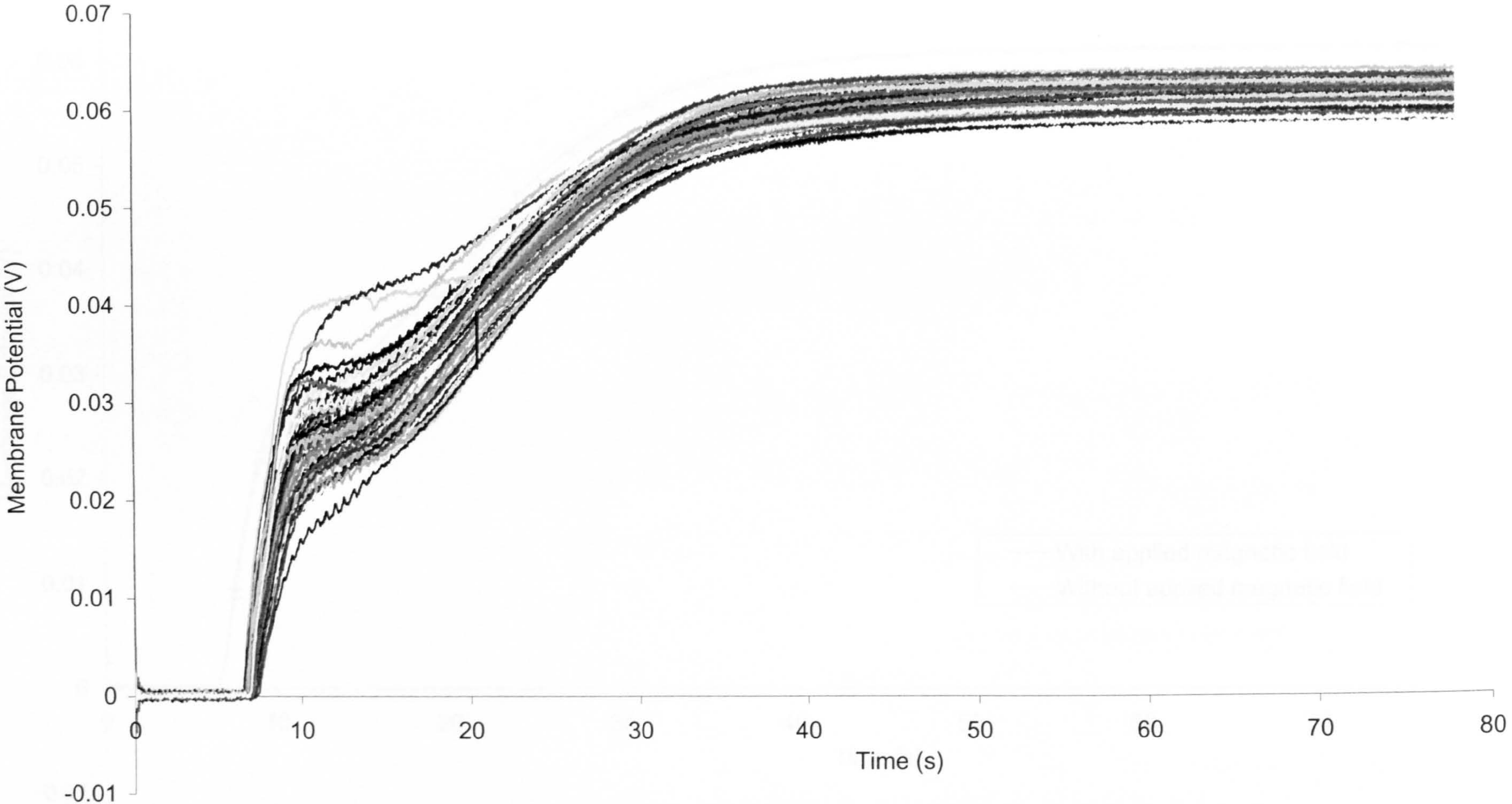

Figure 8.4 Mean membrane potentials measured during first series of experiments

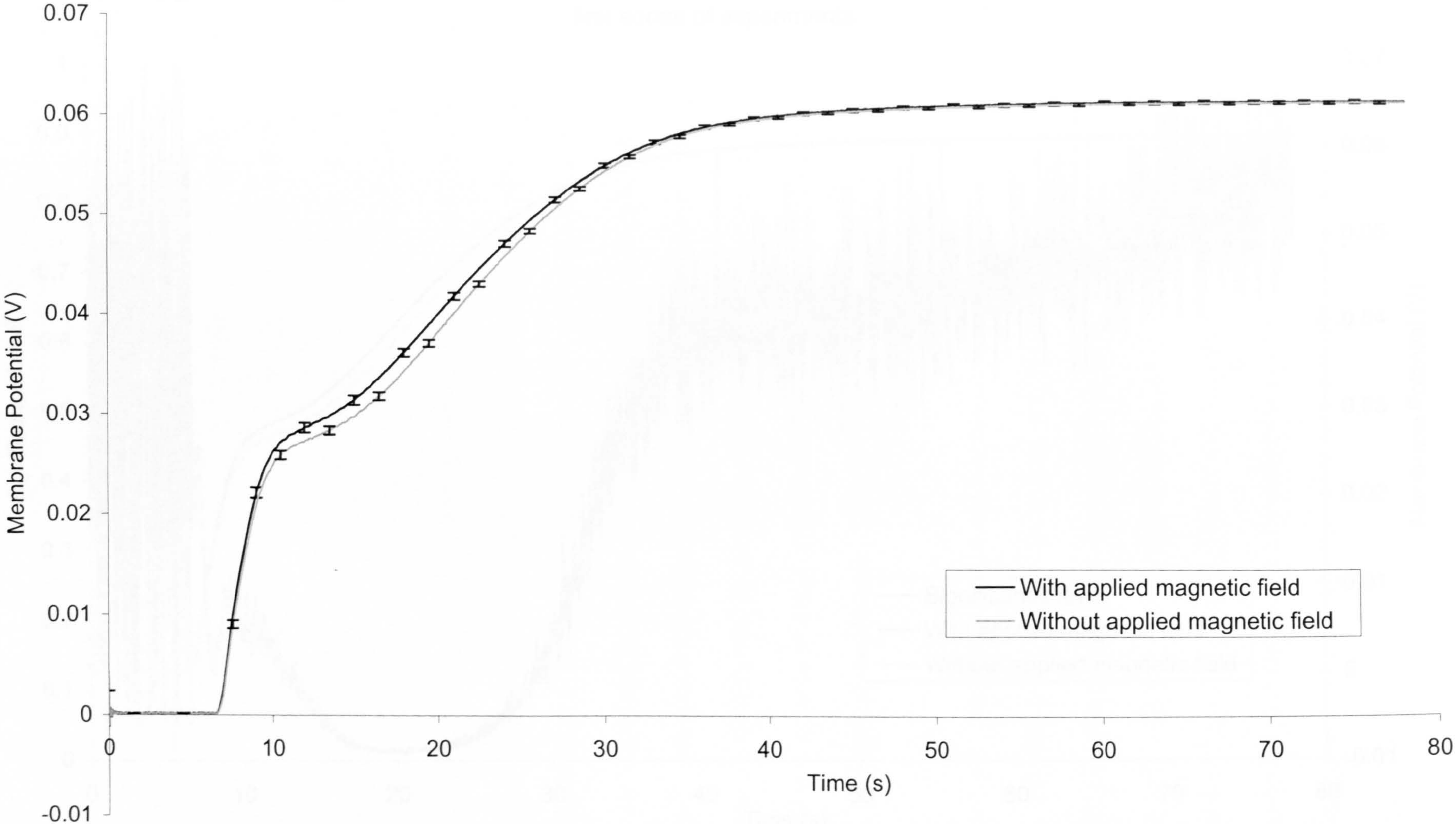

Figure 8.5 Significance levels of differences between mean membrane potentials measured during first series of experiments

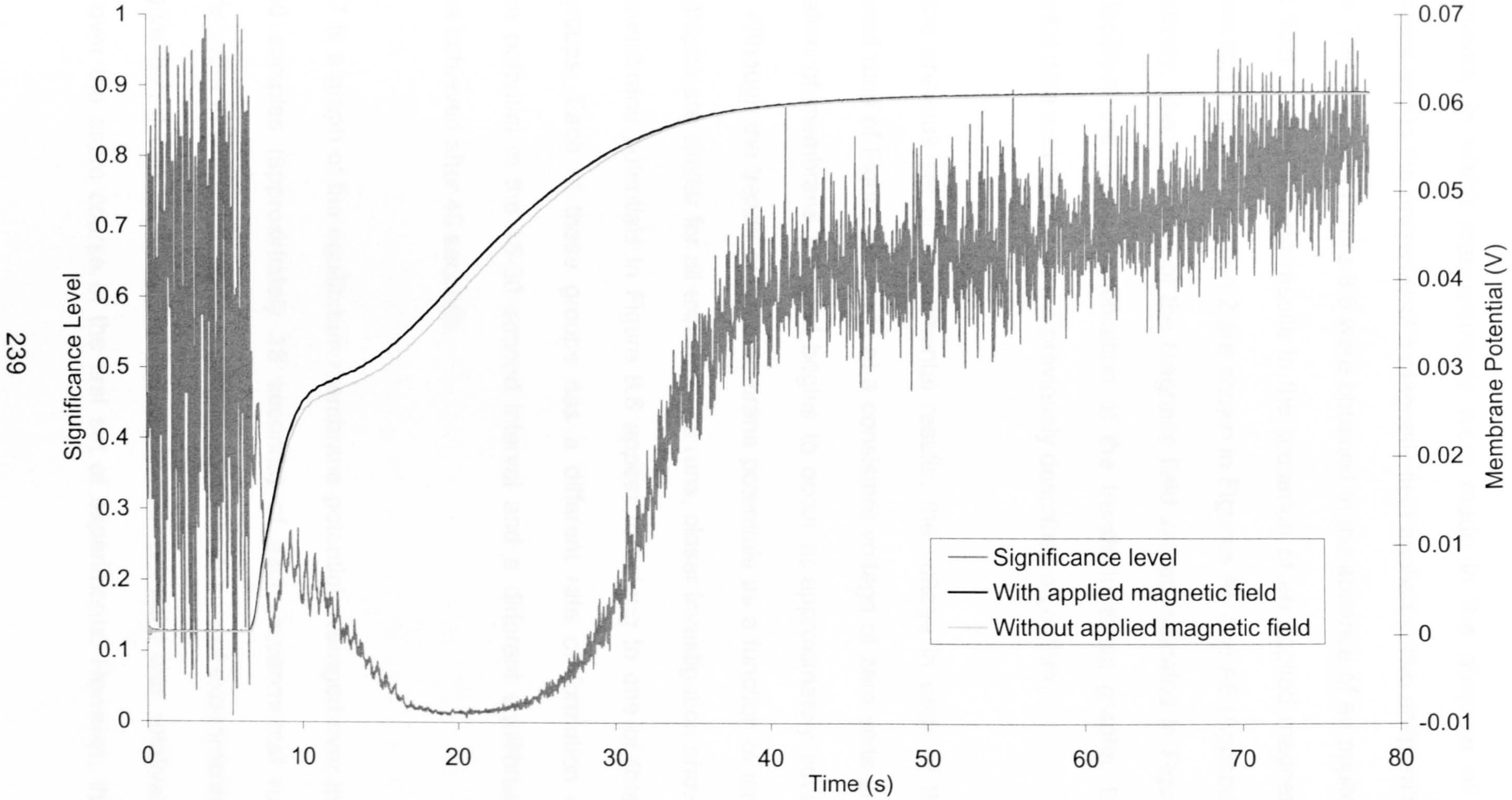

Figure 8.6 shows the results of individual experimental runs from the second set of experiments, in which measurements were made in the absence of a magnetic field and in the presence of a magnetic field applied in two antiparallel directions. The results of Figure 8.6 were obtained in the absence of an applied magnetic field. Corresponding results in the presence of an applied magnetic field in direction 1 and in direction 2 are shown in Figures A5 and A6 (Appendix 2) respectively. The directions of the magnetic field are as indicated in Figure 8.1. To facilitate the visual identification of the trends in these graphs, the experimental data was filtered by the previously described algorithm.

As with the previous set of experimental results, the voltage in each of the experimental runs of Figure 8.6 starts at a consistent voltage of zero volts and the formation of membrane potential begins to occur at approximately seven seconds. Although the trends of the membrane potentials as a function of time in these graphs are similar for all experimental runs, closer investigation shows that the membrane potentials in Figure 8.6 appear to belong to one of three distinct groups. Each of these groups has a different rate of formation of membrane potential in the 15-30 second interval and a different equilibrium potential is achieved after 40 seconds.

Figure 8.7 is a graph of the equilibrium membrane potential averaged over the final 6000 samples (approximately 18 seconds) of each experimental run against the order in which the run was performed, for both sets of experiments. From Figure 8.7, it can be seen that the equilibrium potential was relatively constant over the entire course of the first set of experiments. However, the

equilibrium potentials increase over the course of the second set of experiments and the equilibrium potential appears to increase in three distinct "steps" as a function of the experimental order. No satisfactory explanation for the drift in equilibrium potential or the existence of the three distinct groups of equilibrium potential can be proposed. The same sample of membrane and batch of sodium chloride solution were used in each experimental run, there were no perceptible changes in ambient conditions and the experimental technique was consistent over the entire course of these experiments. Fortunately, the randomised experimental order can be expected to prevent any systematic error which may occur as the result of this drift in experimental results.

A comparison of the rate of formation of membrane potential was performed upon the data from the second set of experiments, using the same method that was used previously. Gradients were calculated in the two most linear regions of the voltage against time graphs common to all experimental runs, which were found to be the 4-14 mV and 28-40 mV intervals. Additionally, an individual statistical analysis was performed on gradients belonging to each of the three distinct groups observed in Figure 8.7. The results were classified into three groups, consisting of experimental runs 1-31, runs 32-65 and runs 66-99. Gradients were calculated individually for each of these groups over the 24-40 mV interval, which was the largest linear region of the graph common to all experimental runs. Furthermore, the gradients for results 32-65 were calculated over the 28-50 mV interval and the gradients for results 66-99 were calculated over the 28-56 mV interval. These intervals were chosen since they were the largest linear regions of the graph common to all experimental runs within a

particular group. The mean gradients for all magnetic field configurations are presented in Table 8.2 and plotted in Figure 8.8.

Voltage range (mV)	Mean rate of formation of membrane potential ($mV\ s^{-1}$)		
	Without applied field	With applied field in direction 1	With applied field in direction 2
4-14 (all results)	6.92	6.54	7.16
28-40 (all results)	2.17	2.10	2.18
28-40 (results 1-31)	1.84	1.71	1.75
28-40 (results 32-65)	2.16	2.22	2.23
28-40 (results 66-99)	2.52	2.68	2.66
28-50 (results 32-65)	1.94	2.06	2.01
28-56 (results 66-99)	2.45	2.47	2.46

Table 8.2 Mean rates of formation of membrane potential for second series of experiments

The significance levels of the difference between the mean gradients for the second set of experiments are shown in Table 8.3 and plotted in Figure 8.9. In most cases the differences between the rate of formation of membrane potential are insignificant. The difference between mean gradients approaches a low significance level in only two cases, both of which are when the gradients under a magnetic field applied in direction 1 are compared to those in the absence of a magnetic field. In the 28-40 mV interval for results 1-31 this significance level

is calculated as 0.033 and in the 28-50 mV interval for results 32-65 the significance level is calculated as 0.069.

Voltage range (mV)	Significance level of difference between mean rate of formation of membrane potential		
	Applied field in direction 1 vs. No applied field	Applied field in direction 2 vs. No applied field	Applied field in direction 1 vs. Applied field in direction 2
4-14 (all results)	0.404	0.493	0.174
28-40 (all results)	0.474	0.945	0.458
28-40 (results 1-31)	0.033	0.136	0.285
28-40 (results 32-65)	0.290	0.290	0.966
28-40 (results 66-99)	0.282	0.335	0.727
28-50 (results 32-65)	0.069	0.335	0.564
28-56 (results 66-99)	0.778	0.846	0.853

Table 8.3 Significance levels of differences between mean rates of formation of membrane potential for second series of experiments

Figure 8.10 shows the mean membrane potentials measured during the second set of experiments. The mean membrane potentials in the absence of a magnetic field and with an applied field in direction 2 are almost identical. However, the mean membrane potential when a magnetic field was applied in direction 1 is now of a smaller magnitude than that measured in the absence of an applied field for the period of time between 10 and 15 seconds. This contradicts the results of the previous set of experiments, in which it was

observed that an applied magnetic field in direction 1 increased the mean membrane potential with respect to that measured in the absence of an applied field. The equilibrium value of the membrane potential, achieved after approximately forty seconds, is also of a smaller magnitude for measurements with a magnetic field applied in direction 1 compared to those in the absence of a magnetic field or with an applied magnetic field in direction 2. This steady state difference was not observed in the previous set of experiments but, due to the randomised experimental order which was used, cannot be attributed to the drift in the value of the equilibrium potentials that was observed over the course of the experiments.

The significance levels of the differences in mean membrane potentials between each of the possible pairings of results are presented in Figures 8.11-8.13. For reference, the mean membrane potentials are also shown in these figures. The *t*-test was performed upon membrane potential data which was processed by the previously described filter algorithm, in order to improve the clarity of presentation of the significance results. Figures 8.11 and 8.12 show the significance of the differences between mean membrane potentials measured with an applied magnetic field in direction 1, compared to those measured in the absence of a magnetic field and with an applied magnetic field in direction 2 respectively. In both Figures 8.11 and 8.12, the difference between mean membrane potentials approaches a low significance level during the initial formation of the membrane potential between 9 and 15 seconds. The lowest significance levels measured during this time period are 0.035 and 0.046 in Figures 8.11 and 8.12 respectively. The differences between the equilibrium

values of the mean membrane potential, measured after forty seconds, are not significant ($p > 0.4$).

Figure 8.13 shows the significance levels of the difference between mean membrane potentials measured in the absence of an applied magnetic field and in the presence of an applied magnetic field in direction 2. After the initial formation of membrane potential, the differences between these two sets of results are insignificant ($p > 0.05$).

A statistical analysis of the differences between membrane potentials when the results were separated into the three groups described earlier (runs 1-31, runs 32-65 and runs 66-99) showed no evidence that the magnetic field affects the mean membrane potential. For the sake of brevity, this statistical analysis has not been shown.

Figure 8.6 Membrane potentials measured in the absence of an applied magnetic field during second series of experiments

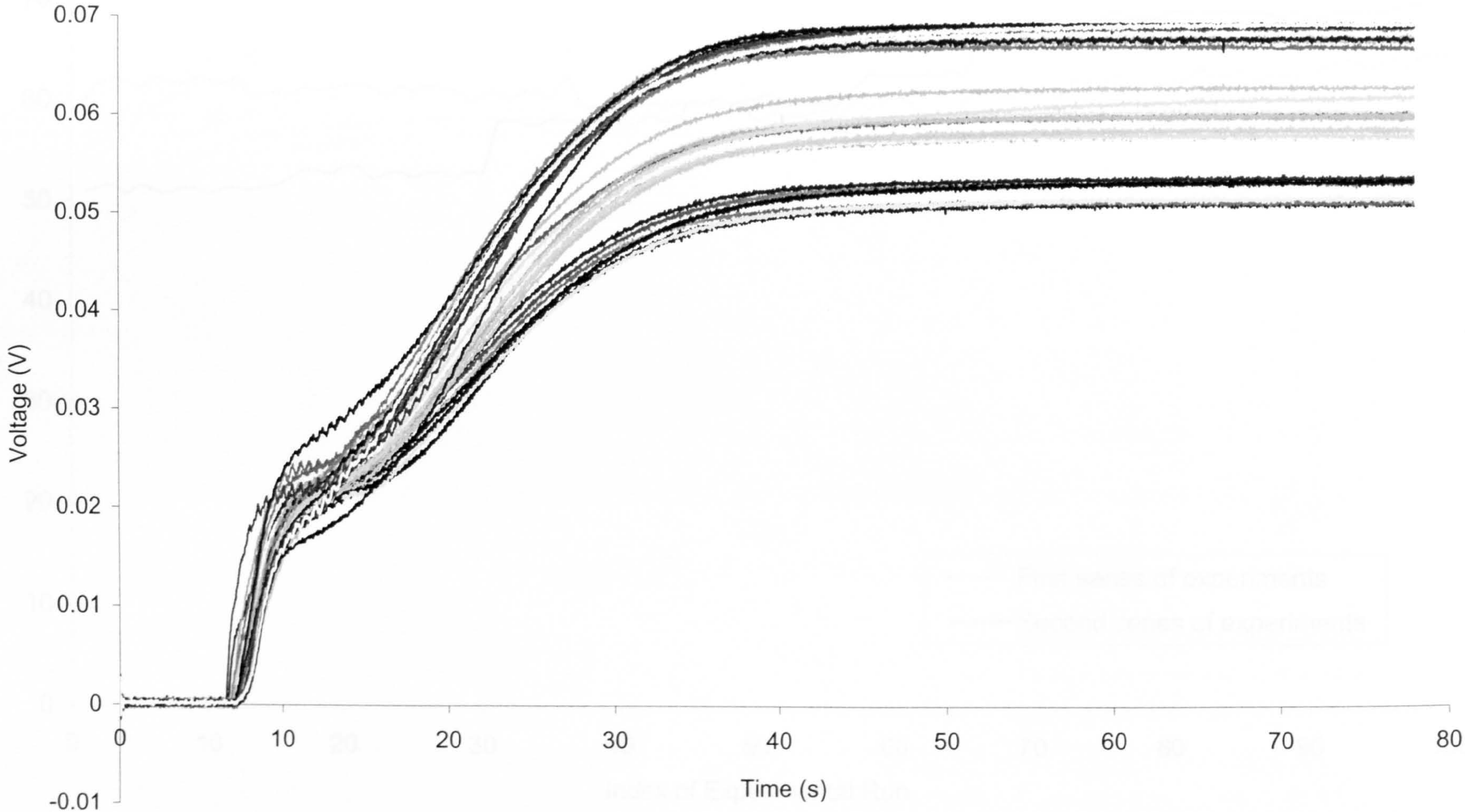

Figure 8.7 Variation of equilibrium membrane potential over a series of experimental runs

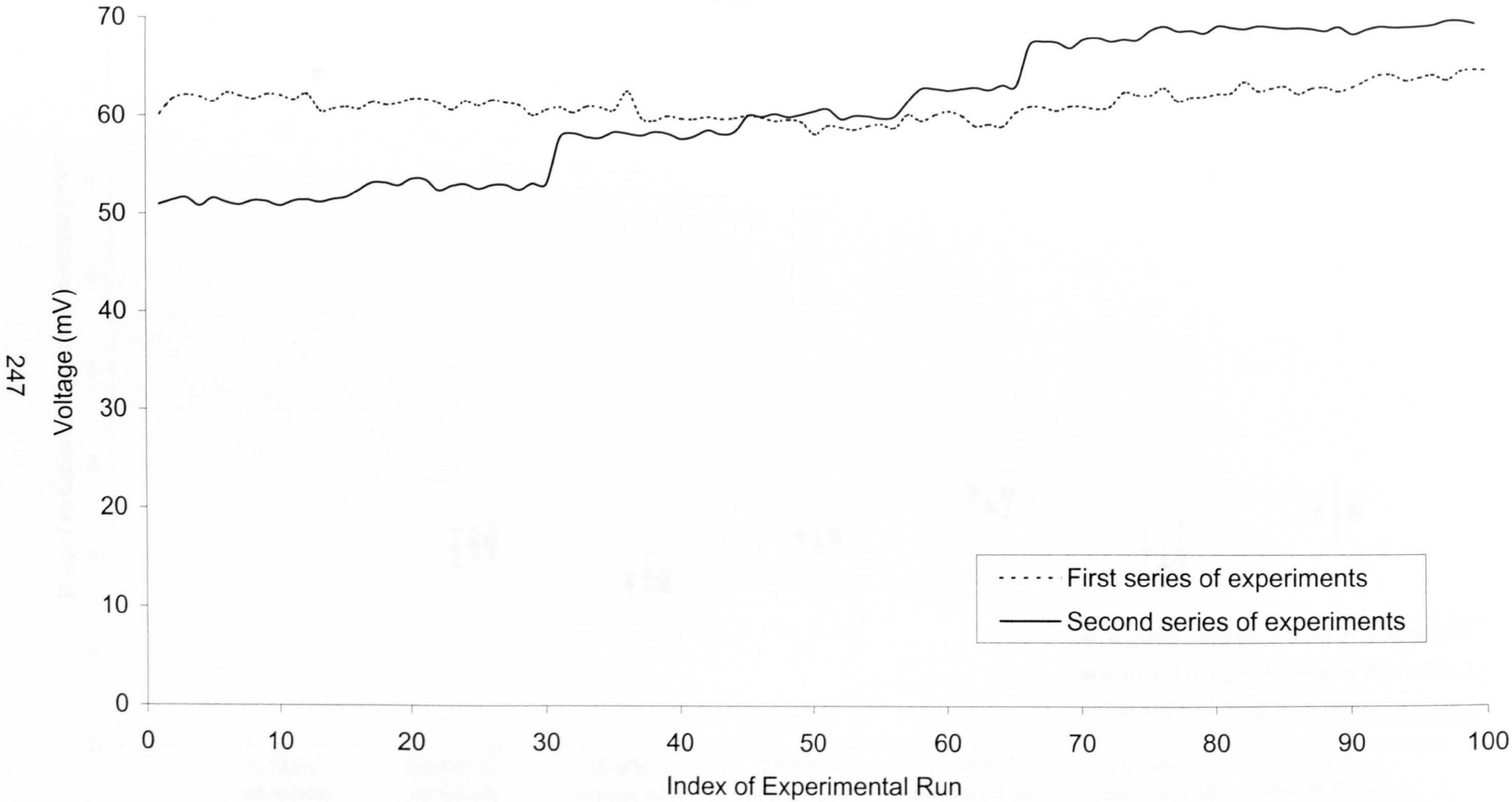

Figure 8.8 Mean rates of formation of membrane potential measured during second series of experiments

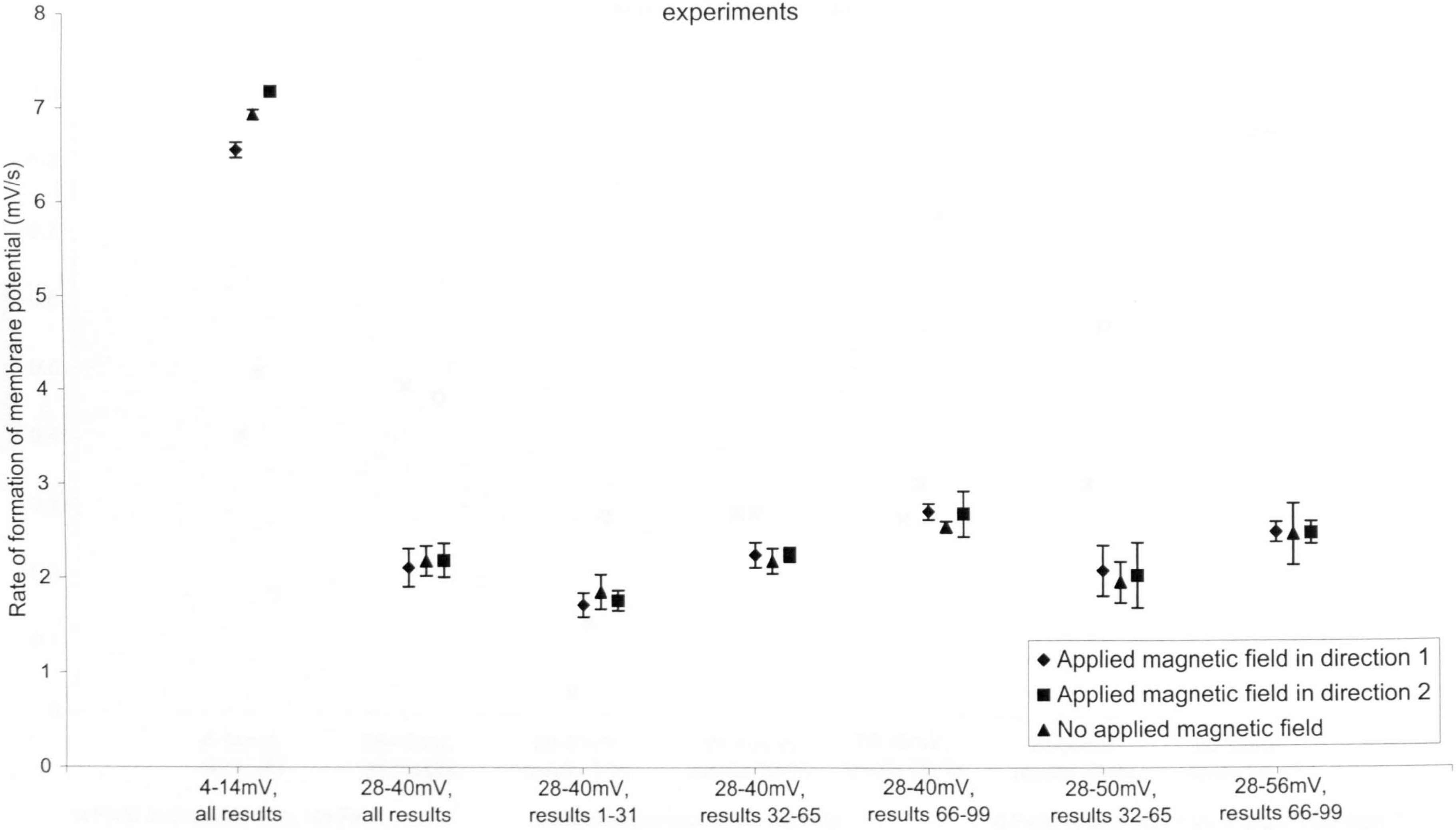

Figure 8.9 Significance of differences of mean rate of formation of membrane potential for second series of experiments

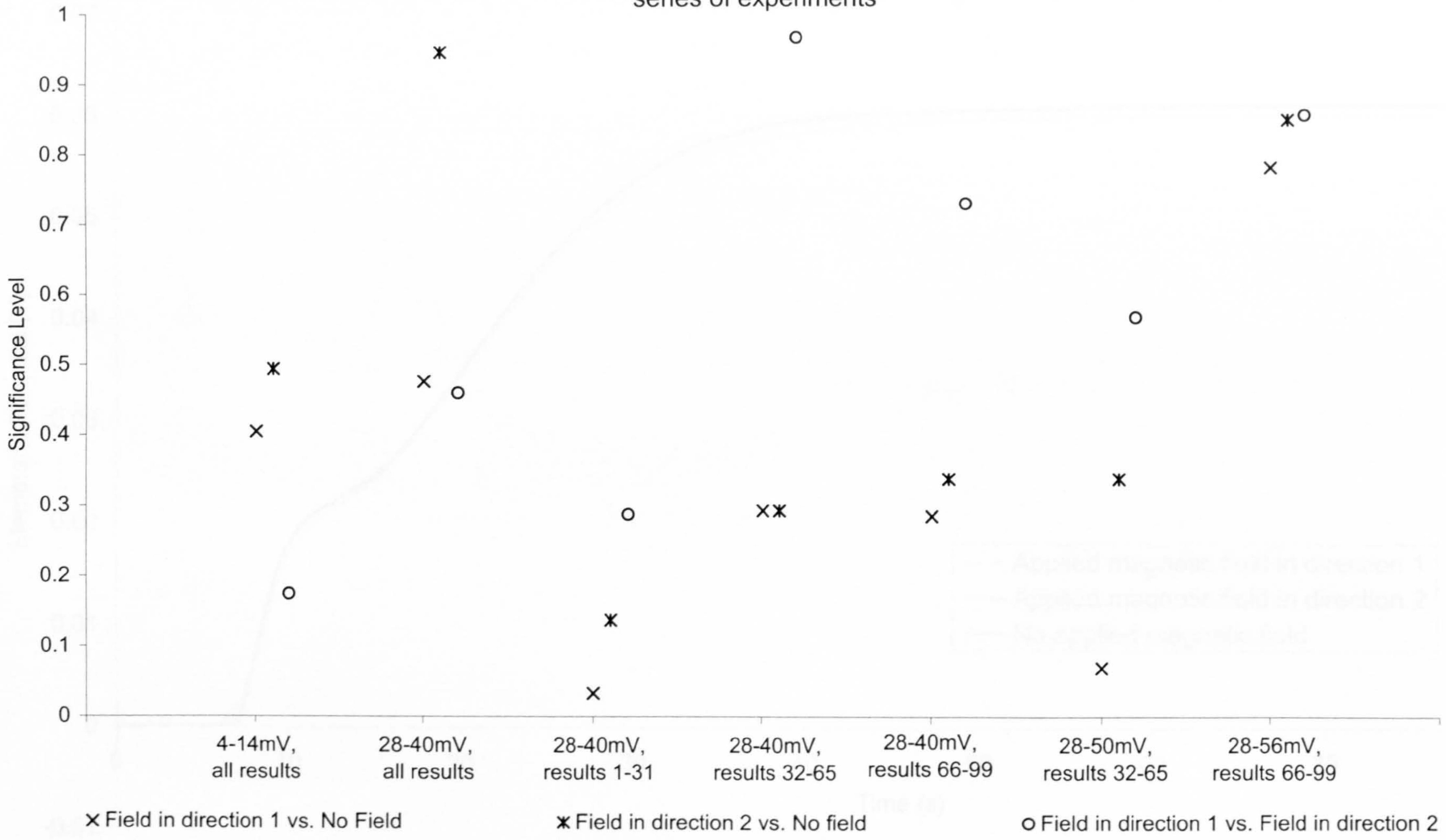

Figure 8.10 Mean membrane potentials measured during second series of experiments

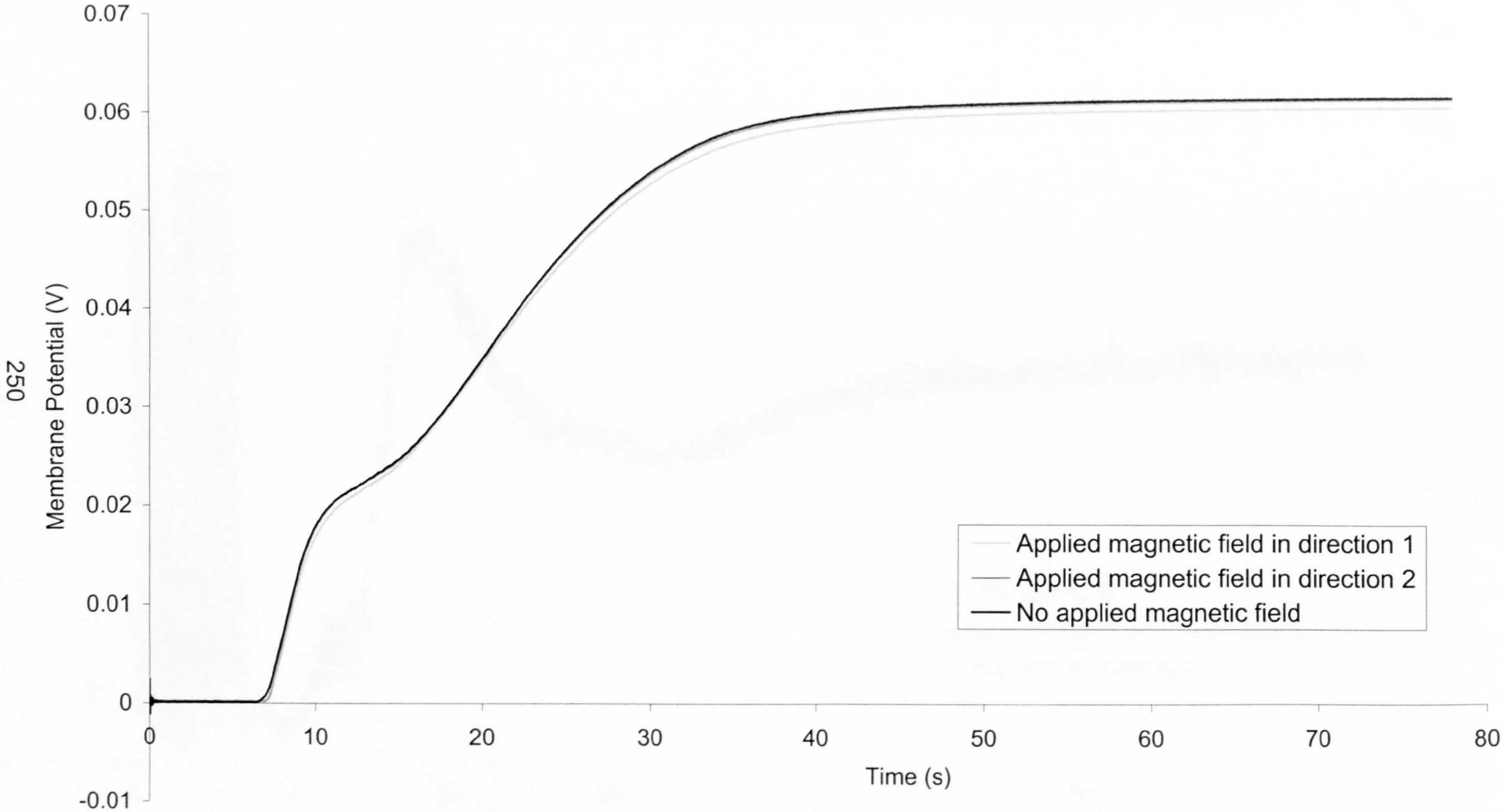

Figure 8.11 Significance levels of differences between mean membrane potentials measured in the absence of a magnetic field and in the presence of an applied field in direction 1 during second series of experiments

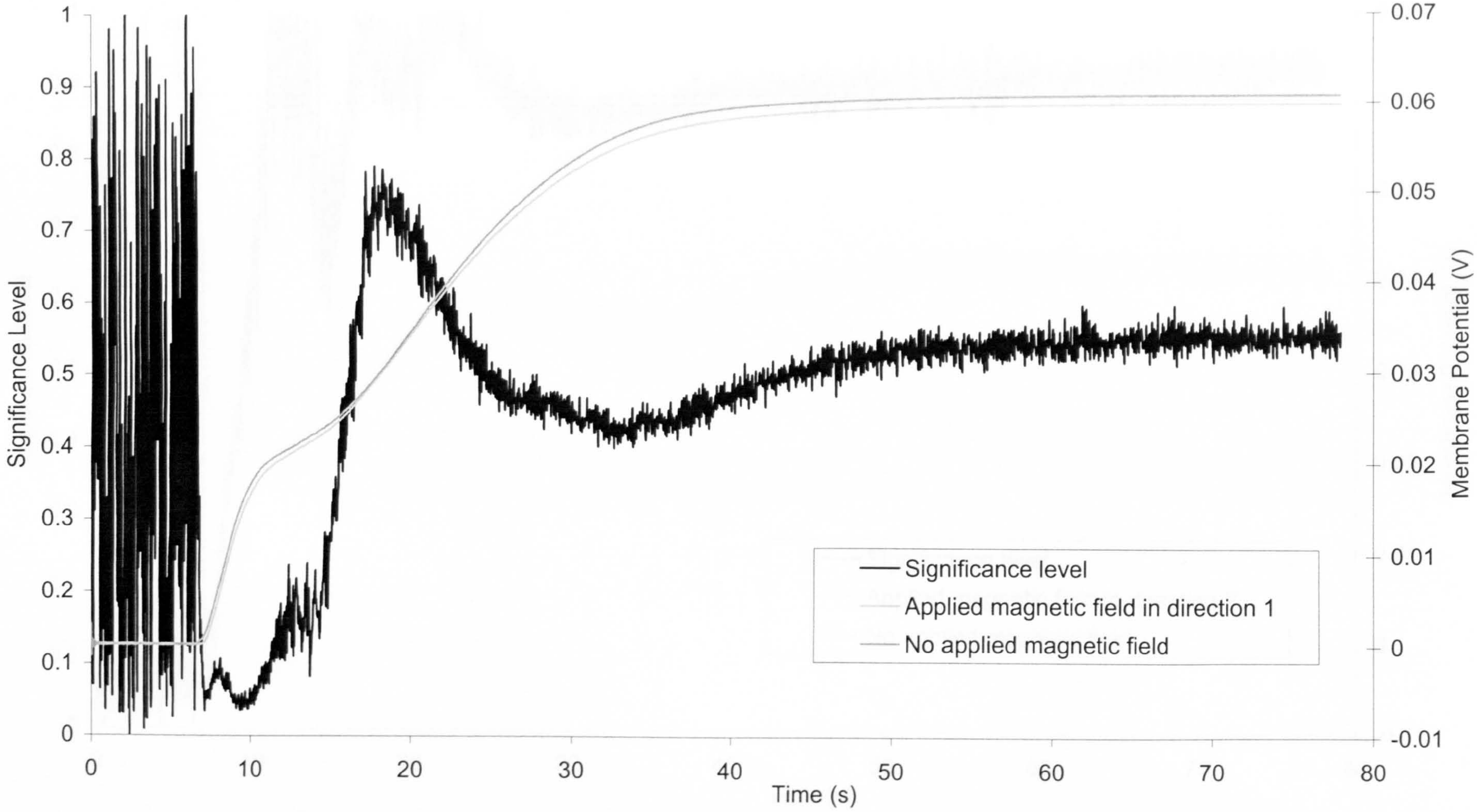

Figure 8.12 Significance levels of differences between mean membrane potentials measured in the absence of a magnetic field and in the presence of an applied field in direction 2 during second series of experiments

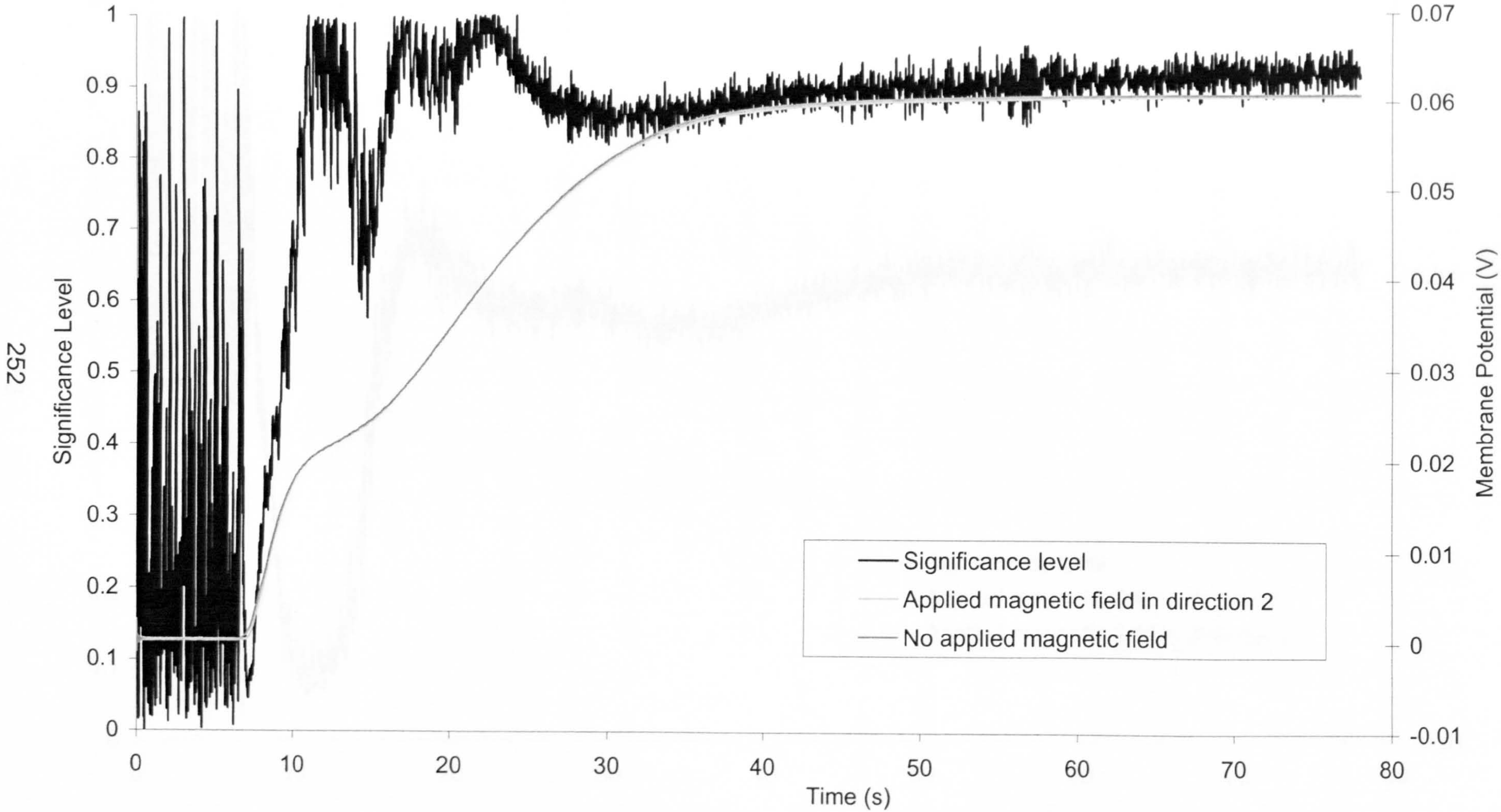

Figure 8.13 Significance levels of differences between mean membrane potentials measured in the presence of an applied magnetic field in directions 1 and 2 during second series of experiments

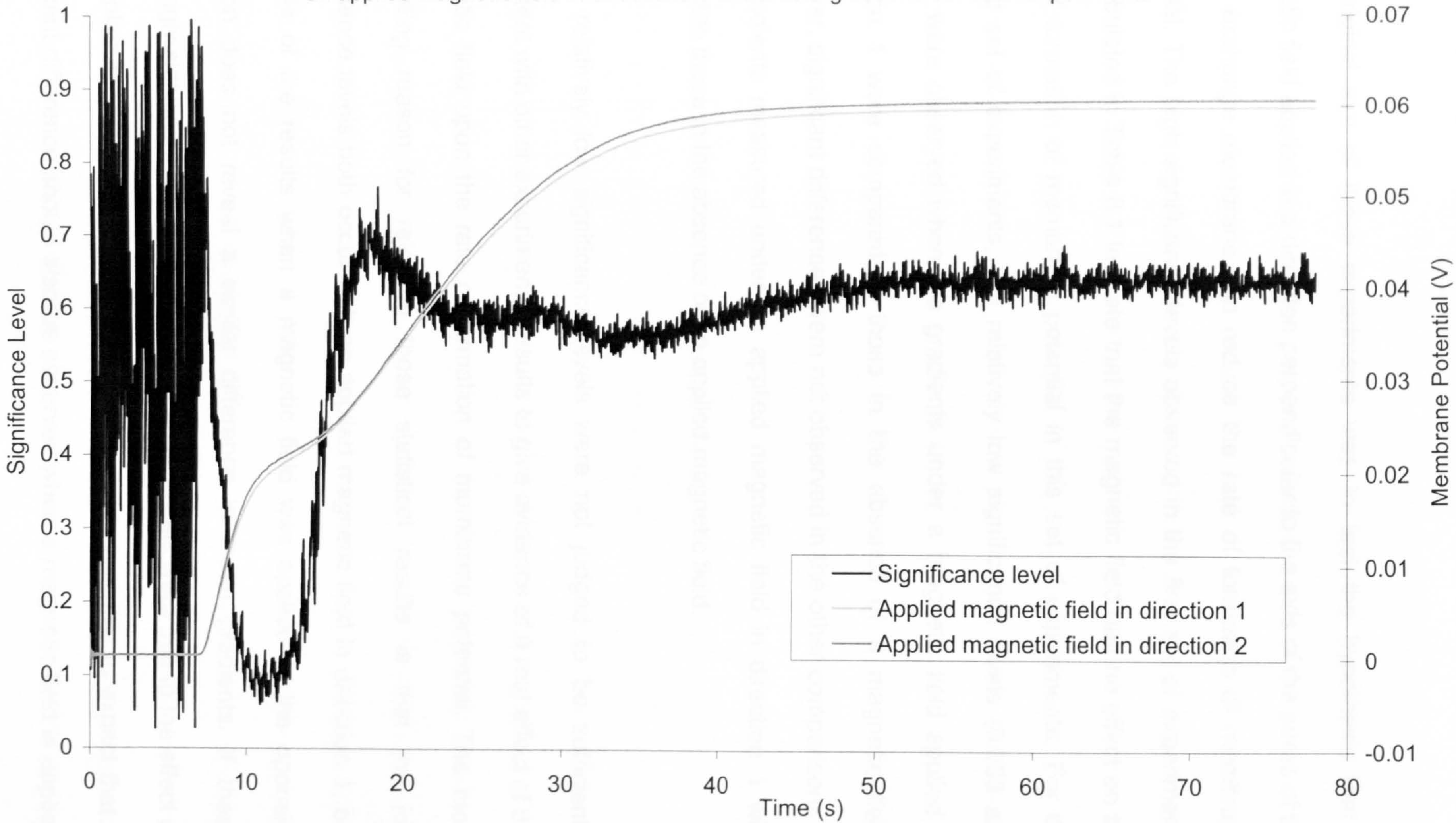

8.3. Discussion

The original aim of these experiments was to test the hypothesis that a magnetic field applied in a direction perpendicular to the axis of the pores of the cation exchange membrane can reduce the rate of formation of membrane potential. The high significance levels observed in the first set of experiments and tabulated in Table 8.1 indicate that the magnetic field had no effect on the rate of formation of membrane potential in this set of experiments. For the second set of experiments, two relatively low significance levels (0.033 and 0.069) were observed when the gradients under a magnetic field applied in direction 1 were compared to those in the absence of a magnetic field. However, significant differences were not observed in the other comparisons of the gradients measured under an applied magnetic field in direction 1 with respect to those in the absence of an applied magnetic field.

These relatively low significance levels were not judged to be sufficiently consistent with other experimental results to give evidence of a real effect of the magnetic field upon the rate of formation of membrane potential. The most compelling reason for rejecting these statistical results is that the low significance levels both occur with an applied magnetic field in direction 1, but analysis of the results when a magnetic field was applied in the opposite direction does not reveal a similar difference in mean gradients. If these seemingly significant differences in the mean gradients were due to the effect of the applied magnetic field in direction 1, it seems reasonable to expect that a significant difference should also be observed when a magnetic field is applied

in the opposite direction. The absence of a significant effect with an applied magnetic field in direction 2 under the same experimental conditions, together with the absence of significant effects in the previous set of experiments or when gradients are compared over other intervals in this set of experiments, indicate that the magnets did not affect the rate of formation of membrane potential. Furthermore, closer examination of the differences in means with low significance levels shows that in the 28-40 mV interval for results 1-31, the mean gradient in the presence of an applied magnetic field is greater than that measured in the absence of a field. However, in the 38-50 mV interval for results 32-67, the gradient in the presence of a field is actually less than that in the absence of a field. Therefore, it was concluded that the magnetic field did not affect the rate of formation of membrane potential in these experiments.

A significant ($p < 0.02$) increase in measurements of mean membrane potential was observed in the presence of an applied magnetic field during the first set of experiments. This effect was not predicted by the hypothetical mechanism of collisions between sodium ions and the walls of the cation exchange membrane pores due to an applied magnetic field. Therefore, the second set of experiments in which a magnetic field was applied in two antiparallel directions was designed to determine the reason for the increase in membrane potential.

Prior to conducting the second set of experiments, two experimental outcomes were considered possible. The potential outcomes were based on the assumption that the previously observed increase in the mean membrane potential in the presence of a magnetic field was caused by an interaction

between the magnetic field and the sodium chloride solution. If the previous observations were caused by collisions between sodium ions and the membrane pores, then it was expected that applying a magnetic field in the reverse direction would also cause the same effect. In this case, the mean membrane potential measured in the presence of a magnetic field in direction 1 was expected to be equal to that measured with an applied magnetic field in direction 2. Furthermore, mean membrane potentials measured in the presence of an applied field in either direction were expected to be of a greater magnitude than that measured in the absence of a magnetic field. This situation is illustrated in Figure 8.14 (a).

If the previous observations were due to some other effect, there is a possibility that this effect may be dependent upon the direction of the applied magnetic field. In this case, the application of a magnetic field in the same direction (direction 1) should again show an increase in mean membrane potential, compared to that observed in the absence of a magnetic field. Application of a magnetic field in the opposite direction (direction 2) would be expected to show a reduction in mean membrane potential measurements with respect to those in the absence of an applied field. This situation is illustrated in Figure 8.14 (b). Furthermore, the differences between each of the two sets of mean membrane potentials measured in the presence of a magnetic field and that in the absence of a field (shown as ΔV_2 for a magnetic field in direction 2 in Figure 8.14 (b)) were expected to be equal. Any combination of results other than those shown in Figure 8.14 would suggest that the unexpected results of the previous

experiment were due to a factor other than the interaction of the applied magnetic field with the sodium chloride solution.

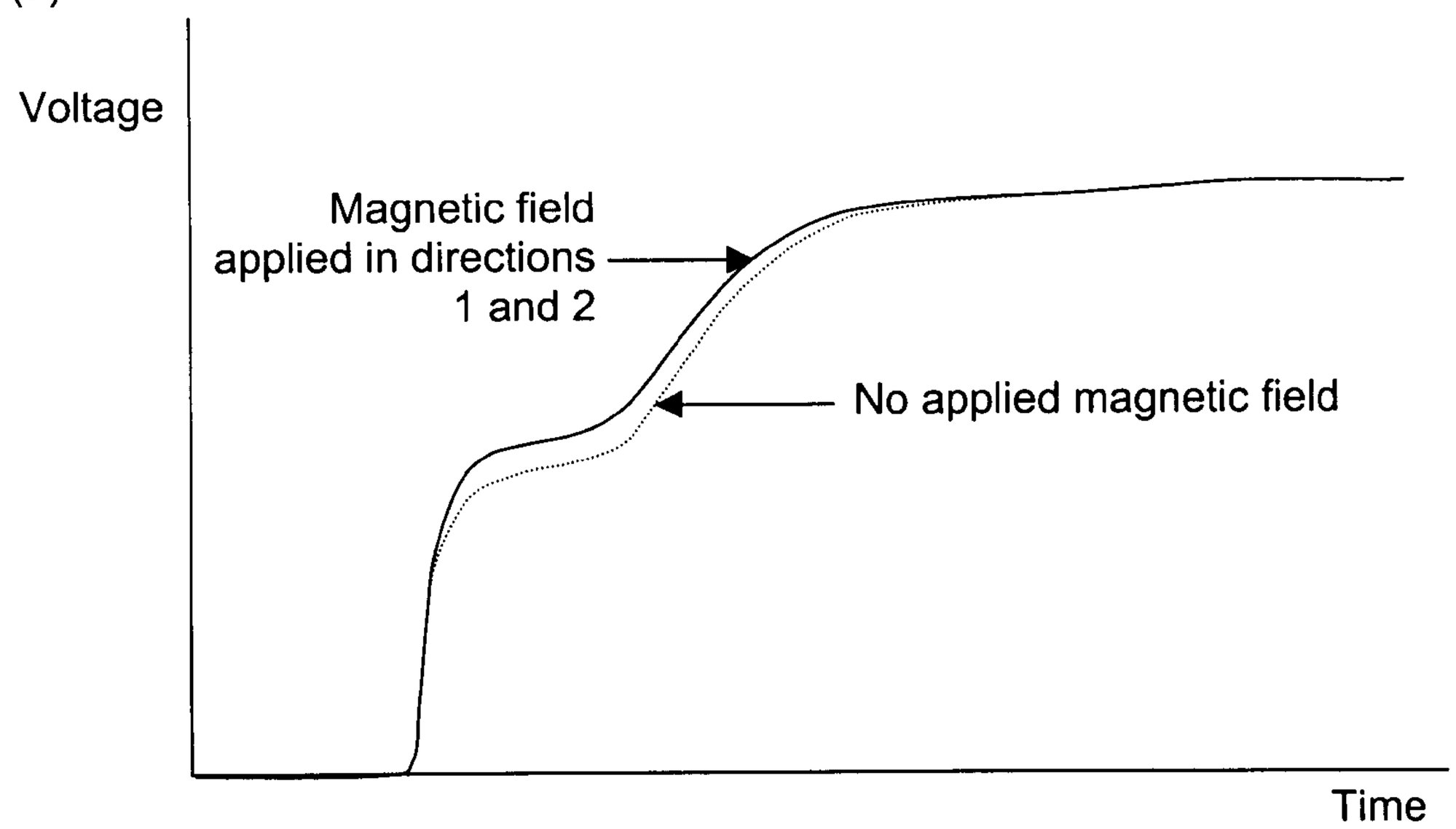

Figure 8.14 Expected results from second set of transient experiments

It is considered that the increase in the mean membrane potential measured in the presence of an applied magnetic field during the first set of experiments was not due to the effect of the magnetic field on the motion of ions. The failure to replicate the results of the first set of experiments suggests that the observed difference between membrane potentials was due to an experimental artefact rather than an interaction between the magnetic field and sodium ions. Although a difference between membrane potentials measured in the absence of a magnetic field and in the presence of a magnetic field applied in direction 1 was observed in the second set of experiments, this difference was not as significant as that measured previously. The argument that the differences in mean membrane potential are due to an experimental artefact is supported by the observation that the membrane potentials measured in the presence of a magnetic field in direction 1 were greater than those in the absence of a field in the first set of experiments, yet this situation was reversed in the second set of experiments. The failure to observe either of the effects on membrane potential that were suggested in Figure 8.14 when a magnetic field was applied in the opposite direction provides additional proof that the magnetic field has no effect on membrane potential.

It was concluded that the results of these experiments offer no evidence of an interaction between the sodium ions and an applied magnetic field. The rate of formation of membrane potential was not significantly reduced by an applied static magnetic field. The mean membrane potential was unaffected by the application of a magnetic field.

A perceived shortcoming of the experimental method is the absence of temperature regulation. The Nernst equation (1.1) shows that membrane potential is proportional to absolute temperature. Since the temperatures of the sodium chloride solutions used in the experiment were not controlled, it is possible that variations in their temperatures may have affected the rate of formation of membrane potential. At the start of every experiment both solutions of sodium chloride were at room temperature, which was estimated to be consistent for each experimental run within the 20 ± 5 °C range. Therefore, fluctuations in temperature would result in less than a ± 1.7% variation in membrane potential. It is considered that such a small variation in membrane potential is unlikely to have had a significant effect on the outcome of the experiments, or on the conclusions drawn from the experimental results.

To support the conclusion that the diffusion of sodium ions through the ion exchange membrane was unaffected by an applied magnetic field, a literature search was conducted to find similar studies of diffusion through artificial membranes in the presence of magnetic fields. Since the literature search revealed no previous investigations involving ion exchange membranes, it is thought that the experiments described in this chapter are unique. However, several papers were found that describe the effect of a magnetic field on diffusion through other types of artificial membrane.

The first such investigations appear to have been conducted by Lielmezs *et al.*, who measured the diffusion coefficients of alkali chloride solutions through a fritted glass diaphragm in the presence of a 0.5 T field [6, 7]. Lielmezs *et al.*

reported that while the diffusion coefficients of hydrogen chloride, sodium chloride and potassium chloride increased when the magnetic field was applied, the rates of diffusion of lithium chloride and caesium chloride were reduced by the magnetic field. The researchers suggested that the effect may be due to interactions between the solvent, the solute and the glass diaphragm, or due to magnetically mediated changes in fluid properties, such as the slight increase in the viscosity of water which the researchers had previously observed. Lielmezs *et al.* also observed that the rate of diffusion of saccharides through an inert polycarbonate membrane was reduced by magnetic fields of up to 1.1 T [8]. The magnetic field was thought to reduce the diffusion rate by affecting the hydration of the saccharide molecules.

Waskaas reported that the rate of diffusion of paramagnetic nickel (II) chloride solution through an inert cellulose acetate membrane was increased by a magnetic field in the 0-0.82 T range [9]. Waskaas argued that the increase in diffusion rate was caused by a magnetomotive force which developed in response to the different reluctances of the paramagnetic solutions on either side of the membrane.

Mogi *et al.* measured the mixing rate of various ionic solutions separated by a porous paper membrane in 8 T magnetic field [10]. The rate of mixing was found to increase, decrease or be unaffected by the magnetic field, depending on the solution under observation. Mogi *et al.* specifically discounted any effect of the magnetic field on the rate of diffusion as an explanation for this phenomenon, instead suggesting that bulk solution flow, occurring due to

differences in the densities of the solutions, was enhanced or suppressed by the magnetic field.

These publications provide evidence that the rate of diffusion through an artificial membrane may be increased or decreased by a magnetic field, depending on the properties of the solution. It is significant that none of the researchers suggested the mechanism of collisions between ions and the pores as proposed in Section 4.2 to explain their results. This supports the conclusion that collisions between the ions and the membrane caused by the applied magnetic field did not influence the rate of formation of membrane potential in the experiments reported in this chapter.

The conclusion that the rate of formation of membrane potential is not reduced by an applied magnetic field casts severe doubt upon the hypothesis that anaesthesia can be induced by an axially aligned static magnetic field. The absence of a measurable effect in experiments with an artificial membrane suggests it may not be possible to reduce the rate of formation of action potentials in a nerve fibre using an applied magnetic field. It was estimated in Section 5.1 that the minimum applied magnetic flux density required to cause a collision between a sodium ion and the walls of an ion exchange membrane pore was 40×10^{-6} T. The corresponding minimum flux density for a biological ion channel was estimated to be 356 T (Section 4.2). The absence of a measurable effect on cation exchange membranes with an applied magnetic field of 0.3 T, well in excess of the estimated minimum field, suggests that applied flux densities even greater than 356 T may be necessary to induce an effect in

nerve fibres. Therefore, it may not be possible to induce an anaesthetic effect by this mechanism, even if generation of 356 T static magnetic field were feasible.

It must be remembered that experiments performed upon artificial membranes can never give a completely accurate prediction of the behaviour of biological membranes. Despite the absence of an effect in the experiments with a sample of cation exchange membrane, there is still a possibility that an applied magnetic field may produce a significant effect upon the motion of ions through a biological ion channel. To assess the validity of extrapolating the results from the artificial membrane experiments to biological membranes, it is worthwhile to compare the major structural features of biological and artificial ion channels.

When the hypothetical mechanism for inducing an anaesthetic effect was postulated, the ion channel was approximated by a smooth, perfect cylinder with no electrostatic charge. In reality, the structure of both biological ion channels and the pores of ion exchange membranes are much more complicated than this model suggests, to the extent that the neither structure is completely understood. Recent research [11, 12] in which the sodium channel was investigated by cryo-electron microscopy has illustrated the complexity of biological ion channels. Rather than being a single cylindrical pore, the cryo-electron microscope images show that the transmembrane protein which forms the sodium channel actually contains four individual pores connecting the intra- and extra-cellular regions. These pores, through which sodium ions diffuse, are not perfectly straight and may even interconnect within a central cavity inside

the pore. Unfortunately, the limited resolution (19 angstrom) of these images of the ion channel does not allow the exact structure of the sodium channel to be determined.

In the absence of accurate information on the structure of the voltage-gated sodium channel, some of the important differences between the structure of biological pores and the approximated ion channel can be illustrated by examining the features of the potassium channel. The potassium channel is the most understood biological ion channel, as the result of 3.2 angstrom resolution images produced by x-ray crystallography [13]. These images show that the potassium channel consists of three distinct regions, as opposed to the perfectly cylindrical shape used in these approximations. The main structural features of the potassium channel are summarised in Figure 8.15.

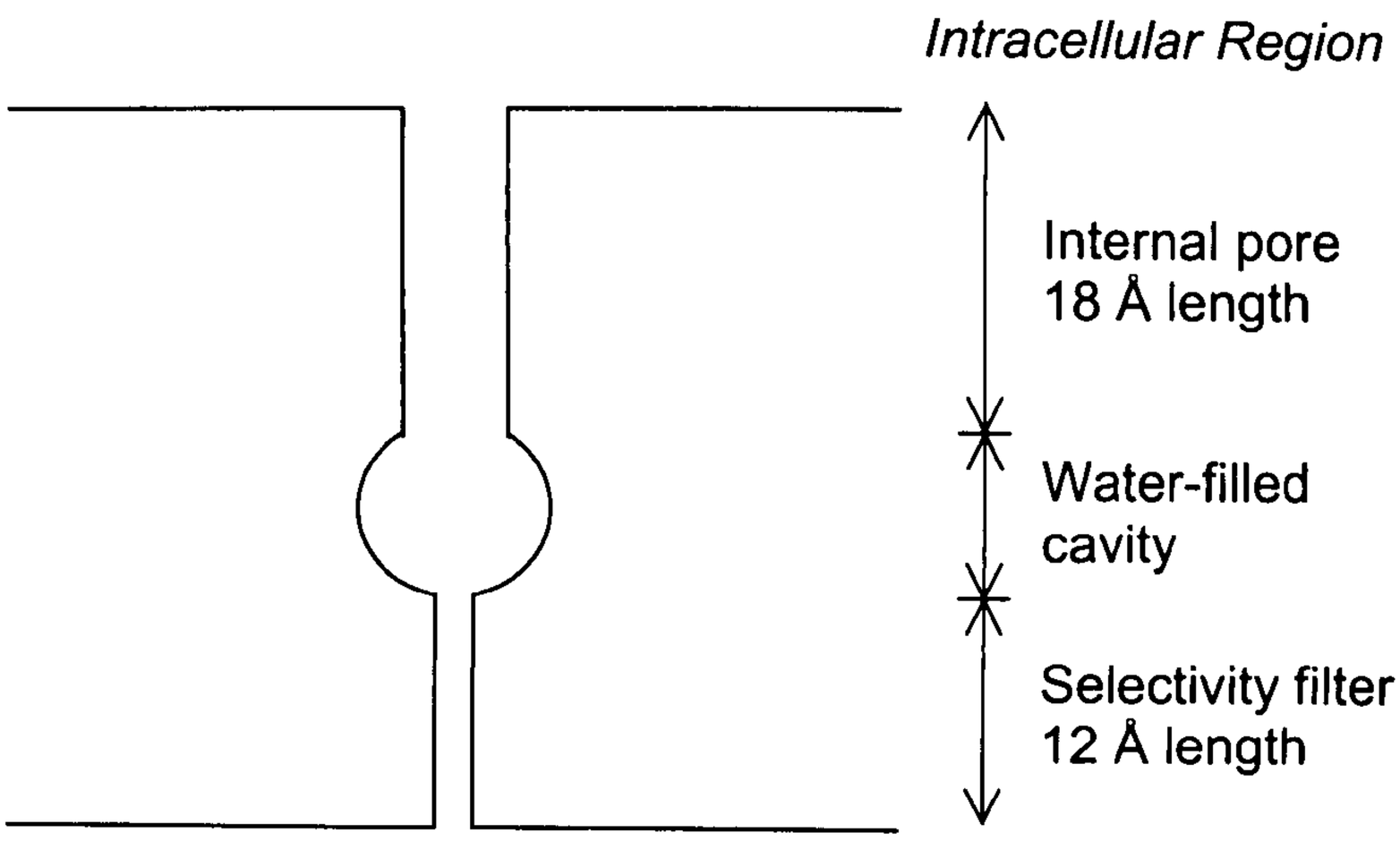

Figure 8.15 Structure of a potassium channel

The first part of the channel is an approximately cylindrical region known as the internal pore, which connects the intracellular region to a cavity in the centre of the membrane. This cylindrical region is of a sufficient diameter to allow the passage of a hydrated potassium ion. The cavity in the centre of the membrane has a diameter of approximately 10 Å and is filled with water molecules. Ordinarily, the centre of the membrane contains non-polar groups and a potassium ion would not be energetically stable in this region without being surrounded by charged groups. Therefore, the water molecules are a source of additional charge to stabilise the potassium ion in this region. The final component of the ion channel is a narrow, approximately cylindrical region known as the selectivity filter, which has the purpose of making the channel selectively permeable to potassium ions. The selectivity filter is 12 Å in length, has a narrow diameter and is lined with carbonyl (CO) groups. Upon entering the selectivity filter, the hydrated potassium ion is stripped of most of the water molecules which surround it in the bulk solution. The negatively charged carbonyl oxygen atoms act as "surrogate" water molecules and maintain the energetic stability of the potassium ion as it passes through the selectivity filter. The diameter of the selectivity filter is such that other ions, particularly sodium ions, are unable to get close enough to the carbonyl oxygen atoms to become stable. Thus, the potassium channel achieves its selectivity since it is not energetically favourable for other ions to enter the selectivity filter. The total length of the potassium channel is 45 Å.

Although it has yet to be proven, the sodium channel is likely to contain many of the features of the potassium channel. In particular, the sodium channel is likely

to have a narrow selectivity filter and the cavity which has been observed in the cryo-electron microscope images of the sodium channel [11] may contain water molecules to stabilise sodium ions at the centre of the membrane.

The structure of an ion exchange membrane pore is also considerably different to the perfectly cylindrical pore structure that was originally assumed. The "cluster-network" model, in which the pore consists of a number of spherical cavities of 40 angstrom diameter interconnected by cylindrical channels of 10 angstrom diameter (Figure 8.16) is the most widely accepted structural model of an ion exchange membrane pore [14, 15]. The cavities are considered to be lined with charged groups, negatively charged sulphonic (SO_3^-) groups in the case of a cation exchange membrane, from which the membrane derives its selectivity. However, other researchers have suggested that the pore structure is a tortuous network of channels of uniform cross-section [16].

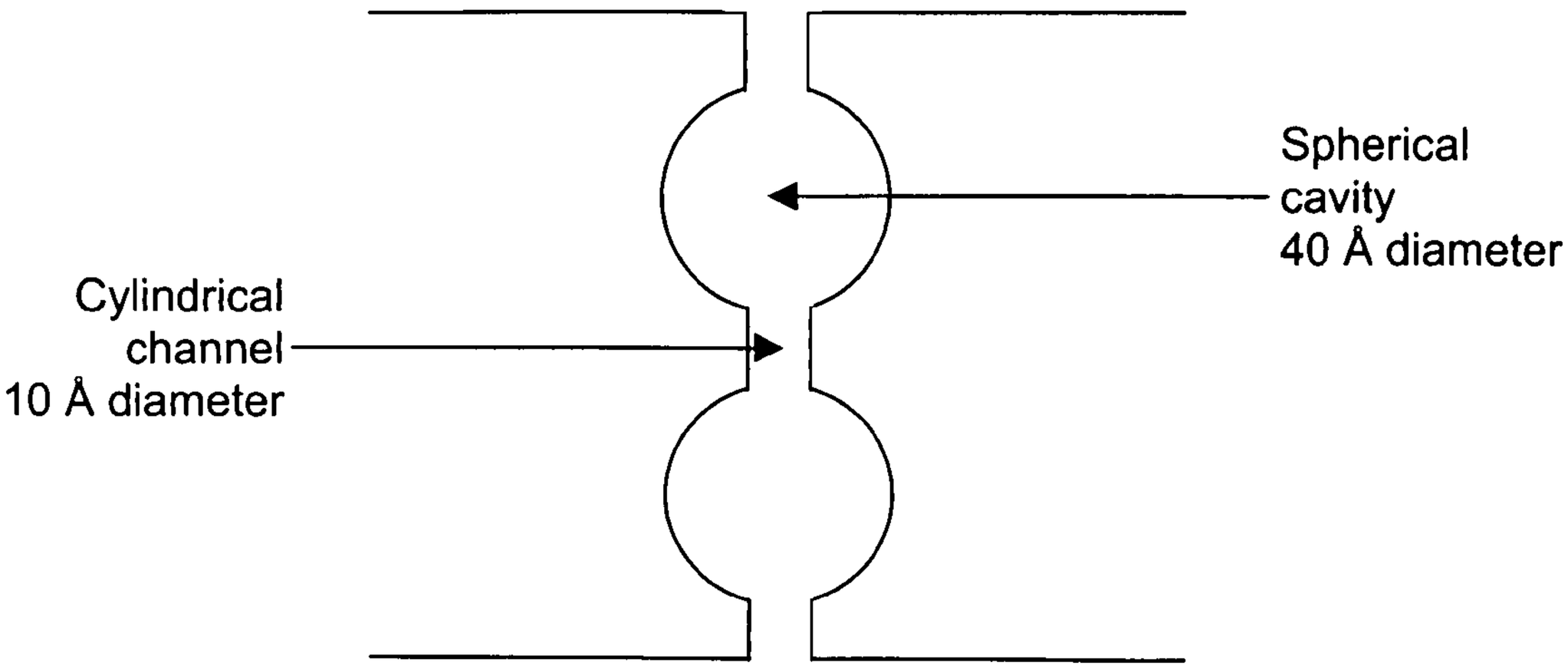

Figure 8.16 Cluster-network model of ion exchange membrane pore structure

Although the structures of sodium channels and ion exchange membrane pores are not completely understood, it is clear that neither structure is well represented by a perfect cylinder. Both pore structures exhibit considerable non-uniformity and it is possible that each type of pore consists of large cavities connected to narrow channels. While the ion exchange membrane does not provide a completely accurate model of a biological membrane, their pores share enough common features for the conclusions of these artificial membrane experiments to be extrapolated to a biological system with reasonable confidence.

One possible explanation for the absence of a measurable effect in the experiments is that the original estimate of the velocity of sodium ions within the ion channels was incorrect. A wide search of both textbooks and papers failed to find a single instance in which the velocity of ions in a biological ion channel was measured directly. In lieu of published values, the velocity of ions was estimated by calculating the gradient of the graph of sodium ion position against time in the simulation of ion transport through a gramicidin channel published in reference [17]. Thus, the sodium ion velocity was estimated to be approximately 9.5 m s^{-1}.

However, the instantaneous speed of sodium ions in bulk solution is far greater than this estimate of ion velocity within the channel. In the bulk fluid, ions will undergo Brownian motion and the speed of a sodium ion can be calculated by equating its thermal energy (8.3) with its kinetic energy (8.4):

$$E_{thermal} = \frac{3kT}{2} \tag{8.3}$$

$$E_{kinetic} = \frac{mv^2}{2} \tag{8.4}$$

where T is absolute temperature, m is the mass of the hydrated ion, v is its speed and k is Boltzmann's constant (1.38×10^{-23} J K^{-1}). At body temperature (310 K), the speed of a hydrated sodium ion with a mass of 1.27×10^{-25} kg is calculated as 318 m s^{-1}. This simple estimate of ionic speed ignores interactions with the solvent and other ions.

If sodium ions are assumed to travel at thermal speeds of 318 m s^{-1} within the ion channel, a new estimate of the applied magnetic flux density required to cause a collision can be calculated from equation (4.2). Using a Larmor radius of 21.2 nm as derived from Figure 4.5, a magnetic field of 11.9×10^{3} T is necessary to cause a collision between a sodium ion and the walls of the ion channel. If this estimate of ionic velocity was correct, the hypothetical technique of non-invasive anaesthesia would be unfeasible due to the large magnetic field required.

However, when the pores of the cation exchange membrane are considered, which would permit a much larger Larmor radius of 0.19 metre, the minimum applied magnetic field required to cause a collision is 1.33×10^{-3} T. Therefore, if the assumption that ions move within the pores of the cation exchange membrane at thermal speeds was correct, collisions between the ions and pores would have occurred during the experiments in an applied magnetic field of 0.3 T. Since the applied magnetic field was three orders of magnitude greater than that required to cause a single collision, the high velocity of ions within the

pores cannot be the only explanation for the lack of an observed effect in these experiments.

An insight into the reason for the absence of an effect in the experiments was provided by papers in which the velocities of various ions and molecules in ion exchange membranes were measured. Bath *et al.* measured the drift velocity of sodium ions through a cation exchange membrane in an applied electric field as 3.5×10^{-5} m s^{-1} [18]. This is seven orders of magnitude less than the estimated thermal velocity of sodium ions of approximately 300 m s^{-1}. The sodium ion velocities published by Bath *et al.* are supported by other researchers' measurements of water velocity in ion exchange membranes. Sims *et al.* [19] published values of water velocity of the order of 1×10^{-5} m s^{-1}, while Dammak *et al.* [20] measured water velocities of the order of 1×10^{-7} m s^{-1}.

Viscous effects, which cause ion motion to be impeded by interactions with other ions and solvent molecules, are a contributing factor in the lower than predicted measurement of sodium ion velocity in the pore. Another explanation for the low velocity of sodium ions was demonstrated in a separate experiment by Bath *et al.* [21]. Bath *et al.* reported that the velocity of an uncharged organic molecule in a cation exchange membrane was almost three orders of magnitude greater than that of an organic monovalent cation of similar mass. The comparatively low velocity of the ion was attributed to electrostatic interaction with charged groups within the pore which are responsible for the selective properties of the membrane. Therefore, the motion of sodium ions

through the cation exchange membrane is likely to be significantly retarded by electrostatic attraction to these fixed charges within the pore.

The absence of an observable effect of the magnetic field on the rate of formation of membrane potential may be explained by comparing the magnitude of the Lorentz force to that of the Coulomb force between the sodium ion and the pore. The Coulomb force F, which measures the electrostatic interaction between two charges Q_1 and Q_2, separated by a distance r in a medium of relative permittivity ε_r is calculated from [22]:

$$F = \frac{Q_1 Q_2}{4\pi\varepsilon_0\varepsilon_r r^2} \qquad (8.5)$$

where ε_0 is the permittivity of free space and has a value of 8.854×10^{-12} F m^{-1}.

To simplify estimation of the Coulomb force, the distributed nature of the fixed charge within the pore is ignored. Although these fixed charges exist at a number of discrete sites, their resultant effect is treated as that of a single point charge. To satisfy the condition of charge neutrality within the pore [23], the point charge is assumed to be equal and opposite to the sodium ion charge of 1.6×10^{-19} C. The separation between the fixed pore charge and the sodium ion is estimated to be 0.52 nm. This value is obtained by assuming that the hydrated sodium ion of 0.24 nm radius [24] is separated from the fixed pore charge only by the pore charge's hydration atmosphere. The pore charge is assumed to be hydrated by a single layer of water molecules of 0.28 nm diameter [24]. The relative permittivity is assumed to 78.5, the value for water

[25]. When these values are substituted into equation (8.5), the Coulomb force is calculated to be 1.08×10^{-11} N.

To calculate the Lorentz force, the velocity of the sodium ion in the ion exchange membrane is assumed to be 3.5×10^{-5} m s^{-1}, as suggested by Bath *et al.* [18]. A static magnetic field of 0.3 T, as used in these experiments, is assumed to be applied in a direction perpendicular to ion motion. Substituting these values into equation (3.1) yields a Lorentz force of 1.68×10^{-24} N.

This simple calculation demonstrates that the Lorentz force is negligible in comparison to the Coulomb force, with a difference of thirteen orders of magnitude between the two forces. In other words, the effect of Lorentz force which attempts to deflect the motion of sodium ions into the walls of the ion exchange membrane pore is insignificant in comparison to the electrostatic attraction that already exists between ions and the pore. Detailed modelling of the interaction between ions and ion channels is non-trivial and is beyond the scope of this thesis. However, the conclusion of this simple calculation, that the Coulomb force is large in comparison to the Lorentz force, is in agreement with the results of Lynden-Bell and Rasaiah who calculated that the force between sodium ions and the walls of idealised ion channels is of the order of 1×10^{-10} N [26]. It is therefore concluded that the rate of diffusion of sodium ions through the pore is unaffected by the presence of an applied magnetic field. This reasoning explains the lack of an observed effect in the transient experiments upon ion exchange membranes described in this chapter.

The presence of charged groups within biological ion channels is also documented. It was originally assumed that sodium ions moved continuously along the axis of an uncharged cylindrical ion channel. However, ions actually move along the channel by passing through a series of discrete electrostatically charged regions known as binding sites [27]. Electrostatic attraction to the binding site causes ions to remain stationary until they can achieve sufficient thermal energy to leave the binding site. Hence, the motion of ions along the channel is discontinuous as the ion 'jumps' between binding sites. This provides evidence that ions within a biological membrane are also strongly influenced by electrostatic attraction to the channels. Thus, the conclusion that the Lorentz force is small in comparison to the Coulomb force is also likely to be valid when a sodium ion within a nerve cell membrane is considered.

It is calculated that an applied magnetic field of the order of 10^{12} T would be required for the magnitudes of the Lorentz and Coulomb forces to be comparable, based on the previous assumptions for ion exchange membranes. For comparison, the strongest permanent magnets produce flux densities of approximately 4 T [28]. However, this magnetic field is produced within the centre of a fully-enclosed sphere, a so-called "magic sphere", meaning that placement of a nerve fibre within the field is impossible. The world's most intense static electromagnet is owned by the National High Magnetic Field Laboratory in Florida, USA, and produces a magnetic field of 45 T [29]. The 32 millimetre bore of this magnet would preclude the insertion of a limb within the magnetic field. The largest man-made magnetic fields are pulsed fields with flux densities of 2.8×10^3 T, produced by magnetocumulative generators [30].

Unfortunately, these electromagnets are only capable of generating a single magnetic pulse of short duration before being destroyed by the intense heat and forces which are created [31]. Magnetocumulative generators would therefore be unsuitable for clinical use. It is clearly not possible to create a magnetic field of sufficient intensity to significantly affect the motion of sodium ions within the ion channel. For this reason, it is considered that the hypothetical method of non-invasive anaesthesia is unfeasible.

An interesting consequence of the recognition of the large electrostatic attraction between the ion and the pore is that Liboff's "biomagnetic hypothesis" may be disproved. In a paper published in 1965, Liboff hypothesised that experimental observations of inhibited growth in cells that were exposed to a magnetic field may have been caused by a reduced rate of diffusion across the cell membrane [32]. By analogy to the diffusion of plasmas [33], Liboff suggested that the diffusion coefficient of an ionic species would be reduced in a direction perpendicular to that of an applied magnetic field. Liboff calculated that this effect would be significant only for cells with a charged cytoplasm, such as nerve cells, for applied flux densities of the order of 10 T. However, assuming that ion channels only allow ions to pass in single file, Liboff's hypothetical mechanism requires collisions between ions and the walls of the ion channel that result in a change in the direction of ion motion. This mechanism is unlikely to occur since the motion of ions will be constrained by their strong electrostatic attraction to the channel, which will prevent the change in the direction of ionic motion that is required to reduce the rate of diffusion.

In summary, the experiments on transient sodium ion flow through a cation exchange membrane in the presence of an applied magnetic field suggest that inducing anaesthesia with an axially aligned magnetic field is not possible. It has been noted that due to the structural differences between the pores of the cation exchange membrane and biological ion channels, the cation exchange membrane does not provide an entirely realistic model of the effect of the magnetic field *in vivo*. The only way to determine whether the hypothetical method of anaesthesia is feasible would be to perform experiments upon real neurons, either *in vivo* or *in vitro*.

The results of several *in vivo* and *in vitro experiments, similar* to those that might be conducted to investigate this technique of non-invasive anaesthesia, were considered in Section 1.3.1. It was noted that many of these experiments had contradictory results and that there was no consensus on the effects of magnetic fields on nerve function. Although some researchers reported that magnetic fields caused a reduction in action potential amplitude [34, 35] and conduction velocity [36], other researchers reported that magnetic fields had no effect on nerve function [37, 38, 39] or that applied magnetic fields increased nerve excitability [40, 41]. None of these *in vivo* and *in vitro* experiments provide evidence to suggest that the mechanism proposed for non-invasive anaesthesia occurs in nerve cells. The magnetic fields used in these experiments were in the 0.1-2.0 T range, several orders of magnitude less than would be required for the Lorentz force to be comparable to the Coulomb force. However, it would not be possible to generate a magnetic field of sufficient intensity for the effect of the Lorentz force to be observed.

The observation that the force exerted on sodium ions by the magnetic field is negligible in comparison to the strong electrostatic force exerted by the ion channel strongly suggests that investigations of this effect on biological systems would yield negative results. It is the author's opinion that further experimental investigation of this hypothetical *mechanism*, *for the purpose* of producing a non-invasive anaesthetic effect, is not worthwhile.

8.4. References

1. Fisher, R.A.
   The Design of Experiments, Fourth Edition.
   Oliver and Boyd, 1947.
2. Cox, D.R.
   Planning of Experiments.
   Wiley, 1958.
3. Kanji, G.K.
   100 Statistical Tests
   SAGE Publications, 1993.
4. Press, W.H., Flannery, B.P., Teukolsky, S.A. and Vetterling, W.T.
   Numerical Recipes in C.
   Cambridge University Press, 1988.
5. Philips, J.L.
   How To Think About Statistics, Revised Edition.
   Freeman, 1992.
6. Lielmezs, J.
   External Transverse Magnetic Field Effect on Electrolyte Diffusion in Alkali Chloride-Water Solutions.
   Thermochimica Acta, Vol. 19, 1977, pp. 249-266
7. Lielmezs, J., Aleman, H.
   External Transverse Magnetic Field Effect on Electrolyte Diffusion in LiCl-H_20 Solutions.
   Biochemistry and Bioenergetics, Vol. 5, 1978, pp. 285-295.
8. Lielmezs, J., Atwal, V. and Aleman, H.
   Magnetic Field Effect on Free Diffusion of Selected Saccharides in Aqueous Solution Through an Inert Porous Membrane.
   Journal of the Electrochemical Society, Vol. 137, 1990, pp. 3809-3814.
9. Waskaas, M.
   Short-Term Effects of Magnetic Fields on Diffusion in Stirred and Unstirred Paramagnetic Solutions.
   Journal of Physical Chemistry, Vol. 97, 1993, pp. 6470-6476.

10. Mogi, K., Sakihama, T., Hirota, N. and Kitazawa, K.
Magnetic Field Effect on the Transport Process of Paramagnetic or Diamagnetic Substances in the Aqueous Solution.
Journal of Applied Physics, Vol. 85, 2001, pp. 5714-5716.
11. Sato, C., Ueno, Y., Asai, K., Takahashi, K., Sato, M., Engel, A. and Fujiyoshi, Y.
The Voltage-Sensitive Sodium Channel is a Bell-Shaped Molecule with Several Cavities.
Nature, Vol. 409, 2001, pp. 1047-1051.
12. Catterall, W.A.
Structural Biology – A 3D View of Sodium Channels.
Nature, Vol. 409, 2001, pp. 988-991.
13. Doyle, D.A., Cabral, J.M., Pfuetzner, R.A., Kuo, A., Gulbis, J.M., Cohen, S.L., Chait, B.T. and MacKinnon, R.
The Structure of the Potassium Channel: Molecular Basis of K+ Conduction and Selectivity.
Science, Vol. 280, 1998, pp. 69-77.
14. Gierke, T.D., Munn, G.E. and Wilson, F.C.
The Morphology in Nafion Perfluorinated Membrane Products as Determined by Wide- and Small-Angle X-Ray Studies.
Journal of Polymer Science: Polymer Physics Edition, Vol. 19, 1981, pp. 1687-1704.
15. Heitner-Wirguin, C.
Recent Advances in Perfluorinated Ionomer Membranes: Structure, Properties and Applications.
Journal of Membrane Science, Vol. 120, 1996, pp. 1-33.
16. Verbrugge, M.W. and Hill, R.F.
Ion and Solvent Transport in Ion-Exchange Membranes: II. A Radiotracer Study of the Sulfuric-Acid, Nafion-117 System.
Journal of the Electrochemical Society, Vol. 137, 1990, pp. 893-899.
17. Skerra, A. and Brickmann J.
Simulation of Voltage-Driven Hydrated Cation Transport Through Narrow Transmembrane Channels.
Biophysical Journal, Vol. 51, 1987, pp. 977-983.

18. Bath, B.D., Lee, R.D., White, H.S. and Scott, E.R.
Imaging Molecular Transport in Porous Membranes. Observation and Analysis of Electroosmotic Flow in Individual Pores Using the Scanning Electrochemical Microscope.
Analytical Chemistry, Vol. 70, 1998, pp. 1047-1058.

19. Sims, S.M., Higuchi, W.I., Srinivasan, V. and Peck, K.
Ionic Partition Coefficients and Electroosmotic Flow in Cylindrical Pores: Comparison of the Predictions of the Poisson-Boltzmann Equation with Experiment.
Journal of Colloid and Interface Science, Vol. 155, 1993, pp. 210-220.

20. Dammak, L., Tourreuil, V., Larchet, C. and Auclair, B.
Experimental Determination of the Water Flow Through Charged Membranes in Bi-Ionic Systems.
New Journal of Chemistry, Vol. 21, 1997, pp. 1291-1296.

21. Bath, B.D., White, H.S. and Scott, E.R.
Electrically Facilitated Molecular Transport. Analysis of the Relative Contributions of Diffusion, Migration and Electroosmosis to Solute Transport in an Ion-Exchange Membrane.
Analytical Chemistry, Vol. 72, 2000, pp. 433-442.

22. Carter, R.G.
Electromagnetism for Electronic Engineers, Second Edition.
Chapman & Hall, 1992.

23. Lakshminarayanaiah, N.
Transport Phenomena in Membranes.
Academic Press, 1969.

24. Moore, W.J.
Physical Chemistry, 5th Edition.
Prentice-Hall, 1972.

25. Atkins, P.W.
Physical Chemistry, Fourth Edition.
Oxford University Press, 1990.

26. Lynden-Bell, R. M. and Rasaiah, J.C.
Mobility and Solvation of Ions in Channels.
Journal of Chemical Physics, Vol. 105, 1996, pp. 9266-9280.

27. Aidley, D.J. and Stanfield, P.R.
Ion Channels.
Cambridge University Press, 1996.
28. Leupold, H.A., Tilak, A. and Potenziani, E.
Permanent Magnet Spheres: Design, Construction and Application.
Journal of Applied Physics, Vol. 87, 2000, pp. 4730-4734.
29. Bird, M.D., Bole, S., Dixon, I., Eyssa, Y.M., Gao, B.J. and Schneider-Muntau, H.J.
The 45 T Hybrid Insert: Recent Achievements.
Physica B, Vol. 294-295, 2001, pp. 639-642.
30. Bykov, A.I., Dolotenko, M.I., Kolokolchikov, N.P., Selemir, V.D. and Tatsenko, O.M.
VNIIEF Achievements on Ultra-High Magnetic Fields Generation.
Physica B, Vol. 294-295, 2001, pp. 574-578.
31. Herlach, F.
Innovations and Trends in Magnet Laboratories and Techniques.
Physica B, Vol. 294-295, 2001, pp. 500-504.
32. Liboff, R.L.
A Biomagnetic Hypothesis.
Biophysical Journal, Vol. 5, 1965, pp. 845-853.
33. Chen, F.F.
Introduction to Plasma Physics.
Plenum, 1974.
34. Edelman, A., Teulon, J. and Puhalska, I.B.
Influence of the Magnetic Fields on Frog Sciatic Nerve.
Biochemical and Biophysical Research Communications, Vol. 91, 1979, pp. 118-122.
35. Azanza, M.J. and del Moral, A.
Isolated Neuron Amplitude Spike Decrease Under Static Magnetic Fields.
Journal of Magnetism and Magnetic Materials, Vol. 158, 1996, pp. 593-594.

36. Reno, V.R.
Conduction Velocity in Nerve Exposed to a High Magnetic Field.
NASA Report NAMI-1089, 1969.

37. Schwarz, J.L.
Influence of a Constant Magnetic Field on Nervous Tissues: I. Nerve Conduction Velocity Studies.
IEEE Transactions on Biomedical Engineering, Vol. 25, 1978, pp. 467-473.

38. Schwarz, J.L.
Influence of a Constant Magnetic Field on Nervous Tissues: II. Voltage-Clamp Studies.
IEEE Transactions on Biomedical Engineering, Vol. 26, 1979, pp. 238-243.

39. Gaffey, C.T. and Tenforde, T.S.
Bioelectric Properties of Frog Sciatic Nerves During Exposure to Stationary Magnetic Fields.
Radiation and Environmental Biophysics, Vol. 22, 1983. pp. 61-73.

40. Hong, C-Z., Harmon, B.S. and Yu, J.
Static Magnetic Field Influence on Rat Tail Nerve Function.
Archives of Physical Medicine and Rehabilitation, Vol. 67, 1986, pp. 746-749.

41. Hong, C-Z.
Static Magnetic Field Influence on Human Nerve Function.
Archives of Physical Medicine and Rehabilitation, Vol. 68, 1987, pp. 162-164.

9. CONCLUSIONS

Two methods by which it was hypothesised that a non-invasive effect could be achieved were evaluated. The first hypothetical method of non-invasive anaesthesia proposed that a rotating magnetic field could be used to hyperpolarise a nerve and thus prevent the propagation of action potentials. It was hypothesised that the Lorentz force experienced by ions in the nerve fibre and extracellular fluid due to the motion of the magnetic field would cause a redistribution of charge along the axis of the nerve. By connecting the extracellular region to earth, it was thought that the nerve fibre could be hyperpolarised.

Although a computer simulation demonstrated that hyperpolarisation of the nerve fibre could prevent the propagation of action potentials, an *in-vivo* experiment failed to produce an anaesthetic effect. It was concluded that the hypothetical method of non-invasive anaesthesia was unfeasible, for either of two reasons. Firstly, hyperpolarisation of the nerve fibre could not be achieved with the proposed apparatus since the Lorentz force is opposed by an electrostatic force between ions which results from the redistribution of charge. Alternatively, it may be argued that rotation of the magnets does not result in a rotating magnetic field, thus precluding the possibility that ions experience a Lorentz force. This research highlighted the disagreement between scientists over the effect of rotating a magnet, even 150 years after Faraday performed the first such experiments.

For the second method of non-invasive anaesthesia, it was hypothesised that a static magnetic field aligned with the axis of the nerve could be used to block action potentials. It was proposed that sodium ions diffusing into the axon during the depolarising phase of the action potential would experience a Lorentz force, which would reduce the rate of diffusion by causing collisions between ions and the ion channel. By reducing the rate of diffusion, it was hypothesised that the rate of depolarisation could be significantly reduced, thus preventing the propagation of action potentials. A computer simulation confirmed that action potentials may be blocked if the quantity of sodium ions diffusing into the nerve fibre is sufficiently reduced.

The first experiment to assess the feasibility of this hypothetical non-invasive anaesthetic technique demonstrated that the potential difference across a cation exchange membrane was affected by the presence of a magnetic field when a steady current or voltage was applied to the membrane. A reversible increase or decrease in membrane potential was observed, dependent upon the directions of the applied magnetic field and current flow. However, it was demonstrated that this phenomenon was not caused by collisions between sodium ions and the pores of the membrane. The observed results are consistent with a magnetically mediated variation in the conductivity of the electrolyte. It is unlikely that this phenomenon may be put to use as a non-invasive anaesthetic technique, since a greater flow of current than is normally present in nerve cells is required for the magnetic field to have a significant effect.

In the second set of experiments to evaluate the proposed method of non-invasive anaesthesia, the rate of diffusion of sodium ions through a cation exchange membrane was unaffected by a 0.3 T magnetic field. The failure of the magnetic field to reduce the rate of ion diffusion may be attributed to the large electrostatic force that exists between ions and charged groups within the ion channel. The magnitude of the Lorentz force is small in comparison to the electrostatic force, thus preventing the magnetic field from significantly influencing the motion of sodium ions. It was concluded that this hypothetical non-invasive anaesthetic effect is unfeasible.

Although it is disappointing that both hypothetical non-invasive anaesthetic techniques have not been proven, an encouraging conclusion may also be drawn from this research. It was noted in Chapter 1 that there has been much concern about the possible detrimental effects to human health caused by exposure to magnetic fields. While there may be other mechanisms by which magnetism may interact with the nervous system or other parts of the body, these results indicate that the Lorentz force experienced by ions in a static magnetic field is unlikely to have a significant physiological effect. Both hypothetical techniques of non-invasive anaesthesia were disproved on the grounds that the Lorentz force is insignificant in comparison to the electrostatic forces experienced by ions. Similarly, hypothetical mechanisms of interaction between magnetic fields and living organisms which speculate that the Lorentz force will affect ion behaviour (such as that proposed by Liboff [1] and discussed in Section 8.3) are unlikely to occur. Ions will be greatly influenced by electrostatic forces arising from the charged groups which are prevalent in

physiological media, thus precluding the possibility that the Lorentz force will significantly influence their behaviour. This conclusion illustrates the tremendous resilience of the nervous system to the often large magnetic fields that are encountered in everyday life.

9.1 Further Work

Despite the discouraging conclusion that both of the proposed techniques are unfeasible, non-invasive anaesthesia remains a desirable goal. Non-invasive anaesthesia could provide many benefits, including elimination of the risks associated with anaesthetic drugs and minimising the cost of surgery. Therefore, it is worthwhile to consider alternative techniques which may produce a non-invasive anaesthetic effect.

The literature review of Section 1.3 highlighted the lack of consensus on the effects of magnetic fields on nerve function. The results of many of these publications are contradictory and there is clearly a need for further fundamental research into the effects of both static and time-varying magnetic fields on the nervous system. Not only will such research facilitate the development of techniques for non-invasive anaesthesia and pain relief, but will also clarify the health risks associated with exposure to magnetic fields.

The most promising experimental results as far as non-invasive anaesthesia is concerned *are those published by Azanza and* del Moral and McLean, Holcomb *et al.,* since the research led by these scientists has produced consistent results over a period of several years. Azanza and del Moral have demonstrated that relatively weak magnetic fields of less than one tesla can modulate the activity [2, 3, 4] or reduce the magnitude of action potentials [5] in snail nerve fibres. Furthermore, del Moral and Azanza [6] have proposed a mechanism by which the magnetic field interacts with the nerve through the alignment of

diamagnetically anisotropic groups which is consistent with all of their experimental results. Although it is unclear why this mechanism did not cause observable results in experiments conducted by other researchers, future non-invasive anaesthetic techniques may attempt to take advantage of the hypothetical diamagnetic anisotropy.

McLean, Holcomb *et al.* observed that an array of permanent magnets with flux densities in the range of 1-35 mT blocked action potentials *in vitro* [7, 8, 9] and reduced pain in clinical trials [10, 11]. A magnetic array was also found to reduce pain in clinical experiments conducted by Vallbona *et al.* [12]. Although the researchers have not identified the mechanism by which the magnetic array prevents the propagation of action potentials, it is possible that their techniques could be refined to produce an anaesthetic effect. The use of magnetic arrays with a greater flux density or the application of arrays to several locations along the nerve are considered to be worthy of investigation.

Alternatively, it may be possible to produce a non-invasive anaesthetic effect via the use of a pulsed magnetic field. There is evidence to suggest that magnetic stimulation of the brain [13, 14] or body [15] may provide pain relief. Therefore, it is hypothesised that stimulation with a time-varying magnetic field could be used to produce anaesthesia. Such a technique may attempt to elicit additional action potentials in sensory nerves, in order to interfere with the brain's ability to correctly interpret painful stimuli. However, the use of magnetic stimulation must be treated with caution since tissue damage may result from the heating effect

of induced eddy currents. Furthermore, there are reports that transcranial magnetic stimulation can cause seizures in healthy patients [16, 17].

It is clear that non-invasive anaesthesia could revolutionise surgery and potentially save lives. The possible benefits are so great that any future hypothetical techniques to induce non-invasive anaesthesia are worthy of investigation. However, any such techniques must be treated with due caution and some degree of scepticism, due to the long history of charlatanism and quackery that is associated with the use of electromagnetic phenomena in healthcare [18].

9.2 References

1. Liboff, R.L.
   A Biomagnetic Hypothesis.
   Biophysical Journal, Vol. 5, 1965, pp. 845-853.
2. Azanza, M.J. and del Moral, A.
   Effects of Static Magnetic Fields on Isolated Neurons.
   Journal de Physique, Vol. 49, 1988, pp. C8 2059-2060.
3. Azanza, M.J.
   Characterization of Neuronal Membrane K^+ and Ca^{2+} Channels Operated Under Steady Magnetic Fields Exposure.
   Journal of Magnetism and Magnetic Materials, Vol. 83, 1990, pp. 527-529.
4. Azanza, M.J. and del Moral, A.
   Neuron Firing Frequency Dependence on the Static Magnetic Field Intensity.
   Journal of Magnetism and Magnetic Materials, Vol. 140, 1995, pp. 1464-1465.
5. Azanza, M.J. and del Moral, A.
   Isolated Neuron Amplitude Spike Decrease Under Static Magnetic Fields.
   Journal of Magnetism and Magnetic Materials, Vol. 158, 1996, pp. 593-594.
6. del Moral, A. and Azanza, M.J.
   Model for the Effect of Static Magnetic Fields on Isolated Neurons.
   Journal of Magnetism and Magnetic Materials, Vol. 114, 1992, pp. 240-242.
7. McLean, M.J., Holcomb, R.R., Wamil, A.W. and Pickett, J.D.
   Effects of Steady Magnetic Fields on Action Potentials of Sensory Neurons in Vitro.
   Environmental Medicine, Vol. 8, 1991, pp. 36-45.

8. McLean, M.J., Holcomb, R.R., Wamil, A.W., Pickett, J.D. and Cavopol, A.V.
Blockade of Sensory Neuron Action Potentials by a Static Magnetic Field in the 10 mT Range.
Bioelectromagnetics, Vol. 16, 1995, pp. 20-32.

9. Cavopol, A.V., Wamil, A.W., Holcomb, R.R. and McLean, M.J.
Measurement and Analysis of Static Magnetic Fields which Block Action Potentials in Cultured Neurons.
Bioelectromagnetics, Vol. 16, 1995, pp. 197-206.

10. Holcomb, R.R., Parker, R.A. and Harrison, M.S.
Biomagnetics in the Treatment of Human Pain – Past, Present, Future.
Environmental Medicine, Vol. 8, 1991, pp. 24-30.

11. Segal, N., Houston, J., Fuchs, H., Holcomb, R. and McLean, M.J.
Efficacy of a Static Magnetic Device Against Knee Pain Associated with Inflammatory Arthritis.
Journal of Clinical Rheumatology, Vol. 5, 1999, pp. 302-305.

12. Vallbona, C., Hazlewood, C.F. and Jurida, G.
Response of Pain to Static Magnetic Fields in Postpolio Patients: A Double-Blind Pilot Study.
Archives of Physical Medicine and Rehabilitation, Vol. 78, 1997, pp. 1200-1203.

13. Migita, K., Uozumi, T., Arita, K. and Monden, S.
Transcranial Magnetic Coil Stimulation of Motor Cortex in Patients with Central Pain.
Neurosurgery, Vol. 36, 1995, pp. 1037-1039.

14. Amassian, V.E., Vergara, M., Somasundaram, M., Maccabee, P.J. and Cracco, R.Q.
Temporary Relief of Induced Pain by Repetitive Magnetic Stimulation of Human Parietal Lobe.
Journal of Physiology, Vol. 499, pp. P88-89.

15. Ellis, W.V.
Pain Control Using High-Intensity Pulsed Magnetic Stimulation.
Bioelectromagnetics, Vol. 14, 1993, pp. 553-556.

16. Pascual-Leone, A., Valls-Solé, J., Brasil-Neto, J.P., Cohen, L.G. and Hallett, M.
Seizure Induction and Transcranial Magnetic Stimulation.
The Lancet, Vol. 339, 1992, p. 997.

17. Wassermann, E.M., Cohen, L.G., Flitman, S.S., Chen, R. and Hallett, M.
Seizures in Healthy People with Repeated "Safe" Trains of Transcranial Magnetic Stimuli.
The Lancet, Vol. 347, 1996, pp. 825-826.

18. Fishlock, D.
Doctor Volts.
IEE Review, Vol. 47, No. 3, 2001, pp. 23-28.

APPENDIX 1 TECHNICAL DRAWINGS

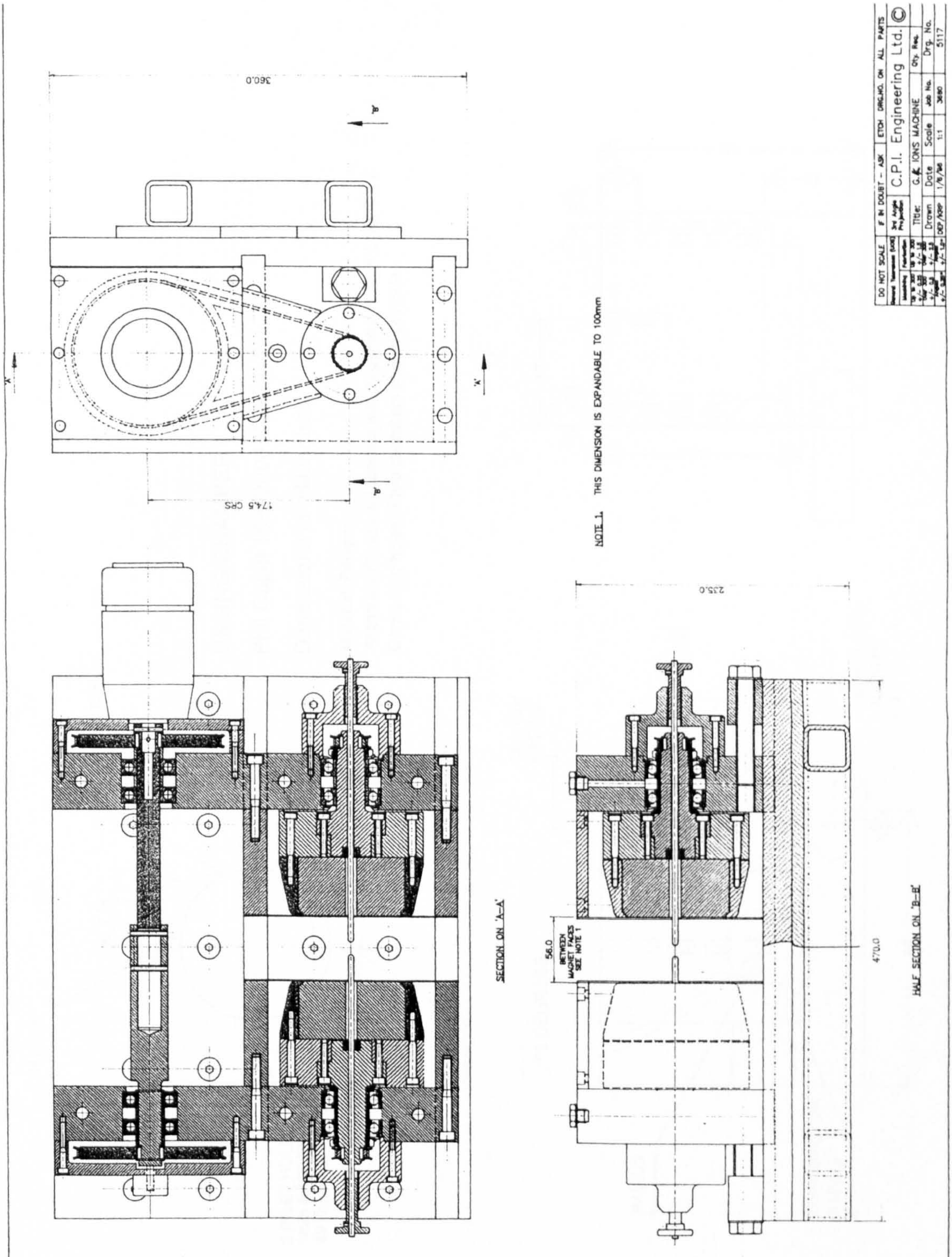

Figure A1 Rotating magnet apparatus

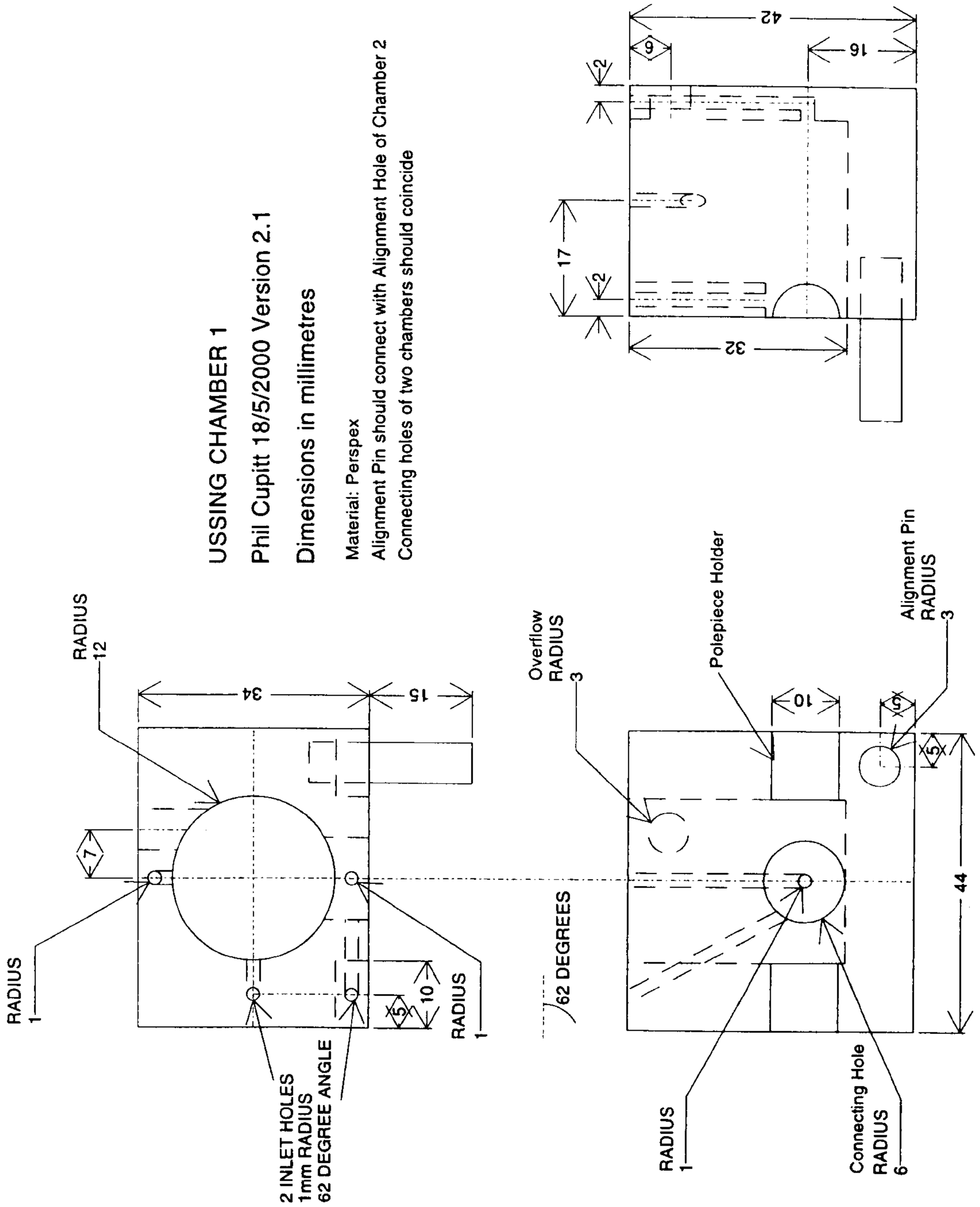

Figure A2 Ussing chamber (bath 1)

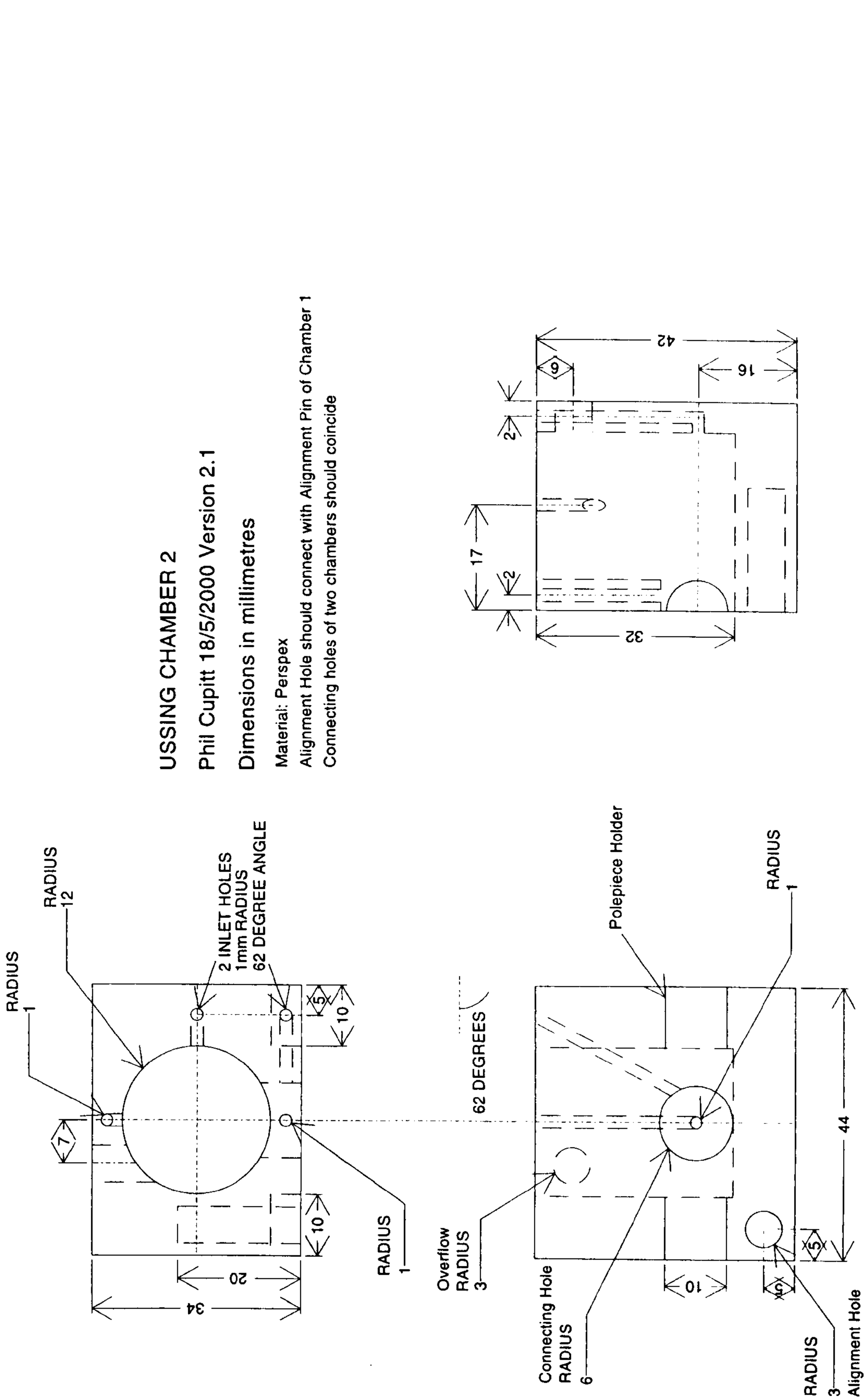

Figure A3 Ussing chamber (bath 2)

APPENDIX 2 SUPPLEMENTARY RESULTS

Figure A4 Membrane potentials measured in the presence of an applied magnetic field during first series of experiments

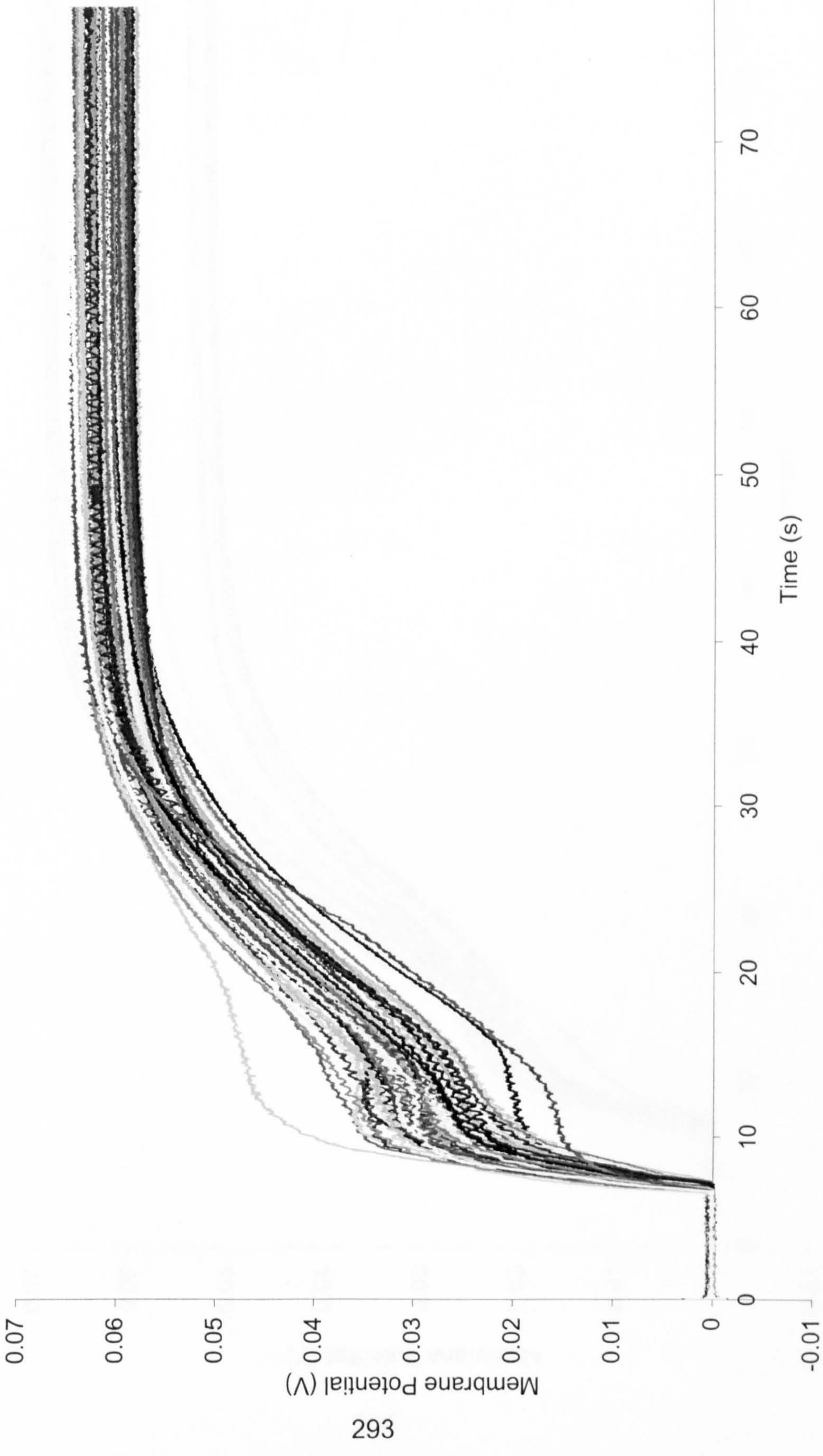

Figure A5 Membrane potentials measured in the presence of a magnetic field applied in direction 1 during second series of experiments

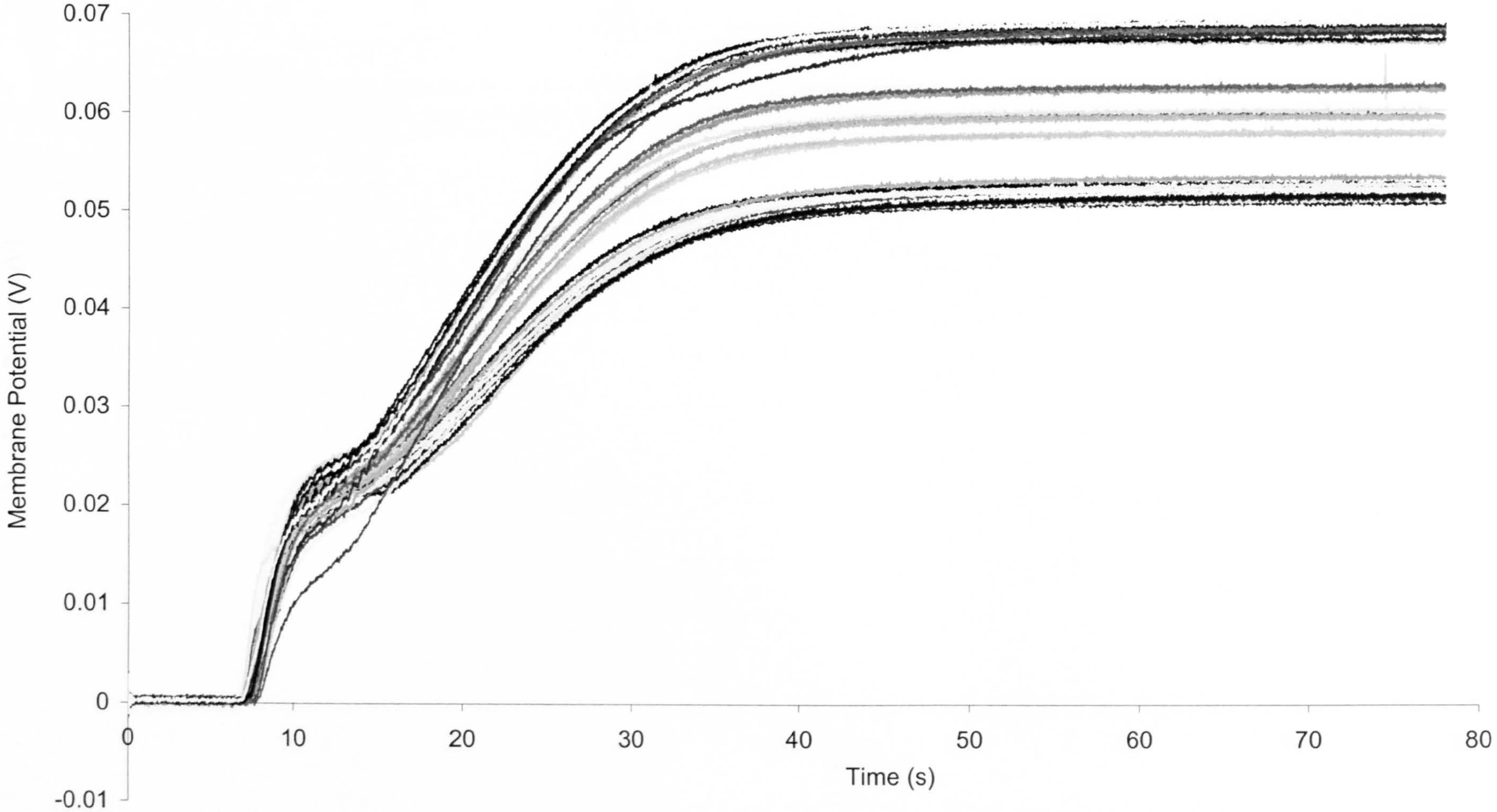

Figure A6 Membrane potentials measured in the presence of magnetic field applied in direction 2 during second series of experiments